VARIABLE FREQUENCY INDUCTION MOTOR DRIVE DYNAMICS

by

V. R. Stefanovic, Dipl.Ing., Belgrade U., M.Eng.

Department of Electrical Engineering

McGill University
Montreal, Quebec

August 1975

VARIABLE FREQUENCY INDUCTION MOTOR DRIVE DYNAMICS

by

V. R. Stefanovic, Dipl.Ing., Belgrade U., M.Eng.

A thesis submitted to the Faculty of Graduate Studies and Research in partial fulfillment of the requirements for the degree of Doctor of Philosophy.

Department of Electrical Engineering,
McGill University
Montreal, Quebec

August 1975

ABSTRACT

Several strategies for controlling the speed of a closed loop induction motor drive, supplied from a variable frequency source are discussed. Both static and dynamic characteristics are considered. The speed response to all drive inputs is analyzed using both time and frequency domain techniques. The results are reviewed to include practical limitations such as inverter characteristics and motor nonlinearity. It is concluded that the best dynamic performance is obtained by using a constant airgap flux control and supplying the motor from an inverter of the pulse width modulated type.

A new method for predicting the structure and the zero location of the speed-torque transfer functions is presented. The method is general and applicable to any motor drive, operating in open or closed loop and described by a set of linearized equations.

The experimental results support the validity of the motor dynamic model as well as the predictions of the drive transfer functions and the extension of the stability results to the motor nonlinear behaviour.

RESUME

Cette thèse présente une étude de plusieurs méthodes pour le contrôle de la vitesse d'un moteur à induction à circuit bouclé et dont la source est à fréquence variable.

Les caractéristiques statiques et dynamiques sont considérés, et la fonction réponse de la vitesse pour tous les signaux d'entrée, est analysée dans les domaines du temps et de la fréquence respectivement.

Les résultats sont interprétés de manière à tenir compte de certaines limitations pratiques, telles que les caractéristiques de l'inverseur et la non-linéarité du moteur. On aboutit à la conclusion que la meilleure performance dynamique est obtenue en utilisant un entrefer à flux constant, et en alimentant le moteur avec un inverseur à modulation par impulsions de largeur variable.

On présente une nouvelle méthode pour prédire la structure et l'emplacement des zéros des fonctions de transfert vitesse-couple. La méthode est générale et peut être appliquée à la commande de n'importe quel moteur, en circuit ouvert ou fermé et representé par des équations linéarisées.

Les résultats expérimentaux confirment la validité du model dynamique du moteur, ainsi que les prédictions des fonctions de transfert de commande et l'extension des résultats sur la stabilité du compartement non-linéaire du moteur.

CLAIM OF ORIGINALITY

To the best of the author's knowledge, the following contributions are original.

1) The formulation and proof of two theorems which predict the structure of speed-torque transfer functions as well as the nature and the location of their zeros. The theorems are general, simple, and valid for any motor drive, operating in an open or closed control loop and described by a set of linearized equations.

2) The presentation of the dynamic characteristics of a closed loop, variable frequency induction motor drive, operating with a constant volts per hertz control strategy.

3) The statement of the dynamic characteristics of a variable frequency induction motor drive, operating with constant slip speed control strategy.

4) The formulation of the dynamic characteristics of a variable frequency induction motor drive, supplied by a current source and operating with constant airgap flux control strategy.

5) The investigation of inverter effects on the dynamic performance of induction motor drives.

6) The application of modal analysis to the study of practical stability of induction motor drives.

7) The proof tha[redacted]oncepts of observability and controllability are inadequate to deal wi[redacted] dynamic behaviour of practical linear systems and the definition of two new terms, pseudo-observability and pseudo-controllability, which are more relevant to engineering applications.

ACKNOWLEDGEMENTS

I wish to express my gratitude to Dr. T. H. Barton for his guidance and help during the course of this study.

The whole Electrical Engineering Department has been most helpful during these years, but especially Mr. W. Taal, Mr. J. Foldvari and Mr. S. Henry, who provided their expert assistance whenever it was needed.

Sincere appreciation goes to Bill Scott for his invaluable advice and time spent in many discussions.

My gratitude extends to Ted Goodman for his good will to endure the proof reading of this thesis.

Many thanks to Dr. H. Nakra who always provided an optimistic outlook on the future.

Very special thanks go to my brother, Michael, for putting his artistic talents to work during the technical preparation of this thesis.

Additional thanks are extended to the Engineering secretaries on the Loyola Campus for their expert help in typing when it was most needed.

I would like to acknowledge my gratitude to the Department of Electrical Engineering, Concordia University, Loyola Campus, and in particular to Dr. S. J. Kubina for arranging the leave of absence from my work, which enabled me to complete this study.

Finally, I want to thank, in a very special way, my wife, Biljana, for her companionship, optimism and help during these years.

TABLE OF CONTENTS

LIST OF ILLUSTRATIONS

LIST OF SYMBOLS

$[A]$	General state matrix
$[B]$	General input matrix vector of state derivatives
$[P]$	General coefficient matrix
$[Q]$	General coefficient matrix, state vector
$[M]$	Modal (eigenvector) matrix
$[I]$	Identity matrix, also vector of steady state currents
$[A_r]$	State matrix of a reduced system
$[\Lambda]$	Jordan eigenvalue matrix
$[H]$	Input mode coupling matrix
$[I_v]$	Unity vector, Appendix B
Adj.[ ]	Adjoint matrix
Det.[ ]	Determinant of a matrix
T	Transposed
U	Input vector
$[V_r]$	Reference (speed) input signal
$[G]$	General speed matrix
$[F]$	General reference frame matrix
X	General vector of state variables
$\dot{X}$	General vector of state variable derivatives
Y	Vector of output variables
y_s	Motor speed
$[R]$, $[L]$	General resistance, inductance matrices
$I_{s/m/r}$	Stator/magnetizing/rotor current, motor equivalent circuit
I_o	General vector of steady state currents

$I_{\gamma\delta}$	Vector of steady state currents in synchronous (γ-δ) reference frame
$I_{1/2}$	Stator γ-coil/δ-coil steady state currents
$I_{3/4}$	Rotor γ-coil/δ-coil steady state currents
i	Vector of instantaneous currents
v	Vector of instantaneous voltages
V_{ph}	Phase rms voltage, 3-phase abc reference frame
V	Line rms voltage, 3-phase abc reference frame
E	Airgap voltage, motor equivalent circuit. Also inverter dc link voltage
$V_{\gamma\delta}$	Voltage vector in synchronous (γ-δ) reference frame
$R_{1/2}$	Stator/rotor resistance
$L_{s/r}$	Stator/rotor leakage inductances, 3-phase abc frame
$L_{1/2}$	Stator/rotor leakage inductances, synchronous reference frame
f	Input frequency in hz
ω	Instantaneous input frequency in electrical rad/sec
Ω	Steady state input frequency in electrical rad/sec
ω_c	Instantaneous speed of a reference frame in electrical rad/sec
Ω_c	Steady state speed of a reference frame in electrical rad/sec
ω_s	Instantaneous slip speed in electrical rad/sec
Ω_s	Steady state slip speed in electrical rad/sec
ω_m	Instantaneous motor speed in mechanical rad/sec
Ω_m	Steady state motor speed in mechanical rad/sec
mmf	Magnetomotive force
ψ	Phase angle mmf vector

f_T	Total friction of a rotating system
J_T	Total inertia of rotating masses
T_e	Motor electrical torque in N_m
T_L	Motor load torque in N_m
ρ	Slope of a static torque-speed curve
n	Number of motor pole-pairs
N	Number of equations
λ_k	k-th eigenvalue
z_k	k-th zero, $G_2(s)$ transfer function
q_k	k-th modal state
m_{kj}	k-th component of a j-th eigenvector
h_{kj}	k-th component of a j-th input-mode coupling vector
p	d/dt operator
δ	Operator denoting a perturbation of variable which follows. Also a subscript for δ-axis variables.
γ	Subscript for γ-axis variables
s	Complex variable
$G_1(s)$	Speed-input (speed) reference transfer function
$G_2(s)$	Speed-load torque transfer function (motor mechanical output impedance)
N(s)	Numerator polynomial of a transfer function
D(s)	Characteristic polynomial of a transfer function
$T_c(s)$	Transfer function, speed controller
A_c	Proportional gain of a speed controller
k_c	Integrator gain, speed controller
k_t	Tachogenerator constant

A_3	Conversion gain, closed loop drives equal to n/k_t
A_1	Voltage gain constant V/hz, open loop drive equal to k/6.2832
k	Proportionality constant for V/hz control; also a dummy subscript
τ	Dummy variable

LIST OF TABLES

CHAPTER I

INTRODUCTION

1.1 Applications of variable speed induction motor drives

Since its invention in 1888, the induction motor has been one of the most widely used motors in industry. However, until recently, its application was mainly limited to drives with constant or near constant speed. Whenever a process required a wide speed range, the historically older dc motor was generally used. Over the last fifteen years, two main factors have emerged which promise to change this:

1) The trend towards automation of manufacturing processes which is placing more stringent requirements on the drive reliability and dynamic performance.

2) The development of thyristors with adequate power and switching capabilities which makes the use of variable frequency drives practical. Of all the methods for changing the speed of an induction motor, only control of the input frequency gives continuous speed regulation and high starting torque while using maintenance free squirrel cage motors.

Both factors have resulted in a gradually increasing use of variable speed induction motors. Consequently, there has been an increasing interest in their dynamic behaviour.

It is appropriate to review the main advantages of an induction over a dc motor in variable speed drives.

1) Maintenance. The squirrel cage induction motor is the simplest and most rugged of all electrical machines, while a dc motor has all the disadvantages of a commutator machine. (Frequent maintenance, arcing, susceptibility to chemically aggressive atmosphere and vibrations, flash-over, etc.)

2) Very wide speed range. Dc motors are normally restricted to 4:1

speed range, at most. An induction motor, supplied from an appropriate variable frequency source can operate from zero up to 12,000 rpm.[1] Thus, practically any speed requirement can be satisfied without the additional mechanical gearing.

3) Power to weight ratio (specific power). For a given torque output, an induction motor weighs only about 60% of its dc counterpart. Operation at higher speeds, for which the dc motor is ill suited, may further increase the motor specific power:

   - For the same torque and, thus, size, the power output is higher
   - With the higher input frequencies, and the same power output the iron in the machine can be reduced, thereby reducing its weight.

   Liquid cooling is possible with induction motors and this further increases its power/weight ratio. Motors with more than 1 hp/1 lb. at 12,000 rpm (power supply included) have been manufactured.[1]

4) Superior transient response. During fast speed changes, an induction motor has a double advantage over its dc counterpart:

   - It has a lower rotor inertia
   - It can better sustain large accelerating torques.

5) Cost. An induction motor has a much lower first cost than an equivalent dc machine. However, the cost comparison for a complete drive, including a power supply and controls depends on the power range and motor application.[18]

The following examples illustrate applications of variable frequency induction motor drives over the past decade:

Traction application[1-7] where the requirements for low maintenance, good power to weight ratio and general ruggedness will continue to favor the induction motor.

Aerospace[10-11]; the main reasons for using induction motors in this case are the superior reliability and power to weight ratio.

Mining,[16] where motor compactness and explosion proof quality have been dominant factors in some specific applications.

Steel industry,[13-14] for multimotor drives, where the induction machine has not only a technical but also an economic advantage over its dc counterpart.

Nuclear reactor pump drives,[8,9] which are required to operate reliably, without maintenance over prolonged periods of time.

Automatic tool machines,[15] where the combination of good power/weight ratio, total enclosure, good power factor and good speed control have favored the induction motor.

Fan and pump drives,[17] where variable frequency induction motors are becoming a viable alternative as the price of thyristors is reduced.

One should not conclude from these examples that induction motors will entirely replace the dc machines in the foreseeable future. The main reason is that the cost of a complete drive is usually 2-3 times higher when an induction motor is used.[19,20] A variable frequency induction motor will be selected only when a particular application makes it more economical,[18] or, when critical performance requirements make the dc motor unsuitable.

1.2 Review of previous work

Induction motor dynamic studies have preceded the development of variable frequency drives. Weygandt and Charp have investigated the motor transients in a servo system by using an analog computer.[21] Kovacs and Racz have applied rotating reference frames and space vectors to the study of motor transients.[22]

The development of the thyristor gave a great impetus to motor dynamic studies. First Pfaf[24] and then Rogers[25] pointed to motor stability problems at low input frequencies. They both used the linearized motor equations; Pfaf giving the time and frequency domain analysis for different

values of the rotor inertia; Rogers applying the synchronous frame representation and root-locus method to investigate the effects of motor parameters on the stability.

A stream of papers, proposing various control strategies and giving motor steady state characteristics followed. Heumann presented several drive configurations and showed the advantage of the constant airgap flux operation;[27] Heck and Meyer,[26] West et al[23] and Heumann and Jordan[28] pointed out certain advantages of current over voltage control. Abraham et al[29] and Mokrytzki[31] proposed constant slip control which results in a constant power factor operation. Slabiak and Lawson discussed the torque controlled motor, suitable for traction applications.[30] The Brown Boveri engineers, involved in induction motor railway applications, have published a number of detailed papers,[32,34] the most important being that by Shönung and Stemmler[33]. They were one of the first to recognize the superiority of the pulse width modulated inverter and to investigate its harmonic content. Furthermore, they clearly formulated, if not analyzed, all control strategies for speed regulation in variable frequency induction motors.

Although most of these studies gave drive control schematics and outlined methods of operation, none has presented a detailed analysis of motor dynamics.

One of the first comprehensive stability studies, after the work of Rogers, was done by Fallside and Wortley in 1968 and published in 1969.[36] The root locus method was applied to predict the motor stability boundaries and two stabilizing feedbacks were used to improve the drive dynamic performance.

At almost the same time, but independent of this study, a sequence of papers followed, inspired by previous work of Krause and Lipo on synchronous and reluctance variable frequency supplied motors. Krause and Woloszyk compared computer and actual test results[35] for an induction motor drive. Nelson et al[38] and Lipo and Krause[39] investigated the effects of different drive parameters on the motor stability in great detail. Krause and Lipo showed that the higher harmonics in the inverter output voltage may be neglected without significantly affecting motor stability.[40] Ooi and Barton identified motor modes and used sensitivity functions to investigate

the effect of motor parameters on the drive eigenvalues.[42]

By that time, the representation of the motor linearized equations in the synchronous reference frame and the use of the state space method in the dynamic analysis had become the most favored approach. A few studies of the motor nonlinear equations were made, with varying degress of success. They proceeded either by using the equivalent circuit while introducing substantial approximations,[43] by directly solving the motor equations on an analog[45] or digital[46] computer, or by applying the Liapunov method.[47]

All these studies were done for constant V/hz motor control.

Although several authors[26,31,29,58,80,83] have proposed closed loop speed operation, and Landau[49] presented the experimental results for one such drive, there are no corresponding dynamic studies available. This is in spite of the fact that there are a number of closed speed loop drives in operation.[6,11,12]

The development of variable frequency supplies proceeded in parallel with the study of induction motors. The basic theory for both line and force commutated inverters was developed in the era of mercury arc devices,[50,51] and was ready for use when thyristors became available.

One of the first inverter types to be applied in variable frequency induction motor drives was a line commutated cycloconverter,[30] which requires lower grade thyristors than other types. Due to its restricted ouput frequency range, it is being gradually replaced by force commutated inverters.

The ~~most~~ common inverter circuit in use to-day was proposed by McMurray and Shattuck[52] in 1961. Bradley et al gave detailed analysis of various commutation methods. Shönung and Stemmler,[32] Mokrytzki,[54] Heumann,[55] Veres[57] and many others recognized the advantages of pulse width modulated inverter. Espelage et al[56] proposed an inverter with externally injected commutation pulses. Phillips[58] presented a very interesting current controlled inverter which generated further study.[63] As the pulse width modulated inverter is becoming an obvious choice for better drive performance, a number of recent studies[59 62] analyzed various aspects of its operation. It is evident from this review that variable frequency supplied induction motor drives are becoming a viable alternative to dc motors and that their

development is proceeding rapidly.

1.3 Present study

Although the literature shows that there has been considerable research on the dynamics of variable frequency induction motor drives, many important aspects have been neglected:

1) Only constant V/hz control has been analyzed. There have been, apparently, no dynamic studies of other (and possibly better) control strategies.

2) A great effort has been made to identify combinations of motor parameters which ensure stable drive operation and improve its dynamic response. Very often such combinations lead to poor steady state performance. Only Fallside and Wortley[36] have considered a more logical approach: the motor parameters are selected to optimize drive efficiency and process requirements, while stabilizing feedback loops improve motor dynamic performance.

3) No dynamic study has been made for closed speed loop drives, which are becoming increasingly important in automatic process control.

4) Practically all previous studies have used motor linearized equations, which has proved to be the most fruitful approach. However, most conclusions about motor dynamics were made by considering only the drive eigenvalues, which determine only the asymptotic stability. This is insufficient for practical motor applications, where relative damping and output rise times are much more relevant. Where the input-output couplings have been taken into account, the results are pertinent only to constant V/hz drives.

5) A large number of studies have equated constant V/hz with constant airgap flux operation. The two are, however, entirely different, in both the static and dynamic performance.

This discussion indicates the areas requiring further investigation and clarification. In an attempt to improve the pertinent knowledge and to further the development of variable frequency induction motor drives, the following are the main objectives of this thesis:

1) Control strategies

All the most important control strategies are clearly formulated and examined. The merits of each with respect to the motor dynamic performance are critically evaluated.

2) Closed loop operation

For the first time the closed speed loop operation is analyzed for different control strategies. By designing speed controller for each drive configuration, it is possible to improve the dynamic performance of a standard induction motor, without placing uneconomical constraints on its parameters.

3) Practical stability

All results are presented in both the time and the frequency domain and include the effects of various drive inputs on the motor speed. In this way, the drive practical stability is evaluated and presented in a form readily understood by practicing engineers.

4) Realistic limitations

Dynamic results are first obtained for an ideal, sinusoidal power supply and are then reviewed to assess the effect of practical inverters, tachogenerator and motor nonlinearity.

Thus, the final results consist of two parts: the first is independent of inverter technology and reflects the nature of induction machines, and the second, which takes into account all the limitations caused by imperfect drive components and which depends on the future developments of variable frequency supplies.

5) Experimental verification

The dynamic model for the induction machine and the theoretical

results are confirmed experimentally. Again, both time and frequency domain techniques are used.

In addition to these stated objectives, a new method for predicting the structure and location of zeros in the speed-torque transfer function is developed. The method is general, applicable to any motor drive operating in open or closed loop, and described by a set of linearized equations.

CHAPTER II

SPEED CONTROL--STATIC CHARACTERISTICS

2.1 Introduction

Three strategies for controlling the torque and thus the speed of an induction motor are presented, together with the corresponding static torque curves. The effects of the saturation of the main flux path are included. Since most of these results are available in the literature, the static characteristics are presented here only for the sake of completeness.

While the speed control of dc motors obeys a simple law, the corresponding relationship for induction machines is much more complex. Basically, there are two independent inputs which are used to control the motor speed. They are:

- Applied stator voltage
- Applied stator frequency

In addition to these two inputs the speed depends also on the motor load. A control strategy may be now defined as the law which determines how each of these inputs should be manipulated in order to obtain a desired motor behaviour. It will be seen that the same motor has significantly different static and dynamic characteristics with different control strategies.

While there are many possible strategies, only the three which are most often used are considered in this study. They are:

1) Constant volts/hz control
2) Constant slip speed control
3) Constant airgap flux control

The drive configurations which implement these strategies are described in the study of the motor dynamic behaviour (Chapter IV).

The motor static characteristics for each strategy are obtained by using the standard equivalent circuit (Fig. 2.1) and are then modified to allow for magnetic nonlinearity. All results are expressed in per unit (P.U.)

values, with the motor rated values used as the base.

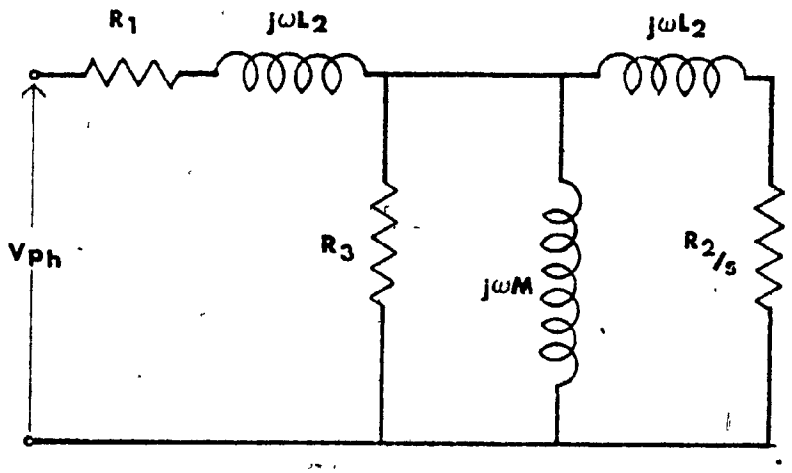

Fig. 2.1: Standard per phase equivalent circuit of an induction motor.

The parameters of the motor used in this study are given in Appendix A. It is useful to restate at this point the expression for the electrical torque of a 3-phase induction motor. From the equivalent circuit, it follows:

$$T_e = 3 \frac{(M I_m)^2 R_2/\omega_s}{(R_2/\omega_s)^2 + (L_2)^2} \qquad (2\text{-}1)$$

where ω_s is the slip speed. When the motor operates within rated load, the slip speed is small. Therefore:

$$(R_2/\omega_s)^2 \gg (L_2)^2$$

so that the rotor leakage inductance can be neglected. The equation (2-1)

then becomes:

$$T_e = \frac{3 M^2 I_m^2 \omega_s}{R_2} \qquad (2\text{-}2)$$

or

$$T_e = c_t \omega_s \Phi^2 \qquad (2\text{-}3)$$

where Φ is the airgap flux, while c_t is a constant given by:

$$c_t = 3/R_2$$

The last expression shows that the electrical torque can be controlled either by manipulating the slip speed or the airgap flux.

2.2 Constant Volts/hz Control

This strategy results in a fixed, linear relationship between the applied voltage and frequency (Fig. 2.2). The aim is to maintain the airgap flux density approximately constant as the applied frequency is changed while avoiding any feedbacks for direct or indirect flux measurement. In order to prevent a pronounced decrease in the electrical torque at low input frequencies, a fixed component V_o is added to the applied voltage so that it becomes:

$$V = V_o + kf \qquad (2\text{-}4)$$

The constant component V_o is usually chosen so that rated stator current flows at 0 hz while the proportionality constant k gives the rated motor line voltage at 60 hz (Fig. 2.2).

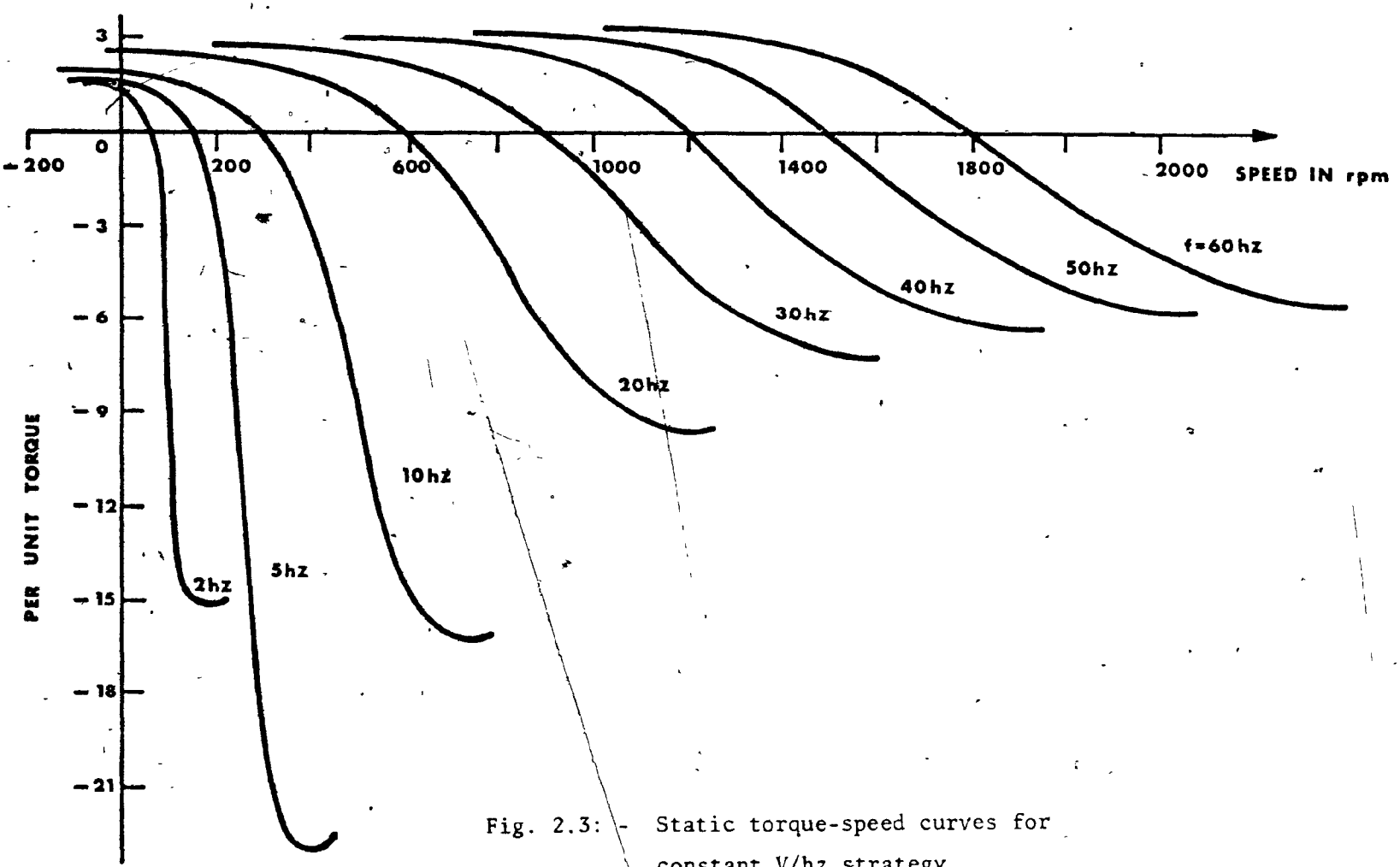

Fig. 2.3: - Static torque-speed curves for constant V/hz strategy.

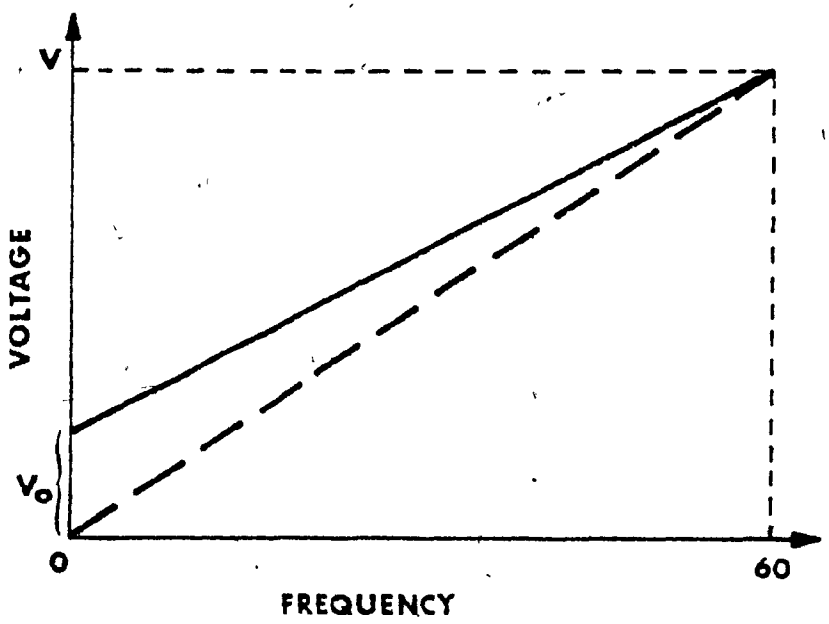

Fig. 2.2: Voltage-frequency relationship for constant V/hz strategy.

The constant V/hz control is the simplest to implement since it does not require any feedbacks. Consequently, it has received most of attention in the literature.[33,39,42,64]

The static torque-speed curves for this control strategy are presented in Fig. 2.3. The natural starting torque of this machine is relatively high due to the large rotor resistance.

When all points of the positive and negative peak torques in Fig. 2.3 are connected, an envelope of the static torque-speed curves is obtained (Fig. 2.4). It has been shown before[64] that the very large negative peak torques at low input frequencies are incompatible with the nature of the magnetic circuits in electrical machines. Therefore, the saturation of the main flux path has to be taken into account. This is done by treating the magnetizing inductance in the equivalent circuit as a nonlinear function of the motor magnetizing current (Fig. 2.5). The computation of the peak torque requires an iterative procedure which was found to converge to the correct values of the terminal voltage and magnetizing current in three to five steps. The envelopes of the torque-speed curves so obtained, which allow for magnetic saturation, are presented in Fig. 2.4.

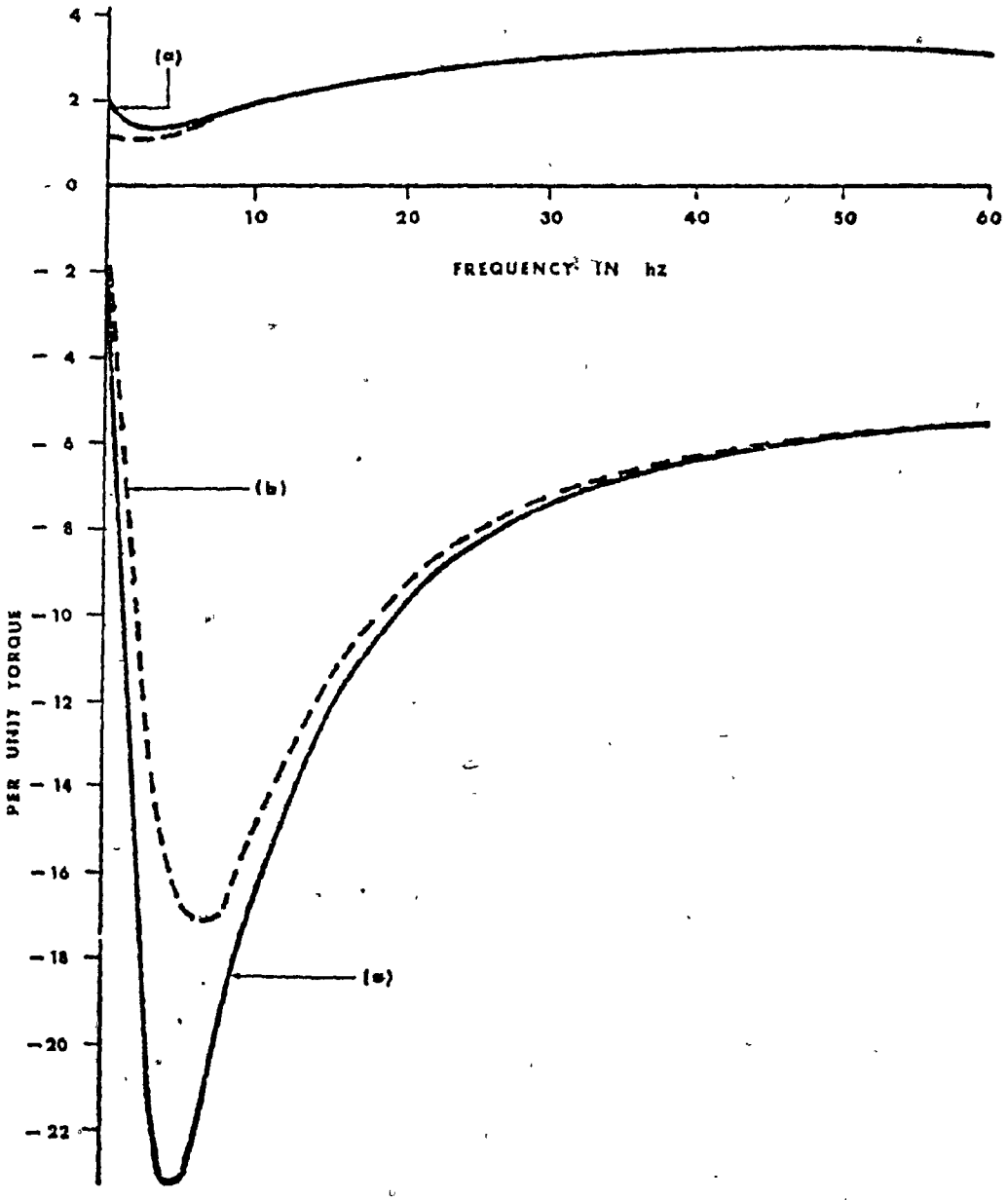

Fig. 2.4: Static peak torques for constant V/hz control

A) linear circuit model

B) with saturation of main flux path included.

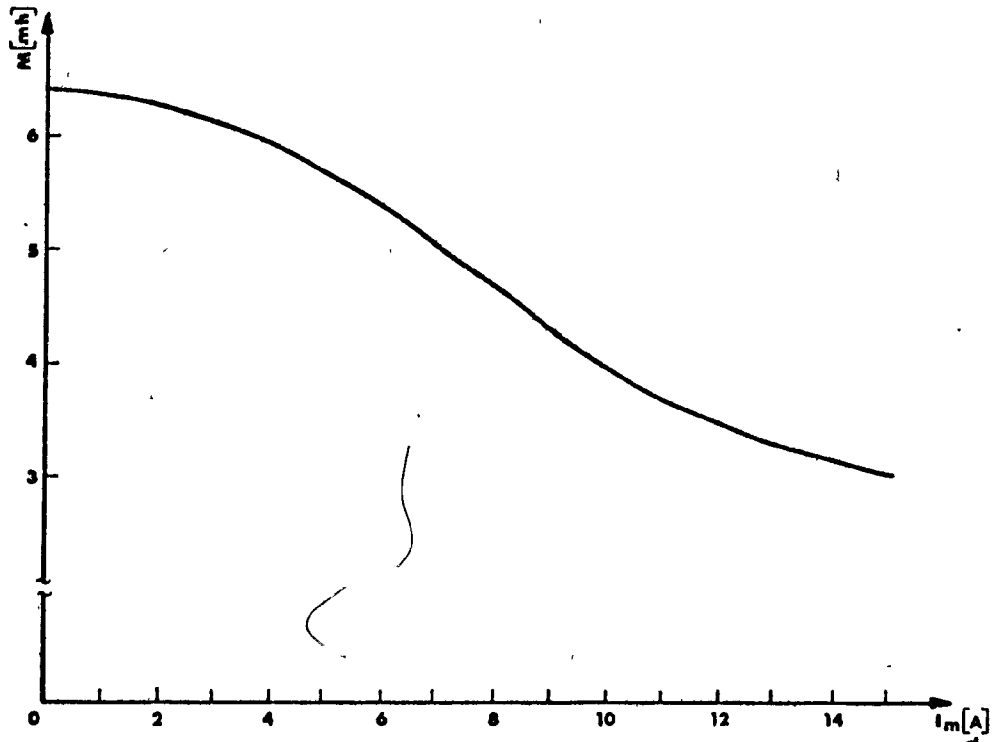

Fig. 2.5: Motor magnetizing inductance as a function of the magnetizing current. The curve was obtained experimentally.

A few comments can be made with respect to these results:

1) The effects of magnetic saturation ought to be included when considering the constant V/hz operation of induction motors in:
   - Generating mode, when the motor acts as a brake.
   - Motoring mode at very low input frequencies (below 5-6 hz)
2) The motoring torque is significantly decreased as the supply

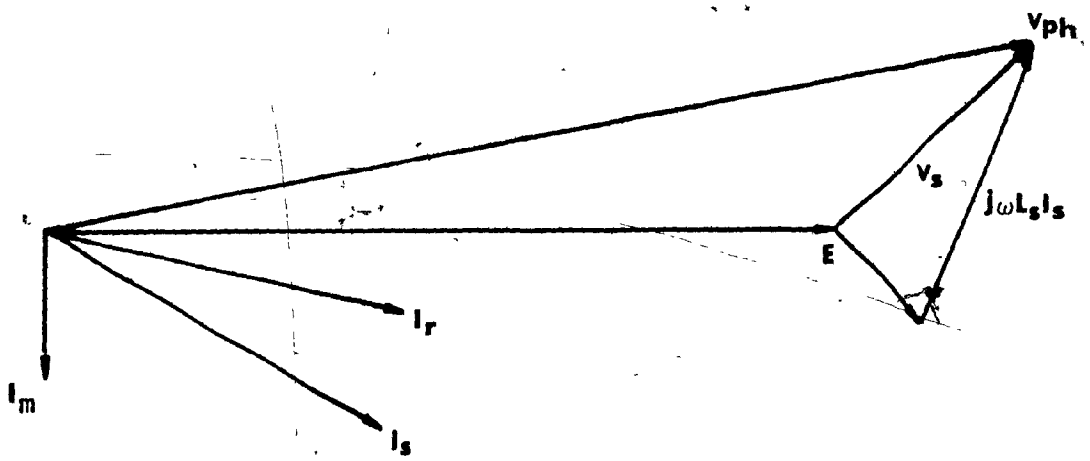

Fig. 2.6a: The machine is in the motoring mode. The airgap voltage E is smaller than the input voltage V.

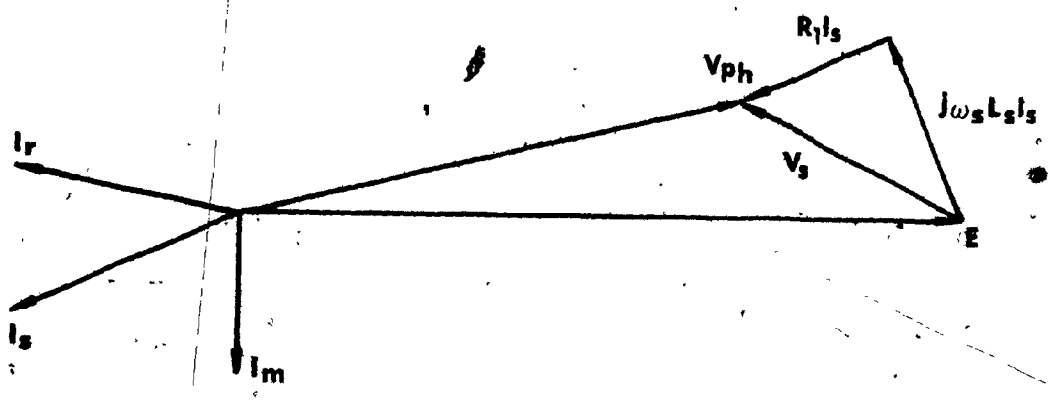

Fig. 2.6b: The machine is in the braking mode. The airgap voltage E is larger than the input voltage V.

frequency is reduced. For example, it falls to 1.46 P.U. at 5 hz as compared with 3.25 P.U. at 60 hz. Besides limiting the motor loading capabilities in this frequency range, this decrease results in a reduced slope of the torque-speed curves which is detrimental to the motor dynamic behaviour, as will be seen in Chapter IV.

3) The decrease in the peak motoring torques is the result of a reduced airgap flux, which in turn is due to a relative increase of the stator resistive voltage drop at the lower input frequencies. Consider the motor voltage equation (Fig. 2.1) when the supply frequency is reduced:

$$\bar{V}_{ph} = \bar{V}_s + \bar{E} = \lim_{\omega \to 0} \{(R_s + j\omega L_s)\bar{I}_s + j\omega M \bar{I}_m\}$$

Obviously, as the frequency is reduced, an increasing portion of the applied voltage is required to cover the stator resistive voltage drop.

4) The torque-speed curves are not symmetrical with respect to the synchronous speed point. The difference between the motoring and braking peak torques is most evident at the lower supply frequencies. The reason for this difference is best understood by considering the corresponding phasor diagrams (Figs. 2.6a and 2.6b). It is evident from these diagrams that for the same applied voltage V, the airgap flux is larger in the braking than in the motoring operation. For a given input frequency the difference will increase with the increase in the magnitude of the rotor slip speed. For a given slip speed this difference becomes more pronounced at lower supply frequencies, when the stator resistive voltage drop starts to dominate the machine voltage equation.

2.3 Constant slip speed control

This type of control has been proposed by several authors.[29,31] It has the advantage of reducing the motor core losses at light loads by

decreasing the value of the airgap flux. Furthermore, this control yields a constant power factor over the whole speed range. In this strategy there is no fixed relationship between the input voltage and frequency. The input frequency reference is obtained as the sum of the actual motor speed and selected slip speed, which is, therefore, maintained constant. The input voltage is changed independently to control the electrical torque by controlling the airgap flux--Equation (2-3).

Since the motor operates with the constant slip speed, the standard torque-speed curves are not well defined for this type of control. Consider, for example, the motor operation at point A, Fig. 2.7

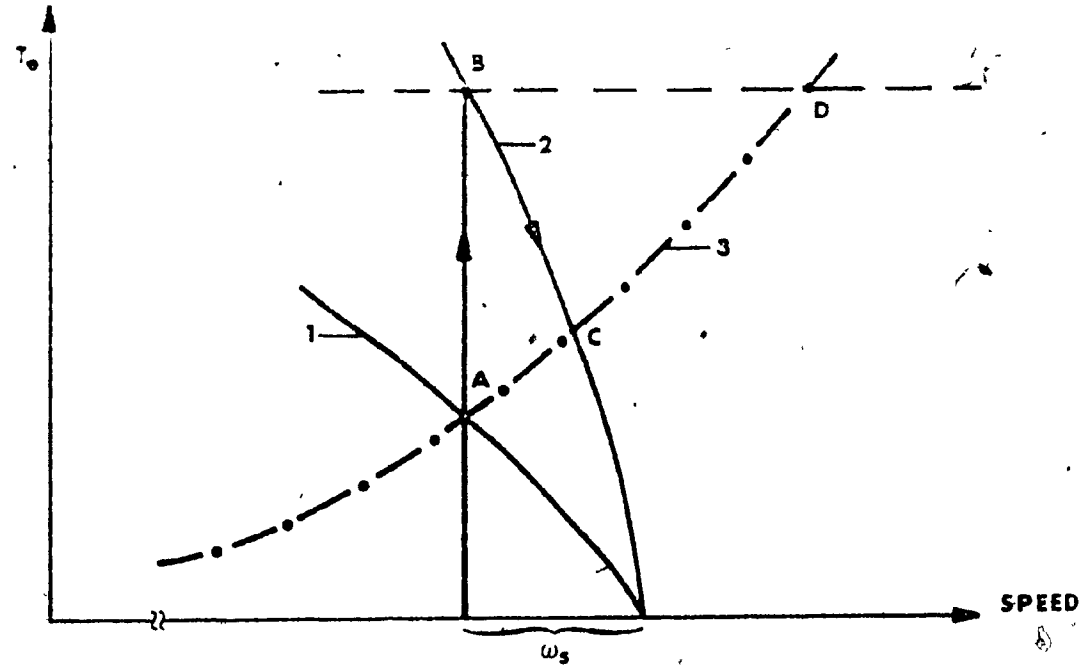

Fig. 2.7: The trajectory of the operating point with the constant slip speed control. 1) and 2) are the motor torque curves while 3) is the load torque curve.

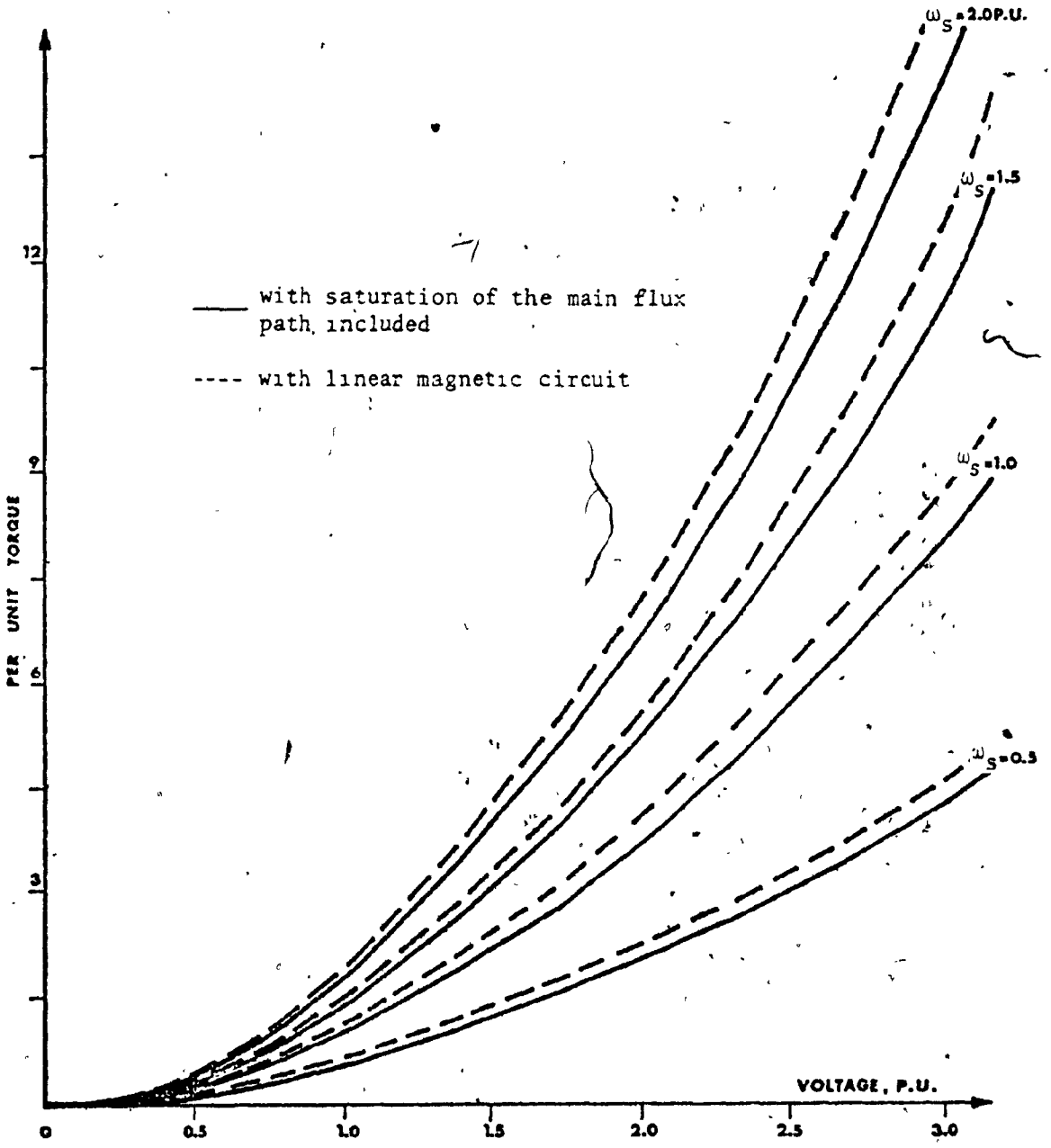

Fig. 2.8a: Static torque-voltage characteristics at 60hz constant slip speed control.

The selected slip speed is ω_s, the airgap flux is Φ_1, resulting in motor torque curve 1). When a request for a speed increase is given, the motor terminal voltage increases, strengthening the airgap flux and transferring the motor operation to point B on curve 2). Since the input frequency has not changed, the motor starts to accelerate along curve 2) from B to C, reducing the slip speed ω_s. This triggers an increase in the supply frequency which moves to keep the slip speed constant. Due to this, the motor continues to accelerate, following this pattern, until the new electrical torque equals the load torque, point D. The motor dynamic behaviour is described in greater detail in Section 4.5.

Since the standard torque - speed curves are not well defined for this strategy, the torque - voltage curves are presented instead (Fig. 2.8a and 2.8b). They correspond to Equation (2-3) with four different slip speeds. Both linear and nonlinear magnetic circuits are considered. It is seen that magnetic saturation lowers the value of the output torque for a given slip speed and input voltage. In addition, the saturation greatly increases the motor magnetizing current, this effect being more pronounced at the higher input voltages and the lower input and slip frequencies. For example, at 100 r.p.m. slip speed, 60 hz input frequency and 3 P.U. applied voltage, the magnetizing current is 3.03 P.U. for linear and 6.88 for the nonlinear magnetic circuit. The corresponding values at 10 hz input frequency are 3.18 P.U. and 7.22 P.U.

When calculating the torque curves, the input voltage was changed from zero to 3 P.U. at 60 hz and from zero to three times the corresponding constant V/hz voltage at 10 hz input frequency. Although such a voltage range is impractical for the steady state motor operation, it may be required during transients in order to produce the large electrical torques necessary for fast speed changes.

2.4 Constant airgap flux control

If the flux is maintained constant in Equation (2-3), the electrical torque varies linearly with the slip speed. While this arrangement requires

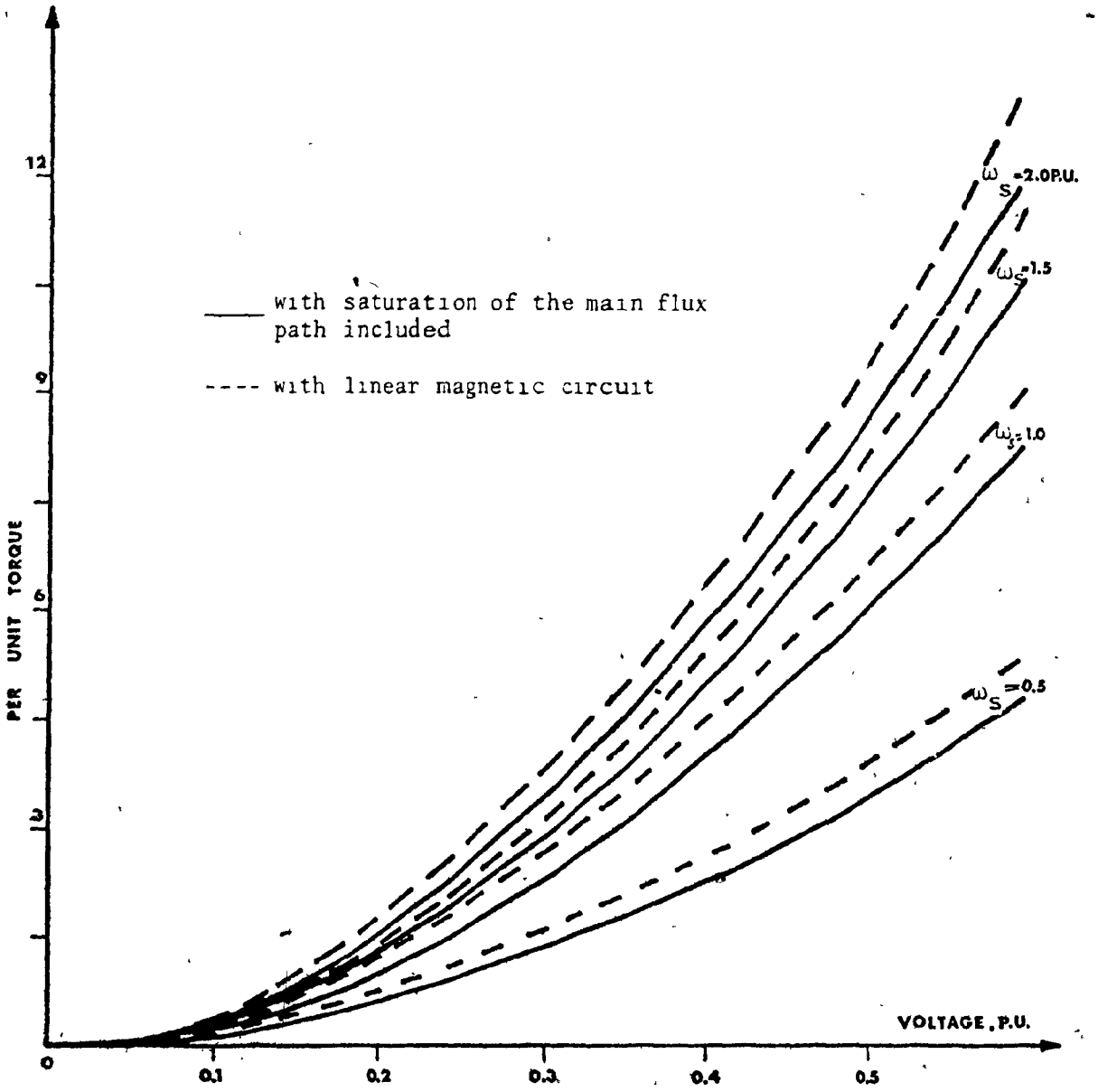

Fig. 2.8b: Static torque-voltage characteristics at 10hz input frequency constant slip speed control

somewhat complex feedback loops for flux measurement, it has many advantages and has been the subject of numerous studies.[27,65,66]

In addition to the linear relationship between the slip speed and torque (which exists for sufficiently small values of the slip speed), the salient characteristics of the constant airgap flux operation are:

1) The positive and negative peak torques are constant and equal over the whole input frequency range. This is a direct consequence of the constant airgap flux operation. The electrical torque is given by:

$$T_e = \frac{R_2 I_r^2}{\omega_s} = 3\,\Phi^2 R_2 \frac{\omega_s}{R_2^2 + (\omega_s L_r)^2} \qquad (2\text{-}5)$$

The last expression has its extrema at:

$$\omega_s = \pm \frac{R_2}{L_r} \qquad (2\text{-}6)$$

This indicates that the torque speed curves are symmetrical with respect to the synchronous speed point. The maximum torque is obtained by substituting the positive value of ω_s from (2-6) into (2-5):

$$T_m = \frac{3\,\Phi^2}{2\,L_r} \qquad (2\text{-}7)$$

With constant flux Φ the last expression is independent of the applied frequency. It is interesting to observe the effect of the rotor leakage inductance on the value of the maximum motor torque.

2) The maximum torques are much larger than those obtained with the constant V/hz control. It was shown[64] that for this particular motor, the respective values at 60 hz are 8.25 P.U. and 3.25 P.U. The difference becomes even greater at lower input frequencies. At 5 hz the values are 8.25 P.U. for the constant flux and 1.46 P.U.

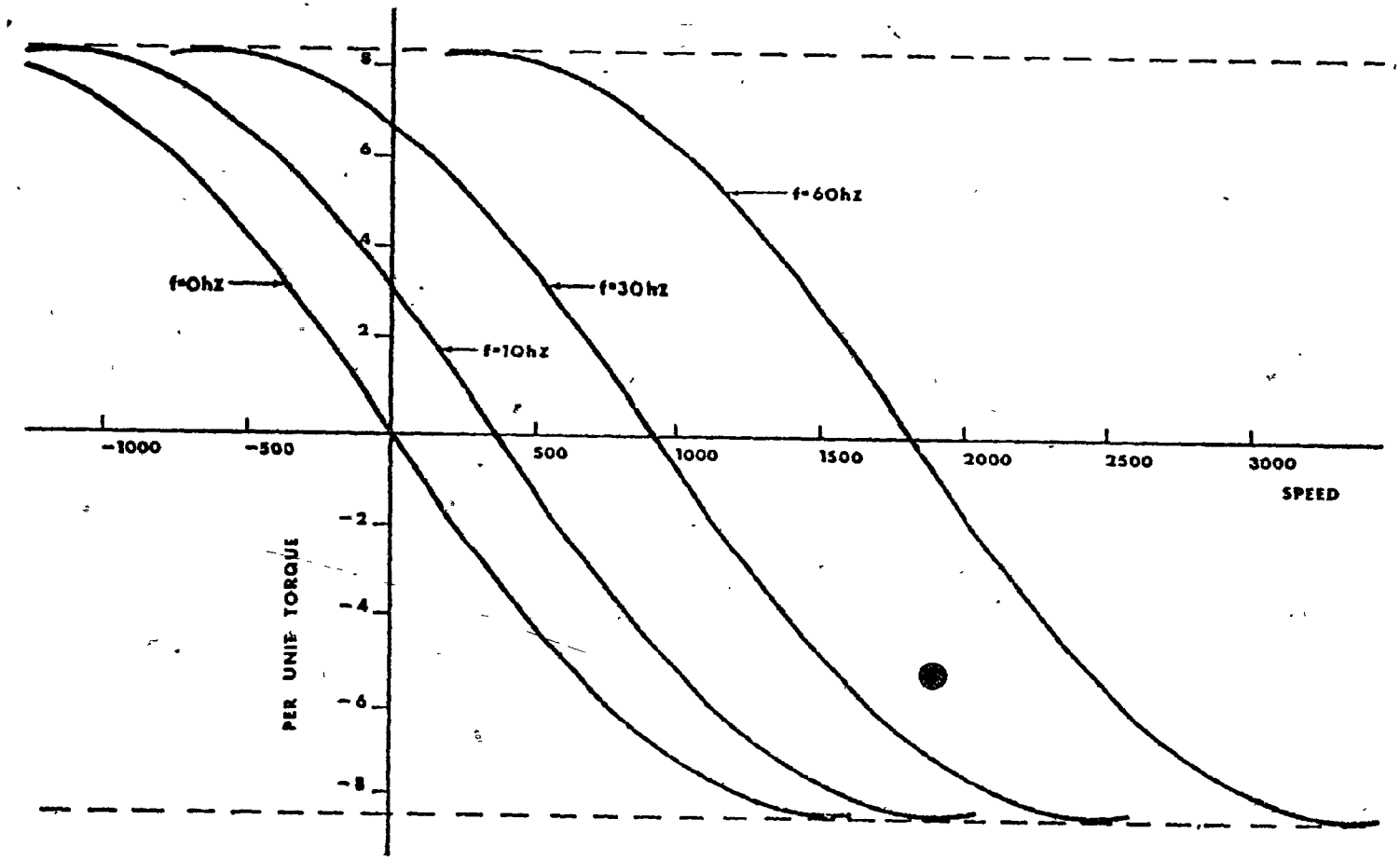

Fig. 2.9: Static torque-speed curves for constant airgap flux control.

for the constant V/hz control. Therefore, the constant flux control can produce much larger starting torques.

3) The slip speed at which the peak torques occur is constant and larger than for the constant V/hz control. For the constant flux operation, the maximum power transfer occurs when

$$S_{max} = \frac{R_r}{L_r}$$

this giving then equation 2-6. For the constant V/hz control, the stator impedance must be included so that

$$S_{max} = \frac{R_2}{\sqrt{R_1^2 + \omega^2 (L_s + L_r)^2}}$$

4) There is no magnetic saturation at lower input frequencies as in the case of constant V/hz operation since the applied voltage is continuously adjusted to maintain the desired flux level.

The torque-speed curves for the constant airgap flux control are presented in Fig. 2.9. The flux level is the same as for the 60 hz synchronous speed operating point. The input voltage must change considerably to keep the flux constant as the load is increased. For example, at 60 hz the voltage reaches 1.75 P.U. at the maximum torque point. If the voltage increase is limited, the demagnetization of the airgap will start as the load is increased and the motor will revert to the operation at a constant stator voltage (Fig. 2.10). The slope of these curves is small because of the high rotor resistance of this particular machine. Squirrel cage motors, generally used in variable frequency drives, will normally have much steeper torque speed curves.

2.5 Summary

The motor static characteristics for three different control strategies were presented. Although these characteristics are not of direct interest

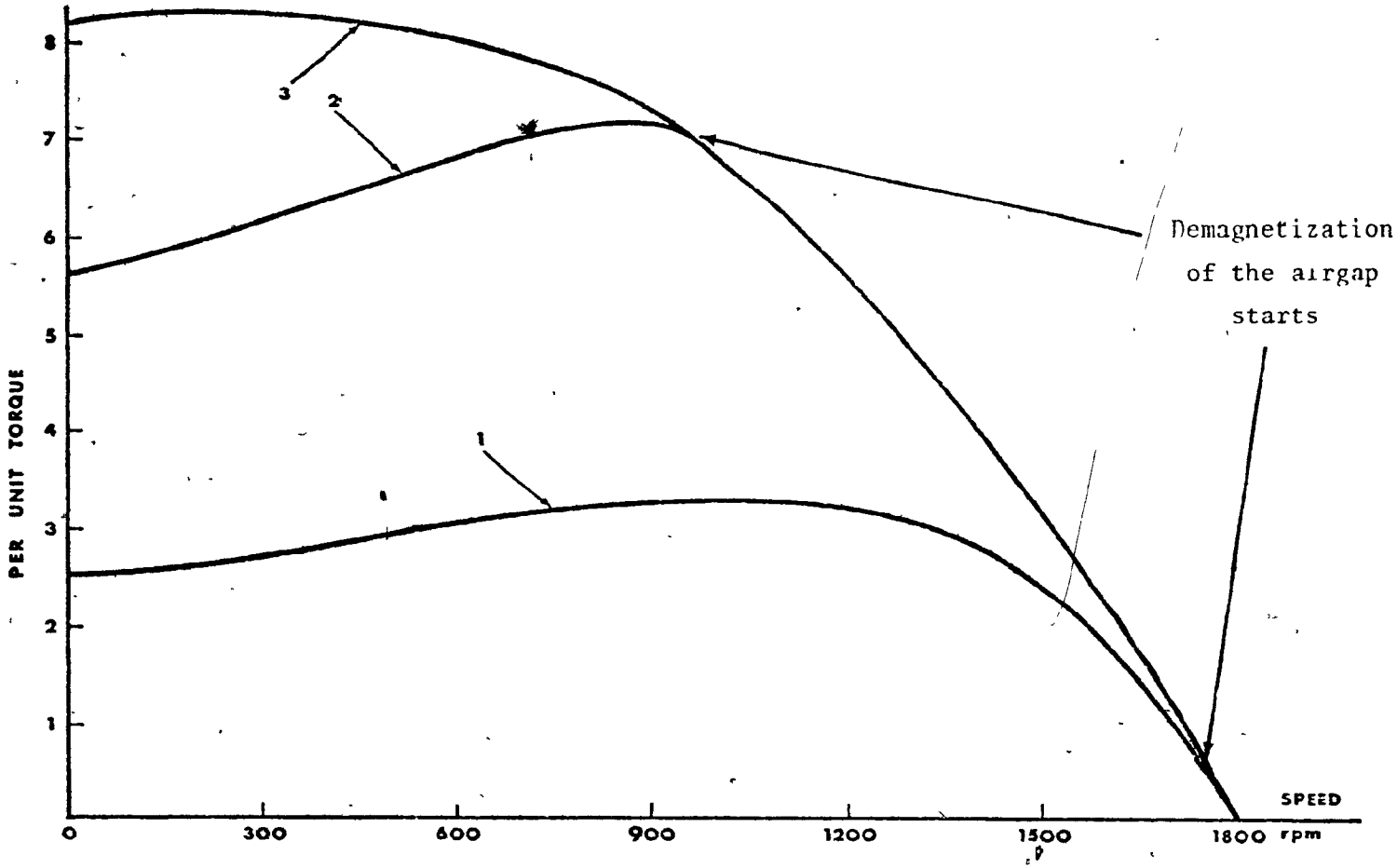

Fig. 2.10: Static torque-speed curves of 60 hz input frequency.

(1) Voltage increase limited to 1.0 P.U.
(2) Voltage increase limited to 1.5 P.U.
(3) Voltage increase is not limited.

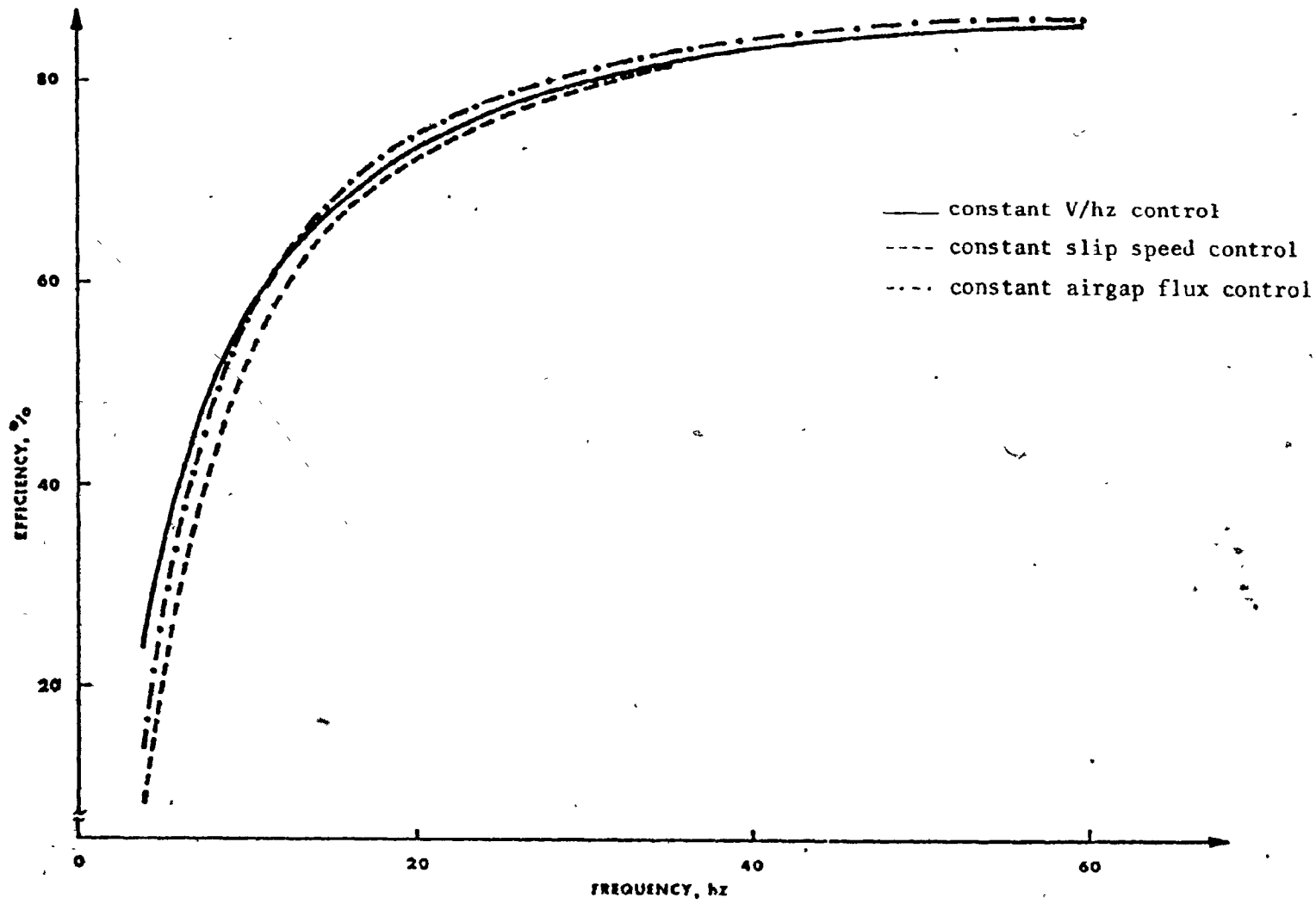

Fig. 2.11: Motor efficiency at rated torque, 60hz sinusoidal input voltage and different control strategies.

in the motor dynamic study, they provide some insight into the motor transient performance. Since for fast speed response large electrical torques are required, the importance of the motor torque capabilities in the dynamic behaviour is obvious. With this criterion in mind, the following conclusion can be made:

1) While the early studies[30,32] of variable frequency induction motors have equated the constant V/hz control with the constant airgap flux operation, these two strategies result in significantly different drive characteristics. The constant V/hz control results in a reduction of the peak motor torques as the input frequency is reduced. This reduction becomes even more pronounced when magnetic saturation is taken into account. Thus, an inferior dynamic performance at the lower input frequencies may be expected.

2) The constant slip speed control is capable of providing large torques at any supply frequency. However, if the selected slip speed is small, these large torques lead to magnetic saturation, and very high magnetizing currents. Thus, the motor static and dynamic operations have contradictory requirements in the choice of the slip speed: it should be small for high steady state efficiency and preferably large for the large torques necessary for fast speed response. A compromise between these two requirements leads to suboptimal motor performance in both the steady state and the transient motor operation.

3) The constant airgap flux control can give large torques while avoiding magnetic saturation. Therefore, this control is potentially superior than any other considered, for both dynamic and steady state motor operation. The main disadvantage is the relatively complex drive configuration necessary for implementing the constant flux strategy. Furthermore, the associated power source must be able to operate over a considerably wider voltage range than in the case of the constant V/hz control.

The efficiency curves for each control strategy and changing supply frequency are presented in Fig. 2.11. The curves were obtained for the rated

motor torque. The values of the airgap flux at 60 hz, synchronous speed and the rated slip speed were used for the corresponding control strategies. Magnetic saturation is included but the motor mechanical losses are neglected. Note that below 4 hz, the motor efficiency becomes meaningless since the rated torque can be obtained only for the negative machine speeds.

These results should be considered only as a guideline since the actual motor efficiency depends largely on the voltage waveforms of the particular power source.

CHAPTER III

DYNAMIC STUDY--METHODS OF ANALYSIS

3.1 Introduction

Before considering the analysis of the motor dynamic performance, one should define the methods which will be used in such a study. This approach offers several advantages:

- A uniform basis is provided for the treatment of all three control strategies presented in the last chapter.
- A justification for a particular method is given only once and does not have to be repeated in the study of each drive structure.
- A single framework is specified so that dynamic characteristics of various drive configurations are easily compared.

For these reasons, this chapter reviews the methods which will be later applied in the study of variable frequency drives.

The machine equations in the synchronous reference frame are first presented. In addition to reducing the number of motor equations, the treatment in this reference frame yields constant, dc, steady state motor currents. Therefore, when the motor equations are linearized, a constant state matrix is obtained so that the linear control theory can be applied to the machine transient analysis.

Both time and frequency domain techniques are briefly reviewed. The presentation of the state space method is included for the sake of completeness. A considerable number of previous studies has proceeded to conclude about the induction motor stability only on the basis of the motor eigenvalue location. This is used, then, as a reminder that the complete convolution integral has to be considered before any statements on the drive transient response can be made.

Since the frequency domain technique proved to be superior in the design of speed controllers for the closed loop drives, various methods for

the transfer function derivation are also reviewed. In addition to the other well-known techniques, a new method for the calculation of the speed-torque transfer function is presented. This method is given in the analytical form, is general, and is applicable to any motor drive described by a set of linearized equations.

3.2 Motor equations

Induction motor equations in the synchronously rotating reference frame are used. These equations are then linearized and written in standard state space form, so that linear control theory can be applied to the motor dynamic study.

3.2.1 Machine reference frames

The transformations from an original, physical, machine system to that described in an arbitrary reference frame is well explained in many textbooks and papers.[2,68,63] Within the standard assumptions of:

- negligible core losses, hysteresis and saturation
- operation with sinusoidal airgap flux,

an electrical machine can be represented in a reference frame, which rotates with the speed of ω_c rad/sec, by these equations:

$$V = \{[R] + n\,\omega_m[G] + \omega_c[F] + [L]_p\}\,i \qquad (3\text{-}1)$$

$$T_L = n\,i^T[G]i - f_T\omega_m - J_T\,p\,\omega_m \qquad (3\text{-}2)$$

In the case of an induction motor, with uniform airgap and ungrounded stator, (3-1) is a 4 x 4 matrix equation, describing a machine electrical system. The machine mechanical part is characterized by (3-2).

For an induction motor the matrices R, L, F and G are:

$$[R] = \begin{bmatrix} R_1 & 0 & 0 & 0 \\ 0 & R_1 & 0 & 0 \\ 0 & 0 & R_2 & 0 \\ 0 & 0 & 0 & R_2 \end{bmatrix} \tag{3-3a}$$

$$[L] = \begin{bmatrix} L_1 & 0 & M & 0 \\ 0 & L_1 & 0 & M \\ M & 0 & L_2 & 0 \\ 0 & M & 0 & L_2 \end{bmatrix} \tag{3-3b}$$

$$[F] = \begin{bmatrix} 0 & -L_1 & 0 & -M \\ L_1 & 0 & M & 0 \\ 0 & -M_1 & 0 & -L_2 \\ M & 0 & L_2 & 0 \end{bmatrix} \tag{3-3c}$$

$$[G] = \begin{bmatrix} 0 & 0 & 0 & 0 \\ 0 & 0 & 0 & 0 \\ 0 & -M & 0 & -L_2 \\ M & 0 & L_2 & 0 \end{bmatrix} \tag{3-3d}$$

where R_1 and R_2 are motor stator and rotor resistances, respectively, M is a magnetizing inductance in the motor equivalent circuit, while L_1 and L_2 are given as:

$$L_1 = M + L_s$$

$$L_2 = M + L_r$$

L_s and L_r being respectively the stator and rotor leakage inductances.

With the stator winding supplied and the rotor short circuited, the voltage vector in (3-1) is:

$$v = \sqrt{\frac{3}{2}} \begin{bmatrix} V_m \cos((\omega - \omega_c)t + \alpha) \\ V_m \sin((\omega - \omega_c)t + \alpha) \\ 0 \\ 0 \end{bmatrix} \qquad (3\text{-}4)$$

where V_m is the peak voltage of each motor phase.

If the speed of the reference frame, ω_c, is chosen to be equal to the radian supply frequency ω, machine representation in the synchronous (γ-δ) reference frame is obtained. Choosing $\alpha = 0$ at $t = 0$ in (3-4) and denoting the rms motor line voltage by V, the steady state voltage vector in the γ-δ frame becomes:

$$V_{\gamma\delta} = \begin{bmatrix} V \\ 0 \\ 0 \\ 0 \end{bmatrix} \qquad (3\text{-}5)$$

The current vector in (3-1) contains stator and rotor currents in the synchronous reference frame:

$$i_{\gamma\delta} \equiv \begin{bmatrix} i^s_\gamma \\ i^s_\delta \\ i^r_\gamma \\ i^r_\delta \end{bmatrix}$$

Representation in the synchronous reference frame offers the following advantages:

1) The motor equations become independent of a rotor position angle θ_m.
2) All steady state voltages and currents become dc. Therefore, when the motor equations are linearized around an operating point, the state matrix [A] in $\dot{x}$ = [A] X + [B] U will be constant.
3) The number of equations is reduced to 5 from the original 8 used in the 3-phase motor representation.

While 3) is desirable, 1) and 2) are indispensable for an efficient computer application to the drive dynamic analysis.

Since shaft speed transients are of the greatest interest in this study, the speed is chosen as the motor output variable, and equation (3-1) becomes nonlinear. Furthermore, a nonlinear mechanical equation (3-2) has to be included for a full description of motor dynamics.

3.2.2 Linearization of motor equations

Before the state space control theory can be applied to the analysis of motor dynamic behaviour, motor equations (3-1) and (3-2) have to be linearized. This is achieved by perturbing the supply frequency and the magnitude of input voltage from their steady state (operating point) values. Such perturbations cause a corresponding change in motor currents, speed and output torque.

The motor variables will be, after perturbation:

	New Variable	=	Steady State	+	Perturbed
Input frequency	ω	=	Ω	+	δ_ω
Motor speed	ω_m	=	Ω_m	+	$\delta\omega_m$
Motor current vector	$i_{\gamma\delta}$	=	$I_{\gamma\delta}$	+	$\delta i_{\gamma\delta}$
Input voltage vector	$v_{\gamma\delta}$	=	$V_{\gamma\delta}$	+	$\delta V_{\gamma\delta}$
Load torque	T_{L1}	=	T_L	+	δT_L
Reference frame speed	ω_c	=	Ω_c		

Note that the speed of the reference frame remains unperturbed and constant.

By substituting expression for the new variables into equations (3-1) and (3-2) one obtains:

$$V_{\gamma\delta} + \delta V_{\gamma\delta} = \{[R] + n\,\Omega_m[G] + \Omega_c[F]\}\, I_{\gamma\delta} +$$

$$+ \{[R] + n\,\Omega_m[G] + \Omega_c[F] + [L]p\}\, \delta i_{\gamma\delta} +$$

$$+ n\,\delta\omega_m[G]\,[I_{\gamma\delta}] + n\,\delta\omega_m[G]\,[\delta i_{\gamma\delta}] \qquad (3\text{-}6a)$$

and

$$T_L + \delta T_L = \Omega_m\, f_T + \delta\omega_m\, f_T + J_T\, p\, \delta\omega_m$$

$$+ n[I_{\gamma\delta}]^T[G]\,[I_{\gamma\delta}] + n[I_{\gamma\delta}]^T([G] + [G]^T)[\delta i_{\gamma\delta}] +$$

$$+ n[\delta i_{\gamma\delta}]^T[G]\,[\delta i_{\gamma\delta}] \qquad (3\text{-}6b)$$

Note that $[L]\,p\,[I_{\gamma\delta}] = 0 = J_T\,p\,\Omega_m$ since at an operating point all currents are dc and the speed is constant. If the steady state equation is taken out from (3-6) and if the perturbations are small enough, so that cross products of perturbed variables can be neglected, the motor linearized equations become:

$$\delta V_{\gamma\delta} = \{[R] + n\,\Omega_m[G] + \Omega_c[F] + [L]p\}\,\delta i_{\gamma\delta} + n\,\delta\omega_m[G]\,[I_{\gamma\delta}] \qquad (3\text{-}7a)$$

$$\delta T_L = [I_{\gamma\delta}]^T\{[G] + [G]^T\}\,\delta i_{\gamma\delta} - f_T\,\delta\omega_m - J_T\,p\,\delta\omega_m \qquad (3\text{-}7b)$$

where matrices R, F, G and L are given by equation 3-3.

The voltage vector $[\delta V_{\gamma\delta}]$ requires special attention since the speed of the reference frame, Ω_c, is constant, while the input frequency is perturbed. If corresponding new variables, defined on the last page are inserted into equation (3-4), it becomes:

$$[V_{\gamma\delta}] + [\delta V_{\gamma\delta}] = \begin{bmatrix} (V + \delta V)\cos(\Omega - \Omega_c + \delta\omega)t \\ (V + \delta V)\sin(\Omega - \Omega_c + \delta\omega)t \\ 0 \\ 0 \end{bmatrix}$$

Since $\Omega_c = \Omega$, the perturbed voltage vector is obtained when the steady state solution, given by equation (3-5), is taken out from the last expression. Thus:

$$[\delta V_{\gamma\delta}] = \begin{bmatrix} V(\cos\delta\omega t - 1) + \delta V\cos\delta\omega t \\ V\sin\delta\omega t + \delta V\sin\delta\omega t \\ 0 \\ 0 \end{bmatrix} \qquad (3\text{-}8)$$

If the supply frequency perturbations, $\delta\omega$, are small and of short duration, equation (3-8) can be linearized by approximating:

$$\cos\omega t \cong 1 \; ; \; \sin \delta\omega t \cong \delta\omega t,$$

$$\delta V \sin \delta\omega t \cong \delta V \, \delta\omega t$$

Furthermore, $\delta V \, \delta\omega t \cong 0$ as a second order effect. The perturbed voltage vector thus becomes:

$$[\, \delta V_{\gamma\delta} \,] = \begin{bmatrix} \delta V \\ V\delta\psi \\ 0 \\ 0 \end{bmatrix} \tag{3-9}$$

where $\delta\psi = \delta\omega \, t$. The geometric interpretation of input frequency perturbations is given in Fig. 3.1. At constant supply frequency the input vector V coincides with the γ-axis and only the γ-coil is energized while δ-coil is short circuited, equation (3 - 5). When the applied frequency is perturbed by $\delta\omega$, the vector V departs from γ-axis with the speed of $\delta\omega$ el. rad./sec., while the whole reference frame continues to rotate at constant speed of $\Omega_c = \Omega$ el. rad./sec. Physically it means that any change in the input frequency will result in a change of speed of the rotating electromagnetic field (emf). In the constant speed synchronous reference frame this change can be produced only by another voltage component along the δ-axis--hence, $V \, \delta\psi$ term.

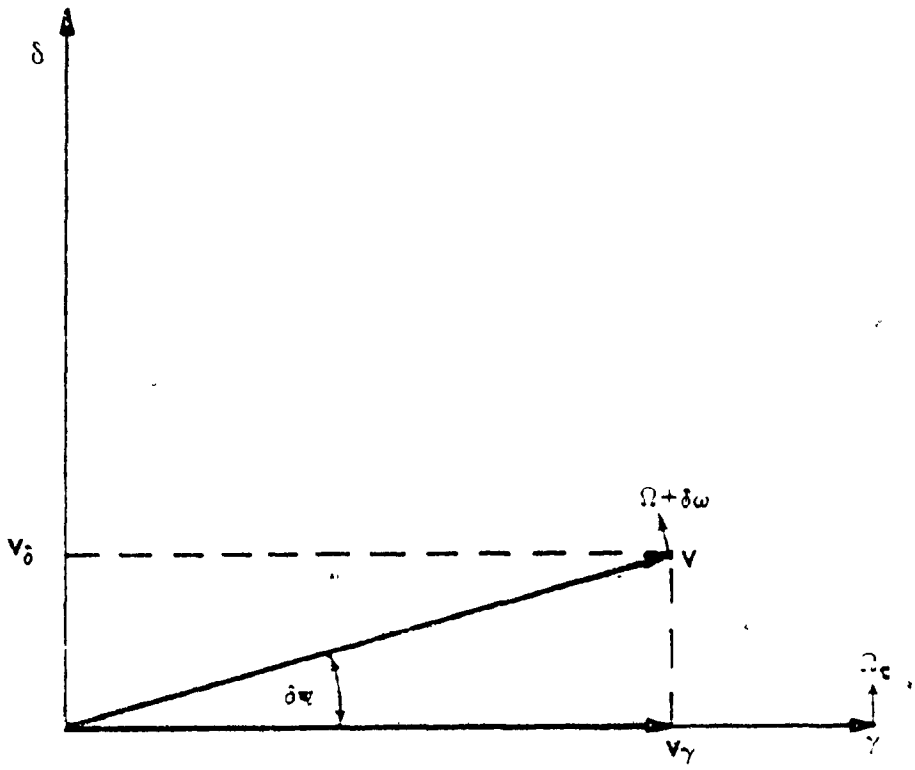

Fig. 3.1 Input frequency perturbation in the synchronously rotating reference frame.

3.2.3 State space equations

The linearized equations (3-7a) and (3-7b) can be written in a compact form as:

$$\begin{bmatrix} L & 0 \\ 0 & J_T \end{bmatrix} p \begin{bmatrix} \delta i_{\gamma\delta} \\ \delta\omega_m \end{bmatrix} = \begin{bmatrix} -(R + n\Omega_m G + \Omega_c F) & nGI_{\gamma\delta} \\ nI_{\gamma\delta}^T (G + G^T) & -f_T \end{bmatrix} \begin{bmatrix} \delta i_{\gamma\delta} \\ \delta\omega_m \end{bmatrix} + \begin{bmatrix} \delta V_{\gamma\delta} \\ -\delta T_L \end{bmatrix} \quad (3\text{-}10)$$

where matrix notation for R, G, L, F, $I_{\gamma\delta}$, $\delta i_{\gamma}\delta$ and $\delta V_{\gamma\delta}$ is understood.

If the motor state vector is defined as

$$X = \begin{bmatrix} x_1 \\ x_2 \\ x_3 \\ x_4 \\ x_5 \end{bmatrix} = \begin{bmatrix} \delta i_\gamma^s \\ \delta i_\delta^s \\ \delta i_\gamma^r \\ \delta i_\delta^r \\ \delta \dot{\omega}_m \end{bmatrix} \tag{3-11a}$$

and the input vector as:

$$U = \begin{bmatrix} \delta V \\ V\delta\psi \\ 0 \\ 0 \\ -\delta T_L \end{bmatrix} \tag{3.11b}$$

the equation (3-10) can be written as

$$P[\dot{X}] = [Q]X + U \tag{3-12}$$

or

$$\dot{X} = [P]^{-1}[Q]X + [P]^{-1}U \tag{3-13}$$

which then identifies the state A and input B matrices in

$$\dot{X} = [A]X + [B]U$$

as

$$[A] = [P]^{-1}Q \tag{3-14a}$$

and

$$[B] = [P]^{-1} \tag{3-14b}$$

Matrix P can be inverted by hand to give:

$$[P]^{-1} = \begin{bmatrix} [L]^{-1} & 0 \\ 0 & 1/J_T \end{bmatrix} \tag{3-15a}$$

where

$$[L]^{-1} = \frac{1}{L_1L_2 - M} \begin{bmatrix} L_2 & 0 & -M & 0 \\ 0 & L_2 & 0 & -M \\ -M & 0 & L_1 & 0 \\ 0 & -M & 0 & L_1 \end{bmatrix} \tag{3-15b}$$

while matrix Q is given by:

$$[Q] = \begin{bmatrix} -R_1 & \Omega_c L_1 & 0 & \Omega_c M & 0 \\ -\Omega_c L_1 & -R_1 & -\Omega_c M & 0 & 0 \\ 0 & \Omega_s M & -R_2 & \Omega_s L_2 & -n(MI_2 + L_2I_4) \\ -\Omega_s M & 0 & -\Omega_s L_2 & -R_2 & n(MI_1 + L_2I_3) \\ -nMI_4 & nMI_3 & nMI_2 & -nMI_1 & -f_T \end{bmatrix} \tag{3-16a}$$

where motor slip speed is $\Omega_s = \Omega_c - n\Omega_m$ in el. rad./sec. while the vector of the steady state motor currents is:

$$I_{\gamma\delta} = \begin{bmatrix} I_1 \\ I_2 \\ I_3 \\ I_4 \end{bmatrix} \tag{3-16b}$$

When supply frequency and load are specified the motor operating point is defined so that its steady state currents and speed can be computed. Equation (3-12) describes then fully motor dynamics behaviour at that point. The eigenvalues of the state matrix A are the poles of the system and are used to establish motor asymptotic stability. Together with corresponding eigenvectors, they determine the motor response to the perturbation from a point of equilibrium, caused by initial conditions. If a response to any drive input is desired, the input matrix B has to be taken into account.

Since input frequency, slip speed and steady state motor currents all appear in the state matrix A (equation 3-14a), the resulting eigenvalues and eigenvectors (i.e. motor dynamics) will depend on both applied frequency and motor load. As it will be seen later, this dependence complicates the analysis of the induction motor dynamic behaviour.

The methods used in the analysis of local stability are discussed in the next section.

3.3 Methods of analysis

The methods used in the analysis and interpretation of dynamic behaviour of induction motor drives are outlined in this section. In this way, a necessary notation is established and a uniform basis for drive comparison is defined.

The section starts by reviewing some of the basic concepts of the linear control theory. It continues the review by showing that a transient response of an autonomous system, determined by its eigenvalues and eigenvectors, cannot be directly correlated to the system practical stability. In other words results of asymptotic stability alone are not sufficent to provide answers to more practical questions, such as how does a system output track an input reference signal, or, how does it respond to a disturbance.

Since these questions are sometimes better answered by a study of the corresponding transfer functions, the second part of this section presents a short review of techniques for motor transfer function derivation. In addition to well known methods of canonical controllable forms, Laplace

transform of state equations, partial fraction expansion and frequency response of state equations, a new approach to derivation of speed--torque transfer functions is presented. Termed the Direct Method, it permits a better insight into speed--torque interaction for a very large group of electric drives.

3.3.1 Review of the state space techniques

Any linear system can be described by the following set of equations.[71]

$$\dot{X} = [A]X + [B]U \tag{3-17a}$$

$$Y = [C]X + [D]U \tag{3-17b}$$

where U, X and Y are N x 1 input, state and output vectors respectively, A and B are N x N state and input matrices, respectively, C is an output and D an input-output matrix. If these matrices are all time invariant, the system (3-17) is a fixed one.

Since most physical systems (motor drives included) do not have inputs directly coupled to outputs, the matrix D is zero. Then, in order to simplify the following discussion, the states X are chosen as the system outputs Y, so that the redefined system is:

$$\dot{X} = [A]X + [B]U \tag{3-18a}$$

$$Y = [I]X \tag{3-18b}$$

Characteristic values (or eigenvalues) of this system, denoted by $\lambda_1, \lambda_2 \ldots \lambda_N$, are the roots of a characteristic polynomial:

$$\text{DET} \mid \lambda I - A \mid = 0$$

System eigenvectors, m_k^o, are obtained from:

$$[\lambda_k I - A] m_k^o = 0, \qquad k = 1 \ldots N$$

The modal or eigenvector matrix is a matrix having for its columns the corresponding eigenvectors:

$$[M] = [m_1^0\ m_2^0 \ldots m_N^0] = \begin{bmatrix} m_{11} & m_{12} \ldots m_{1N} \\ m_{21} & m_{22} \ldots m_{2N} \\ \ldots\ldots\ldots\ldots \\ m_{N1} & m_{N2} \ldots m_{NN} \end{bmatrix} \tag{3-19}$$

The system described by (3-18) is asymptotically stable if every one of its eigenvalues has a negative real part. This implies that all states will return to their respective points of equilibrium, defined by $\dot{X} = 0$, after the system has been perturbed instantenously and then left free. This can be best understood if the state equations become decoupled: Define a new state variable vector q as:

$$X = [M]q \qquad \text{and} \qquad q = [M]^{-1}X \tag{3-20}$$

Substituting (3-20) into (3-18a) and premultuplying by M^{-1}, system uncoupled equations in the space of q states are obtained:[72]

$$\dot{q} = [M]^{-1}[A][M]q + [M][B]^{-1}U \tag{3-21a}$$

$$Y = [M]q \tag{3-21b}$$

The first matrix equation can be written as:

$$\dot{q} = [\Lambda]q + [H]U \tag{3-22a}$$

where $[\Lambda]$ is a Jordan matrix and $[H]$ is the input-mode coupling matrix. Assuming distinct eigenvalues, the last equation can be presented in the expanded form:

$$\begin{bmatrix} \dot{q}_1 \\ \dot{q}_2 \\ \vdots \\ \dot{q}_N \end{bmatrix} = \begin{bmatrix} \lambda_1 & 0 & 0 & \cdots & 0 \\ 0 & \lambda_2 & 0 & \cdots & 0 \\ \vdots & \vdots & \vdots & \vdots & \vdots \\ 0 & 0 & 0 & \cdots & \lambda_N \end{bmatrix} \begin{bmatrix} q_1 \\ q_2 \\ \vdots \\ q_N \end{bmatrix} + \begin{bmatrix} h_{11} & h_{12} & \cdots & h_{1N} \\ h_{21} & h_{22} & \cdots & h_{2N} \\ \vdots & \vdots & \vdots & \vdots \\ h_{N_1} & h_{N_2} & \cdots & h_{NN} \end{bmatrix} \begin{bmatrix} U_1 \\ U_2 \\ \vdots \\ U_N \end{bmatrix} \qquad (3\text{-}22b)$$

The response of each q_k state to initial condition is:

$$q_k(t) = q_k(0)e^{\lambda_k t} = q_k(0)e^{a_k t}(\cos b_k t + j \sin b_k t) \qquad (3\text{-}23)$$

where:

$$\lambda_k = a_k + jb_k$$

Term $e^{\lambda_k t}$ is called a mode of a system,[72] while $q_k(t)$ is its modal state.* In the space of q variables, response of each state $q_k(t)$ is decoupled from responses of the remaining states. Obviously, for $a_k < 0$ the k-th mode approaches zero as $t \to \infty$, and the response of k-th modal state, $q_k(t)$, is asymptotically stable.

When input signals are applied to the system (3-22) the forced response of each modal state, with zero initial conditions and $t_o = 0$, is given by a convolution integral:

$$q_k(t) = \int_0^t e^{\lambda_k (t-\tau)} \sum_{j=1}^{N} h_{kj} U_j(\tau) d\tau, \qquad k = 1 \ldots N \qquad (3\text{-}24)$$

where h_{kj} is the corresponding element of the input-mode coupling matrix H in (3-22). If the system is excited by both initial conditions and its inputs, the modal state response is given by the sum of (3-23) and (3-24).

The system response in the space of the original states is given by (3-20). Or, in scalar form:

---

* Modal state, $q_k(t)$ is sometimes called a canonical state.

$$x_j(t) = \sum_{k=1}^{N} m_{jk} q_k(t) \qquad j=1 \ldots N \qquad (3\text{-}25)$$

Thus, each original state $x_j(t)$ is obtained as a linear combination of all modal states $q_k(t)$ and corresponding eigenvector components. The last equation holds regardless whether modes are excited by initial conditions, by input signals or by both. Normally, in real physical systems the modes are perturbed by input functions and equation (3-24) would apply. The following discussion will be thus limited to this, more general, case.

Although the property of asymptotic stability is a very important one, it satisfies only the first, most basic dynamic requirement, namely that each system mode is stable and that it will return to rest after being perturbed from its equilibrium point. This information is, however, not sufficient to determine the dynamic characteristic of a practical system. For example, not all modes have to be present in the system output. Specifically, a mode will not appear in the output $X_j(t)$ if either of these two conditions is satisfied: [73 75]

1) The mode $e^{\lambda_k t}$ is not excited by any of the system inputs. This means that the corresponding k-th row of the input-mode coupling matrix H has only zero elements (equations 3-22b and 3-24). This is called uncontrollability.

2) The modal state $q_k(t)$ is not coupled to the particular output $x_j(t)$. This means that the corresponding element m_{jk} of the modal matrix M is zero, equation (3-25). Obviously, if the whole k-th column of the matrix M has only zero elements, the k-th modal state (and thus the k-th mode) will not appear in any of the system outputs $x_j(t)$, j = 1 . . . N. This is called unobservability.

Although very important, the definitions of controllability and observability represent more a mathematical than an engineering concept. For example one could have a system which satisfies the observability criterion, but where the coupling of one particular modal state, $q_k(t)$ into the system outputs is much weaker than the coupling of the remaining states. That modal

state will be then practically unobservable in the system response. Similar argument can be made for the concept of controllability. For this reason, and in order to deal with the practical case of motor drives, two new concepts are defined:

1) Pseudo-observability: "Pseudo-observable modes are the modes which appear in the system output, but which can be neglected without noticeably affecting the output response."

2) Pseudo-controllability: "Pseudo-controllable modes are the modes which have sufficiently weak coupling to the input vector U to be considered unexcited when the inputs are applied."

To establish whether a given system has any mode which is either pseudo-observable or pseudo-controllable, one has to look into relative magnitudes of elements on the corresponding row or column in the system input-mode coupling or eigenvector matrices.

The discussion can be now directed towards the induction motor case.

From equation (3.11b), an open loop induction motor drive has three independent inputs:

$$U = \begin{bmatrix} \delta V \\ V\delta\psi \\ 0 \\ 0 \\ \delta T_L \end{bmatrix}$$

Normally, one is interested in finding the drive response when one single input is applied. Inspection of corresponding column in the input-mode coupling matrix H then gives information about the coupling between this input and the drive modes. For example, if the change in the load torque is applied, the excitation of the drive modes will be determined by the elements on the 5-th column of the H matrix, as seen from equation (3-22b). Once the modes are excited they may, but do not have to appear in the drive output. As stated earlier, the stability of a motor drive really means the stability of its speed response. Thus, the speed becomes the only output of interest

and the matrix C in (3-17b) becomes a row vector:

$$y(t) = [C]X(t) = [0\ 0\ 0\ 0\ 1] \begin{bmatrix} x_1 \\ x_2 \\ x_3 \\ x_4 \\ x_5 \end{bmatrix} \tag{3-26}$$

If every drive state $x_k(t)$ were present in the output $y(t)$, an induction motor would qualify as an observable system since all its eigenvalues are distinct and, thus, its modal matrix M is nonsingular. However, with the speed as the only output, it is sufficient to have a single zero element on the 5-th row in the M matrix (i.e. $m_{5k} = 0$) to have a corresponding modal state, $q_k(t)$ suppressed

The terms "controllable" and "observable" mean usually desirable system properties in the context of the state space techniques. The same properties may be, under some conditions, undesirable in the case of an induction motor. Consider, for example, the load torque. Ideally, it will not be coupled to any of the modes, so that the drive is not sensitive to the load variations. As well, it is desirable that none of more oscillatory modes is strongly present in the speed response.

At this point a brief recapitulation can be made:

1) The dynamic behaviour of an induction motor drive cannot be studied by looking at its eigenvalues and eigenvectors only. The whole system, together with its inputs has to be considered.

2) The input-mode coupling matrix [H] is crucial in finding the effects of a given input on each motor mode. Specifically, elements of a j-th column in the matrix [H] determine how much will the corresponding input $u_j(t)$ excite each of the modes.

3) The elements on the 5-th row in the modal matrix M determine the participation of each modal state $q_k(t)$ (and thus of each mode $e^{\lambda_k t}$) in the motor speed response.

With this discussion, the framework for the drive analysis in the time domain is defined. The speed response to the known input function can be obtained in two steps:

1) Compute the excitation of each modal state, using equation (3-24).

2) Write the speed response as the linear combination of modal states, using equations (3-25) and (3-26).

3.3.2 Review of the transfer function methods

Several steps have to be performed in the study of the motor linearized equations, before the motor dynamic characteristics for any particular control strategy can be firmly stated. Roughly, the study can be broken into three main steps:

1) Design of the drive controller for a given control strategy, with some specified performance as the objective.

2) Theoretical analysis and prediction of the dynamic behaviour of the drive so obtained.

3) Verification of theoretical results by an experiment.

The second step, theoretical analysis, is straight forward when the state space techniques, presented in the last subsection, are used. The first and third step need some discussion.

The first step, design of a drive controller could be performed equally well in the time domain, using the state feedback method.[76] (Briefly, the method consists of restructuring the state matrix to obtain the desired eigenvalue location). Since the rotor currents are not available for measurements, state estimators would have to be used.[78] Although it is mathematically very elegant, this method is not the most suitable one for this problem. Its shortcomings have been discussed in some detail recently.[70]

For these reasons, the frequency domain technique is used in the drive controller design. The method is well known and uses Bode plots, to represent the system open loop transfer functions.

The third step, experimental verification of the theoretical results, is fully discussed in Chapter VI. Since this step was performed in the frequency domain, it would be desirable to have the theoretical results in the same form, for an easy comparison. For this reason, the motor drive analysis (step 2) is done in both time and frequency domains.

The attention is now turned to the derivation of the motor transfer functions. Two expressions are needed: $G_1(s)$ and $G_2(s)$, representing respectively the speed-speed reference and speed-load torque transfer functions:

$$\frac{\delta\omega_m}{\delta V_r} = G_1(s) = \frac{N_V(s)}{D(s)} \tag{3-27}$$

and

$$\frac{\delta\omega_m}{\delta T_L} = G_2(s) = \frac{N_T(s)}{D(s)} \tag{3-28}$$

where, generally

$$N(s) = \sum_{j=1}^{N} b_j s^{N-j} \tag{3-29a}$$

and

$$D(s) = \sum_{k=1}^{N+1} a_{N+1-j}\, s^{j-1} \tag{3-29b}$$

Solutions of $N(s) = 0$ represent transfer function zeros while $D(s) = 0$ gives the system poles (eigenvalues). The transfer function $G_2(s)$ can be regarded as the motor equivalent output impedance, which relates the load torque to the speed. It will be seen that, in the analogy with electrical networks, this impedance can be reduced by closing the speed feedback loop.

There are many ways of finding system transfer functions. Four methods, pertinent to the induction motor drives will be now discussed:

1) Controllable canonical form

This method is general and applicable to any system. The a's and b's coefficients in (3-29) are directly obtainable from the controllable canonical form of the motor state equations.[77,79] However,

as it will be seen later, one can better understand, and thus use, a transfer function represented by a Bode plot, rather than by a polynomial. It is true that once the numerator and denominator coefficients are found from the canonical form, the corresponding Bode plot is obtained easily. However, if only the Bode diagram is desired, there are more direct and more efficient methods to find it than the canonical form.

2) State equations

This method is the most efficient one when the graphical (Bode plot) representation of the transfer function is sufficient. The transfer function poles and zeros are not explicitly calculated. Instead, a frequency response of the system state equations is computed. Consider a linear, time invariant system, represented by a matrix equation:

$$\dot{X} = [A]X + [B]U$$

After applying the Laplace transform, this equation, in the sinusoidally steady state, becomes:

$$j\omega X(j\omega) = [A]X(j\omega) + [B]U(j\omega)$$

or

$$X(j\omega) = [j\omega I - A]^{-1}[B]U(j\omega) \qquad (3\text{-}30)$$

It is easy to write a computer program which evaluates the phase and magnitude of $X(j\omega)$ at each ω and for a given input $u_j(\omega)$ with all other inputs set to zero. These results can be used to obtain a Bode plot for each state x_k. Every Bode plot represents then a frequency response of the transfer function between an output x_k and an input u_j: For induction motor drives x_k becomes x_5 (the speed), while u_j can be either a speed reference or a load torque.

Since this method is straight forward, it will be used in the design of drive speed controllers and as a check of the partial fraction method.

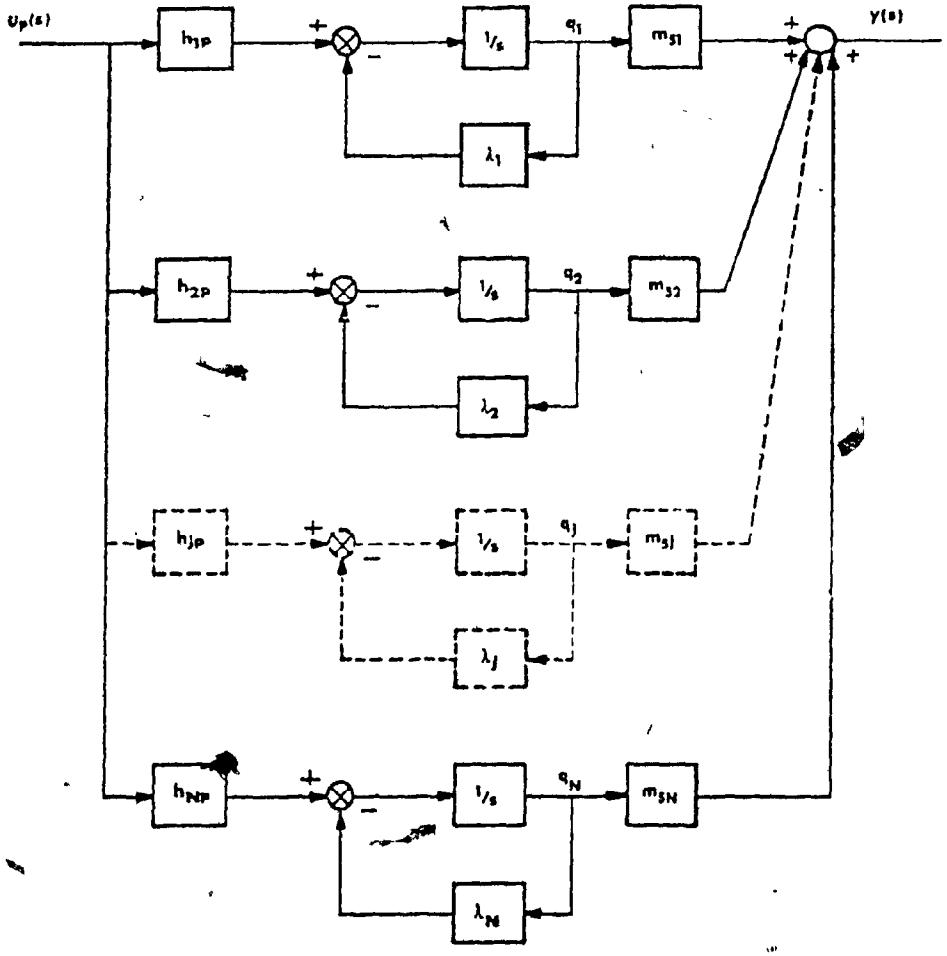

Fig. 3.2: Simulation diagram for partial fraction expansion.

3) Partial fraction expansion [74]

Transfer functions $G_1(s)$ and $G_2(s)$ can be decomposed into terms corresponding to each eigenvalue. This is best illustrated by considering the decoupled state equation (3-22a). Its scalar form, for any modal state $q_k(t)$ is:

$$\dot{q}_k(t) = \lambda_k q_k(t) + \sum_{j=1}^{N} h_{kj} u_j(t) \qquad k = 1 \ldots N$$

When the Laplace transform is applied, with zero initial conditions, this equation becomes:

$$q_k(s) = \frac{\sum_{j=1}^{N} h_{kj} u_j(s)}{s - \lambda_k} \tag{3-31}$$

For motor drives the output speed is given by equations (3-25) and (3-26). Or, in s-domain:

$$y(s) = x_5(s) = \sum_{K=1}^{N} m_{5k} q_k(s)$$

By considering only one input $u_p(s)$ in equation (3-31), with all others set to zero, the desired input-output relationship is obtained:

$$y(s) = \sum_{K=1}^{N} \frac{m_{5k}\, h_{kp}}{s - \lambda_k} u_p(s) \qquad p = 1 \ldots N \tag{3-32}$$

This expression enables the evaluation of the transfer function between the motor speed y and any of the drive inputs u_p. When presented in the form of a simulation diagram, it makes the input-mode-output coupling obvious, Fig. 3.2. This diagram deserves some comments. Elements of the input-mode coupling matrix show how much will each modal state q_k be excited by an input u_p. The 5-th component of each eigenvector, m_{5k}, gives the coupling of each modal state q_k into the motor speed, $y(t) = x_5(t)$. The product between these

two couplings, i.e., $h_{kp} m_{5k}$, divided by the eigenvalue λ_k gives the dc gain of each term in (3-32). The total speed-input dc gain is the sum of all term gains.

It is clear from Fig. 3.2 why the eigenvectors and input-mode coupling vectors are both so important in evaluating the output response. Note that the equation (3-32) could have been obtained as well by taking the Laplace transform of the convolution integral (equation 3-24).

Since both modal, M, and coupling, H, matrices have to be computed to evaluate the convolution integral (3-24), no additional effort is needed when calcuating the motor transfer functions by equation (3-32). This method will then be used to obtain both $G_1(s)$ and $G_2(s)$ transfer functions at each operating point.

4) Direct Method

Since this is a new method for the calculation of the speed-torque transfer functions, which is not limited to induction motors, and which gives an analytic expression for this transfer function, it will be treated separately.

3.3.3 Direct Method

The Direct Method will be formulated by using two theorems which correspond to open and closed loop machine operation. Since this method is applicable to any rotating electrical machine described by a set of linearized equations, the output-input transfer function is first presented.

Consider a linear system described by equations (3-18). Its transfer function matrix is obtained by performing the Laplace transform on (3-18a) with all initial conditions set to zero:

$$X(s) = [sI - A]^{-1}[B]\,U(s)$$

or

$$X(s) = \frac{\text{Adj}[sI - A]}{\text{Det}[sI - A]}\,[B]\,U(s)$$

Define now matrices C_o and N_o as:

$$[C_o] = Adj[sI - A] \tag{3-34a}$$

$$[N_o] = Adj[sI - A][B] = [C_o][B] \tag{3-34b}$$

The relationship between an input $u_k(s)$ and an output $x_j(s)$ is given then by a corresponding transfer function $T_{jk}(s)$.

$$x_j(s) = T_{jk}(s)u_k(s) \qquad \frac{N_{jk}(s)}{D(s)} \; u_k(s) \tag{3-35}$$

where D(s) is the system characteristic equation given by:

$$D(s) = Det[sI - A]$$

while $N_{jk}(s)$ is the j-th row, k-th column element of the matrix N_o in (3-34b). If C_{jl} is a j-th row, l-th column element of the matrix C_o in (3-34a), the numerator of $T_{jk}(s)$ is:

$$N_{jk}(s) = \sum_{m=1}^{N} C_{jm}(s) \; B_{mk} \tag{3-36}$$

where N is the order of the state matrix A in (3-18a).

From the definition of an adjoint of a matrix, $C_{jm}(s)$ is a minor of j-th row, m-th column of the matrix [sI - A].

While the roots of D(s), which represent the poles of the system, are readily obtained using one of the computer eigenvalue subroutines, roots of $N_{jk}(s)$ are more difficult to compute. In a general case equation (3-36) requires calculation of N determinates of N-1 order to find the corresponding polynomials $C_{jm}(s)$.

Consider now the case of a rotating electrical machine. In most cases, such a machine will be represented in its corresponding reference frame by the following generalized equations:[69]

$$v = \{[R] + n\omega_m[G] + \omega_c[F] + [L]p\}i \tag{3-37a}$$

$$T_L = n i^T[G] i - f_T\omega_m - J_T p\,\omega_m \tag{3-37b}$$

The matrices R, G, F, and L, as well as the column vectors v and i assume different forms, depending on the machine. The number of electrical equations in (3-37a) is 3 for a dc compound machine, 4 for an induction machine, and 5 for a salient rotor synchronous machine.

The reference frame rotates at the radial speed ω_c which is equal to the machine supply frequency. For a dc machine this results in a stationary, d-q reference frame and the term $\omega_c[F]$ in (3-37a) is zero.

When equations (3-37a) and (3-37b) are linearized around an operating point, as described in the subsection 3.2.2, the result is

$$\delta V = \{[R] + n\Omega_m[G] + \Omega_c[F] + [L]p\}\delta i + n[G]I_o\delta\omega_m \tag{3-38a}$$

$$\delta T_L = I_o^T\{[G] + [G]^T\}\delta i - f_T\delta\omega_m - J_T p\delta\omega_m \tag{3-38b}$$

where I_o and Ω_m represent the machine steady state currents and speed, respectively. The speed of the reference frame, Ω_c is unperturbed and is equal to the operating point supply frequency.

It is useful to define at this point the machine decoupled electrical system as the one described by (3-38a) with the rotor speed constant, i.e., $\delta\omega_m=0$.

The last equation can be written now with all state derivations on one side:

$$\begin{bmatrix} L & 0 \\ 0 & J_T \end{bmatrix} p \begin{bmatrix} \delta i \\ \delta\omega_m \end{bmatrix} = \begin{bmatrix} -R-n\Omega_m G-\Omega_c F & -n\,G\,I_o \\ nI_o^T\{G+G^T\} & -f_T \end{bmatrix} \begin{bmatrix} \delta i \\ \delta\omega_m \end{bmatrix} + \begin{bmatrix} \delta V \\ -\delta T_L \end{bmatrix} \tag{3-39}$$

Since speed and torque will appear always on the same, k-th row in the machine equations, the speed-transfer function is, from (3-35):

$$\frac{\delta\omega_m}{\delta T_L} = \frac{x_k(s)}{u_k(s)} = \frac{N_{kk}(s)}{D(s)} \qquad (3\text{-}40)$$

where D(s) is the system characteristic equation, while $N_{kk}(s)$ is given by (3-36).

The Direct Method, as applied to the open and closed loop operation is now formulated.

Open loop

The relationship between speed ω_m and torque T_L is given by the following theorem.

Theorem 1: The speed-torque transfer function $G_2(s)$ of any rotating machine, which is operating in open loop and which is described by a set of linearized equations, will have N-1 zeros, N being the number of machine eigenvalues. Furthermore, all zeros of $G_2(s)$ will be identical with the eigenvalues of the machine decoupled electrical system.

Proof: The open loop machine is fully described by (3-39), which can be written in a compact form as:

$$[P_1]\dot{X} = [Q_1]X + U \qquad (3.41a)$$

thus defining the state (A) and input (B) matrices in (3-18) as:

$$[A] = [P_1]^{-1}[Q_1]$$

and (3.41b)

$$[B] = [P_1]^{-1}$$

where

$$[P_1]^{-1} = \begin{bmatrix} [L]^{-1} & 0 \\ 0 & 1/J_T \end{bmatrix} \tag{3-42}$$

The speed torque transfer function is given by (3-40) Note that for the open-loop system k = N. From 3-36 and 3-41 the transfer function numerator, $N_{kk}(s)$, is:

$$N_{kk}(s) = \sum_{j=1}^{N} C_{kj}(s) B_{jk} = \sum_{j=1}^{N} C_{kj}(s) P_{1jk}^{-1}$$

However, from (3-42) all elements on the k-th column in $[P_1]^{-1}$ are zero except k-th one, which is equal to $1/J_T$. Thus, the numerator is:

$$N_{kk}(s) = C_{kk}(s)/J_T \tag{3-43}$$

where $C_{kk}(s)$ represents the k-th row k-th column element of the matrix C_o. From equations (3-34a) and (3-41) this matrix is

$$[C_o] = \text{Adj}\,[sI - P_1^{-1} Q_1] \tag{3-44}$$

The zeros of the speed-torque transfer function $T_{kk}(s)$ are the roots of

$$N_{kk}(s) = C_{kk}(s)/J_T = 0$$

From the definition of an adjoint of a matrix, $C_{kk}(s)$ is the minor, M_{kk}, of the k-th row, k-th column element of the $(sI - P_1^{-1}Q_1)$ matrix.

This matrix is given by

$$[sI - P_1^{-1} Q_1] = \begin{bmatrix} sI + [L]^{-1}\{[R] + n\Omega_m [G] + \Omega_c [F]\} & [L]^{-1} n [G] I_o \\ -I_o^T \{[G] + [G]^T\} n/J_T & s + f_T/J_T \end{bmatrix} \tag{3-46}$$

Thus, the k-th row, k-th column element is $s + f_T/J_T$.

To find the minor $M_{kk}=C_{kk}(s)$ one has to delete k-th row and k-th column in (3-46) and then to find the determinant of so obtained matrix:

$$C_{kk}(s) = \text{Det}[sI + [L]^{-1}]([R] + n\Omega_m[G] + \Omega_c[F]\} \tag{3-47}$$

Since this determinant represents the characteristic equation of the machine decoupled electrical system, the roots of $C_{kk}(s)=0$ are the eigenvalues (poles) of that system. From (3-40), (3-43) and (3-47) the speed-torque transfer function of an open loop electrical machine is:

$$\frac{\delta\omega_m}{\delta T_L} = G_2(s) = \frac{\prod_{j=1}^{N-1}(s-z_j)}{J_T \prod_{j=1}^{N}(s-\lambda_j)} \tag{3-48}$$

where z_j's are the eigenvalues of the machine decoupled electrical system, while λ_j's are the poles of the total system, described by (3-39).

Q.E.D.

Discussion

1) Theorem-1 is equally valid for motors and generators. For motors, equation (3-48) gives the machine equivalent output impedance. For generators, (3-48) represents the input impedance which will an external device, such as a diesel engine, encounter while maintaining the generator speed.

2) If the machine is operating in an open loop, the coupling between its electrical and mechanical parts becomes usually very weak. This means that the electrical eigenvalues are little affected when the mechanical equation is added.[42] Because of this, the N-1 values of z_j's are almost identical with the first N-1 values of λ_j's in (3-48).

Consequently, pole-zero cancellation occurs, so that the speed-torque transfer function is reduced to first order and can be approximated by:

$$G_2(s) \cong \frac{1}{J_T(s-\lambda_m)} \tag{3-49}$$

where λ_m is the mechanical, non-cancelled, eigenvalue of the complete system (3-39).

It is instructive to find λ_m using an approximate, analytical method. The machine mechanical system, with positive signs for motor operation is described by:

$$\delta T_L = \delta T_e - f_T \delta\omega_m - J_T p \delta\omega_m$$

Performing Laplace transform with all initial conditions set to zero and introducing $\delta T = \delta T_e - \delta T_L$ the last equation gives:

$$\lambda_m = s = \frac{1}{J_T}\left(\frac{\delta T}{\delta\omega_m} - f_T\right) \tag{3-50}$$

Since for most load characteristics

$$\frac{\delta T_e}{\delta\omega_m} \gg \frac{\delta T_L}{\delta\omega_m}$$

it follows that:

$$\rho = \delta T/\delta\omega_m \cong \delta T_c/\delta\omega_m$$

This means that ρ can be approximated with the slope of the machine torque-speed curve at the operating point. If friction f_T in (3-50) is neglected the speed-torque transfer function becomes:

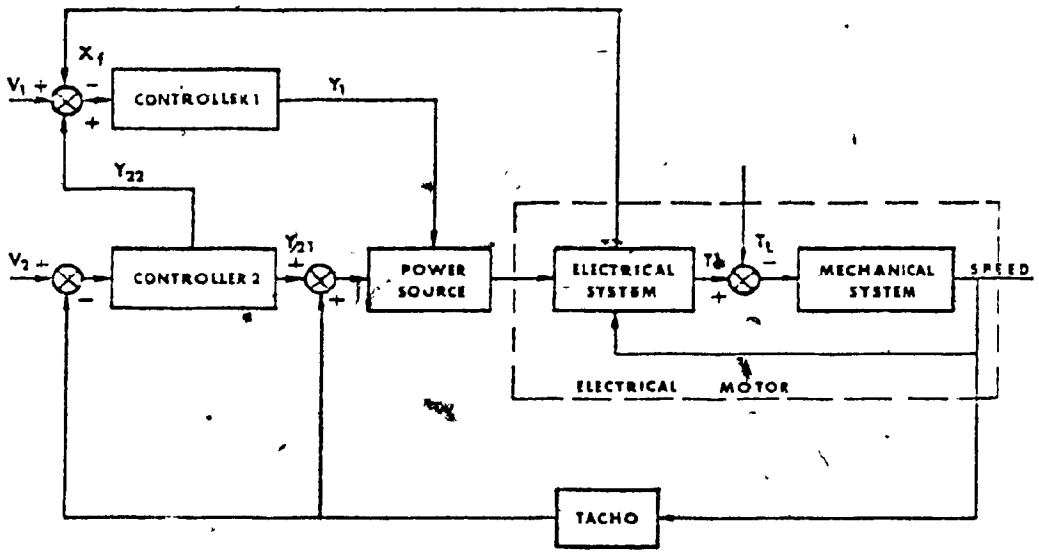

Fig. 3.3: Closed loop, multifeedback drive.

$$G_2(s) = \frac{1}{(J_T s - \rho)} \qquad (3\text{-}51)$$

An increase in the static slope results in a lower motor output impedance $G_2(s)$ and, therefore, makes speed less sensitive to the load variations--a well known fact. The increase in the total inertia produces the same effect by reducing the break frequency of the mechanical eigenvalue, λ_m. In giving dynamic interpretations to equation (3-51) one should, however, keep in mind the approximations under which this equation was obtained

Closed loop

Consider a general, multifeedback motor drive, represented in Fig. 3.3.

In this drive, the output vector Y_1 of controller 1 can depend on any number of drive variables, input references V_1 and V_2 or their combination. Typically, the feedback vector x_f can contain motor currents, airgap flux, torque, voltages, temperature, or any other controlled motor variable except the speed. The input reference vector, V_1, specifies the desired values for all states contained in the feedback vector x_f.

The outputs Y_{21} and Y_{22} of controller 2 contain speed and speed reference, V_2.

In this way, there is no restriction on the number of controlled variables in this drive structure (Fig. 3.3).

The following two definitions are now needed:

Definition 1: A speed controller is the controller which has the outputs dependent on motor speed and speed reference.

Controller 2 is obviously the speed controller for the drive presented in Fig. 3.2.

Definition 2: The drive reduced system is obtained by removing the speed controller and the motor mechanical system from the drive structure.

Most power sources have time constants which are much shorter than those of rotating machines. Therefore, the power source in Fig. 3.3 will be represented by a simple gain, K_s.

Denote by N_1 and N_2 the number of eigenvalues in the drive reduced system and speed controller, respectively. Then, if both controllers are linear and time invariant, the speed-load relationship is given by the following theorem:

Theorem 2: The speed-torque transfer function of any closed loop electric drive, described by a set of linearized equations and having N eigenvalues, will have N-1 zeros. N_1 of these zeros will be the eigenvalues of the drive reduced system, while the remaining N_2 will be the eigenvalues of the drive speed controller.

The proof of this theorem is given in Appendix B. As a consequence of this theorem and from the results in Appendix B the speed-torque transfer function of a closed loop drive can be written as:

$$G_2(s) = \frac{\prod_{j=1}^{N_1}(s-z_j)\prod_{i=1}^{N_2}(s-z_i)}{J_T\prod_{k=1}^{N}(s-\lambda_k)} \qquad (3\text{-}52)$$

where z_j's and z_i's are respectively the eigenvalues of the reduced system and speed controller, while λ_k's are the eigenvalues of the complete drive. It is obvious that Theorem 1 represents a special case of Theorem 2, when both controllers are removed from the drive structure.

Discussion

1) Within stated linearity constraints, Theorem 2 is applicable to any closed loop motor drive encountered in practice.

   For example, it is valid for the class of multifeedback drives, such as dc drives, which normally have an inner current loop, in addition

to the outer speed loop. Induction motor drives, with directly controlled airgap flux, belong to the same class.

Another group for which the Theorem 2 is valid consists of drives where the motor electrical torque, rather than speed, is the controlled output variable. Note that in this case, the speed controller vanishes from the drive structure so that all transfer function zeros become the eigenvalues of the reduced system (equation 3-52). Representatives of this group are all automotive drives, steel and paper mill coiler drives, etc.

2) Theorem 2 can be directly extended to multimachine groups such as Ward-Leonard or generator-induction motor groups. With closed loops acting on a generator, it can be treated as a combination of controller and a power source. Obviously, in this case its time constants have to be taken into account.

3) The pole-zero cancellation, encountered in open loop drive transfer functions is generally not expected here. The reasons are following: When the speed feedback loop is closed, the electro-mechanical coupling becomes usually much stronger, depending on the location of the eigenvalues of the speed controller. The stronger coupling is necessary, if better speed regulation, associated with closed loop drives, is to be realized. Due to this, the eigenvalues of a reduced system are significantly moved when speed equations are added. Consequently, N_1 zeros and N_1 poles in equation (3-52) associated with a reduced system will differ and will not cancel each other.

If, however, all poles of the speed controller have larger time constants than the eigenvalues of a reduced system, the pole-zero cancellation will take place. Note that in this case the speed response cannot be better than in a corresponding open loop drive.

After this discussion, a brief summary of the Direct Method can be given:

1) It is the general method for finding a speed-torque transfer

function and is independent of motor type, supply frequency, load or drive structure.

2) Its prime merit lies in producing conceptually clear results which give a direct physical insight into speed-load interaction. Since it predicts the form of the transfer function as well as the nature of its zeros, the Method can be useful to the system designer in selecting a drive structure.

3) In addition to this, the Method offers a computationally attractive alternative since the calculation of speed-torque transfer functions is reduced to an eigenvalue problem.

3.4 Summary

In this chapter a uniform basis for the dynamic analysis of induction motors was outlined. Both time and frequency domain techniques were reviewed, since the parallel presentation in both domains gives the best insight into the drive transient behaviour. The frequency techniques are also applied to the design of drive speed controllers.

As a considerable number of studies used only eigenvalues to draw conclusions about the motor dynamic behaviour, it was felt necessary to emphasize the importance of the input-output couplings when the practical motor performance is analyzed.

Two new concepts of pseudo-observability and pseudo-controllability were loosely defined. They are more pertinent to engineering applications than the classical notions of observability and controllability.

While searching for a more convenient model of the induction motor, a new method for the calculation of speed-torque transfer function was discovered. It is applicable to any motor drive, operating in an open or closed loop and described by a set of linearized equations. In transcending the class of induction motors, the method underlines the basic similarity of all rotating machinery.

CHAPTER IV

DYNAMIC STUDY--DRIVE CHARACTERISTICS

4.1 Introduction

Three control strategies were introduced in Chapter II, together with the corresponding static drive characteristics. However, in the study of variable speed drives, the dynamic performance is of much greater interest. Specifically, the following questions have to be answered before the merits of a particular control strategy can be evaluated:

1) Which control of the airgap flux gives the best drive performance in terms of stability and speed of response?

2) Which drive structure is least sensitive to the load variations?

Since for all practical purposes the drive output of interest is its shaft speed, the answers to these questions require the study of the relationship between motor speed and each of the two drive inputs:

- speed reference
- load torque

The methods for such study were outlined in the last chapter.

While one could look into stator and rotor currents and discuss their transient response as well, only the speed is considered in this study. This was done for the following reasons:

1) The speed is the most important output in drive applications. The currents represent only an intermediary between drive inputs and the speed.

2) The dynamic requirements are much more stringent for the speed than for the currents. Although undesirable, an underdamped current response is tolerated. At the same time the speed should not contain any oscillations.

3) Large current surges are prevented by the limiting elements built

into power supplies. Thus, one knows in advance that the current swings will not exceed the preset level. There is no similar device for speed changes.

4) The scope of this study precludes the detailed analysis of both speed and currents.

Although the current response is not computed explicitly, it can be determined qualitatively from the obtained results by remembering that very fast speed response requires large electrical torques and thus large motor currents. This means that the speed rise time can be used to estimate the magnitude of the current swing.

Note, however, that if desired, a complete, exact current response can be obtained from the calculated eigenvalue and eigenvector results, using the same method as for the speed.

Each variable frequency ac drive consists basically of two different segments: one is an induction motor with its electromechanical couplings; the other being a corresponding power source, i.e., an inverter. Each segment has its own characteristics, which, when combined, define the overall drive performance. The problem of drive dynamic behaviour is then decomposed into two parts.

1) The merits of each control strategy are evaluated for a drive connected to an infinite bus, sinusoidal voltage (current) supply. The results so obtained are decoupled from the effect of inverter structures and represent an upper, theoretical limit of drive performance for each control strategy.

2) The limitations imposed by inverter characteristics, tachogenerator noise and motor nonlinearity are examined and results obtained in the first part are reviewed to indicate the capabilities of realistic ac drives.

The study of the first part is given in this chapter, that of the second in Chapter V. In order to study the drive closed loop behaviour, a speed controller is designed for each control strategy. As the drive dynamics depend, in general, on the input frequency, the optimal motor performance is possible

only with an adaptive controller This is, however, ruled out for general drive applications, since the control for variable speed induction motors is already more complex than that of their competitor, the dc machine Consequently, the fixed structure controllers presented in this study are only a compromise between the contradictory requirements at the two ends of the operating frequency range

Once the speed controller is selected and the drive structure is thus determined, the study starts from the corresponding linearized equations. In order to present the material methodically, a few steps in the analysis, common to all drives, are outlined.

STEP 1: For a specific supply frequency and the range of motor loads, calculate the drive eigenvalues. If the operating point is at the rated motor load, in addition to this, compute the drive coupling and modal matrices. (The load changes from 20% to 220% in steps of 40% of the motor rated load).

STEP 2: Calculate motor transfer functions using the results from step 1 for the rated load and equation (3-32).

STEP 3: For the rated load calculate the speed response to the drive unit step inputs using equation (3-24) and (3-25) and display the results graphically. In addition to this, find and display the Bode plots of the drive transfer functions.

These steps will produce enough information to draw conclusions, without uncertainty, about the motor dynamic response at that operating point.

Due to space limitation, only three operating points for each drive are fully analyzed by using these three steps. These points correspond to the motor rated load at 60, 30 and 5 hz input frequency. However, the eigenvalues are computed for a total of seven input frequencies. In addition to this, eigenvalues corresponding to six different loads are also obtained at each input frequency.

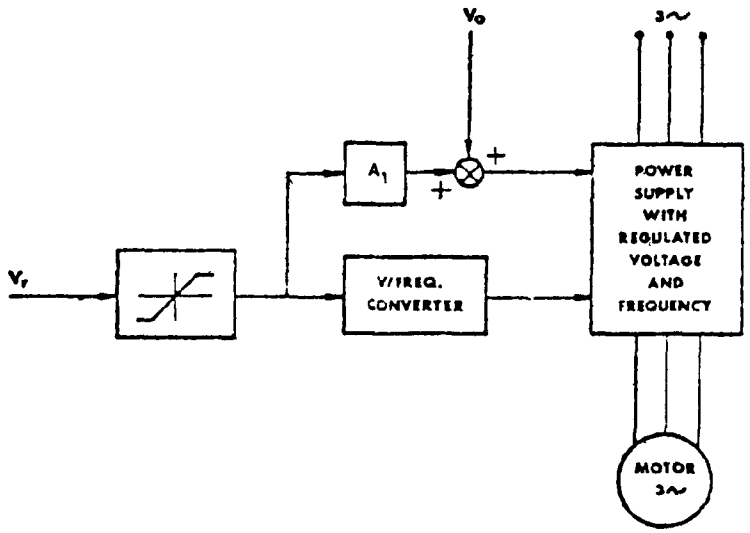

Fig. 4.1: Constant V/hz, open loop drive.

4.2 Constant V/hz control

As described earlier, this control strategy maintains the ratio of the stator voltage and frequency constant during every moment of motor operation (Fig. 2.2).

Since the constant V/hz strategy is most commonly used and since it does not require any speed measurement for its implementation both open and closed loop drives are considered.

4.2.1 Part I. Open loop drive

The constant V/hz control strategy is realized by the motor drive presented in Fig. 4.1.

As was explained earlier, all power supplies and control components are approximated by unity transfer functions. The limiting element confines the motor operation to the stable portion of the speed-torque curve by restricting the value of the motor slip speed. It, thus, yields the optimal accelerating torques during large speed changes.

The drive presented in Fig. 4.1 is fully described at each operating point by the equation (3-10). The state equation is (3-13). The state matrix is given by (3-14a).

Note that for the constant V/hz control the two electrical inputs $u_1 = V$ and $u_2 = V\dot{\psi}$ in (3-11b) are no longer mutually independent, but are related through the equation (2-4). Thus, the input speed reference, V_r, determines both the applied voltage and frequency. The constant V/hz relationship is maintained through the amplifier A_1. From the drive structure, Fig. 4.1, it follows that:

$$\omega = V_r$$

$$V = V_o + A_1 V_r$$

When perturbed these equations give:

$$\delta\omega = \delta V_r$$

$$\delta V = A_1 \delta V_r$$

However, since for small perturbations:

$$\delta\psi = \delta\omega\, t$$

where $\delta\psi$ is defined in Fig. 3.1, it follows that:

$$\delta\psi = \delta V_r\, t$$

combining these equations with the equation (3-11b) one obtains the drive inputs for constant V/hz control

$$u_1(t) = \delta V = A\, \delta V_r \qquad (4\text{-}1a)$$

$$u_2(t) = V\delta\psi = V\, \delta V_r\, t \qquad (4\text{-}1b)$$

where V is the steady state value of the stator line voltage.

Drive Analysis

With the drive structure and corresponding equations specified, the analysis of each operating point can proceed using the three steps outlined in the last section. Results for all three operating points (60, 30 and 5 hz) will be given simultaneously at each step.

STEP 1: Eigenvalues, eigenvectors and input-mode coupling matrix

The results are given in Tables 4.1, 4.2 and 4.3 while the eigenvalue loci for changing supply frequency and changing load are presented in Fig. 4.2. The effect of the change in load (from 20% to 220% of the rated

TABLE 4.1

MOTOR DRIVE WITH CONSTANT V/HZ CONTROL,OPEN LOOP

OPERATING POINT VALUES:	FREQUENCY(HZ)	VOLTAGE(VOLTS)	SPEED(RPM)	TORQUE(NM)
	60.00	127.0	1700.0	17.42

OPERATING POINT CURRENTS:		E-VALUES,REAL	E-VALUES,IMAG.	BREAK FREQUENCY(HZ)	DAMPING
STATOR 1 15.61	1	-36.72	0.00	5.84	1.00
STATOR 2 -9.85	2	-153.34	-73.40	27.06	..90
ROTOR 1 -15.96	3	-153.34	73.40	27.06	0.90
ROTOR 2 1.72	4	-92.24	-328.19	54.26	0.27
	5	-92.24	328.19	54.26	..27

ZEROS OF SPEED-TORQUE TRANSFER F-TION BY DIRECT METHOD:	ZEROS,REAL	ZEROS,IMAG.	BREAK FREQUENCY(HZ)	DAMPING
1	-89.91	-329.67	54.38	..26
2	-89.91	329.67	54.38	0.26
3	-174.01	-68.26	29.75	0.93
4	-174.01	68.26	29.75	..93

E-VECTORS IN POLAR COORDINATES:

E-VECTOR 1	E-VECTOR 2	E-VECTOR 3	E-VECTOR 4	E-VECTOR 5
0.9695E 0C 0.0000E 00	0.7691E 00 -0.7127E 02	0.7691E 00 0.7127E 02	0.7280E 00 -0.5876E 02	0.7280E 00 0.5876E 02
0.3126E 00 0.1800E 03	0.6660E 00 -0.1743E 03	0.6660E 00 0.1743E 03	0.7006E 00 -0.1490E 03	0.7C.6E C0 0.149.E 03
0.9946E 0v 0.1800E 03	0.7860E 0C 0.1079E 03	0.7860E 00 -0.1079E 03	0.7126E 00 0.1196E 03	0.7126E 00 -0.1196E 03
0.3392E 00 0.0000E 00	0.6849E 00 0.4630E 01	0.6849E 00 -0.4630E 01	0.6845E 00 0.2922E 02	0.6845E 00 -0.2922E 02
0.570CE 00 0.1800E 03	0.9762E-01 0.8200E 02	0.9762E-01 -0.8200E 02	0.4268E-01 0.5305E 02	0.4268E-01 -0.5305E 02

INPUT-MODE COUPLING MATRIX IN POLAR COORDINATES:

0.9938E C1 0.1800E 03	0.5769E 01 -0.1161E-10	0.7637E 02 -0.8806E-14	0.1893E 02 0.3798E-11	0.4373E 02 -0.1800E 03
0.1087E 03 0.1617E 03	0.1029E 03 -0.9516E 02	0.2498E 03 -0.8901E 02	0.2084E 03 -0.1069E 02	0.3126E C2 0.6027E 02
0.1087E 03 -0.1617E 03	0.1029E 03 0.9516E 02	0.2498E 03 0.8901E 02	0.2084E 03 0.1069E 02	0.3126E 02 -0.6027E 02
0.1946E C3 0.2701E 02	0.1954E 03 C.1173E 03	0.6345E 02 0.1040E 03	0.6081E 02 -0.1657E 03	0.4042E 01 -0.1563E 03
0.1946E 03 -0.2701E 02	0.1954E 03 -0.1173E 03	0.6345E 02 -0.1040E 03	0.6081E 02 0.1657E 03	0.4042E 01 0.1563E 03

TABLE 4.2

MOTOR DRIVE WITH CONSTANT V/HZ CONTROL.OPEN LOOP

OPERATING POINT VALUES:	FREQUENCY(HZ)	VOLTAGE(VOLTS)	SPEED(RPM)	TORQUE(NM)
	30.00	66.5	800.0	17.95

OPERATING POINT CURRENTS:		E-VALUES.REAL	E-VALUES.IMAG.	BREAK FREQUENCY(HZ)	DAMPING
STATOR 1 16.03	1	-33.51	0.00	5.33	1.00
STATOR 2 -9.70	2	-27.08	-127.06	20.68	0.21
ROTOR 1 -16.23	3	-27.08	127.06	20.68	0.21
ROTOR 2 1.44	4	-220.10	-86.98	37.67	0.93
	5	-220.10	86.98	37.67	0.93

ZEROS OF SPEED-TORQUE TRANSFER F-TION BY DIRECT METHOD:	ZEROS.REAL	ZEROS.IMAG.	BREAK FREQUENCY(HZ)	DAMPING
1	-232.09	-78.88	39.01	0.95
2	-232.09	78.88	39.01	0.95
3	-31.83	130.55	21.39	0.24
4	31.83	130.55	21.39	0.24

E-VECTORS IN POLAR COORDINATES:

E-VECTOR 1	E-VECTOR 2	E-VECTOR 3	E-VECTOR 4	E-VECTOR 5
0.9727E 00 0.0000E 00	0.7082E 00 -0.1302E 03	0.7082E 00 0.1302E 03	0.8038E 00 -0.1198E 02	0.8038E 00 0.1198E 02
0.3646E 00 0.1800E 03	0.6298E 00 0.1457E 03	0.6298E 00 -0.1457E 03	0.7716E 00 -0.1114E 03	0.7716E 00 0.1114E 03
0.9889E 00 0.1800E 03	0.7114E 00 0.4491E 02	0.7114E 00 -0.4491E 02	0.8094E 00 0.1675E 03	0.8094E 00 -0.1675E 03
0.3458E 00 0.0000E 00	0.6232E 00 -0.3975E 02	0.6232E 00 0.3975E 02	0.7798E 00 0.6786E 02	0.7798E 00 -0.6786E 02
0.8059E 00 0.1800E 03	0.1008E 00 -0.3302E 02	0.1008E 00 0.3302E 02	0.7386E-01 0.1462E 03	0.7386E-01 -0.1462E 03

INPUT-MODE COUPLING MATRIX IN POLAR COORDINATES:

0.1645E 02 -0.1800E 03	0.6421E 01 0.8770E-12	0.5866E 02 0.1008E-12	0.1727E 02 -0.3479E-12	0.3746E 02 -0.1800E 03
0.8603E 02 0.3394E 02	0.9115E 02 0.1224E 03	0.5868E 02 0.6119E 02	0.5109E 02 0.1587E 03	0.1004E 02 0.1589E 03
0.8603E 02 -0.3394E 02	0.9115E 02 -0.1224E 03	0.5868E 02 -0.6119E 02	0.5109E 02 -0.1587E 03	0.1004E 02 -0.1589E 03
0.1870E 03 0.4240E 02	0.1637E 03 0.1326E 03	0.1938E 03 -0.1749E 03	0.1819E 03 -0.9398E 02	0.1780E 02 -0.2119E 02
0.1870E 03 -0.4240E 02	0.1637E 03 -0.1326E 03	0.1938E 03 0.1749E 03	0.1819E 03 0.9398E 02	0.1780E 02 0.2119E 02

TABLE 4.3

MOTOR DRIVE WITH CONSTANT V/HZ CONTROL,OPEN LOOP

OPERATING POINT VALUES:	FREQUENCY(HZ)	VOLTAGE(VOLTS)	SPEED(RPM)	TORQUE(NM)
	5.00	16.0	50.0	21.59

OPERATING POINT CURRENTS:		E-VALUES,REAL	E-VALUES,IMAG.	BREAK FREQUENCY(HZ)	DAMPING
STATOR 1	18.90	1	-19.83	0.00	3.16	1.00
STATOR 2	-8.06	2	-8.17	-26.37	4.39	0.30
ROTOR 1	-17.84	3	-8.17	26.37	4.39	0.30
ROTOR 2	-0.94	4	-245.85	-23.85	39.31	1.00
		5	-245.85	23.85	39.31	1.00

ZEROS OF SPEED-TORQUE TRANSFER F-TION BY DIRECT METHOD:

	ZEROS,REAL	ZEROS,IMAG.	BREAK FREQUENCY(HZ)	DAMPING
1	-259.83	-24.91	41.54	1.00
2	-259.83	24.91	41.54	1.00
3	-4.09	-27.44	4.42	0.15
4	-4.09	27.44	4.42	0.15

E-VECTORS IN POLAR COORDINATES:

E-VECTOR 1	E-VECTOR 2	E-VECTOR 3	E-VECTOR 4	E-VECTOR 5
0.1000E 01 0.1800E 03	0.9971E 00 -0.1653E 00	0.9971E 00 0.1653E 00	0.5509E 00 -0.5588E 02	0.5509E 00 0.5588E 02
0.8748E-02 0.0000E 00	0.3973E 00 -0.1107E 03	0.3973E 00 0.1107E 03	0.4774E 00 -0.1759E 03	0.4774E 00 0.1759E 03
0.9374E 00 0.0000E 00	0.6177E 00 0.1637E 03	0.6177E 00 -0.1637E 03	0.5537E 00 0.1241E 03	0.5537E 00 -0.1241E 03
0.1580E 00 0.1800E 03	0.3848E 00 -0.4220E 01	0.3848E 00 0.4220E 01	0.4814E 00 0.4674E 01	0.4814E 00 -0.4674E 01
0.7643E 00 0.0000E 00	0.5659E 00 -0.1724E 03	0.5659E 00 0.1724E 03	0.5093E-01 0.1125E 03	0.5093E-01 -0.1125E 03

INPUT-MODE COUPLING MATRIX IN POLAR COORDINATES:

0.6639E 02 -0.4193E-13	0.1346E 02 -0.2480E-12	0.2875E 02 0.1800E 03	0.7470E 01 0.1800E 03	0.3551E 02 -0.2515E-13
0.1540E 02 0.3081E 01	0.1184E 02 0.6281E 02	0.6977E 01 -0.6843E 02	0.5020E 01 0.7284E 02	0.5923E 01 0.4.12E 02
0.1540E 02 -0.3081E 01	0.1184E 02 -0.6281E 02	0.6977E 01 0.6843E 02	0.5020E 01 -0.7284E 02	0.5923E 01 -0.4.12E 02
0.2698E 03 0.8658E 02	0.2715E 03 0.1454E 03	0.2652E 03 -0.9545E 02	0.2784E 03 -0.3607E 02	0.2667E 02 0.8164E 02
0.2698E 03 -0.8658E 02	0.2715E 03 -0.1454E 03	0.2652E 03 0.9545E 02	0.2784E 03 0.3607E 02	0.2667E 02 -0.8164E 02

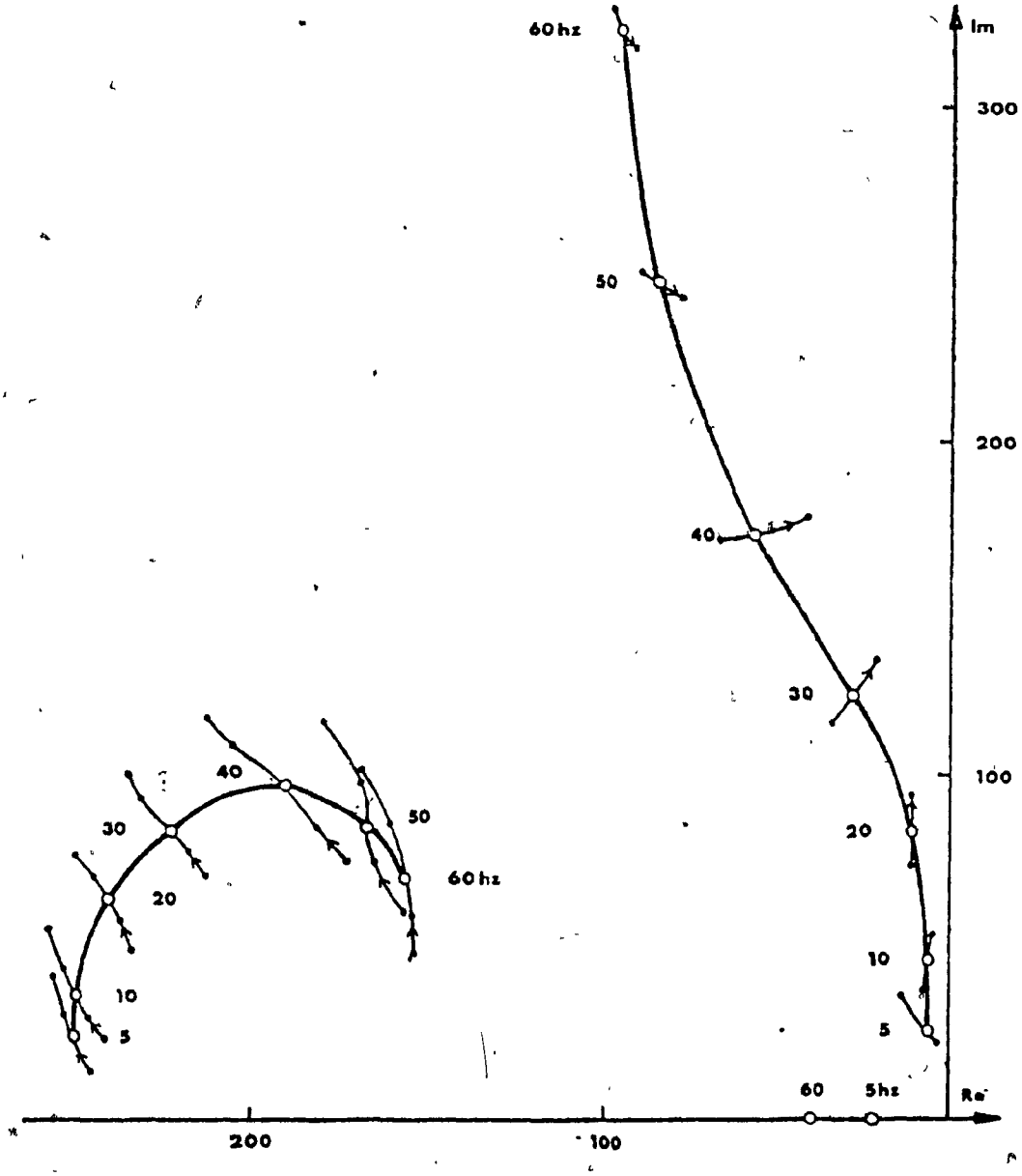

Fig. 4.2: Eigenvalue loci for constant V/hz, open loop drive. The effects of changing load are presented at selected input frequencies.

value) is seen to be small. The motor eigenvalues were previously identified by Ooi and Barton[42] as mechanical (on the real axis and associated with the motor mechanical parameters), magnetizing (complex conjugate, close to the imaginary axis and associated with the motor magnetizing inductance) and leakage (complex conjugate and related to the motor leakage inductance).

From these results, the two leakage modes are well damped. The mechanical mode has a sufficiently small time constant for an acceptable response. However, the two magnetizing modes approach instability as the input frequency is decreased. Note that only the mode response to an initial condition can be analyzed from the eigenvalue results (Fig. 4.2). The excitation of each mode by a particular input is not known nor is the participation of each mode in the output (speed) response. Thus, one has to examine the eigenvectors and the input-mode coupling matrix (Tables 4.1, 4.2 and 4.3).

To illustrate the interpretation of these results, an example is given. Looking at the results for 60 hz operation, one can conclude that the mode corresponding to the real eigenvalue is much less excited by the change in the input voltage than the complex-conjugate modes. (From (4-1a) the input voltage change appears in $u_1(t)$ and one has to look into the first column of the matrix H to find the excitation of each $q_k(t)$--equation (3-24)). The same conclusion about the mode excitation is valid for the change in the supply frequency (input $u_2(t)$ and the second column of the matrix H).

Looking now at the mode-state coupling, one can observe that these highly excited modes, corresponding to the complex conjugate eigenvalues are weakly coupled into the speed, as seen from the 5^{th} row of the eigenvector matrix. Thus one concludes that the input reference V_r (which appears in both $U_1(t)$ and $U_2(t)$) better controls the motor currents (in which the modes $q_k(t)$, $k = 2 - 5$ appear stronger) than the speed itself.

Although this method of analysis is valid and gives a detailed insight into the mechanism of the motor response, it is obviously ill suited for a quantitative study. Still, it is revealing to look into input-mode and mode-state couplings and to understand why the speed response is not oscillatory although some of the eigenvalues are so lightly damped. Thus, the results obtained in this step provide the explanation of the drive response found in step 3.

STEP 2: The drive transfer functions

The two transfer functions of interest are the speed-input reference ($G_1(s)$) and speed-load torque ($G_2(s)$). The latter one represents a drive mechanical output impedance.

When equation (3-32) is applied together with the results of the previous step, $G_1(s)$ and $G_2(s)$ can be obtained at each operating point.

1) Speed-input reference transfer function.

The speed reference signal V_r appears in two drive inputs. When Laplace transform is applied to equations (4-1), these two inputs become:

$$u_1(s) = A_1 V_r(s)$$

$$u_2(s) = \frac{V}{s} V_r(s)$$

From equation (3-32), with these two inputs:

$$Y(s) = \sum_{j=1}^{2} \sum_{k=1}^{5} \frac{m_{5k} h_{kj}}{s-\lambda_k} u_j(s)$$

Replacing $u_1(s)$ and $u_2(s)$ by their expressions and dividing each side by $V_r(s)$

$$\frac{Y(s)}{\delta V_r(s)} = G_1(s) = \sum_{k=1}^{5} \left(\frac{m_{5k} h_{k1}}{s-\lambda_k} A_1 + \frac{m_{52} h_{k2}}{s(s-\lambda_k)} V \right) \qquad (4\text{-}2)$$

Since the four eigenvalues appear in the complex-conjugate pairs, the corresponding eigenvectors (m_{5k}'s) and coupling vectors (h_{kj}'s) appear in the complex conjugate pairs, too. Thus one can write:

$$\lambda_3 = \lambda_2^* \quad ; \quad \lambda_5 = \lambda_4^*$$

$$m_{53} = m_{52}^* \quad ; \quad m_{55} = m_{54}^*$$

$$h_{3j} = h_{2j}^* \quad ; \quad h_{5j} = h_{4j}^* \quad , \quad j = 1, 2$$

Using these equations, (4-2) can be rearranged so that each term denotes a physically realizable system:

$$\frac{y(s)}{\delta V_r(s)} = G_1(s) = \frac{m_{51}h_{11}}{s-\lambda_1} A_1 + \frac{m_{51}h_{12}}{s(s-\lambda_1)} V +$$

$$+ \sum_{\substack{k=2 \\ k\neq 3}}^{4} \frac{2(s\,\mathrm{Re}(m_{5k}\,h_{k1}) - \mathrm{Re}(m_{5k}\,h_{k1}\,\lambda_k^*))}{s(s-\lambda_k)(s-\lambda_k^*)} A_1 +$$

$$+ \sum_{\substack{k=1 \\ k\neq 3}}^{4} \frac{2(s\,\mathrm{Re}(m_{5k}h_{k2}) - \mathrm{Re}(m_{5k}h_{k2}\lambda_k^*)}{s(s-\lambda_k)(s-\lambda_k^*)} V \qquad (4\text{-}3)$$

The last equation gives the speed-input reference transfer function for the open-loop, constant V/hz drive. The presence of an integrator in the second and fourth term in (4-3) reflects the change in the supply frequency. It accounts for the monotonic increase in the mmf phase angle ψ with a fixed change in the speed reference signal V_r. This will be fully discussed in the analysis of the motor step response.

If the numerical values from Table 4.1, 4.2 or 4.3 are inserted into (4-2) or (4-3), the speed-input reference transfer function at the corresponding operating point is obtained. The transfer function Bode plots are presented in Fig. 4.3b, 4.4b and 4.5b. The same results were obtained by applying the Laplace transform to the drive state equations and using equation (3-30).

2) Speed-torque transfer function

From (3-11b), the load torque appears only in the 5th drive input. By straight application of the equation (3-32):

$$y(s) = \sum_{k=1}^{5} \frac{m_{5k}\,h_{k5}}{s-\lambda_k}\, u_5(s)$$

or

$$\frac{y(s)}{\delta T_L(s)} = G_2(s) = \sum_{k=1}^{5} \frac{m_{5k} h_{k5}}{s-\lambda_k} \qquad (4\text{-}4)$$

The last equation gives the speed-torque transfer function which is an equivalent of the drive output impedance.

It is possible to write (4-4) in the physically realizable form, using the same method as for (4-3).

If the results from Table 4.1, 4.2 or 4.3 are inserted into equation (4-4), the drive output impedance is obtained for each corresponding operating point. These results are presented as Bode plots in Fig. 4.6b, 4.7b and 4.8b. Again, the same results were obtained from (3-30) by applying Laplace transform to the drive state equations.

An additional insight into the speed-load interaction is obtained by examining the analytical expression for the output impedance. Applying the Direct Method (Theorem 1) to the drive equations (3-10) one obtains:

$$G_2(s) = \frac{(s-z_1)(s-z_2)(s-z_3)(s-z_4)}{J_T(s-\lambda_1)(s-\lambda_2)(s-\lambda_3)(s-\lambda_4)(s-\lambda_5)} \qquad (4\text{-}5)$$

The zeros of $G_2(s)$, i.e., z_j's, are computed as the eigenvalues of the motor decoupled electrical part and are given in Tables 4.1, 4.2 and 4.3. It is evident from these results that the motor electrical eigenvalues are very little perturbed when the 5^{th}, mechanical equation is added. This indicates weak electromechanical coupling. Note that the same conclusion was made implicitly in Step 1, where it was seen that the changes in input voltage and frequency affect very little the motor speed. Since there will be pole-zero cancellation in (4-5), evident from the computer results in Step 1, $G_2(s)$ can be approximated by the equation (3-51). The validity of this approximation is best perceived from the corresponding Bode plots (Fig. 4.6b, 4.7b and 4.8b).

From the expression for the motor output impedance (4-5) one can easily find the speed steady-state error. If the load step of A units is applied to the shaft while the speed reference V_r is constant, the steady state value of speed will be:

$$y(\infty) = \lim_{s \to 0} s G_2(s) \frac{A}{s}$$

which gives

$$y(\infty) = \frac{z_1 z_2 z_3 z_4}{J_T \lambda_1 \lambda_2 \lambda_3 \lambda_4 \lambda_5} A \qquad (4\text{-}6)$$

with good pole-zero cancellation the last expression becomes:

$$Y(\infty) = \frac{A}{J_T \lambda_5}$$

Using the approximate value of λ_5 given by the equation (3-50):

$$y(\infty) = \frac{A}{\rho - f_T}$$

where ρ is the slope of the static torque-speed curve at the operating point. Since the speed reference V_r has not changed, the last expression denotes the speed error due to the load disturbance. At the same time it shows which factors determine the speed sensitivity to the load changes.

STEP 3: Step and frequency response

The speed response is computed for a unit step change in:

- speed reference, V_r
- load torque, T_L

The results are presented graphically, together with the drive frequency response. The speed step response is calculated in two stages:

First, the response of all modal states q(t) is obtained from the convolution integral, equation (3-24).

Second, modal states, calculated for each input are combined, using

(3-25) and (3-26), to obtain the speed response.

Response to a unit step in the speed reference

The motor load is constant and equal to the rated value. For the step change in V_r, the input $u_1(t)$ follows, while $u_2(t)$ is a ramp (4-1). Thus, the modal states are:

$$q_k(t) = \int_0^t e^{\lambda_k(t-\tau)} h_{k1} A_1 \, d\tau + \int_0^t e^{\lambda_k(t-\tau)} h_{k2} V \tau \, d\tau, \quad k=1 \ldots 5$$

which gives:

$$q_k(t) = \frac{A_1 h_{k1}}{\lambda_k} (e^{\lambda_k t} - 1) + \frac{V h_{k2}}{\lambda^2_k} (e^{\lambda_k t} - \lambda_k t - 1) \qquad (4-7)$$

By using the values for each operating point from Tables 4.1, 4.2 and 4.3, the corresponding step response of each modal state is obtained.

Since the last equation contains a monotonically increasing term, $\lambda_k t$, it is appropriate to discuss it briefly.

The first part in the last expression is due to the step change in the applied stator voltage. Its time varying term will approach zero as the time increases, for all eigenvalues with the negative real part.

The second part of the equation (4-7) is the result of the unit step change in the motor input frequency. Although the input is finite, this part, and therefore all modal states, will increase monotonically with time. Before this response is judged as unstable, one should give it its physical interpretation.

The modal solutions are obtained in the synchronous reference frame which rotates always at the operating point supply frequency. If the motor is in a steady state, the airgap mmf rotates with the same speed and therefore appears to be stationary in this reference frame. Consequently, at the operating point the motor currents appear as dc. As soon as the motor input frequency ω is perturbed, the mmf vector starts to move, sweeping the reference frame (Fig. 3.1). Its projections on the γ and δ axis become time

variant and the motor currents become normally ac. However, since the motor voltages were linearized, the γ and δ axis currents will not be sinusoidal, but will increase linearly with time - the fact reflected by the monotonically increasing term in (4-7). In order to recreate the revolving mmf and thus the ac currents, one should use, in the convolution integral, the full expression for motor γ and δ voltages, given by (3-8). For this case, the modal state response to the unit step change in the speed reference V_r is:

$$q_k(t) = \frac{V+A_1}{\lambda_k^2+1} [h_{k1} (\sin t - \lambda_k \cos t + \lambda_k e^{\lambda_k t}) +$$

$$+ h_{k2} (e^{\lambda_k t} - \lambda_k \sin t - \cos t)] + \frac{V h_{k1}}{\lambda_k} (e^{\lambda_k t} - 1)$$

It is seen that the monotonically increasing term in (4-7) is now replaced by the monotonically oscillating term - reflecting the rotation of the motor mmf vector. The motor currents will now change sinusoidally, with the same frequency with which the mmf vector sweeps the reference frame - which in turn is equal to the frequency increment over its operating point value, as requested by the change in the reference input, δV_r.

From this discussion, it becomes obvious that the apparently unstable (or oscillatory) term in the modal response reflects only the choice of the reference frame. Since the motor speed is invariant with the reference frame transformations, the oscillatory or monotonically increasing terms will not appear in the speed response.

Recapitulating this discussion in simple words, it means that the motor steady state currents will oscillate (i.e., be ac) whenever the speed of the reference frame and the motor supply frequency are not the same. This has nothing to do with the motor speed, which can be constant under these conditions.

One can now look at the speed response which is obtained from (3-25) and (3-26) as:

$$y(t) = \sum_{k=1}^{5} m_{5k} q_k(t)$$

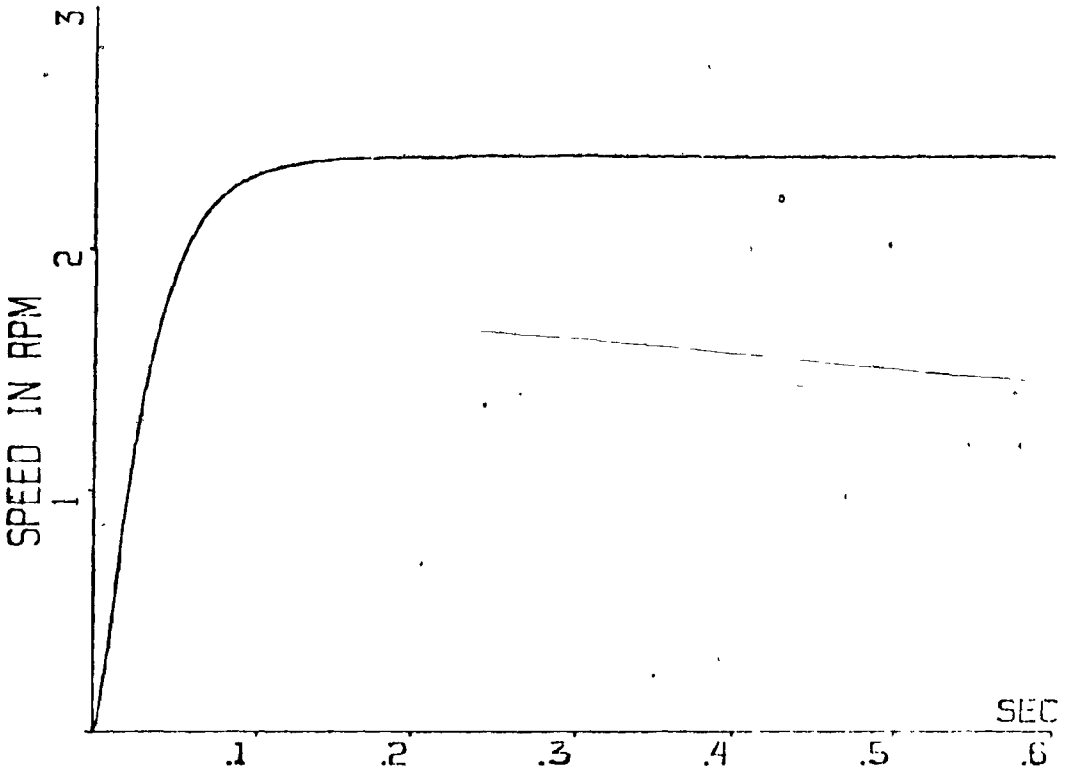

Fig. 4.3a: Speed response to step reference at 60 hz

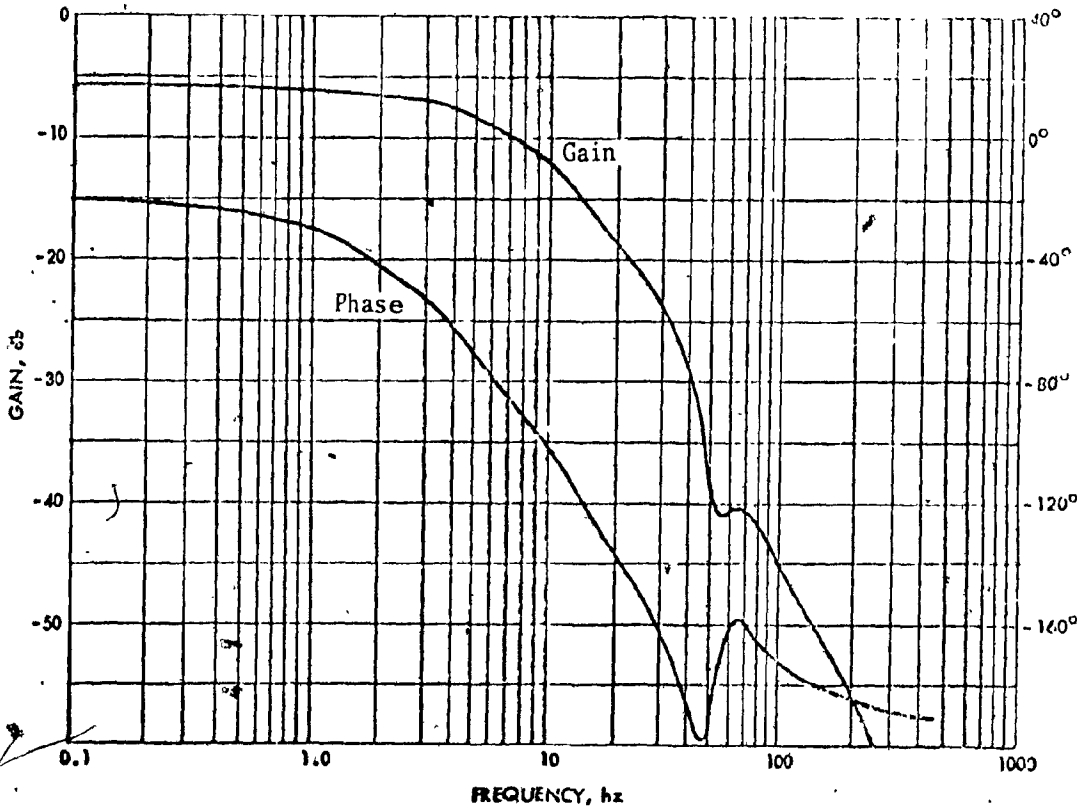

Fig. 4.3b: Frequency response of speed-input reference transfer function at 60 hz.

After the modal states have been calculated at each operating point, the speed step response is obtained and then plotted (Fig. 4.3a, 4.4a amd 4.5a). It obviously does not contain any of the monotonically increasing terms which are present in the modal response. It is interesting to observe the role of the eigenvectors--they filter out from the speed expression that part of the modal response which depends on the reference frame and which will appear in the expression for motor currents.

The attention is now directed to the analysis of the speed response. In order to have more information, the frequency response of $G_1(s)$ is presented in parallel with the speed step response (Fig. 4.3b, 4.4b, 4.5b).

At 60 hz operating point, the speed response (Fig. 4.3a) defines the drive as a second order, overdamped system. The rise time is 62.5 msec. The speed reaches 95% of its steady state value within 90 msec. Thus, the dynamic response is satisfactory. The corresponding Bode plot (Fig. 4.3b) supports this conclusion. At high frequency, the gain drops at 40 db/decade, indicating that in this range the motor behaves as a second order system. Knowing that there are five eigenvalues, this result indicates the presence of three zeros in $G_1(s)$. This conclusion is in agreement with the equation (4-3). The apparent gain peaking in the Bode plot, at 70 hz, is not noticeable in the step response, as it is very attenuated.

Thus, one concludes that the dynamic response of an induction motor at 60 hz, rated load operating point is entirely satisfactory. This fact has been well established for the last 70 years. However, the results at the conventional supply frequency establish the reference against which one will measure dynamic response at other operating points and with different control strategies.

At 30 hz (Fig. 4.4a) the speed response begins to show the high frequency oscillating component. However, the drive still behaves basically as a second order system. The rise and settling times are 72 and 95 msec., respectively. The study of the Bode plot (Fig. 4.4b) gives the same conclusions as for 60 hz point. The only difference is in the gain peaking, which is now decreased but occurs at only 26 db below the dc gain. As a result, an oscillatory component of approximately 20 hz is superimposed on the basic, second order response (Fig. 4.4a). Due to the shape of the Bode plot, it has

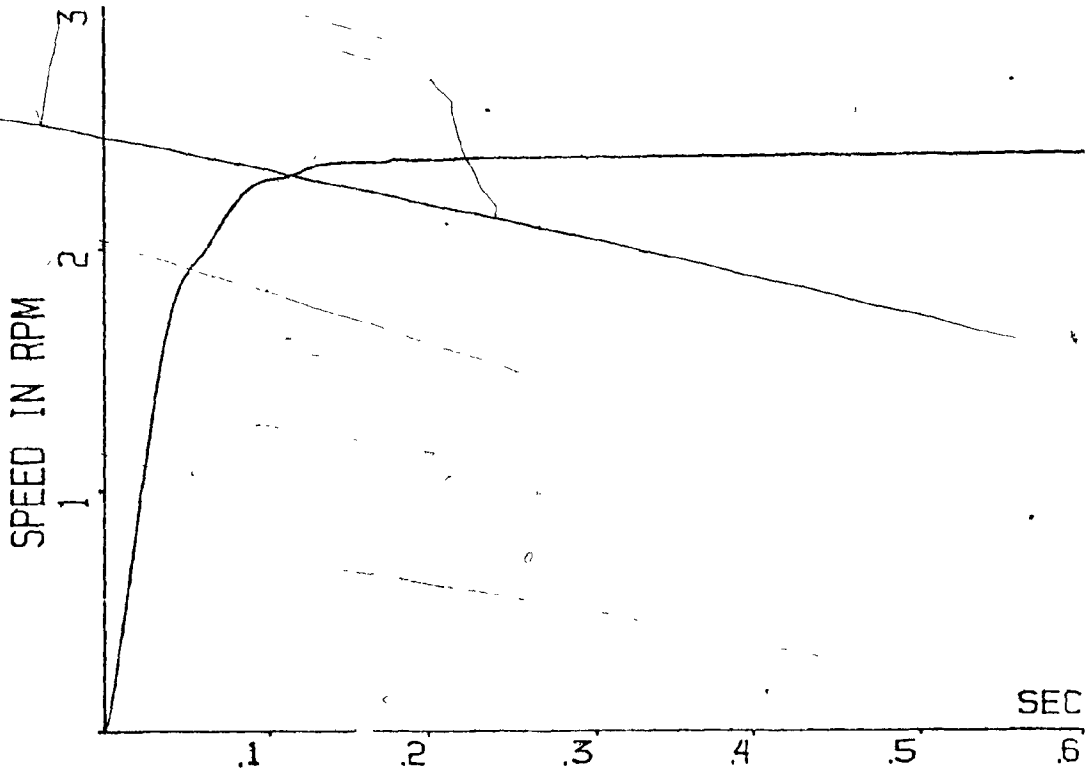

Fig. 4.4a: Speed response to step reference at 30 hz.

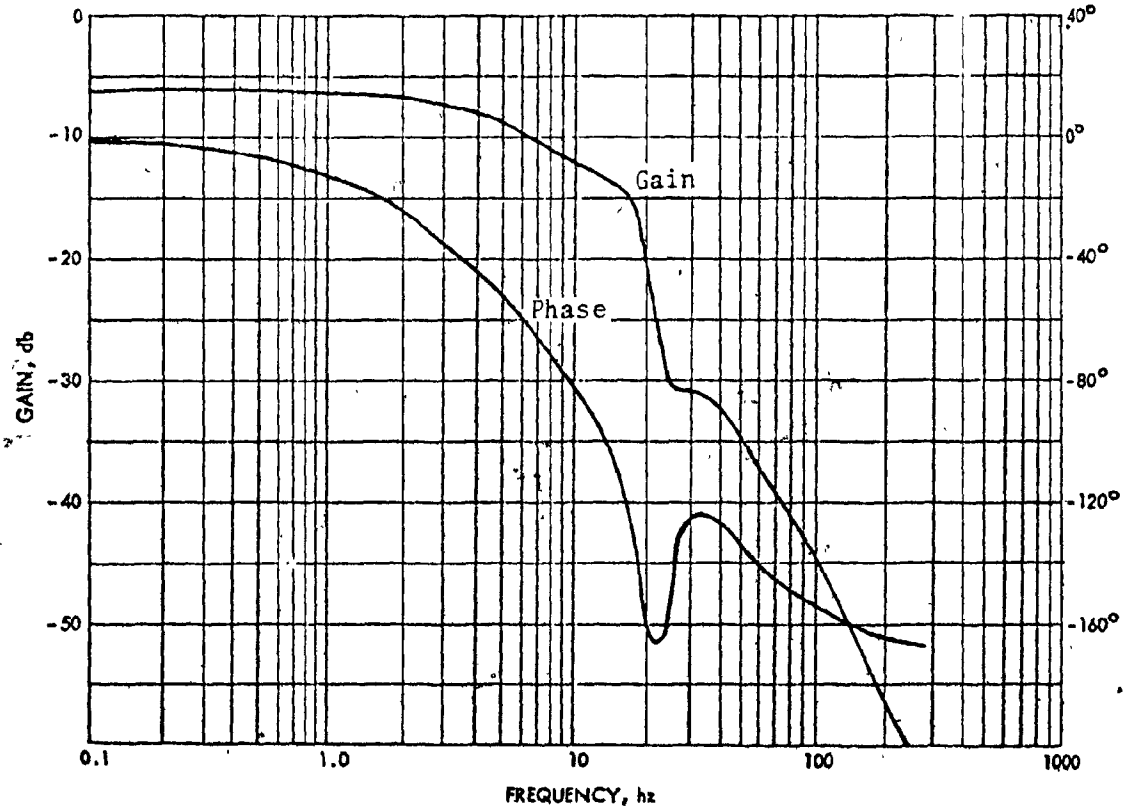

Fig. 4.4b: Frequency response of speed-input reference transfer function at 30 hz.

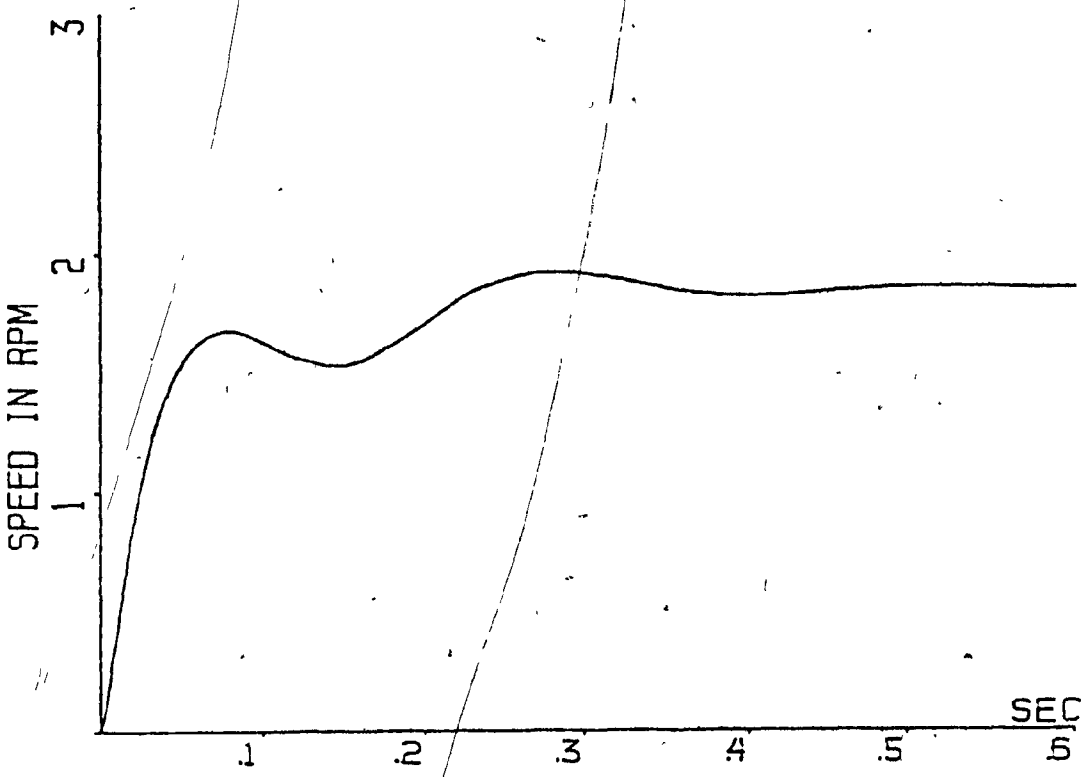

Fig. 4.5a: Speed response to step reference at 5 hz.

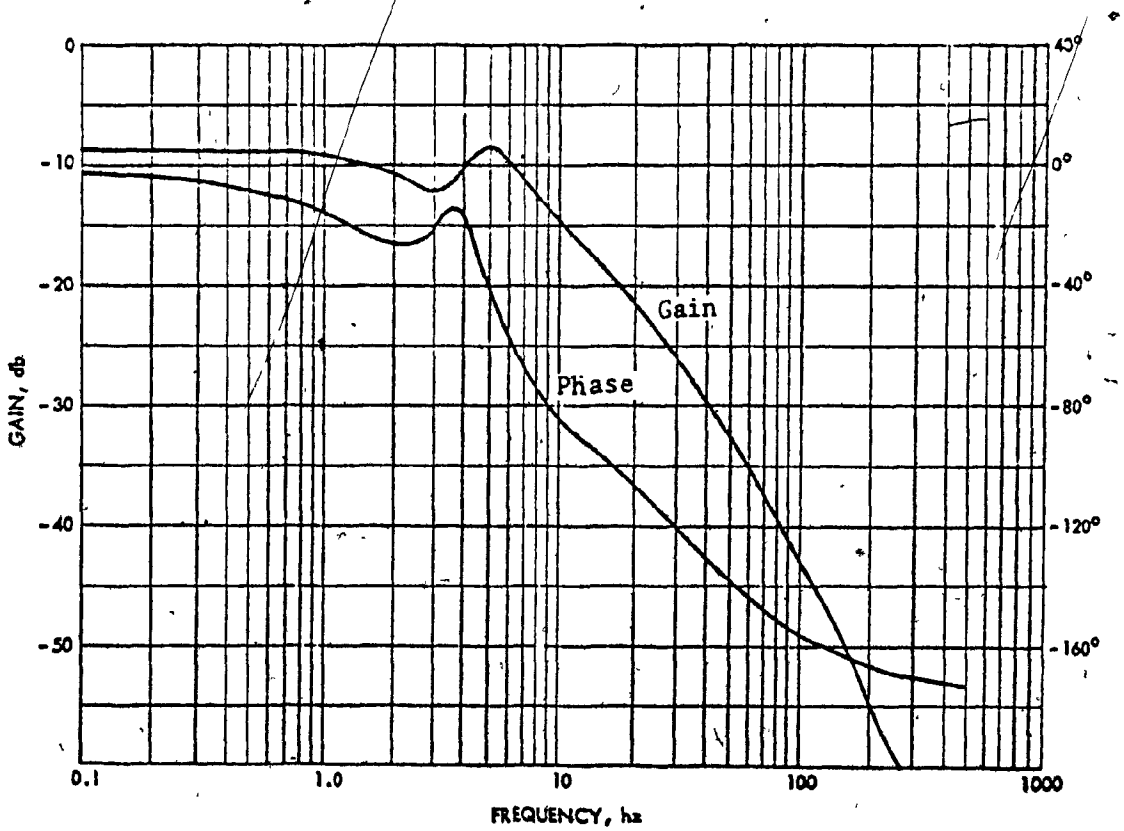

Fig. 4.5b: Frequency response of speed-input reference transfer function at 5 hz.

a small amplitude and dies out quickly.

As a conclusion, the motor dynamic characteristic at 30 hz is only slightly inferior to that at the industrial supply frequency and the drive can give the same performance as before, providing that the precaution is taken to avoid any mechanical resonance.

At 5 hz operating point the dynamic performance has deteriorated significantly, Fig. 4.5a:

1) The speed oscillations are now clearly visible. The response is underdamped and much slower than before. Rise and settling (±5%) times are 210 and 235 msec., respectively. A look at the corresponding Bode plot (Fig. 4.5b) shows a gain peak of 7 db at 5 hz. Since this peak is almost at the dc level, it is very little attenuated and results in a slowly oscillating component superimposed on the second order step response.

2) The dc coupling between the input and the output is reduced, as seen by the lower value of the s.s. speed. (Only 1.84 rpm here against 2.4 rpm for the two previous points with the same unit step change in V_r). The Bode plot supports this by giving the dc gain of -8.5 db, which is a decrease of 2.5 db from the corresponding dc gain at 60 hz. Note that the same conclusion could have been anticipated from the static torque-speed curves, Fig. 2.3.

As a conclusion, the motor dynamic performance at 5 hz is inferior to those at higher input frequencies. It can be shown that the most significant decrease occurs for supply frequencies below 10 hz. Depending on the drive application, this may or may not be acceptable. The most natural method for improving these results is by operating the drive in the closed loop.

Response to a unit step in the load torque

The speed reference is constant at each operating point. From (3-24), the modal state response with $u_5(s) = T_L(s) = 1$ is:

$$q_k(t) = (e^{\lambda_k t} - 1)h_{k5}/\lambda_k \qquad k = 1 \ldots 5$$

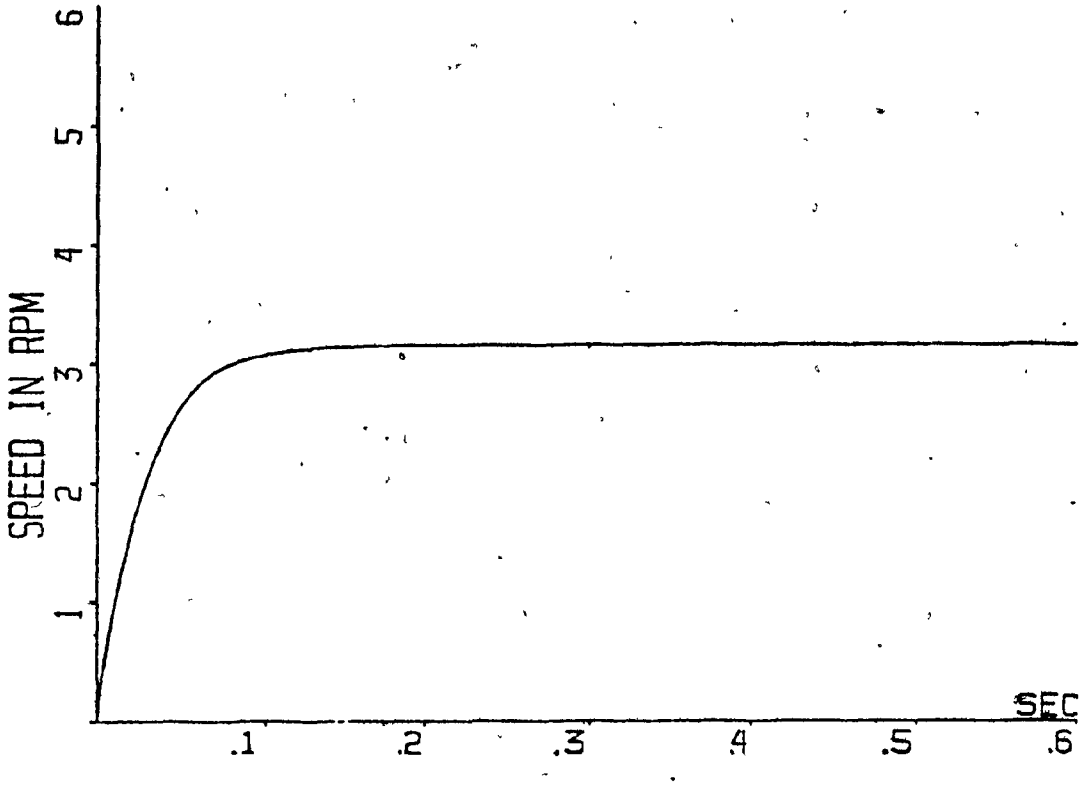

Fig. 4.6a: Speed response to step torque at 60 hz.

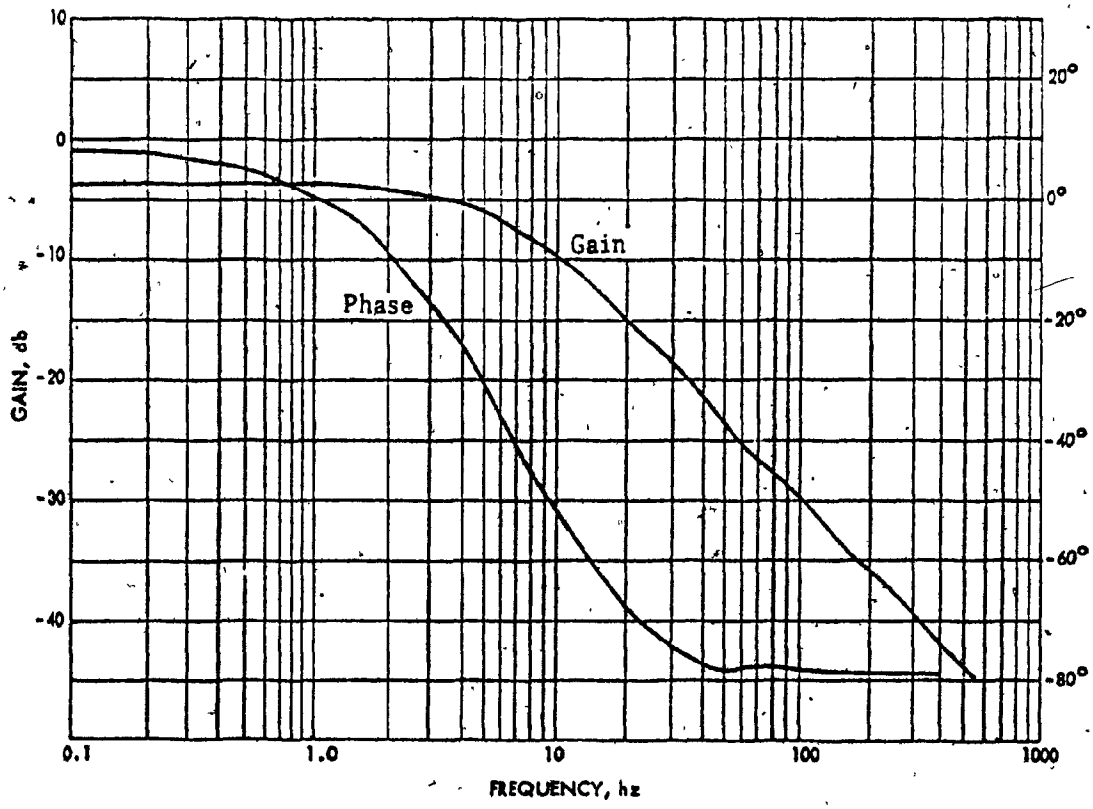

Fig. 4.6b: Frequency response of speed-torque transfer function at 60 hz.

The speed response is obtained as the combination of modal states, equation (3-26).

$$y(t) = \sum_{k=1}^{5} \frac{m_{sk}\, h_{k5}}{\lambda_k} \left(e^{\lambda_k t} - 1\right) \qquad (4\text{-}8)$$

One should remember that any change in the speed due to the torque disturbance represents the speed error since the speed reference has not changed.

Using equation (4-8) and the results in Tables 4.1, 4.2, and 4.3, the speed response at each operating point is obtained, plotted and analysed.

At 60 hz, the speed step response (Fig. 4.6a) corresponds to that of the first order system. The speed settling time (±5%) is 82 msec. The 20 db/decade gain slope of the corresponding Bode plot (Fig. 4.6b) confirms this conclusion. The break point at 5.8 hz defines the drive time constant as T = 27.4 msec. This result checks with the step response as the speed reaches 95% of its final value in 3T.

These results indicate a good pole-zero cancellation in (4-5). Thus, the motor output impedance can be represented accurately at 60 hz by the equation (3-51). The same conclusion was reached in step 2, while discussing the $G_2(s)$.

From the control point of view this represents another example of pseudo-observability. Although the fifth component of each eigenvector is different from zero (Table 4.1) only one mode is visible in the speed output. In this case, it is a desirable characteristic resulting in the first order response.

At 30 hz both the step and frequency response (Fig. 4.7a and b) are essentially identical to those at 60 hz, so that the same comments apply. Note that the complex-conjugate pair starts to appear around 20 hz (Fig. 4.7b). From Table 4.2, this pair corresponds to the magnetizing eigenvalues. However, they are still sufficiently neutralized by the corresponding zeros and do not appear in the step response.

At 5 hz the situation has changed (Fig. 4.8a and b). From the step response the drive still behaves as a first order system, but now with the second order, oscillating term superimposed. The speed settling time is 160 msec. The most significant difference is, however, the magnitude of the speed

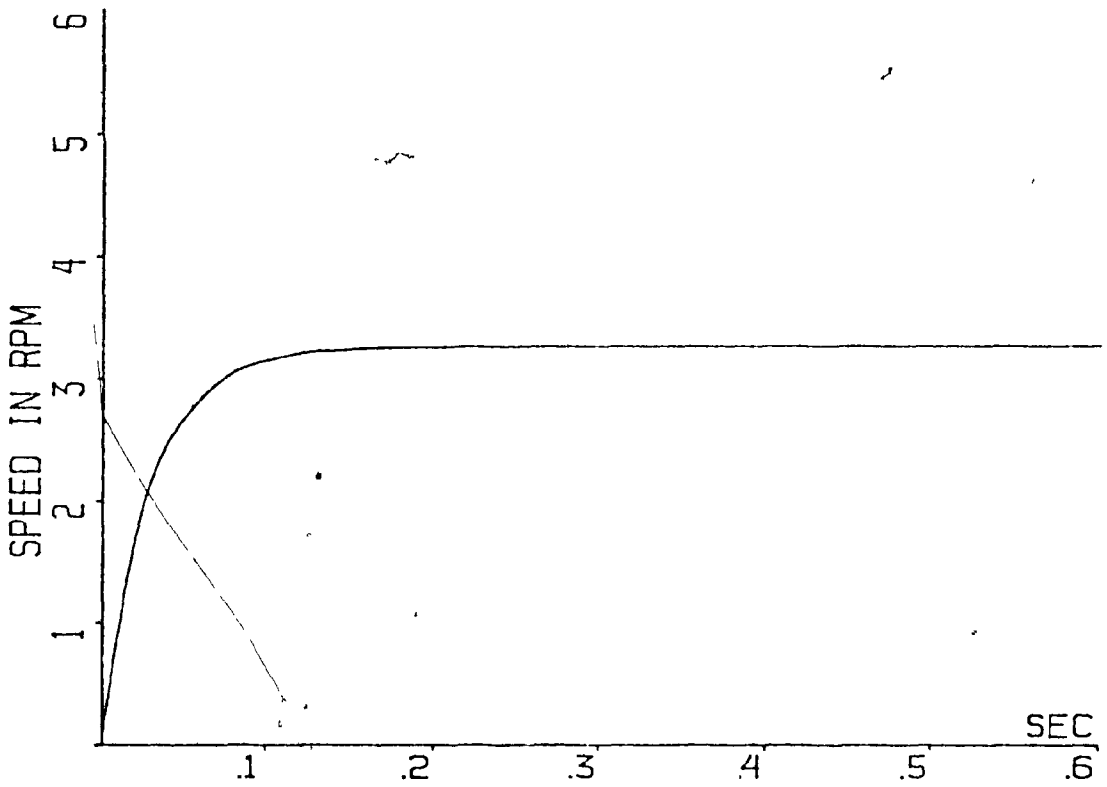

Fig. 4.7a. Speed response to step torque at 30 hz.

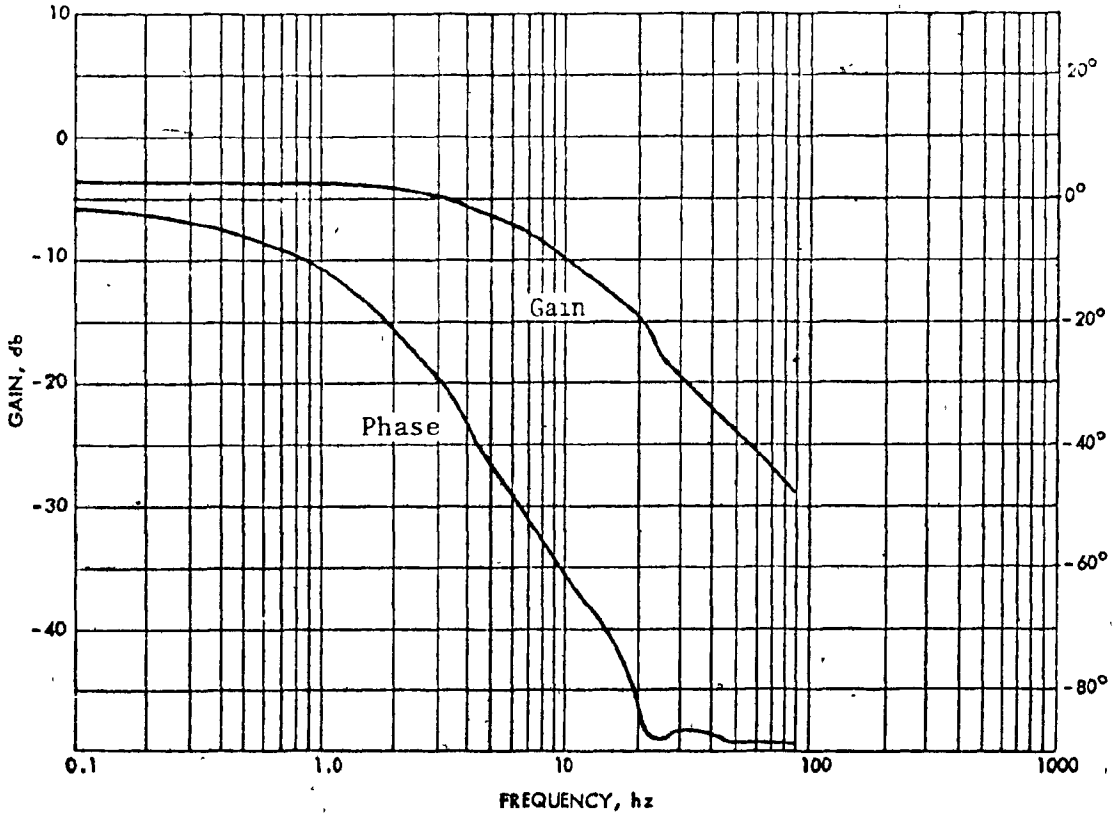

Fig. 4.7b: Frequency response of speed-torque transfer function at 30 hz.

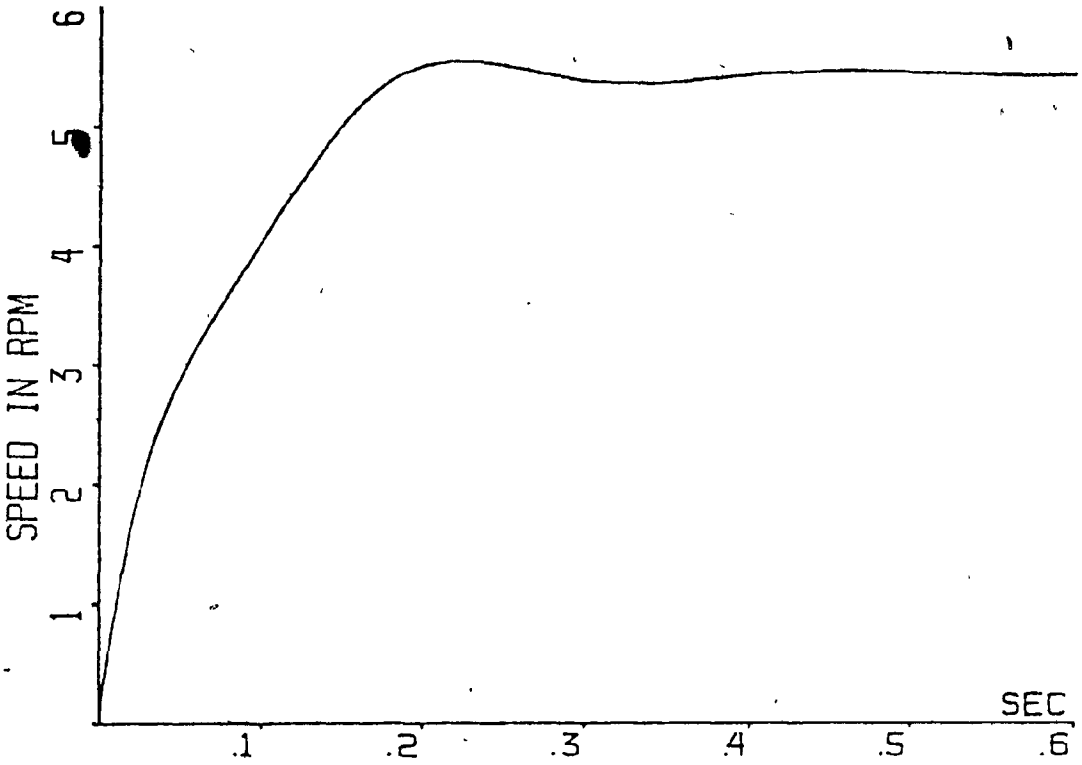

Fig. 4.8a: Speed response to step torque at 5 hz.

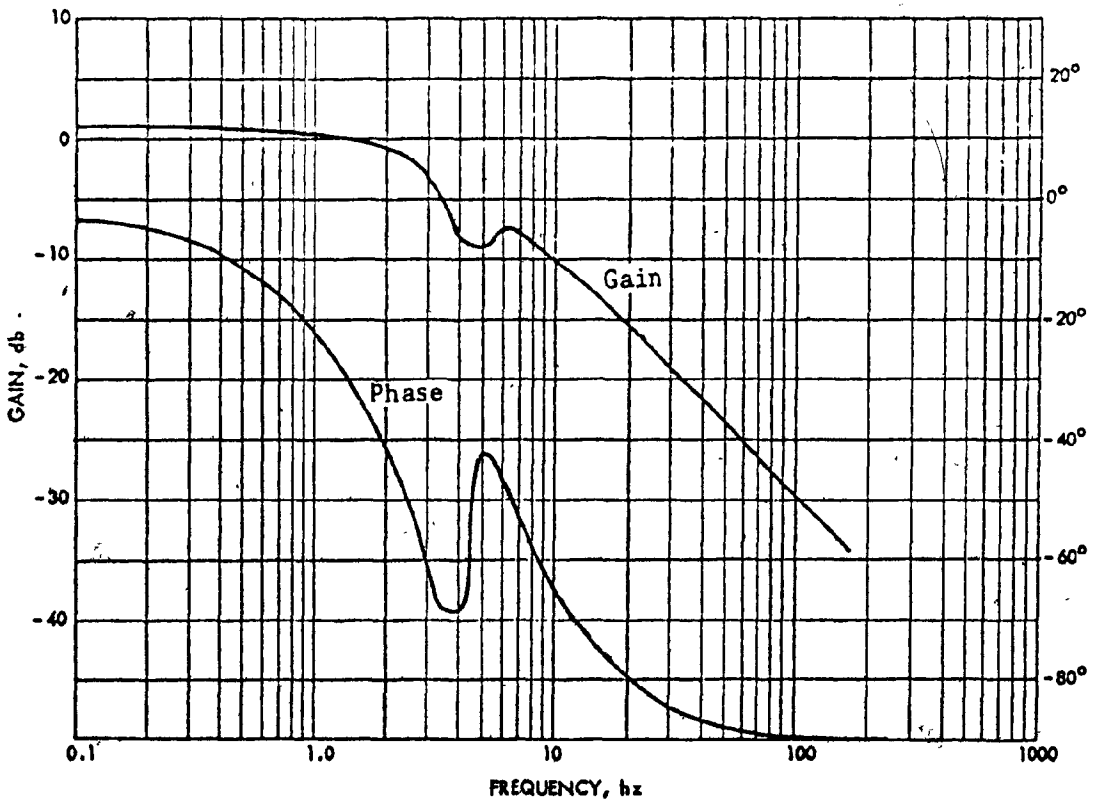

Fig. 4.8b: Frequency response of speed-torque transfer function at 5 hz.

change. With the unit step in the load torque, the speed changed by 3.16 rpm at 60 hz and by 5.44 rpm at 5 hz. This represents an increase of 63% indicating much higher sensitivity to the load disturbances. This rise in the sensitivity could have been predicted from a decrease in the slope of the corresponding static torque-speed curves, Fig. 2.3. Another hint was provided by a decrease of the dc gain in the speed-input reference transfer function at 5 hz, Fig. 4.5. From the network and control theory, such reduction automatically results in an increase of the corresponding output impedance, i.e., higher sensitivity to the disturbances.

A few more comments can be made after examining the drive frequency response (Fig. 4.8b). The $G_2(s)$ dc gain has increased by 3 db over that at 60 hz, giving exactly 63% larger steady state speed value. A second order response, oscillating at approximately 6 hz and caused by the magnetizing modes is superimposed on the basic, first order, drive response. Although this oscillating component is undesirable, it is the magnitude of the speed response, i.e., the increase in the speed sensitivity, which is of greatest concern This again points to the need for a closed loop system which will result in a decreased output impedance

As an overall conclusion, the constant V/hz, open loop drive has a rather poor speed regulation at any frequency, due to the weak electromechanical coupling. The regulation further deteriorates when the load is increased since the mechanical and electrical eigenvalues move further apart. This results in a considerable speed error, especially at the lower input frequencies. The same conclusion is available from the static torque-speed curves presented in Chapter II.

Beside this disadvantage, the speed response is acceptable until the very low supply frequencies (below 10 hz) are reached. Even then, the motor behaviour may be tolerable, depending on its application.

Since the open loop operation is inherently simple, and least expensive to implement, it will always find its use. However, the drive dynamics can be improved while at the same time preserving the simplicity of the constant V/hz control if closed loop operation is considered. Thus, attention is turned to Part II.

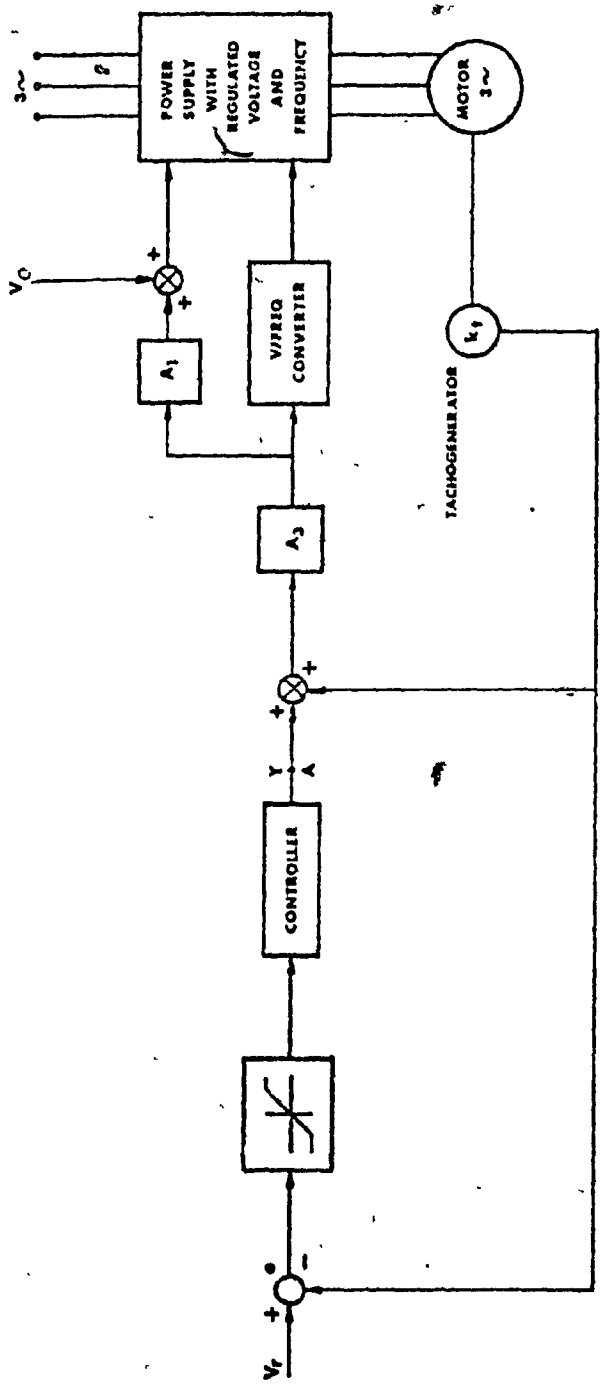

Fig. 4.9: Constant V/hz, closed loop drive.

4.2.2 Part II: Closed loop

Drive Description

The dynamic characteristics of the constant V/hz drive, presented in Fig. 4.1, can be improved by closing the speed feedback loop. The new drive, with speed controller included, is presented in Fig. 4.9.

The closed loop drive operates at a constant speed (within load limits) by continuously adjusting the inverter output frequency and voltage. Any difference e, between the requested and actual speed, is processed through the speed controller and added to the motor actual speed. The signal so obtained represents the inverter frequency reference. The drive operation at a constant speed and varying load is illustrated by using the motor stator curves, Fig. 4.10. The limiter prevents excessive values of slip speed during overloads or large speed changes (Chapter V).

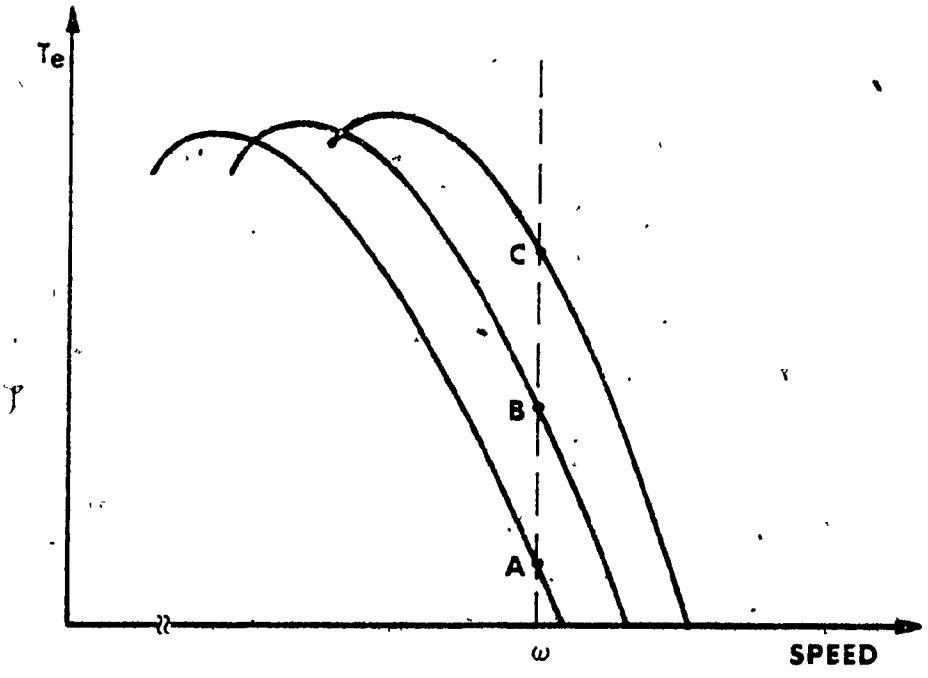

Fig. 4.10: Trajectory of an operating point. Frequency and voltage are both adjusted as the load is changed to keep the motor speed constant, points A, B and C.

Controller Design

Before this drive can be analyzed, its speed controller has to be specified. This is done by considering the drive open-loop frequency response. Note that a controller so designed will have to be a compromise, since the drive dynamics change with the supply frequency and load (equation 3-10). Thus, only an adaptive controller can provide optimal performance over the whole speed range.

The drive open-loop response can be obtained by breaking the feedback loop at point A (Fig. 4.9). The signal Y becomes the input, while the speed is the output of the system so obtained. To establish its equations consider first the expressions for the input frequency and voltage:

$$\omega = (Y + k_t \omega_m) A_3$$

$$V \doteq V_o + A_1 \omega$$

or in the perturbed form

$$\delta\omega = A_3 \delta Y + n \delta\omega_m \qquad (4\text{-}9a)$$

$$\delta V = A_1 \delta\omega = A_1 A_3 \delta Y + A_1 n \delta\omega_m \qquad (4\text{-}9b)$$

because $A_3 = n/k_t$.

Due to the feedback acting on the motor input frequency, the number of drive equations has increased. Therefore, an additional state has to be introduced. It represents a change in the phase angle, $\delta\psi$, between the airgap mmf vector and the γ-axis of the reference frame, as defined in Fig. 3.1. Thus:

$$\frac{d}{dt}(\delta\psi) \doteq \delta\omega = A_3 \delta Y + n\delta\omega_m \qquad (4\text{-}10)$$

Combining (4-9) and (4-10) with the open-loop motor equation (3-10), and the input equation (3-11b), the result becomes:

$$[P_o]\ \dot{X}_o = [Q_o]\ X_o + U \qquad (4\text{-}11)$$

where:

$$P_o = \begin{bmatrix} L_1 & 0 & M & 0 & 0 & 0 \\ 0 & L_1 & 0 & M & 0 & 0 \\ M & 0 & L_2 & 0 & 0 & 0 \\ 0 & M & 0 & L_2 & 0 & 0 \\ 0 & 0 & 0 & 0 & J_T & 0 \\ 0 & 0 & 0 & 0 & 0 & 1 \end{bmatrix} \qquad (4\text{-}12a)$$

$$\dot{Q}_o = \begin{bmatrix} -R_1 & \Omega_c L_1 & 0 & \Omega_c M & n\,\Lambda_1 & 0 \\ -\Omega_c L_1 & -R_1 & -\Omega_c M & 0 & 0 & V \\ 0 & \Omega_s M & -R_2 & \Omega_s L_2 & -n(MI_2+L_2 I_4) & 0 \\ -\Omega_s M & 0 & -\Omega_s L_2 & -R_2 & n(MI_1+L_2 I_3) & 0 \\ -nMI_4 & nMI_3 & nMI_2 & -nMI_1 & -f_T & 0 \\ 0 & 0 & 0 & 0 & n & 0 \end{bmatrix} \qquad (4\text{-}12b)$$

$$X_o = \begin{bmatrix} \delta i_\gamma^s \\ \delta i_\delta^s \\ \delta i_\gamma^r \\ \delta i_\delta^r \\ \delta\omega_m \\ \delta\psi \end{bmatrix} \qquad (4\text{-}12c) \qquad \text{and} \qquad U = \begin{bmatrix} A_1 A_3 \delta\gamma \\ 0 \\ 0 \\ 0 \\ -\delta T_L \\ A_3 \delta\gamma \end{bmatrix} \qquad (4\text{-}12d)$$

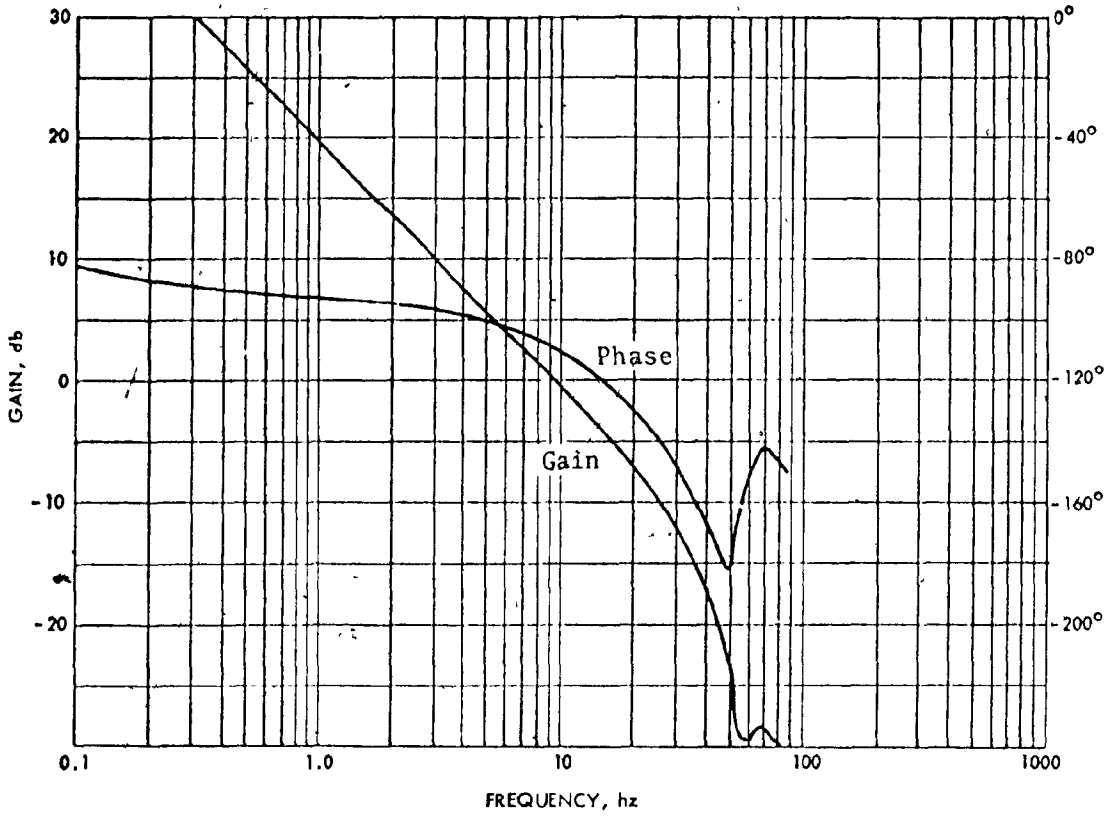

Fig. 4.11a: Frequency response of the open loop system at 1700 rpm.

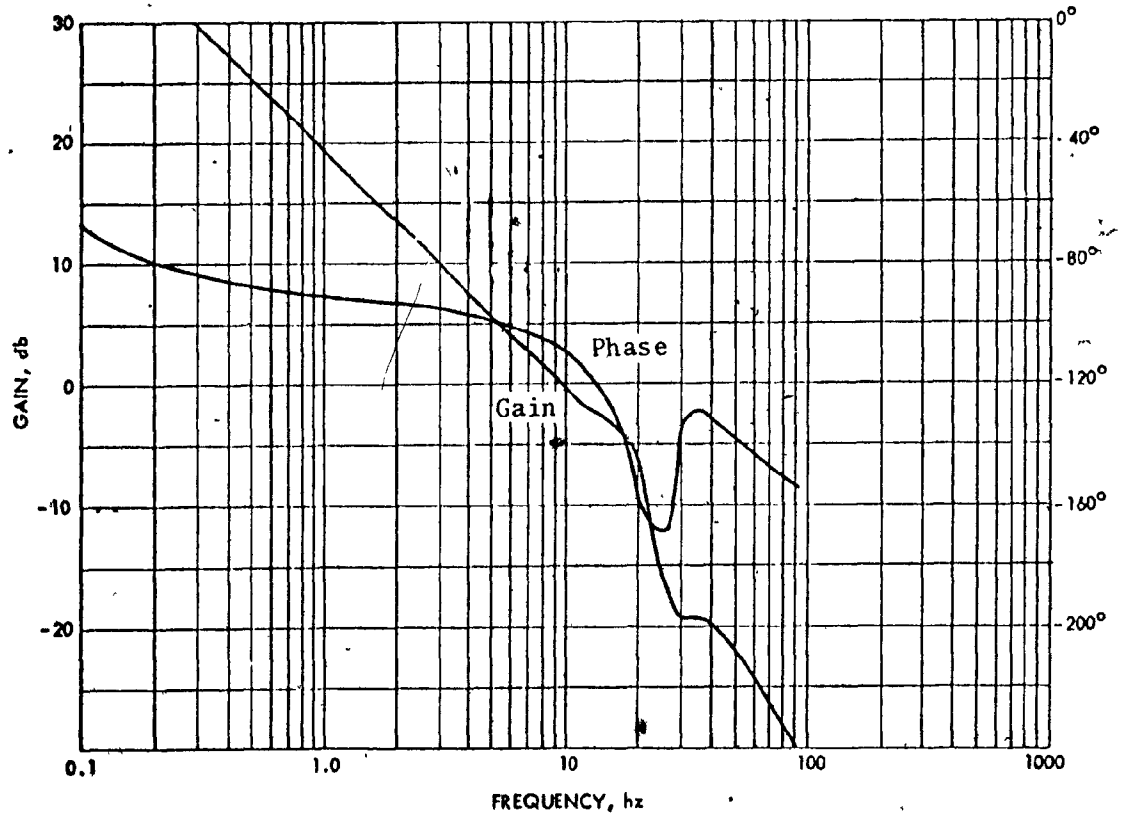

Fig. 4.11b: Frequency response of the open loop system at 800 rpm.

Equation (4-11) describes the closed loop drive (Fig. 4.9) with the speed loop open at point A and signal Y taken as the input. Its frequency response at rated load and three operating speeds (1700, 800 and 100 rpm) is presented in Fig. 4.11a, b and c. From these results the operating point at 1700 rpm (Fig. 4.11a appears to be the most critical one: if the speed loop is closed with the controller having a unity gain, the resulting drive bandwidth will be around 10 hz. This is almost identical to the result obtained in Part I and thus represents no improvement over the open loop operation. Any further increase in the controller gain is not possible due to the ensuing rapid decrease in the phase margin.

The shape of the open-loop frequency response points to the need for a lead compensation which would smooth out the dip in the phase curve. However, since this dip shifts with the change of the motor operating speed (Fig. 4.11b and c) it is impossible to achieve with a fixed controller an optimal compensation over the entire speed range.

On the basis of the drive open loop frequency response (Fig. 4.11) the speed controller is chosen as:

$$T_c(s) = \frac{\delta Y}{\delta e} = \left(\frac{1+a\,d\,s}{1+d\,s}\right)\left(A_c\,\frac{1+s/k_c}{s}\right) \qquad (4\text{-}13)$$

Its frequency response is given in Fig. 4.12. The controller consists of two parts: the lead compensation and the standard proportional-integral (PI) term (Fig. 4.13a). The numerical values in equation (4-13) are selected to obtain the maximum phase lead at 50 hz, where it is most needed (Fig. 4.11a). Furthermore, the controller gain A_c is chosen so that the total gain around the loop is 10. Thus:

$d = 1/(314.16\sqrt{14})$ - determines the upper break frequency of the lead network.

$a = 14$ - determines the separation of break points in the lead network

$k_c = 6.2832$ - integrator gain

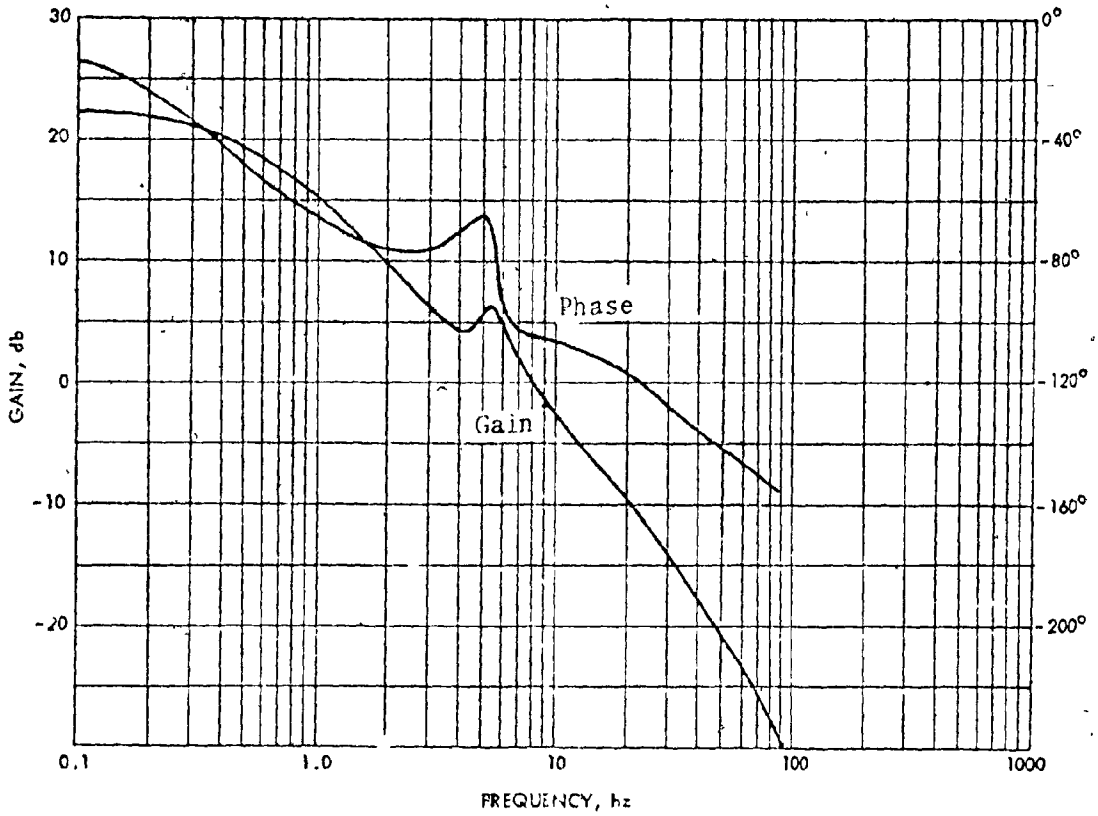

Fig. 4.11c: Frequency response of the open loop system at 100 rpm.

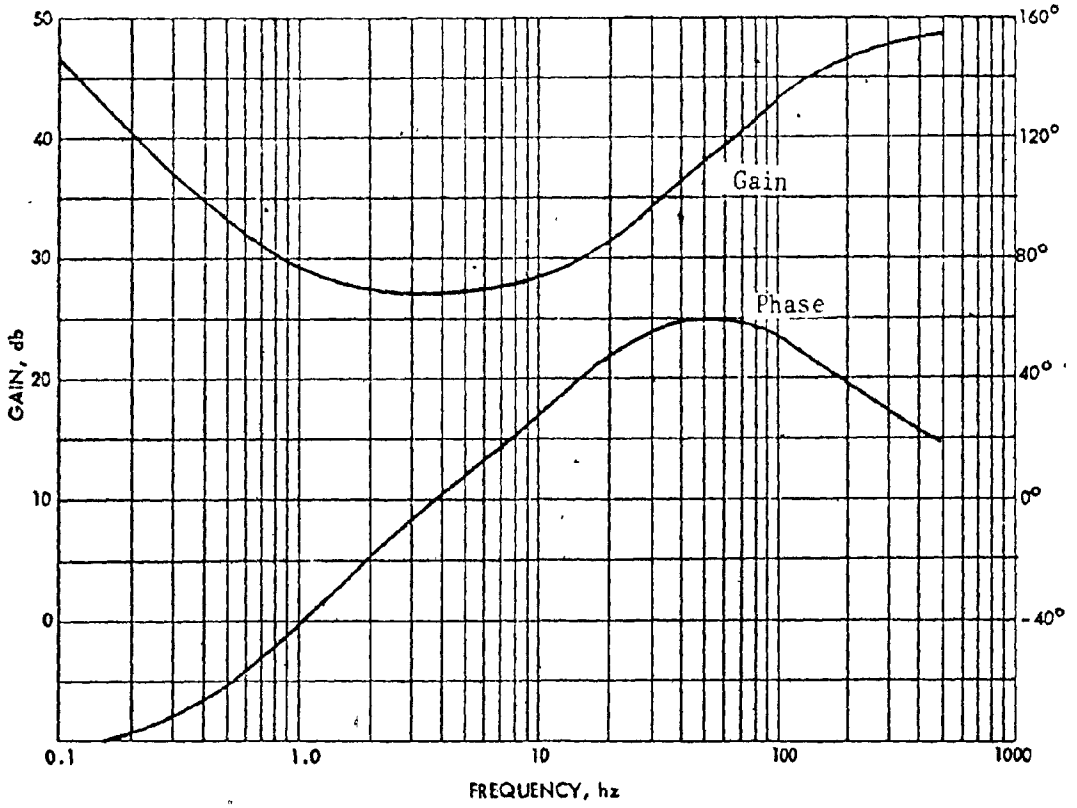

Fig. 4.12: Frequency response of the speed controller, constant V/hz drive.

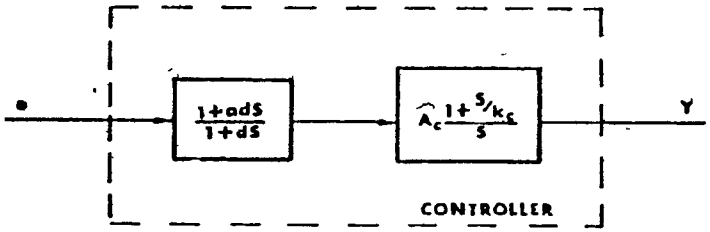

Fig. 4.13a: Speed controller for the constant V/hz drive.

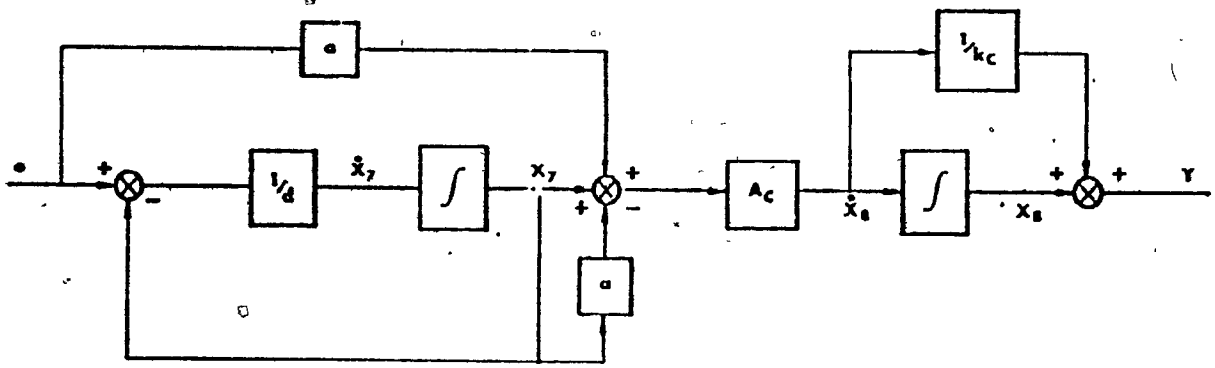

Fig. 4.13b: Speed controller, state diagram representation.

$$A_c = 10\, k_c / k_t = 131.6 \quad \text{- total controller gain}$$

The controller is presented in Fig. 4.13 which should be considered in the context of Fig. 4.9.

Once the controller is specified, the equations for the complete closed loop drive (Fig. 4.9) can be established. Due to two controller integrators, there will be two additional equations in the drive description. They are obtained by choosing the two new states in the standard way, as the outputs from the integrators:

$$\dot{X}_7 = \frac{1}{d}\,(\delta V_r - k_t \delta\omega_m - X_7)$$

$$\dot{X}_8 = A_c(1 - a)X_7 + a\,A_c(\delta V_r - k_t\,\delta\omega_m)$$

while the previous input Y becomes now the controller output:

$$\delta Y = X_8 \quad \frac{A_c}{K_c}(1 - a)X_7 + \frac{a\,A_c}{K_c}(\delta V_r - k_t \delta\omega_m) \qquad (4\text{-}11)$$

When the last three equations are combined with (4-11), the equation of the complete closed loop, constant V/hz drive is obtained:

$$[P]\dot{X} = [Q]X + U \qquad (4\text{-}14)$$

where

$$P = \begin{bmatrix} [P_o] & 0 & 0 \\ 0 & 1 & 0 \\ 0 & 0 & 1 \end{bmatrix} \qquad (4\text{-}15a)$$

with P_o defined by the equation (4-12a).

$$Q = \begin{bmatrix} -R_1 & \Omega_c L_1 & 0 & \Omega_c M & A_1 n(1 - \frac{a A_c}{k_c}) & 0 & \frac{(1-a)A_1 A_3 A_c}{k_c} & A_1 A_3 \\ -\Omega_c L_1 & -R_1 & -\Omega_c M & 0 & 0 & V & 0 & 0 \\ 0 & \Omega_s M & -R_2 & \Omega_s L_2 & -n(MI_2 + L_2 I_4) & 0 & 0 & 0 \\ -\Omega_s M & 0 & -\Omega_s L_2 & -R_2 & n(MI_1 + L_2 I_3) & 0 & 0 & 0 \\ -nMI_4 & nMI_3 & nMI_2 & -nMI_1 & -f_T & 0 & 0 & 0 \\ 0 & 0 & 0 & 0 & n(1 - \frac{a A_c}{k_c}) & 0 & \frac{(1-a)A_3 A_c}{k_c} & A_3 \\ 0 & 0 & 0 & 0 & -k_t/d & 0 & -1/d & 0 \\ 0 & 0 & 0 & 0 & -k_t a A_c & 0 & (1-a)A_c & 0 \end{bmatrix} \quad (4\text{-}15b)$$

$$X = \begin{bmatrix} X_o \\ x_7 \\ x_8 \end{bmatrix} \quad (4\text{-}15c)$$

where X_o vector is defined by equation (4-12c). The input vector U is:

$$U = \begin{bmatrix} u_1(t) \\ u_2(t) \\ u_3(t) \\ u_4(t) \\ u_5(t) \\ u_6(t) \\ u_7(t) \\ u_8(t) \end{bmatrix} = \begin{bmatrix} \frac{a A_1 A_3 A_c \delta V_r}{K_c} \\ 0 \\ 0 \\ 0 \\ -\delta T_L \\ \frac{a A_3 A_c V_r}{K_c} \\ \delta V_r / d \\ a A_c \delta V_r \end{bmatrix} \qquad (4\text{-}15d)$$

The drive state equation is:

$$\dot{X} = [A]X + [B]U$$

where

$$[A] = [P]^{-1}[Q] \qquad (4\text{-}16a)$$

and

$$[B] = [P]^{-1}$$

The P matrix can be inverted by hand to give:

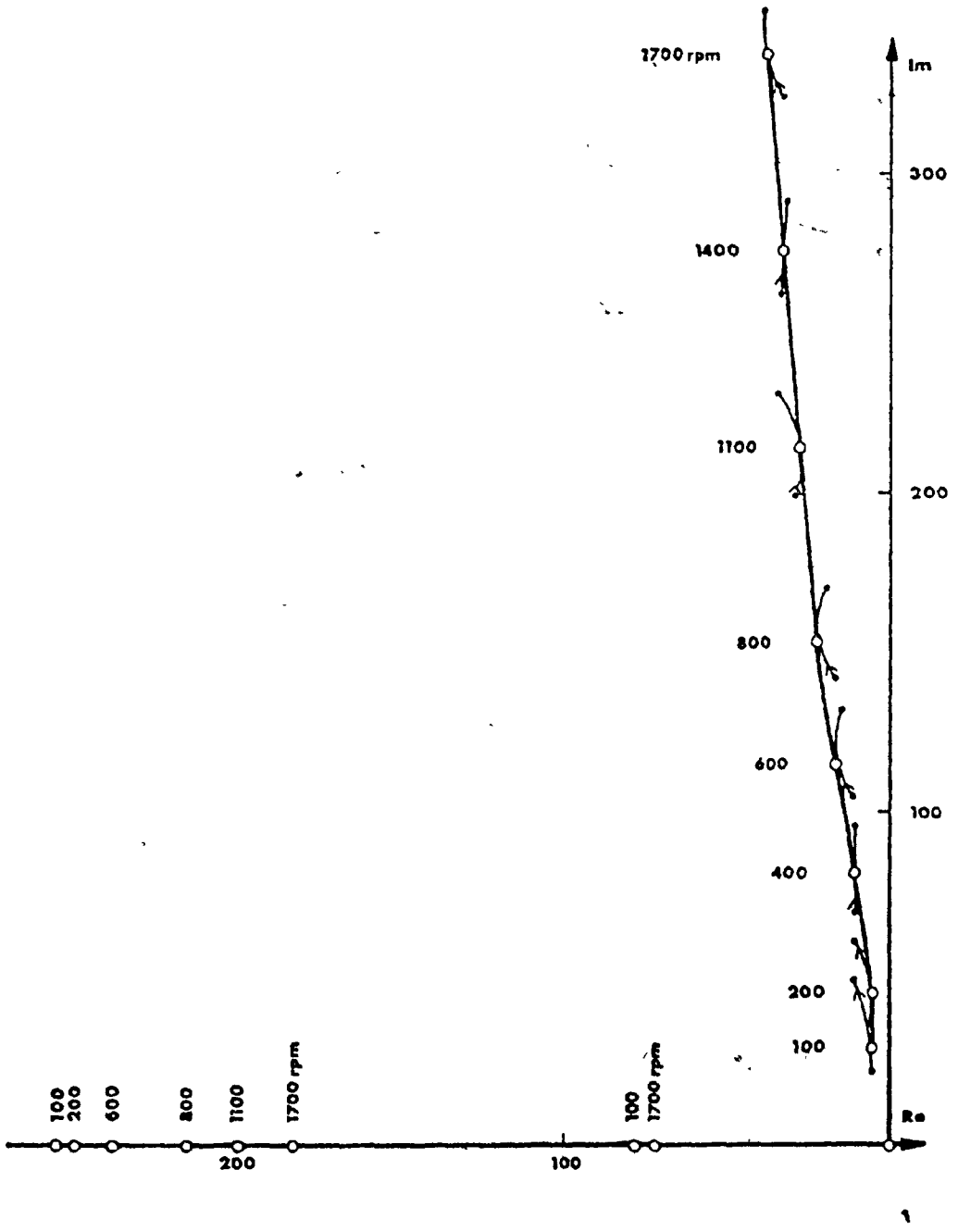

Fig. 4.14: Eigenvalue loci for constant V/hz, closed loop drive. The effects of changing load are presented for selected motor speeds.

$$P^{-1} = \begin{bmatrix} [L]^{-1} & 0 & 0 & 0 & 0 \\ 0 & 1/J_T & 0 & 0 & 0 \\ 0 & 0 & 1 & 0 & 0 \\ 0 & 0 & 0 & 1 & 0 \\ 0 & 0 & 0 & 0 & 1 \end{bmatrix} \quad (4\text{-}17)$$

where L^{-1} matrix is given by equation (3-15).

Drive analysis

With the drive equations specified, the familiar steps in the analysis of motor operating points can be undertaken.

STEP 1: Eigenvalues, eigenvectors and input-mode coupling matrix

The drive is analyzed for speeds of 1700, 800 and 100 rpm. Computer results for these three operating points, and rated load are presented in Tables 4.4, 4.5 and 4.6. The eigenvalue loci for larger number of operating points, and rated load, are presented in Fig. 4.14. Note that the last complex conjugate pair with the break frequency above 200 hz is not included in Fig. 4.14. The effects of the load change on the eigenvalues is given by a separate locus at each operating point, Fig. 4.14. It is obvious from these results that the drive is stable. The eigenvalue loci give again only the modal response to the corresponding initial conditions. The excitation of each mode by the drive inputs is determined by the input-mode coupling matrix H, while its participation in the speed response depends on the drive eigenvectors. Take for example, the third mode which is defined by the eigenvalue at the origin and which therefore increases monotonically with time (Table 4.4). The corresponding eigenvector component (5th row, 3rd column)

TABLE 4.4

MOTOR DRIVE WITH CONSTANT V/HZ CONTROL.CLOSED LOOP

OPERATING POINT VALUES:	FREQUENCY(HZ)	VOLTAGE(VOLTS)	SPEED(RPM)	TORQUE(NM)
	60.00	127.0	1700.0	17.42

OPERATING POINT CURRENTS:			E-VALUES.REAL	E-VALUES.IMAG.	BREAK FREQUENCY(HZ)	DAMPING
STATOR 1	15.61	1	-77.01	0.00	12.26	1.00
STATOR 2	-9.85	2	-181.11	0.00	28.82	1.00
ROTOR 1	-15.96	3	0.00	0.00	0.00	1.00
ROTOR 2	1.72	4	-6.35	0.00	1.01	1.00
		5	-36.38	344.95	55.20	0.10
		6	-36.38	-344.95	55.20	0.10
		7	-683.06	-1148.63	212.69	0.51
		8	-683.06	1148.63	212.69	0.51

E-VECTORS IN POLAR COORDINATES:

E-VECTOR 1		E-VECTOR 2		E-VECTOR 3		E-VECTOR 4	
0.9286E 00	0.0000E 00	0.6725E-01	0.1800E 03	0.6312E 00	0.0000E 00	0.3007E 00	0.0000E 00
0.5893E 00	0.1800E 03	0.1000E 01	0.1800E 03	0.1060E 01	0.0000E 00	0.4191E 00	0.0000E 00
0.9898E 00	0.1800E 03	0.6120E-01	0.0000E 00	0.1104E 00	0.1800E 03	0.7953E-01	0.1800E 03
0.6229E 00	0.0000E 00	0.1026E 01	0.0000E 00	0.1022E 01	0.1800E 03	0.4278E 00	0.1800E 03
0.2721E 00	0.1800E 03	0.8035E-02	0.0000E 00	0.2239E-16	0.0000E 00	0.1085E 00	0.1800E 03
0.4988E-02	0.1800E 03	0.2543E-02	0.1800E 03	0.6406E-01	0.0000E 00	0.2731E-01	0.0000E 00
0.1390E 00	0.0000E 00	0.4535E-02	0.1800E 03	0.1104E-16	0.1800E 03	0.5210E-01	0.0000E 00
0.1969E-01	0.1800E 03	0.3813E-02	0.1800E 03	0.2900E-13	0.1800E 03	0.9982E 00	0.1800E 03

E-VECTOR 5		E-VECTOR 6		E-VECTOR 7		E-VECTOR 8	
0.3165E 00	-0.3396E 02	0.3165E 00	0.3396E 02	0.7145E 00	-0.1433E 03	0.7145E 00	0.1433E 03
0.8347E 00	-0.1290E 02	0.8347E 00	0.1290E 02	0.1822E-01	0.5979E 02	0.1822E-01	-0.5979E 02
0.3093E 00	0.1478E 03	0.3093E 00	-0.1478E 03	0.6945E 00	0.3635E 02	0.6945E 00	-0.3635E 02
0.8097E 00	0.1688E 03	0.8097E 00	-0.1688E 03	0.1778E-01	-0.1204E 03	0.1778E-01	0.1204E 03
0.1339E-01	-0.1233E 03	0.1339E-01	0.1233E 03	0.1125E-01	-0.2293E 02	0.1125E-01	0.2293E 02
0.6581E-02	0.2551E 02	0.6581E-02	-0.2551E 02	0.5096E-02	-0.1329E 03	0.5096E-02	0.1329E 03
0.6316E-02	0.3981E 02	0.6316E-02	-0.3981E 02	0.5053E-02	-0.1361E 03	0.5053E-02	0.1361E 03
0.9938E-02	0.2593E 02	0.9938E-02	-0.2593E 02	0.7678E-02	-0.1329E 03	0.7678E-02	0.1329E 03

INPUT-MODE COUPLING MATRIX IN POLAR COORDINATES:

0.2829E 01	0.1800E 03	0.1961E 01	0.1042E-12	0.1395E 02	-0.1687E-12	0.6020E 01	-0.8699E-13
0.1040E 03	0.1800E 03	0.5592E 02	0.1800E 03	0.1316E 02	-0.9046E-12	0.2671E 03	-0.1837E-13
0.3282E 01	0.1800E 03	0.2487E-11	0.4528E-02	0.2946E 02	-0.2226E-14	0.4446E 01	0.2556E-14
0.3252E 00	0.3056E-12	0.3909E-01	0.1800E 03	0.2901E 01	-0.1800E 03	0.4771E 00	-0.1800E 03
0.1326E 03	0.1292E 03	0.1251E 03	0.4705E 02	0.7195E 01	-0.1793E 03	0.3282E 02	-0.2371E 02
0.1326E 03	-0.1292E 03	0.1251E 03	-0.4705E 02	0.7195E 01	0.1793E 03	0.3282E 02	0.2371E 02
0.1831E 03	0.1693E 03	0.6278E 02	-0.5955E 02	0.1862E 03	-0.1574E 02	0.8640E 01	0.4677E 02
0.1831E 03	-0.1693E 03	0.6278E 02	0.5955E 02	0.1862E 03	0.1574E 02	0.8640E 01	-0.4677E 02
0.6362E 01	0.1800E 03	0.5603E 01	-0.1800E 03	0.6843E 01	-0.9016E-13	0.3904E 01	-0.2.58E-14
0.6175E 02	0.1800E 03	0.6792E 02	-0.2288E-14	0.1113E 02	0.1800E 03	0.2325E 00	0.1800E 03
0.2672E 02	0.1800E 03	0.1825E 01	-0.1347E-13	0.7253E 00	-0.1800E 03	0.4983E 03	0.1927E-15
0.1971E 01	-0.8089E-14	0.1354E 01	0.2354E-14	0.1547E-01	0.1800E 03	0.1013E 01	0.1800E 03
0.5997E 02	0.1216E 03	0.7933E 02	-0.4897E 02	0.5794E 01	0.1355E 03	0.7314E-01	-0.1226E 03
0.5997E 02	-0.1216E 03	0.7933E 02	0.4897E 02	0.5794E 01	-0.1355E 03	0.7314E-01	0.1226E 03
0.8998E 03	0.5385E 02	0.1033E 02	0.6119E 02	0.9026E 02	0.5065E 02	0.3108E 00	-0.7564E 02
0.8998E 03	-0.5385E 02	0.1033E 02	-0.6119E 02	0.9026E 02	-0.5065E 02	0.3108E 00	0.7564E 02

TABLE 4.5

MOTOR DRIVE WITH CONSTANT V/HZ CONTROL,CLOSED LOOP

OPERATING POINT VALUES:	FREQUENCY(HZ)	VOLTAGE(VOLTS)	SPEED(RPM)	TORQUE(NM)
	30.00	66.5	800.0	17.95

OPERATING POINT CURRENTS:			E-VALUES,REAL	E-VALUES,IMAG.	BREAK FREQUENCY(HZ)	DAMPING
STATOR 1	16.03	1	-216.85	0.00	34.51	1.00
STATOR 2	-9.70	2	-75.69	0.00	12.05	1.00
ROTOR 1	-16.23	3	-0.00	0.00	0.00	1.00
ROTOR 2	1.44	4	-6.35	0.00	1.01	1.00
		5	-20.47	159.54	25.60	0.13
		6	-20.47	-159.54	25.60	0.13
		7	-681.76	-1156.31	213.64	0.51
		8	-681.76	1156.31	213.64	0.51

E-VECTORS IN POLAR COORDINATES:

E-VECTOR 1		E-VECTOR 2		E-VECTOR 3		E-VECTOR 4	
0.5931E-01	0.1800E 03	0.9111E 00	0.0000E 00	0.6048E 00	0.0000E 00	0.2973E 00	0.0000E 00
0.1000E 01	0.1800E 03	0.6606E 00	0.1800E 03	0.1000E 01	0.0000E 00	0.4317E 00	0.0000E 00
0.5494E-01	0.0000E 00	0.9759E 00	0.1800E 03	0.8928E-01	0.1800E 03	0.7241E-01	0.1800E 03
0.1016E 01	0.0000E 00	0.7040E 00	0.0000E 00	0.1012E 01	0.1800E 03	0.4359E 00	0.1800E 03
0.6284E-02	0.0000E 00	0.2680E 00	0.1800E 03	0.5611E-16	0.1800E 03	0.1091E 00	0.1800E 03
0.2346E-02	0.1800E 03	0.7244E-02	0.1800E 03	0.6238E-01	0.0000E 00	0.2736E-01	0.0000E 00
0.3679E-02	0.1800E 03	0.1368E 00	0.0000E 00	0.3025E-16	0.0000E 00	0.5237E-01	0.0000E 00
0.3534E-02	0.1800E 03	0.2343E-01	0.1800E 03	0.6379E-14	0.1800E 03	0.1003E 01	0.1800E 03

E-VECTOR 5		E-VECTOR 6		E-VECTOR 7		E-VECTOR 8	
0.1800E 00	-0.9030E 02	0.1800E 00	0.9030E 02	0.7642E 00	-0.1573E 03	0.7642E 00	0.1573E 03
0.7072E 00	-0.4567E 02	0.7072E 00	0.4567E 02	0.1213E-01	0.1913E 02	0.1213E-01	-0.1913E 02
0.1815E 00	0.9453E 02	0.1815E 00	-0.9453E 02	0.7427E 00	0.2235E 02	0.7427E 00	-0.2235E 02
0.6882E 00	0.1382E 03	0.6882E 00	-0.1382E 03	0.1183E-01	-0.1608E 03	0.1183E-01	0.1608E 03
0.1216E-01	-0.1595E 03	0.1216E-01	0.1595E 03	0.1217E-01	-0.3720E 02	0.1217E-01	0.3720E 02
0.6425E-02	-0.1744E 02	0.6425E-02	0.1744E 02	0.5479E-02	-0.1471E 03	0.5479E-02	0.1471E 03
0.5855E-02	0.1266E 02	0.5855E-02	-0.1266E 02	0.5432E-02	-0.1503E 03	0.5432E-02	0.1503E 03
0.9796E-02	-0.1636E 02	0.9796E-02	0.1636E 02	0.8256E-02	-0.1471E 03	0.8256E-02	0.1471E 03

INPUT-MODE COUPLING MATRIX IN POLAR COORDINATES:

0.1426E 03	-0.1800E 03	0.1683E 03	-0.1800E 03	0.1834E 02	0.3034E-12	0.2846E 03	0.5927E-13
0.6250E 01	0.1800E 03	0.2371E 01	0.1617E-12	0.1361E 02	-0.2756E-12	0.6812E 01	-0.4783E-13
0.6906E 01	-0.1800E 03	0.2314E-12	-0.3491E 01	0.2989E 02	0.791UE-14	0.5215E 01	0.1563E-12
0.6666E 00	-0.1709E-13	0.6386E-01	-0.1800E 03	0.2853E 01	0.1800E 03	0.5537E 00	0.1800E 03
0.1196E 03	-0.1707E 03	0.9842E 02	0.1090E 03	0.6450E 01	-0.8041E 02	0.4402E 02	0.5774E 02
0.1196E 03	0.1707E 03	0.9842E 02	-0.1090E 03	0.6450E 01	0.8041E 02	0.4402E 02	-0.5774E 02
0.1680E 03	0.1794E 03	0.3140E 02	-0.4056E 02	0.1743E 03	-0.1741E 01	0.8164E 01	0.4004E 02
0.1680E 03	-0.1794E 03	0.3140E 02	0.4056E 02	0.1743E 03	0.1741E 01	0.8164E 01	-0.4004E 02
0.7412E 02	-0.1800E 03	0.6935E 02	-0.9307E-17	0.1158E 02	-0.1800E 03	0.1936E 00	0.1800E 03
0.7604E 01	0.1800E 03	0.3607E 01	-0.1800E 03	0.6736E 01	0.2986E-13	0.3920E 00	-0.8001E-14
0.2215E 02	-0.1800E 03	0.3842E 01	-0.1614E-14	0.7489E 00	-0.1806E 03	0.5146E 00	0.0000E 00
0.2051E 01	0.0000E 00	0.1158E 01	0.9418E-15	0.1573E-01	0.1806E 03	0.1008E 01	-0.1800E 03
0.5234E 02	-0.1717E 03	0.7045E 02	0.1170E 02	0.4712E 01	-0.1433E 03	0.1260E 00	-0.5047E 02
0.5234E 02	0.1717E 03	0.7045E 02	-0.1170E 02	0.4712E 01	0.1433E 03	0.1260E 00	0.5047E 02
0.8396E 03	0.6808E 02	0.2694E 01	0.7996E 02	0.8419E 02	0.6490E 02	0.2903E 00	-0.6169E 02
0.8396E 03	-0.6808E 02	0.2694E 01	-0.7996E 02	0.8419E 02	-0.6490E 02	0.2903E 00	0.6169E 02

TABLE 4.6

MOTOR DRIVE WITH CONSTANT V/HZ CONTROL,CLOSED LOOP

OPERATING POINT VALUES:	FREQUENCY(HZ)	VOLTAGE(VOLTS)	SPEED(RPM)	TORQUE(NM)
	8.67	19.4	100.0	20.74

OPERATING POINT CURRENTS:			E-VALUES,REAL	E-VALUES,IMAG.	BREAK FREQUENCY(HZ)	DAMPING
STATOR 1	16.24	1	-73.39	0.00	11.68	1.00
STATOR 2	-8.54	2	-251.80	0.00	40.07	1.00
ROTOR 1	-17.51	3	-0.00	0.00	0.00	1.00
ROTOR 2	-0.31	4	-6.34	0.00	1.01	1.00
		5	-6.93	-30.96	5.05	0.22
		6	-6.93	30.96	5.05	0.22
		7	-678.98	-1207.46	220.47	.49
		8	-678.98	1207.46	220.47	0.49

E-VECTORS IN POLAR COORDINATES:

E-VECTOR 1		E-VECTOR 2		E-VECTOR 3		E-VECTOR 4	
0.8217E 00	0.0000E 00	0.7264E-01	0.0000E 00	0.4679E 00	0.0000E 00	0.2762E 00	0.1800E 03
0.4572E 00	0.1800E 03	0.1000E 01	0.1800E 03	0.1000E 01	0.0000E 00	0.5231E 00	0.1800E 03
0.8734E 00	0.1800E 03	0.7699E-01	0.1800E 03	0.1715E-01	0.0000E 00	0.2194E-01	0.0000E 00
0.4899E 00	0.0000E 00	0.1009E 01	0.0000E 00	0.9597E 00	0.1800E 03	0.5012E 00	0.0000E 00
0.2470E 00	0.1800E 03	0.2262E-02	0.0000E 00	0.1946E-16	0.0000E 00	0.1102E 00	0.0000E 00
0.1058E-01	0.1800E 03	0.9513E-03	0.1800E 03	0.5482E-01	0.0000E 00	0.2831E-01	0.1800E 03
0.1258E 00	0.0000E 00	0.1374E-02	0.1800E 03	0.9920E-17	0.1800E 03	0.5289E-01	0.1800E 03
0.2839E-01	0.1800E 03	0.1436E-02	0.1800E 03	0.6544E-15	0.1800E 03	0.1014E 01	0.0000E 00

E-VECTOR 5		E-VECTOR 6		E-VECTOR 7		E-VECTOR 8	
0.7558E 00	-0.8512E 01	0.7558E 00	0.8512E 01	0.8394E 00	-0.1676E 03	0.8394E 00	0.1676E 03
0.1668E 00	-0.1647E 03	0.1668E 00	0.1647E 03	0.1054E-01	-0.3037E 02	0.1054E-01	0.3037E 02
0.6843E 00	0.1360E 03	0.6843E 00	-0.1360E 03	0.8157E 00	0.1203E 02	0.8157E 00	-0.1203E 02
0.4371E 00	-0.2594E 02	0.4371E 00	0.2594E 02	0.1022E-01	0.1497E 03	0.1022E-01	-0.1497E 03
0.1561E-01	0.1661E 03	0.1561E-01	-0.1661E 03	0.1394E-01	-0.4860E 02	0.1394E-01	0.4860E 02
0.1903E-01	0.7932E 02	0.1903E-01	-0.7932E 02	0.6058E-02	-0.1578E 03	0.6058E-02	0.1578E 03
0.7496E-02	-0.1237E 02	0.7496E-02	0.1237E 02	0.5993E-02	-0.1610E 03	0.5993E-02	0.1610E 03
0.3074E-01	0.6836E 02	0.3074E-01	-0.6836E 02	0.9126E-02	-0.1578E 03	0.9126E-02	0.1578E 03

INPUT-MODE COUPLING MATRIX IN POLAR COORDINATES:

0.1752E 02	-0.1800E 03	0.4160E 01	-0.1800E 03	0.1540E 02	0.1534E-12	0.4275E 01	-0.1721E-12
0.5040E 02	0.1800E 03	0.2306E 03	0.1800E 03	0.3071E 02	-0.2037E-12	0.2347E 03	-0.1488E-13
0.4919E 02	0.1800E 03	0.1113E-11	0.1779E 03	0.3505E 02	-0.1715E-12	0.1426E 02	-0.2099E-12
0.4318E 01	0.1800E 03	0.1664E 00	0.1800E 03	0.2967E 01	-0.7812E-13	0.1148E 01	-0.1182E-12
0.2718E 02	-0.3506E 02	0.1436E 02	0.4083E 02	0.4060E 01	-0.1693E 03	0.8091E 01	0.7484E 02
0.2718E 02	0.3506E 02	0.1436E 02	-0.4083E 02	0.4060E 01	0.1693E 03	0.8091E 01	-0.7484E 02
0.1518E 03	-0.1727E 03	0.3208E 01	-0.1217E 03	0.1563E 03	0.7431E 01	0.2185E 02	0.1744E 02
0.1518E 03	0.1727E 03	0.3208E 01	0.1217E 03	0.1563E 03	-0.7431E 01	0.2185E 02	-0.1744E 02
0.1171E 02	-0.1800E 03	0.1904E 01	0.3532E-13	0.7419E 01	-0.3141E-13	0.4475E 03	0.0900E 03
0.2620E 02	0.1800E 03	0.3076E 02	-0.3146E-15	0.3279E 01	-0.1800E 03	0.4531E-01	-0.1800E 03
0.3984E 02	-0.1800E 03	0.2736E 02	-0.1172E-14	0.9696E 00	-0.1800E 03	0.6663E 00	0.9243E-15
0.3354E 01	-0.1800E 03	0.8811E 00	-0.6540E-15	0.1408E-01	-0.1784E-11	0.1004E 01	0.9770E-16
0.1199E 02	-0.3143E 02	0.1520E 02	0.1435E 03	0.3817E 00	-0.1010E 03	0.5292E-01	0.1687E 03
0.1199E 02	0.3143E 02	0.1520E 02	-0.1435E 03	0.3817E 00	0.1010E 03	0.5292E-01	-0.1687E 03
0.7351E 03	-0.7832E 02	0.7779E-01	-0.2360E 01	0.7354E 02	0.7519E 02	0.2551E 00	-0.5333E 02
0.7351E 03	-0.7832E 02	0.7779E-01	0.2360E 01	0.7354E 02	-0.7519E 02	0.2551E 00	0.5333E 02

is zero, showing that this mode does not appear at all in the speed response. This situation was fully discussed in Part I, when commenting on the drive step response. While the explanation presented there was based on the physical arguments, the unobservability of the monotonically increasing mode here becomes obvious, since the mmf phase angle ψ was chosen as one of the drive states. Due to this, the integrator associated with the angle ψ was included in the system structure, resulting in one eigenvalue at the origin. The corresponding eigenvector component, reflecting the previously explained physical principles, has to be zero to decouple the speed from this mode and thus from a particular reference frame. Note that this mode is coupled into all four motor currents, in agreement with the previous discussion.

The results given in Fig. 4.14 and Tables 4.4, 4.5 and 4.6 are good starting points in the drive dynamic analysis. However, the eigenvalue loci are insufficient to conclude anything about the drive practical performance, while the eigenvector and coupling matrix results are difficult to interpret. The alternative methods are the study of the drive transfer functions or the computation of the speed time response.

STEP 2: The drive transfer functions

The two transfer functions of interest are:

1) $G_1(s)$ - Speed-input reference

2) $G_2(s)$ - Speed-load torque

These two transfer functions can be obtained at each operating point by using the computer results from the previous step and the equation (3-32).

1) Speed-input reference transfer function

From equation (4-15d) the speed reference signal, V_r, appears in four drive inputs. Define now a new variable vector [UV] ; such that:

$$[U] = [UV]\,\delta V_r \qquad (4\text{-}18)$$

The torque variations, δT_L, are of course set to zero. The value of [UV]

components is obtained from equation (4-15d):

$$uv_1 = A_1 A_3 A_c a/k_c \tag{4-19a}$$

$$uv_2 = uv_3 = uv_4 = uv_5 = 0 \tag{4-19b}$$

$$uv_6 = A_3 A_c a/k_c \tag{4-19c}$$

$$uv_7 = 1/d \tag{4-19d}$$

$$uv_8 = a A_c \tag{4-19e}$$

From equations (3-26) and (4-15d) the expression for the speed is:

$$y(s) = \sum_{k=1}^{8} \frac{m_{5k} h_{k1}}{s-\lambda_k} u_1(s) + \sum_{j=6}^{8} \sum_{k=1}^{8} \frac{m_{5k} h_{kj}}{s-\lambda_k} u_j(s)$$

After dividing both sides by $\delta V_r(s)$, the speed-input reference transfer function is obtained as:

$$G_1(s) = \frac{y(s)}{\delta V_r(s)} = \sum_{j=1}^{8} \sum_{k=1}^{8} \frac{m_{5k} h_{kj}}{s-\lambda_k} (uv_j) \tag{4-20}$$

If desired, the last expression can be written in the physically realizable form, analogous to the equation (4-3) in Part I. When the appropriate values from Tables 4.4, 4.5 and 4.6 are used in equation (4-20), $G_1(s)$ is obtained at corresponding operating points. Its Bode diagrams are displayed in Figures 4.15b, 4.16b and 4.17b. As expected, the identical results were obtained from the Laplace transform of the drive state equations. These diagrams will be discussed in detail in the next step.

2) Speed-load torque transfer functions

The load torque appears only in the drive mechanical equation. Applying equation (3-32) and dividing both sides by δT_L the desired transfer function is:

$$G_2(s) = \frac{y(s)}{\delta T_L} = \sum_{k=1}^{8} \frac{m_{5k} h_{k5}}{s-\lambda_k} \qquad (4\text{-}21)$$

When the results from Tables 4.4, 4.5 and 4.6 are inserted into the last equation, $G_2(s)$ is obtained at corresponding operating points. Although these results, displayed as Bode diagrams in Fig. 4.18b, 4.19b and 4.20b, are adequate to assess the influence of a load on the drive speed, the additional physical insight is obtained by applying the Direct Method.

The drive reduced system consists of controller 1 and the motor decoupled electrical system. The decoupled electrical system is independent of the drive structure and is consequently identical to that of the open-loop drive. Controller 1 has only one state, $\delta\psi$, and is, therefore, described by a single equation:

$$s\delta\psi = (1-a A_c/k_c)n\delta\omega_m \quad A_3 A_c a \delta V_r/k_c$$

Obviously, controller 1 has only one pole, placed at the origin:

$$s = z_5 = 0$$

The poles of the reduced system are, therefore, given by:

$$s \prod_{j=1}^{4} (s-z_j) = 0 \qquad (4\text{-}22)$$

where z_j's are the eigenvalues of the decoupled system.

From equation (4-13) the poles of the speed controller are:

$$z_6 = 0 \qquad (4\text{-}23)$$

$$z_7 = -1/d$$

They obviously do not depend on the drive operating point.

The eigenvalues of the reduced system and speed controller which

OPERATING POINT	ZEROS OF $G_2(s)$	BREAK FREQUENCY (hz)	DAMPING
1700 rpm	$z_{1/2} = -174.0 \pm j68.2$	29.75	0.931
	$z_{3/4} = -89.9 \pm j329.6$	54.39	0.263
	$z_{5/6} = 0$	0	-
	$z_7 = -1175.4$	187.1	1.0
800 rpm	$z_{1/2} = -232.1 \pm j78.9$	59.0	0.947
	$z_{3/4} = -31.8 \pm j28.9$	21.4	0.237
	$z_{5/6} = 0$	0.0	-
	$z_7 = -1175.4$	187.1	1.0
100 rpm	$z_{1/2} = -259.5 \pm j28.9$	41.56	0.99
	$z_{3/4} = -4.4 \pm j33.9$	5.45	0.128
	$z_{5/6} = 0$	0	-
	$z_7 = -1175.4$	187.1	1.0

TABLE 4.7: Zeros of the speed-torque transfer function for the constant V/hz closed loop drive calculated by using the Direct Method.

represent the zeros of $G_2(s)$ are grouped together in Table 4.7:

Note that all z_j's which correspond to the electrical decoupled system are identical to those obtained for the open-loop drive, Tables 4.1, 4.2 and 4.4.

Using Theorem 2. and equations (4-22) and (4-23) the speed-torque transfer function is:

$$G_2(s) = \frac{s^2(s+1/d) \prod_{j=1}^{4} (s-z_j)}{J_T \prod_{k=1}^{8} (s - \lambda_k)} \qquad (4\text{-}24)$$

Equation (4-24) is only another form of the equation (4-21). They both denote the same physical relationship between speed and load.

A few comments can be made regarding the last expression:

1) The near perfect cancellation of all electrical eigenvalues and zeros is not possible as they now differ considerably, (Tables 4.4, 4.5, 4.6 and 4.7). This indicates a stronger electromechanical coupling of the closed loop drive. The corresponding Bode plots indeed confirm this. Evidently, the simplified form of $G_2(s)$, given by (3-51) cannot be used.

2) The only cancellation occurs for the pole and the zero (z_5) in the origin. They both represent the same eigenvalue which belongs to the controller 1, and which integrates the mmf phase angle ψ. This cancellation was expected, since the motor speed is independent of the reference frame. Consequently, the integrator cannot be present in the speed expression, as discussed in Step 3 of Part I. This unobservability is evident in the time domain from the computer results (Tables 4.4, 4.5 and 4.6), where the corresponding eigenvector component, m_{53}, is zero. Equation (4-24) states the same fact analytically. The identical analytical result would have been observed in Part I, had the angle $\delta\psi$ been made the drive state.

3) The second zero (z_6) in the origin represents the integrator of the speed controller. It provides an infinite around-the-loop dc gain

and thus isolates completely the steady state speed from the load disturbance. (Note that $G_2(0)=0$). In other words, this integrator assures zero steady state speed error. Thus, by properly changing the forward transfer function, $G_1(s)$, one can always modify the output impedance, $G_2(s)$, as desired and vice versa. This is a well known fact in the design of two port networks and could be applied to the design of electric drives, since the Direct Method provides an analytical expression for the drive output impedance.

4) Out of the seven zeros, three are independent of the drive operating point. This is expected since both controllers have a fixed structure.

It is seen from this discussion that the output impedance $G_2(s)$ is significantly affected when the speed loop is closed. The effect of the controller is best understood by looking at the corresponding step and frequency response.

STEP 3: Step and frequency response

This part of the analysis is the most interesting one, since both responses give the ultimate understanding of the drive dynamic performance.

The speed responses to unit steps in the speed reference V_r and load torque T_L are calculated and displayed graphically, together with the drive frequency response. As explained earlier, the step response to any of two inputs is obtained in two stages: The modal response is computed first, following which the speed is found as the combination of modal states.

1) Response to a unit step in speed reference

The motor load is constant and equal to the rated load. From the equation (4-15d) the reference δV_r appears in four drive inputs. With a unit step in δV_r these inputs become:

$$[U] = [UV]$$

where the components of [UV] vector are defined by (4-19).

The response of each modal state to unit step in δV_r is given by

equation (3-24):

$$q_k(t) = \int_0^t e^{\lambda_k(t-\tau)} h_{k1}(UV_1)d\tau + \sum_{j=6}^{8} \int_0^t e^{\lambda_k(t-\tau)} h_{kj}(UV_j)d\tau$$

$$k = 1 \ldots 8$$

when solved, this gives:

$$q_k(t) = (h_{k1}(UV_1) + \sum_{j=6}^{8} h_{kj}(UV_j)) (e^{\lambda_k t}-1)/\lambda_k \qquad (3\text{-}25)$$

For the special case of the eigenvalue at the origin the last equation becomes:

$$q_3(t) = t(h_{31}(UV_1) + \sum_{j=6}^{8} h_{3j}(UV_j))$$

Equations (3-25) and (3-26) give the speed response as:

$$y(t) = \sum_{k=1}^{8} m_{5k}\, q_k(t)$$

However, as seen before, the eigenvector component $m_{53}=0$, so that the third modal state is unobservable in the speed output. Therefore:

$$y(t) = \sum_{\substack{k=1 \\ k\neq 3}}^{8} m_{5k} (h_{k1}(UV_1) + \sum_{j=6}^{8} h_{kj}(UV_j)) (e^{\lambda_k t}-1)/\lambda_k \qquad (4\text{-}26)$$

The speed response to the unit step in the input reference is calculated at each operating point when the appropriate values from Table 4.4, 4.5 or 4.6 are inserted into the last equation. The results are plotted and presented in Figures 4.15a, 4.16a and 4.17a. The $G_1(s)$ frequency response, obtained from equation (4-20) is presented for comparison in Figures 4.15b, 4.16b and 4.17b. A brief discussion of these results follows:

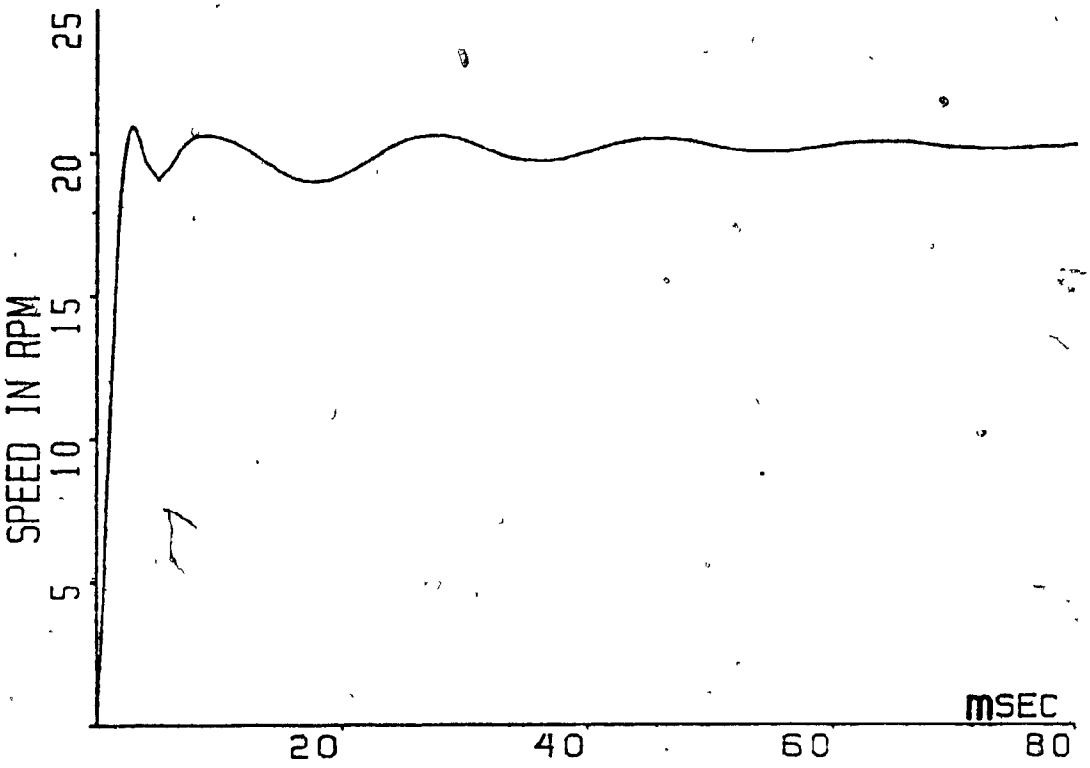

Fig. 4.15a: Speed response to step reference at 1700 rpm.

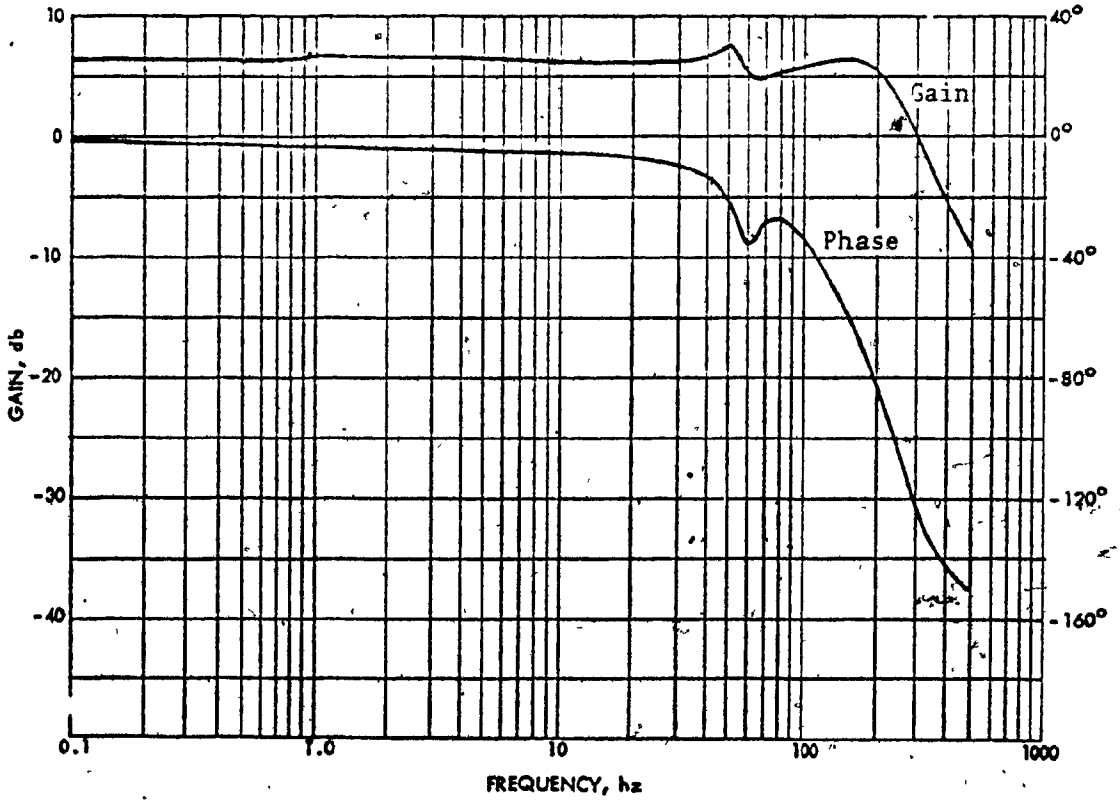

Fig. 4.15b: Frequency response of speed-input reference transfer function at 1700 rpm.

At 60 hz, the speed step response (Fig. 4.15a) has a rise time of 1.5 msec. The settling time, (±5% of the steady state value), is only slightly longer: 2.1 msec. These results represent 2.5% and 2.4% of the respective values for the open-loop drive and give a measure of the improvement in the speed transient response. The short rise time is in a good agreement with the $G_1(s)$ bandwidth of approximately 250 hz (Fig. 4.15b). The step response appears as that of a second order system. The overshoot is less than 5%, corresponding to a gain peak of 160 hz (Fig. 4.15b). As this peak is not very pronounced, the speed oscillations related to it die out quickly, and are replaced by damped oscillations at 50 hz, which are small and entirely contained in the 5% steady state speed band. The speed steady state value is 20 rpm, corresponding to the $G_1(s)$ dc gain of 6.4 db.

At 800 rpm the speed step response is essentially unchanged (Fig. 4.16a). The drive bandwidth (Fig. 4.16b), and consequently the rise time are the same. The gain peak on the Bode plot has shifted now to 25 hz so that the frequency of oscillations in the step response is halved. The speed steady state value is of course unchanged since the feedback gain of 6.4 db is constant.

At 100 rpm the speed rise time is unchanged (Fig. 4.17a). The overshoot is slightly larger, but still less than 7%. It corresponds to a small increase of the gain peak on the Bode plot (Fig. 4.17b). The speed recovers from the subsequent undershoot asymptotically, without any oscillations In this respect, the operation at 100 rpm is superior to those of 1700 and 800 rpm. Note how misleading can be the conclusion about speed response if based only on the drive eigenvalues. The results in Fig. 4.14 would indicate a deteriorating dynamic performance with a decrease in the operating speed.

It is seen from this discussion that the speed response is indeed improved when the feedback loop is closed. The most important change is achieved at the 100 rpm operating point. The conclusion about the performance of the constant V/hz drives is given in the summary, following the analysis of the speed response to the load disturbance.

2) Speed response to a unit step in the load torque

With a unit step in the load torque the only drive input is:

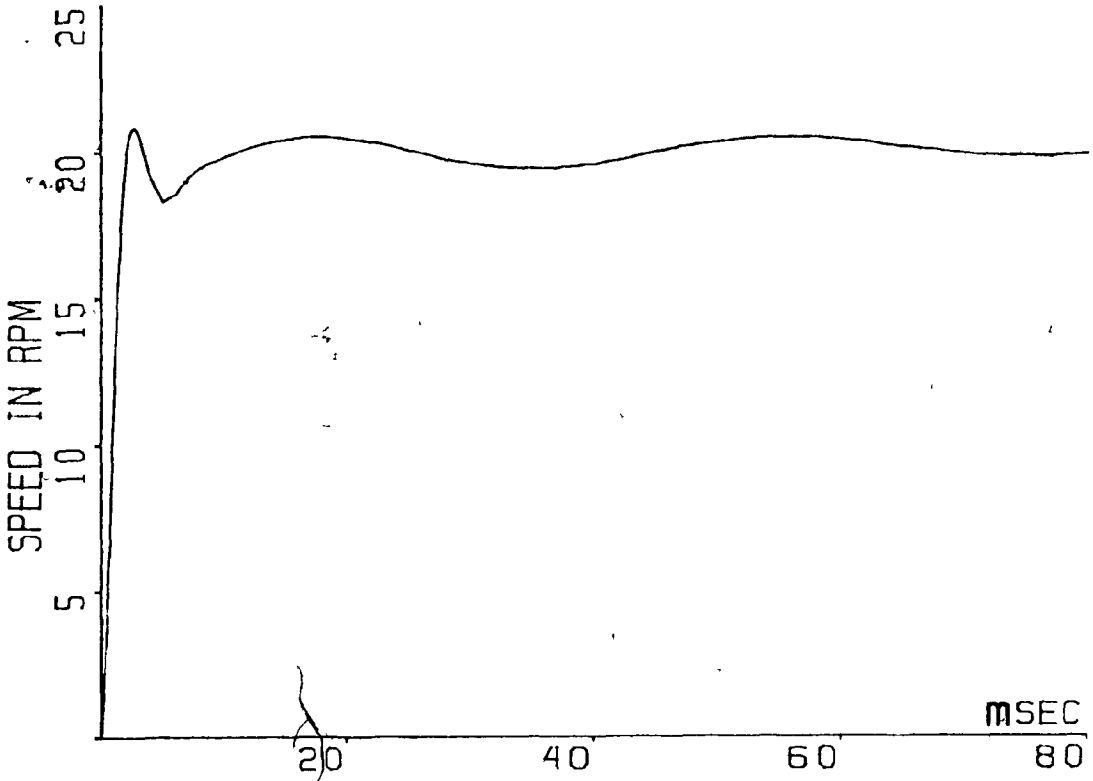

Fig. 4.16a: Speed response to step reference at 800 rpm

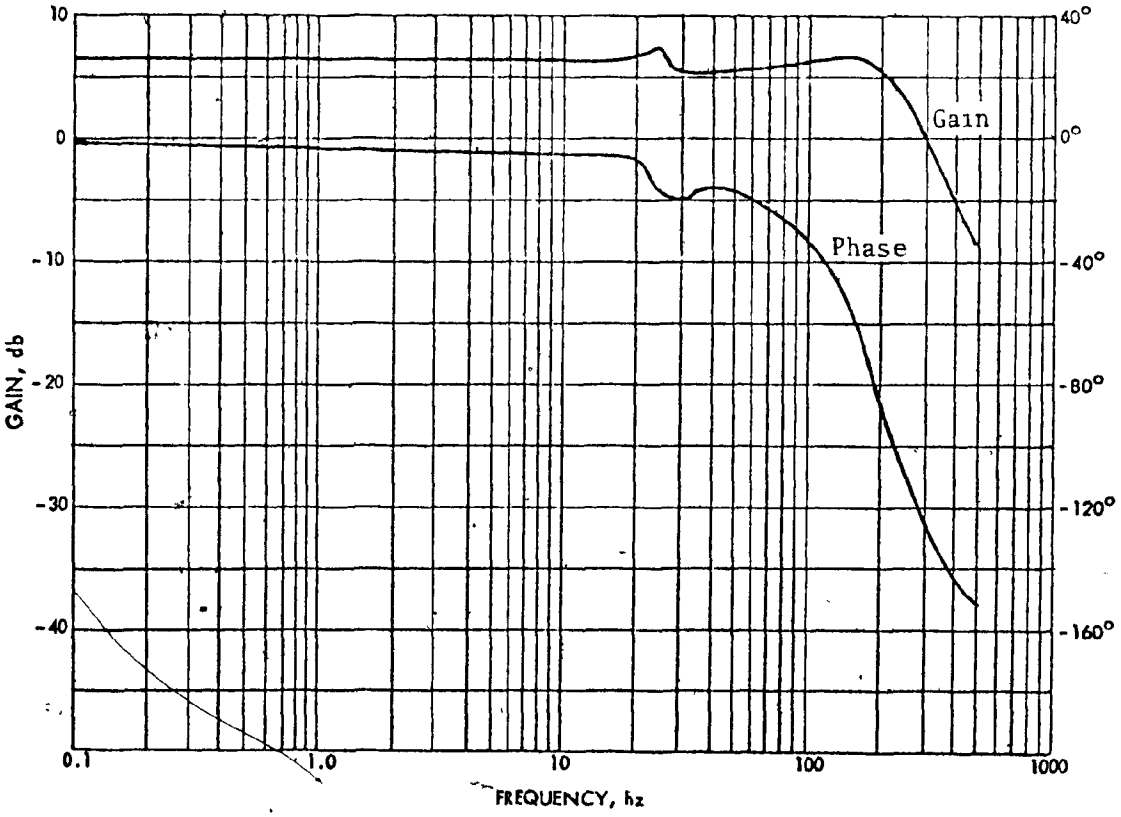

Fig. 4.16b: Frequency response of speed-input reference transfer function at 800 rpm.

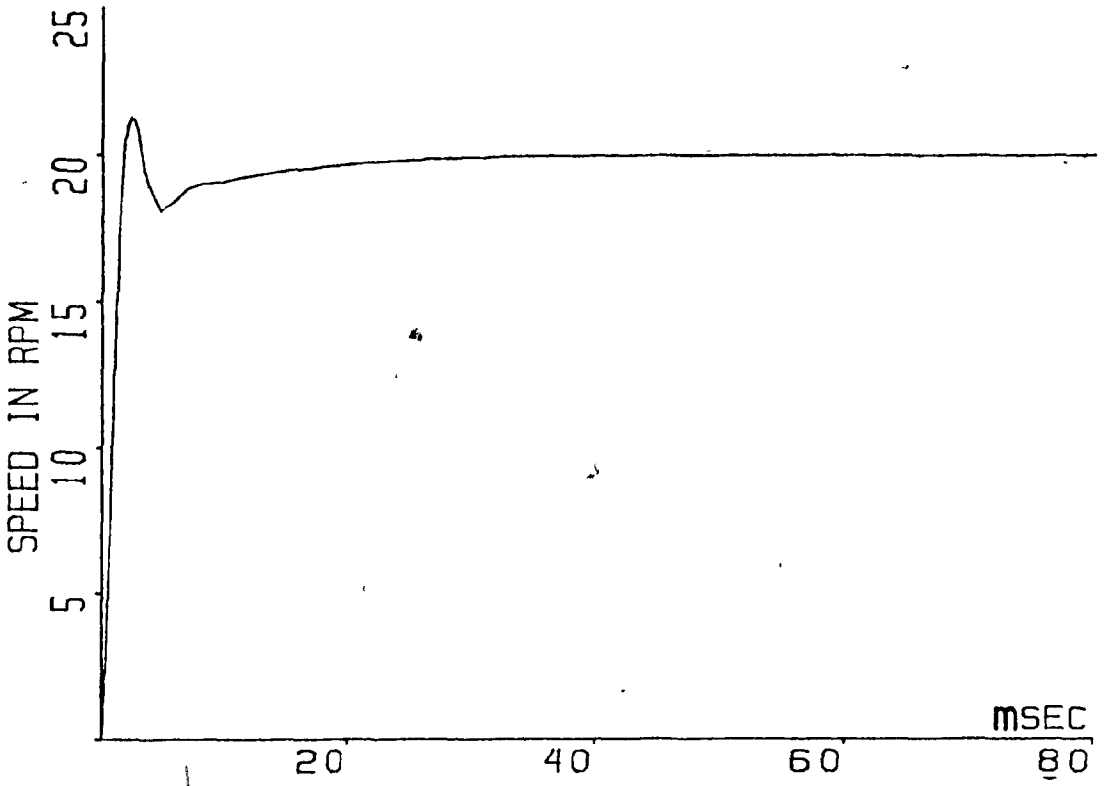

Fig. 4.17a: Speed response to step reference at 100 rpm.

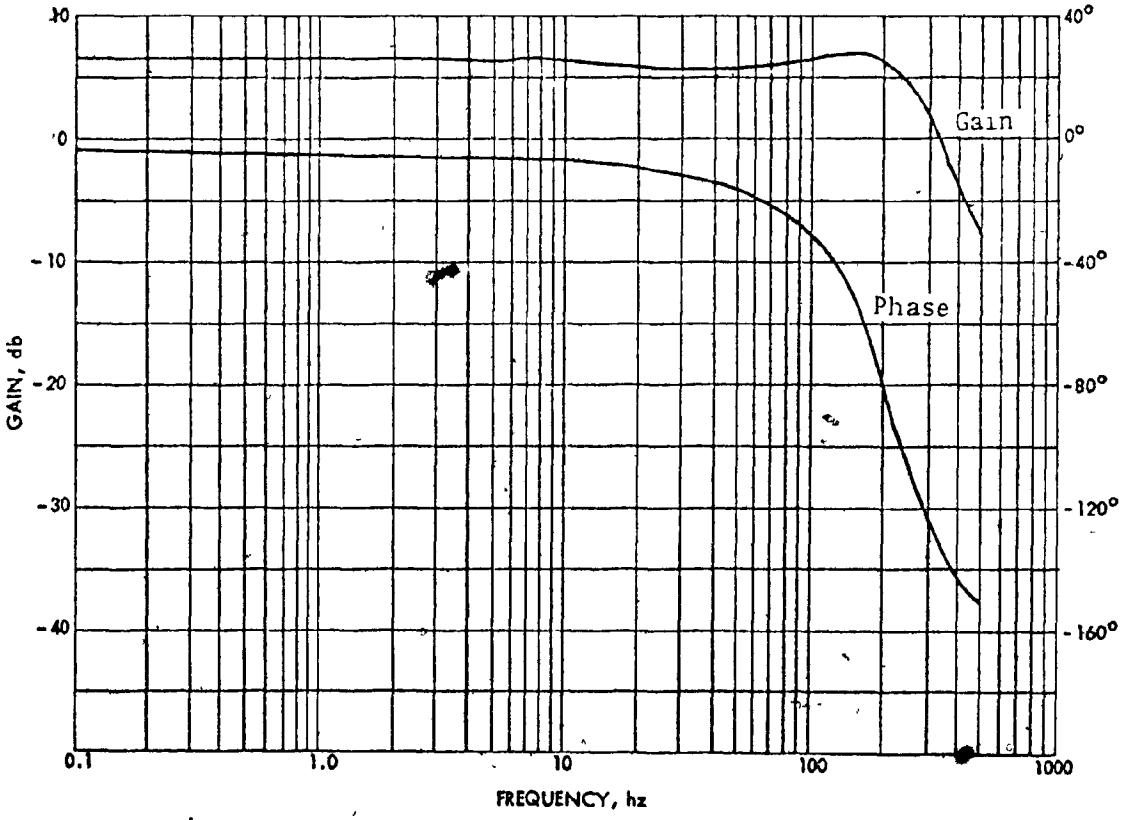

Fig. 4.17b: Frequency response of speed-input reference transfer function at 100 rpm.

$$U_5(t) = 1$$

All other inputs are zero, since the speed reference is constant (4-15d). The modal states are then, from (3-24):

$$q_k(t) = \int_0^t e^{\lambda_k (t-\tau)} h_{k5} \, d\tau \quad , \quad k = 1 \ldots 8$$

When solved this gives:

$$q_k(t) = (e^{\lambda_k t} - 1) \, h_{k5}/\lambda_k \tag{4-27}$$

For the special case of the eigenvalue at the origin, the third modal state becomes:

$$q_3(t) = t \, h_{35}$$

The speed response is obtained by using equations (3-25) and (3-26). However, since the m_{53} element in the eigenvector matrix is zero, the third modal state, $q_3(t)$, is unobserveable. Thus:

$$y(t) = \sum_{\substack{k=1 \\ k\neq 3}}^{8} \frac{m_{5k} \, h_{k5}}{\lambda_k} \, (e^{\lambda_k t} - 1) \tag{4-28}$$

The last expression gives the speed response to the unit step in the torque disturbance. The sum of terms $m_{5k}h_{k5}/\lambda_k$ defines the speed-torque coupling in the steady state. From the analytic expression for $G_2(s)$, equation (4-24), it is obvious that this sum must be zero, due to the integrator in the speed controller. Consequently, the steady state speed is independent of the load torque.

When the appropriate values from Tables 4.4, 4.5 and 4.6 are used in equation (4-28), the speed response at the corresponding operating points is obtained and displayed graphically in Fig. 4-18a, 4.19a and 4.20a. The frequency response of $G_2(s)$ is presented for comparison in Fig. 4.18b, 4.19b and 4.20b.

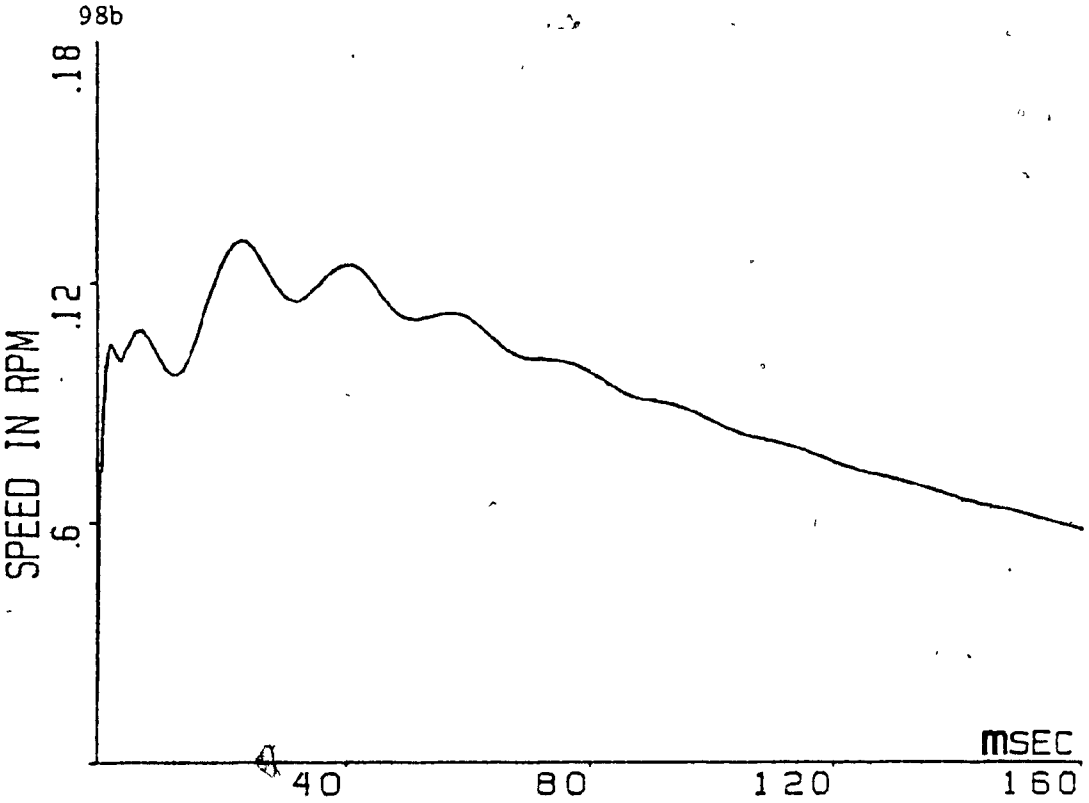

Fig. 4.18a: Speed response to step torque at 1700 rpm.

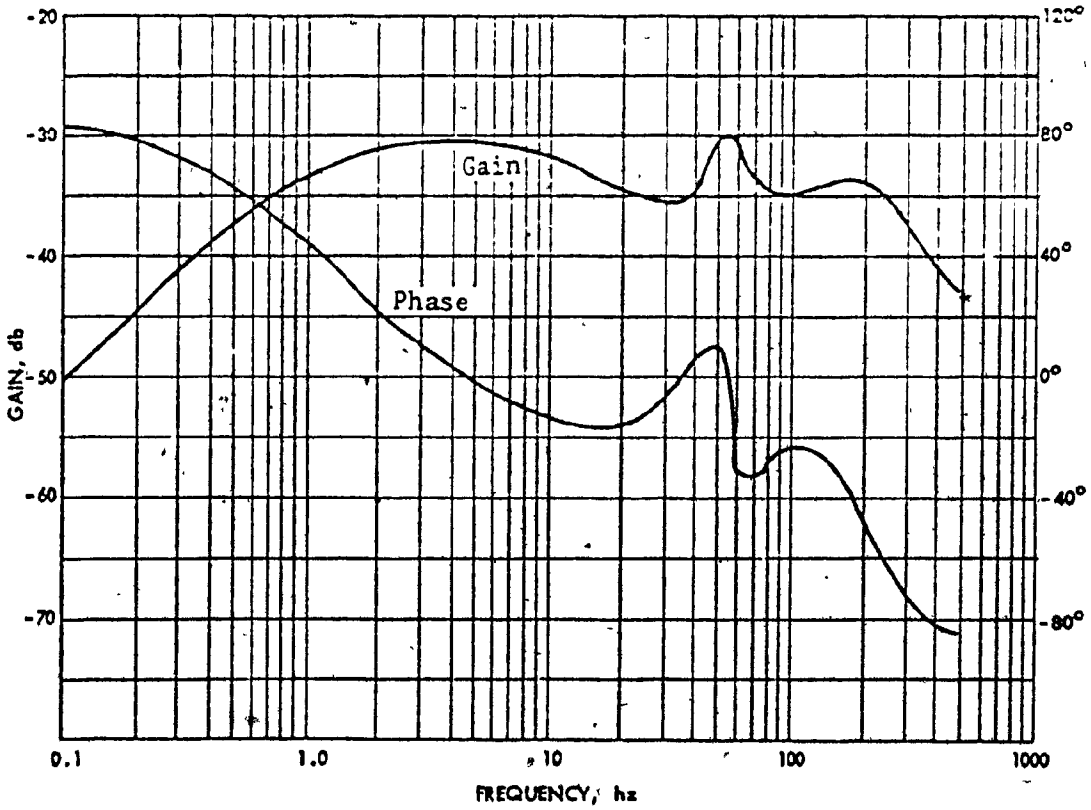

Fig. 4.18b: Frequency response of speed-torque transfer function at 1700 rpm.

When analyzing the motor speed response to load disturbance, one has to keep in mind that it represents a speed error, since the reference, V_r, has not changed. Therefore, what is important is not the speed rise time but its peak and final values, and its settling time.

At 1700 rpm the speed response appears distinctively underdamped (Fig. 4-18a). The main oscillating component has a period of 20 msec. However, to obtain a correct picture, one has to look at the magnitude of the speed change. The response shows, that for 1 N-m step in torque, the maximum change in speed is 0.26 rpm. Furthermore, the largest magnitude of the main oscillating component is only 0.06 rpm. Thus, although the response is underdamped, the speed oscillations are so small that they can usually be neglected.

More information is available from the corresponding Bode plot (Fig. 4.18b). The very attenuated speed-torque coupling which is always below -30 db explains why the speed response (error) is so small. The main oscillating component corresponds to the small gain peaking at 55 hz, caused by an imperfect cancellation of the magnetizing eigenvalues, Tables 4.4 and 4.7. The first oscillating cycle, starting at 2.5 msec., is caused by a pair of complex conjugate eigenvalues, giving the break frequency of 212 hz. The same eigenvalue pair defines the bandwidth of the $G_1(s)$ transfer function. Physically, these eigenvalues determine the rate of change of motor current. Since the pair break frequency is so high, the motor electrical torque can rise very fast. For a step input in the reference signal, this means a very fast speed response. For a step in load disturbance this means a limited build-up of speed error since the electrical torque changes quickly to offset any load variation. Thus, the speed notch at 2.5 msec. in Fig. 4.18a represents the reaction of the electrical torque to an increasing speed error.

The Bode plot shows a steady decrease in a dc value of $G_2(s)$ as the frequency is decreased. The dc value becomes in fact zero, due to the integrator in the speed controller (4-24). Consequently, the steady state speed error has to go to zero. The speed response starts indeed to decrease, 40 msec. after the disturbance was applied. Since the integrator has a break at 1 hz, it will take approximately 0.48 sec. to reduce the speed to 5% of its maximum value (The exact time can be obtained from equation (4-28).

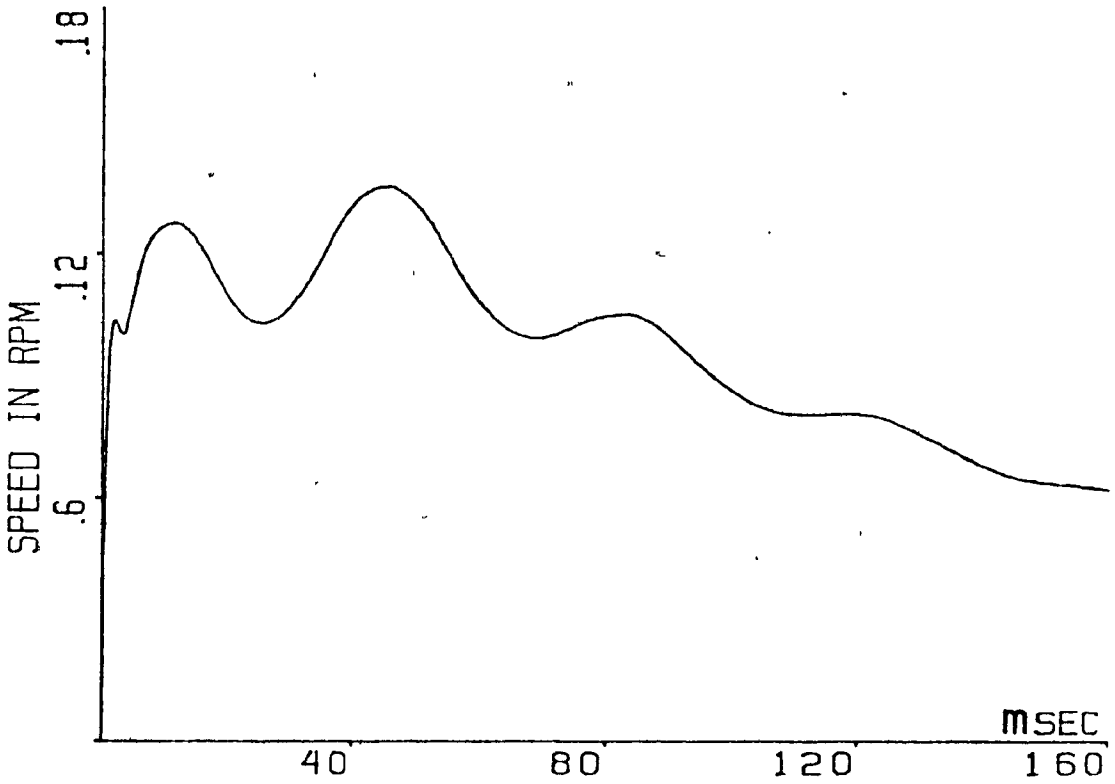

Fig. 4.19a: Speed response to step torque at 800 rpm.

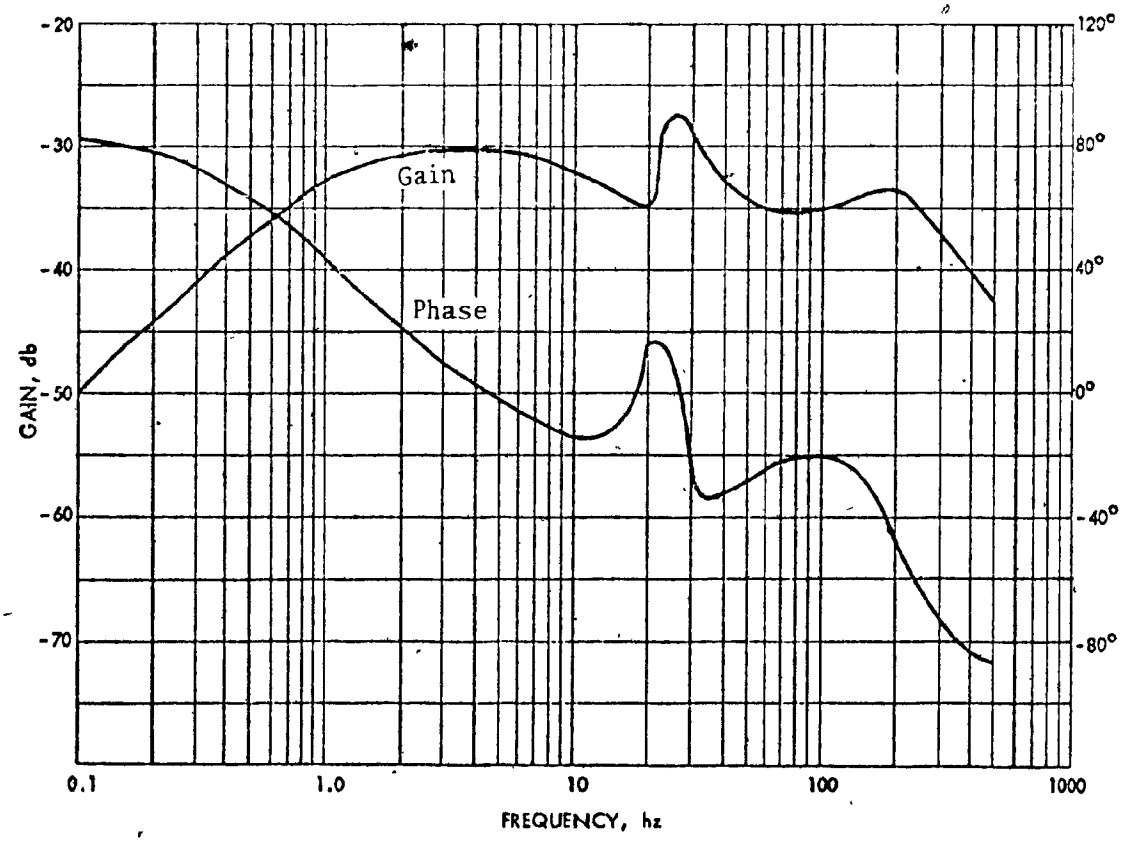

Fig. 4.19b: Frequency response of speed-torque transfer function at 800 rpm.

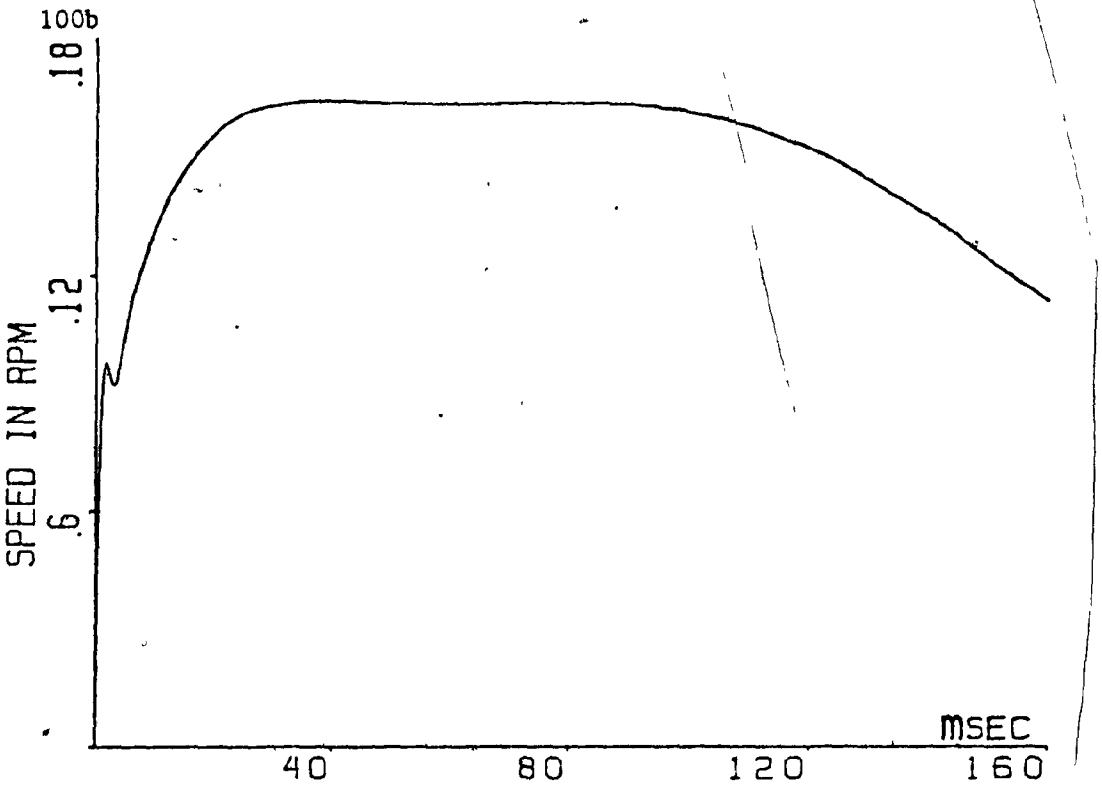

Fig. 4.20a: Speed response to step torque at 100 rpm.

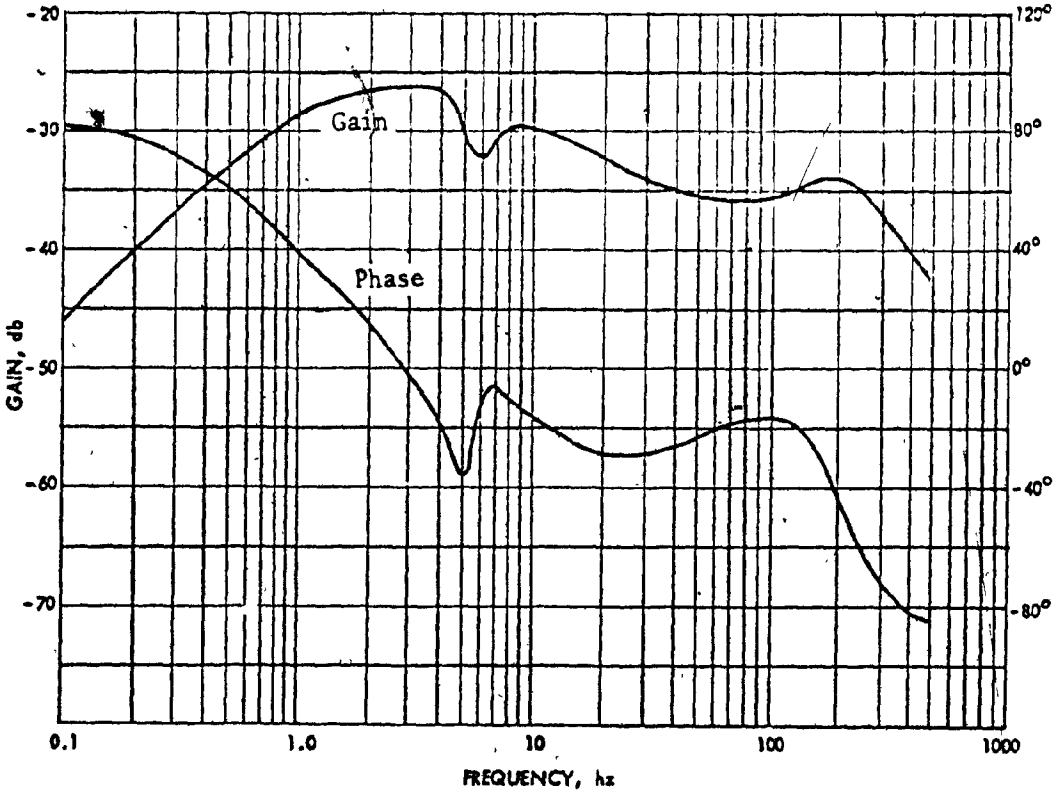

Fig. 4.20b: Frequency response of speed-torque transfer function at 100 rpm.

The brief summary of this analysis is:

1) The oscillations in the speed response can be tolerated since their magnitude is minute, not exceeding 0.06 rpm. Furthermore, all oscillations die out after 80 msec.

2) The maximum speed change is less than 0.26 rpm, making the speed practically insensitive to the load disturbance.

3) The speed error is decreased always to zero due to an integrator in the speed controller.

At 800 rpm the response is essentially unchanged (Fig. 4.19a). The only difference is in the frequency of the oscillating component, which is now at 25 hz, in agreement with the corresponding gain peak on the Bode plot (Fig. 4.19b). All other comments made previously, apply to these results.

At 100 rpm the speed response has only one oscillating cycle, which starts at 2.6 msec. (Fig. 4.20a). As explained, it corresponds to the corrective action of the motor electrical torque. The maximum value of speed change is now 0.326 rpm, 25% higher than before. This increase is caused by a reduction in the forward gain of the motor electrical system, which occurs at lower supply frequencies. This reduction is evident in the open-loop drive, where the $G_1(s)$ dc gain is decreased by 2.5 db at 5 hz supply frequency (figures 4.3b and 4.5b). Note that this decrease results in the corresponding increase in the value of $G_2(s)$, figures 4.6b and 4.8b . For closed loop drives this reduction cannot be seen in the forward $G_1(s)$, transfer function, since it is compensated by the speed controller. However, it still exists as demonstrated by an increase of 1-4 db in the $G_2(s)$ magnitude at 100 rpm operating point (Figures 4.18b and 4.20b, 1-4 hz range). Apart from these differences, all previous comments apply equally to this operating point.

Conclusion

The constant V/hz control strategy, applied to the open-loop drive, gives good dynamic characteristic for supply frequencies above 10 hz. The speed response is fast enough to satisfy most industrial process requirements

while the sensitivity to load disturbances is medium (Note that these conclusions are made for the motor with a high rotor winding resistance. Squirrel cage motors, normally used with variable frequency supplies would have better electromechanical coupling and thus lower speed-torque sensitivity).

Below 10 hz, the open-loop drive exhibits a decrease in the forward loop gain, which results in poor speed response and an increase in the speed sensitivity to load variations. Consequently, the open-loop operation becomes unsuitable for all but most elementary speed regulations in the 0-10 hz range.

If a better dynamic performance is desired, a closed loop drive has to be used. When properly compensated it offers the following advantages:

1) The undesirable speed behaviour at low supply frequencies is eliminated and the drive has a uniform dynamic characteristic over the whole 0 - 60 hz range. In addition to this, it can be shown that the $G_1(s)$ transfer function bandwidth changes very little with the load. For example, at the 800 rpm operating point, it varies from 220 hz at 20% to 205 hz at 220% of the rated load. This means that the speed response is practically independent of the operating point.

2) The speed response is more than forty times faster than in the open-loop drive.

3) The speed has become practically insensitive to the load perturbations.

These results indicate that the closed loop, constant V/hz control is theoretically capable of giving a very high performance drive. In practice, three factors will limit the drive bandwidth and thus the speed of response:

1) The need to filter the high frequency noise in the speed feedback signal.

2) The need to limit the slip speed so that the maximum motor torque is not exceeded.

3) The bandwidth of the drive power source.

More is said about these limitations in Chapter V.

4.3 Constant slip speed control.

Drive Description

It was demonstrated in Chapter II that the motor output torque depends linearly on the slip speed and quadratically on the airgap flux. This section discusses a drive where the slip speed is approximately constant. The output torque is controlled by the airgap flux (ie., applied voltage), while the motor speed is regulated by the applied frequency. This means that the motor voltage and frequency do not form any fixed relationship, as in the constant V/Hz drives, but are manipulated independently

The constant slip speed drive is presented in Fig. 4.21, where $A_3=n/k_t$, n being the number of pole pairs while k_t is the tachogenerator constant. All other power elements are assumed to have unity transfer functions.

The inverter frequency reference is obtained by adding a preset slip speed to the actual motor speed. This then assures constant slip speed operation.

The reference input, V_r, determines the applied motor voltage and, thus, the airgap flux and the motor electrical torque. This torque interacts via slip speed with the applied frequency and, therefore, controls the motor speed. The limiting element prevents sudden large changes in the motor voltage.

To illustrate this principle, consider a drive operation at ω_1 rad/sec. and a constant load. If the input reference is now changed to request ω_2 rad/sec., where $\omega_2 > \omega_1$, the speed error $e = \omega_2 - \omega_1$ is created, the motor voltage is increased, resulting in a higher electrical torque and the motor starts to accelerate. The increase in the motor speed drives the inverter output frequency up, so that a constant slip speed is maintained. If the speed error e is large enough, the element L will saturate. As the motor speed increases, the speed error decreases and the limiter L eventually comes out of saturation. With $e \cong 0$ the motor has arrived at a new, ω_2, operating point, which has the same slip speed as before.

A similar analysis can be made for a deceleration request or for load variations with the speed reference constant. Note that in this latter case

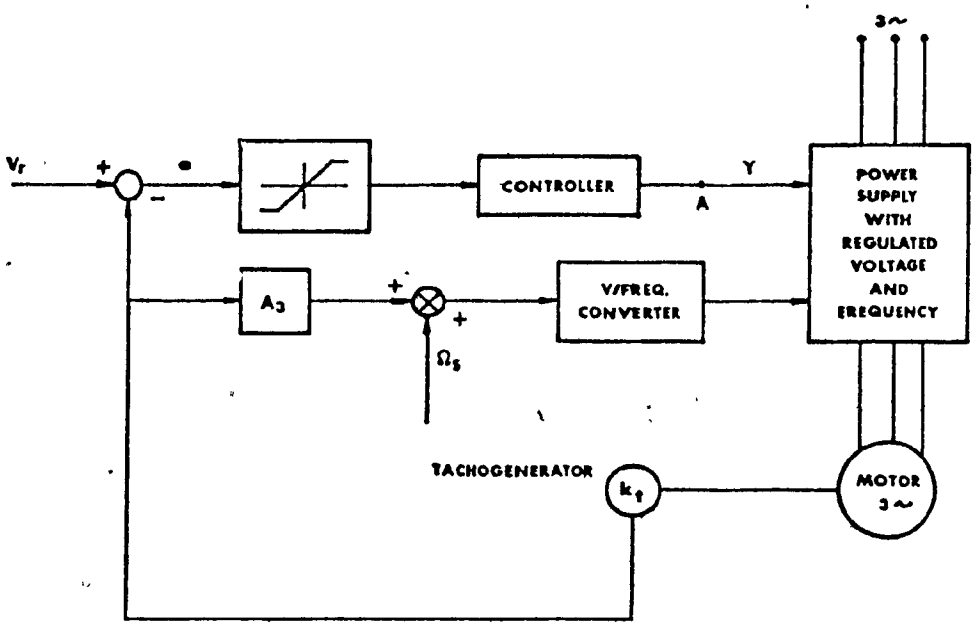

Fig. 4.21: Constant slip speed drive.

the inverter frequency will change during the transient, so as to preserve the constant slip speed, but will assume the same steady state value it had prior to the load perturbation. Thus, the speed is maintained solely by the change in the motor voltage. In this respect, the operation is similar to that of constant frequency, variable voltage induction motors. It is illustrated in Fig. 4.22 using motor static torque-speed curves.

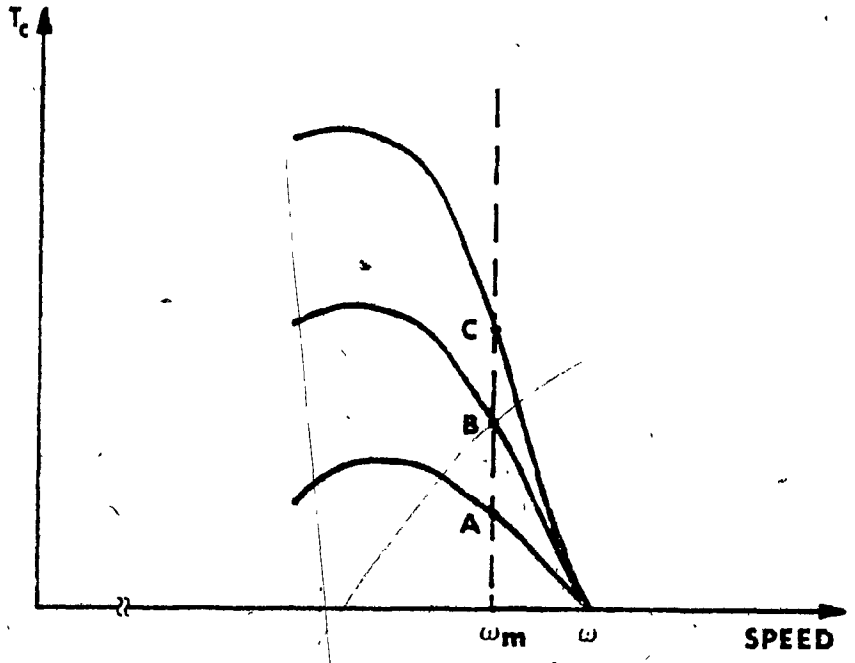

Fig. 4.22: Trajectory of an operating point with changing load: Only the motor voltage is changed to maintain the constant speed ω_m as the load is increased. The steady state value of slip speed is the same for each operating point (A, B, or C).

One can see that if motor stable operation is desired, it is essential that the voltage loop be faster than the positive feedback frequency loop.

Controller design

Before analyzing the drive dynamic behaviour, it is necessary to determine the structure of its speed controller. This is done by considering the drive open loop frequency response. If the voltage loop is broken at point A, Fig. 4.21, with signal Y being the input and speed being the output, the feedback equations are:

$$\omega = A_3 k_t \omega_m + \Omega_s$$

$$V = Y$$

When perturbed, these equations become:

$$\delta\omega = p\delta\psi = pX_6 = n\delta\omega_m \qquad (4\text{-}29a)$$

$$\delta V = \delta Y \qquad (4\text{-}29b)$$

where the already defined value for the gain A_3 was used and where the new state $\delta\psi$ represents the change in the phase angle of the airgap mmf vector, as defined in Fig. 3.1.

When the last two equations are combined with the basic motor equations (3-10) and (3-11) the open-loop drive equations are:

$$[P_o]\dot{X} = [Q_o]X + U \qquad (4\text{-}30)$$

where,

$$P_o = \begin{bmatrix} [L] & 0 & 0 \\ 0 & J_T & 0 \\ 0 & 0 & 1 \end{bmatrix} \qquad (4\text{-}31a)$$

$$Q_o = \begin{bmatrix} -R_1 & \Omega L_1 & 0 & \Omega M & 0 & 0 \\ -\Omega L_1 & -R_1 & -\Omega M & 0 & 0 & V \\ 0 & \Omega_s M & -R_2 & \Omega_s L_2 & -n(MI_2+L_2I_4) & 0 \\ -\Omega_s M & 0 & -\Omega_s L_2 & -R_2 & n(MI_1+L_2I_3) & 0 \\ -nMI_4 & nMI_3 & nMI_2 & -nMI_1 & -f_T & 0 \\ 0 & 0 & 0 & 0 & n & o \end{bmatrix} \qquad (4\text{-}31b)$$

and

$$U = \begin{bmatrix} \delta Y \\ 0 \\ 0 \\ 0 \\ -\delta T_L \\ 0 \end{bmatrix} \qquad (4\text{-}31c)$$

The desired open-loop frequency response is obtained by applying equation (3-30) to equation (4-30), with the constant, rated load. The results at four operating points (1700, 800, 400 and 100 rpm) are plotted in Figures 4.23a, b, c and d. Here, an exception is made in presenting four operating points in order to illustrate the pronounced change in the drive dynamics as the operating speed is changed.

The following conclusions are made from the drive open-loop response:

1) A very pronounced decrease, followed by peaking in the loop gain

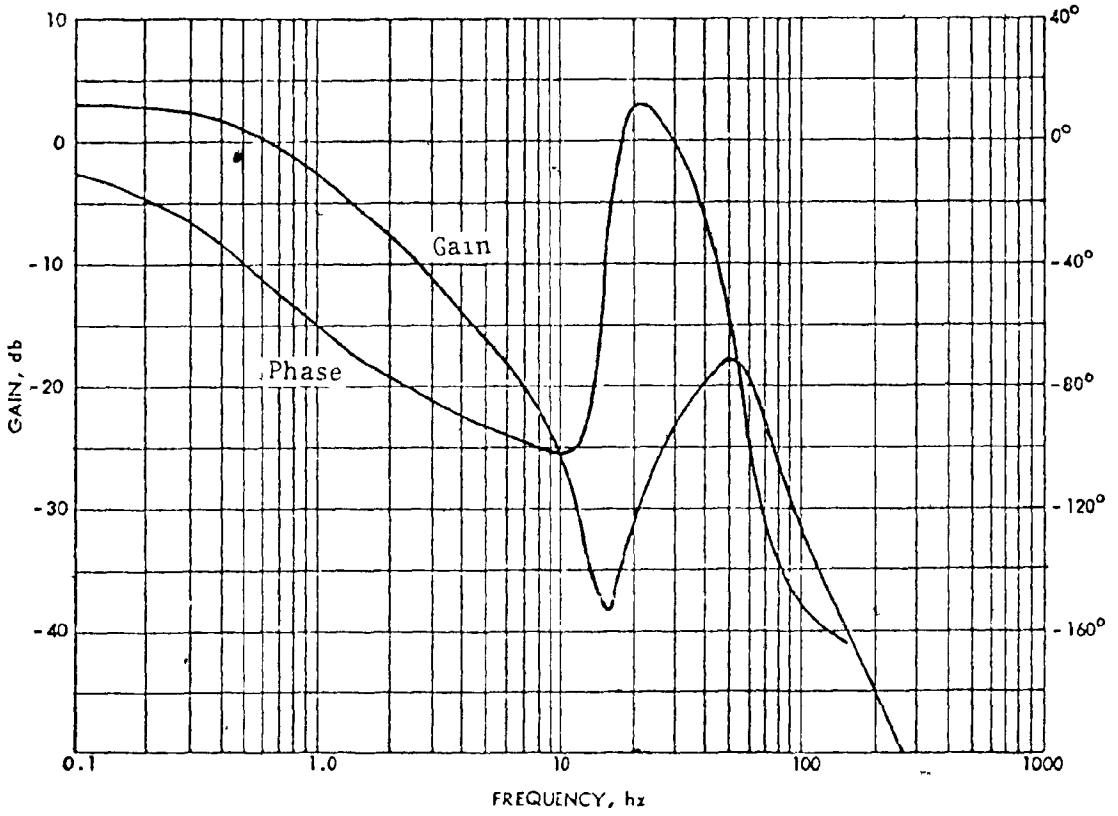

Fig. 4.23a. Frequency response of the open loop system at 1700 rpm.

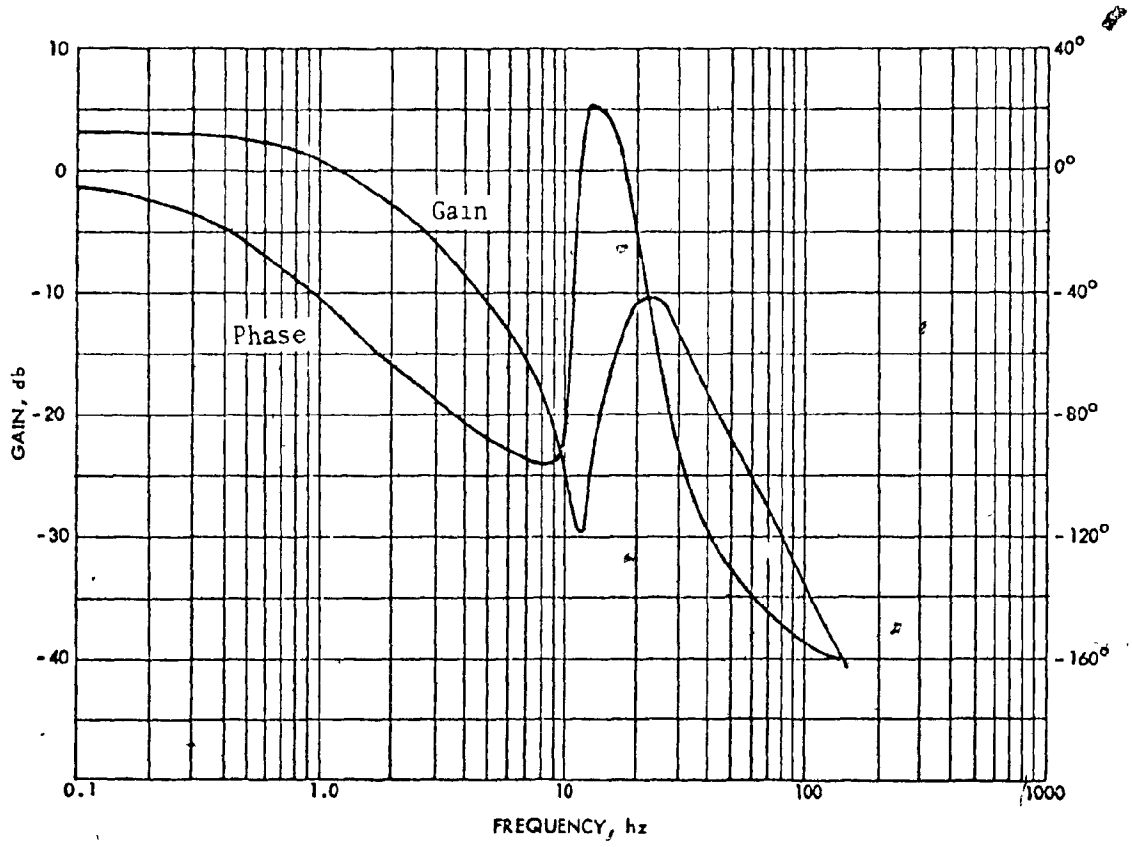

Fig. 4.23b: Frequency response of the open loop system at 800 rpm.

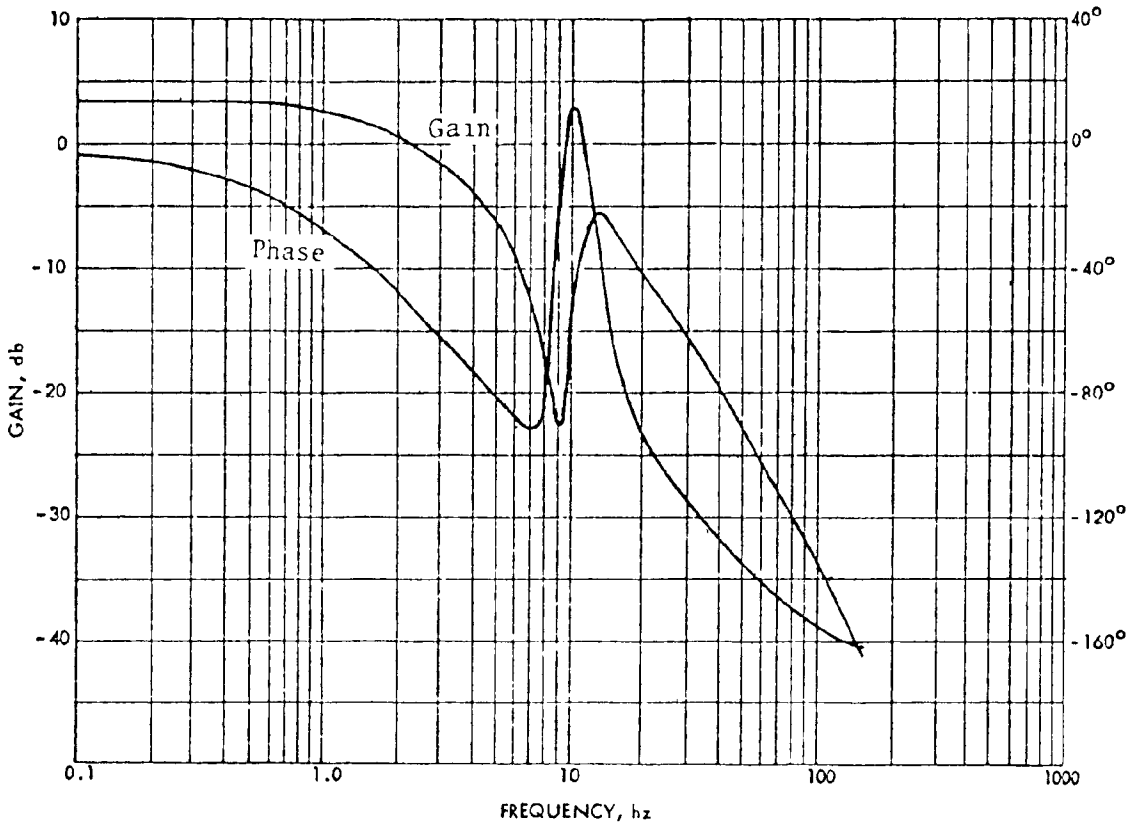

Fig. 4.23c: Frequency response of the open loop system at 400 rpm.

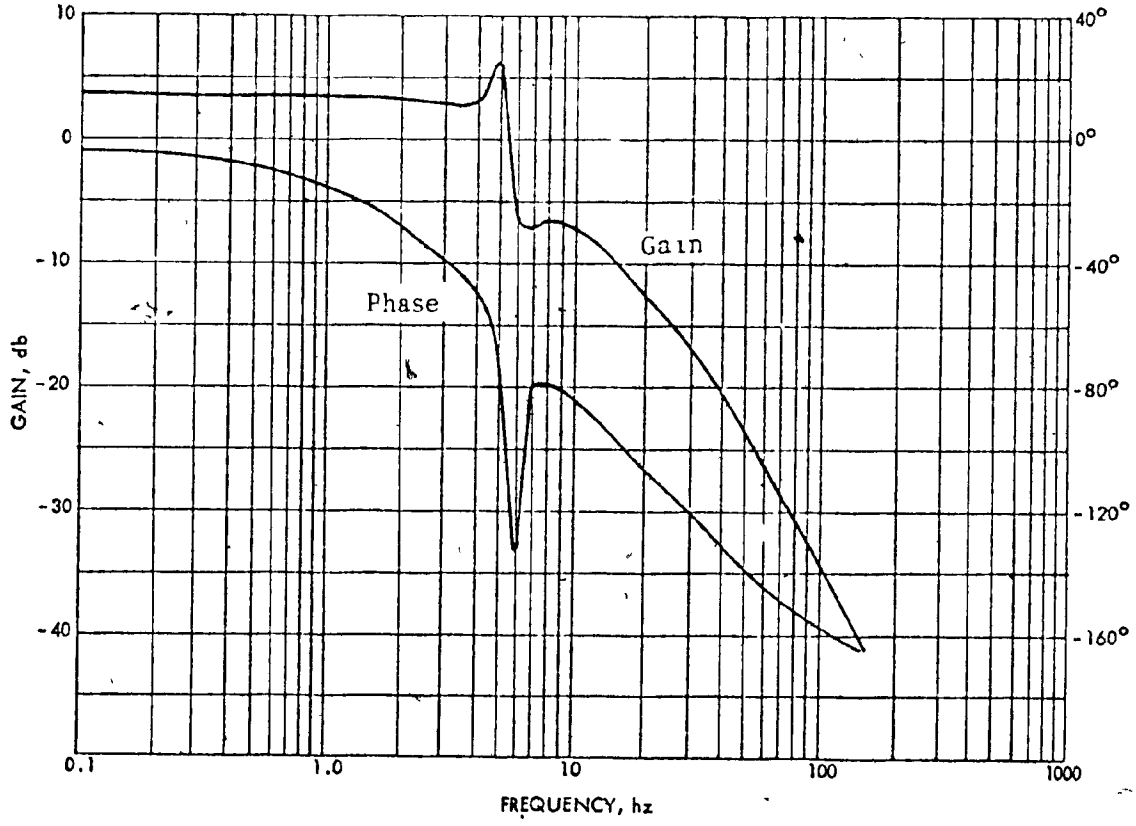

Fig. 4.23d: Frequency response of the open loop system at 100 rpm.

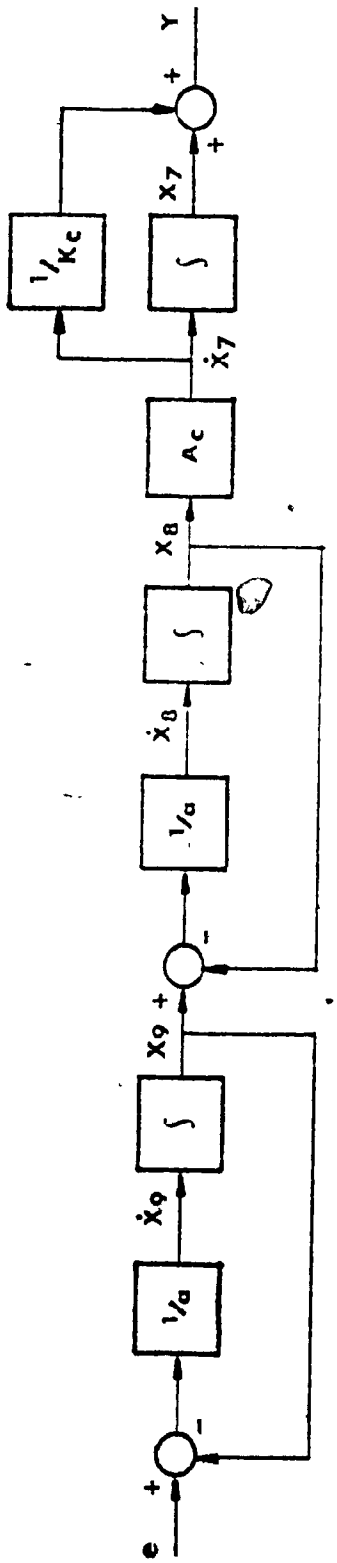

Fig. 4.24: Speed controller for the constant slip speed drive.

requires a controller with compensating network.

2) The frequency at which the drecrease in the loop gain occurs, changes with the motor speed. Thus, any attempt to smooth it out with phase lead or inverted twin-T networks at one operating point will only accentuate the gain peaking at another. Consider, for example, that the controller is chosen to compensate the drive at 1700 rpm (Fig. 4.23a). The resulting controller gain peaking in 10-20 hz region will then only add to the already existing gain peak at 400 rpm operating point (Fig. 4.23c).

3) Considering fixed structure controllers, the only choice left is to attenuate sufficiently all gain peaks by using a phase-lag network with low controller gain. Obviously, this will cut significantly the drive closed loop bandwidth.

As the result of this discussion, the controller transfer function is chosen as:

$$\frac{\delta Y}{\delta e} = T_c(s) = \frac{A_c}{(1+as)^2} \quad \frac{s/k_c+1}{s} \tag{4-32}$$

The numerical values are:

$$k_c = 3.1416; \qquad a = 0.08; \qquad A_c = k_c/k_t$$

The controller consists of the double phase-lag network, (two real poles at 1.83 hz, giving an additional - 40 db roll-off), integrator with the break at 0.5 hz ($k = 3.1416$) and the gain A_c which results in the unity around the loop gain.

The controller structure is given in Fig. 4.24; it should be considered in the context of Fig. 4.21.

With the controller specified, drive close loop equations can be established. If the three controller states are defined in the standard way, as the outputs of the integrators in Fig. 4.23, the controller state equations

are:

$$\dot{x}_7 = A_c\, x_8 \tag{4-33a}$$

$$\dot{x}_8 = x_9/a - x_8/a \tag{4-33b}$$

$$\dot{x}_9 = \delta V_r/a - k_t\, \delta w_m/a - x_9/a \tag{4-33c}$$

since $e = \delta V_r - k_t \delta w_m$

The controller output Y, representing the inverter voltage reference is:

$$\delta Y = x_7 + x_8/k_t \tag{4-34}$$

When the drive loop equation (4-30) is combined with controller equations (4-33) and (4-34), the constant slip speed, closed loop drive from Fig. 4 21 is described by:

$$[P]\,\dot{X} = [Q]\,X + U \tag{4-35}$$

The last equation defines the drive state A and input B matrices as:

$$[A] = [P]^{-1}[Q] \tag{4-36a}$$

$$[B] = [P]^{-1} \tag{4-36b}$$

where

$$[P]^{-1} = \begin{bmatrix} [L]^{-1} & 0 & 0 & 0 & 0 & 0 \\ 0 & 1/J_T & 0 & 0 & 0 & 0 \\ 0 & 0 & 1 & 0 & 0 & 0 \\ 0 & 0 & 0 & 1 & 0 & 0 \\ 0 & 0 & 0 & 0 & 1 & 0 \\ 0 & 0 & 0 & 0 & 0 & 1 \end{bmatrix} \tag{4-37a}$$

(the 4 x 4 matrix L^{-L} is defined by equation 3-15).

$$Q = \begin{bmatrix} -R-n\mathfrak{M}_m G-\Omega_c F & -nGI_{\gamma\delta} & V & 1 & 1/k_t & 0 \\ nI^T_{\gamma\delta}(G+\Theta^T) & -f_T & 0 & 0 & 0 & 0 \\ 0 & n & 0 & 0 & 0 & 0 \\ 0 & 0 & 0 & 0 & A_c & 0 \\ 0 & 0 & 0 & 0 & -1/a & 1/a \\ 0 & -k_t/a & 0 & 0 & 0 & -1/a \end{bmatrix} \quad (4\text{-}37b)$$

The upper 6 x 6 submatrix in (4-37b) is the matrix Q_o, defined by (4-31b). The elements 1 and $1/k_t$ appear in the first row of their corresponding 4 x 1 column vectors, all other remaining entries being zero.

The input vector in (4-35) is:

$$U = \begin{bmatrix} 0 \\ -\delta T_L \\ 0 \\ 0 \\ 0 \\ \delta V_r/a \end{bmatrix} \quad (4\text{-}37c)$$

The first element in (4-37c) represents a 4 x 1 zero vector.

Having established the drive state equations, the analysis of selected operating points (1700, 800 and 100 rpm) will be performed through

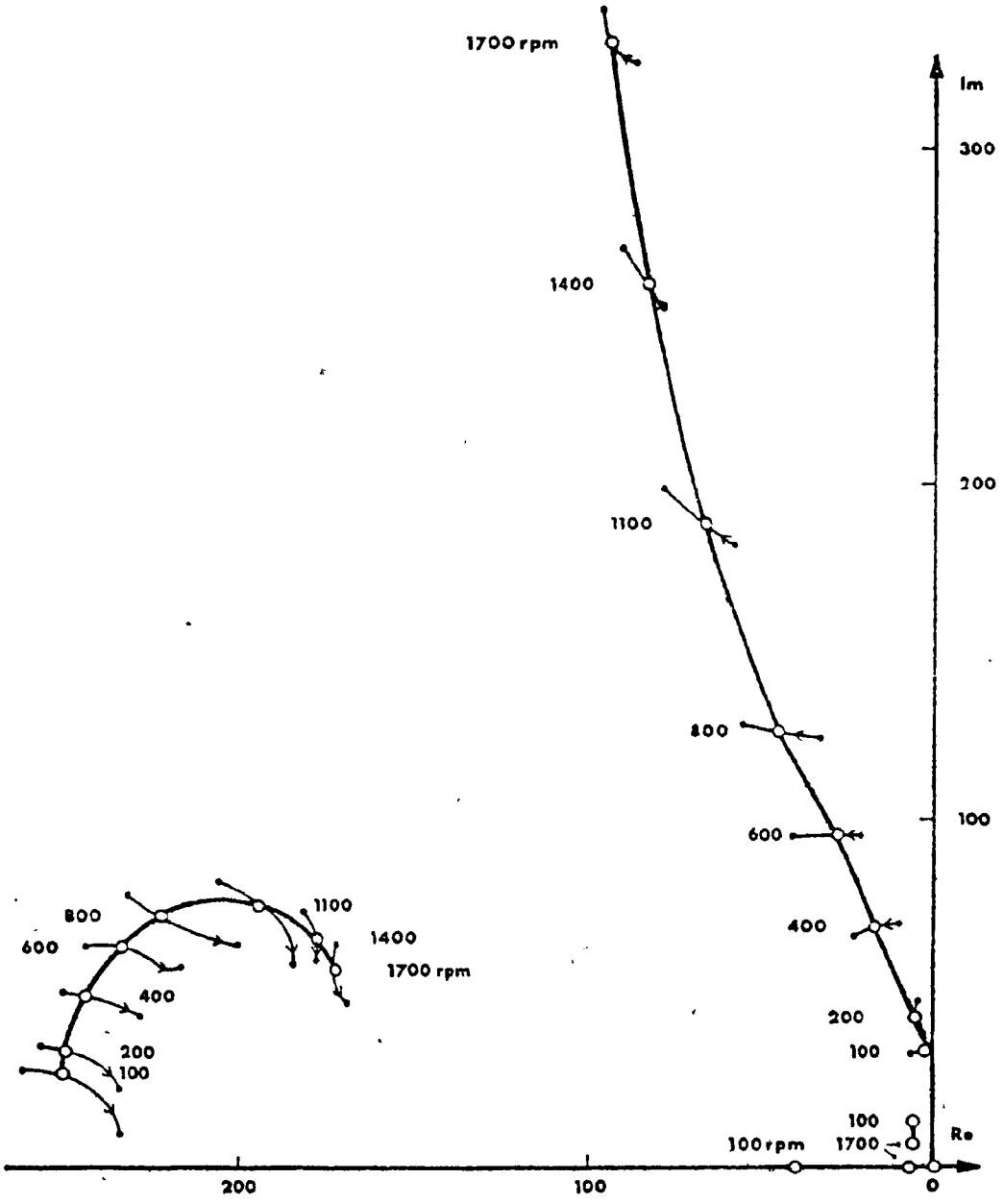

Fig. 4.25: Eigenvalue loci for constant slip speed drive. The effects of changing load are presented for selected motor speeds.

the steps already outlined:

STEP 1: Eigenvalues, eigenvectors and input-mode coupling matrix

The drive is studied at rated load and three different operating speeds. The computer results are presented in Tables 4.8, 4.9 and 4.10. The eigenvalue loci for a larger number of operating points and rated load are presented in Fig. 4.25. The effect of the load change is shown by a separate locus at each operating point (Fig. 4.25).

As explained earlier, the eigenvalue loci permit only the conclusion that the system is stable. The loci do not provide the information how stable it is, how sensitive it is to load and reference input changes or generally, what is the drive dynamic performance. The answers to these questions can be obtained from the input-mode and modal matrices, but they are not easily interpreted in the case of high order systems, when presented in an isolated form as Tables 4.8, 4.9 and 4.10 However, the results obtained in this step can be used to calculate either the drive transfer functions or its time response which are both easily understood.

STEP 2: The drive transfer functions

The two transfer functions of interest are:

1) $G_1(s)$: the speed-input reference

2) $G_2(s)$: the speed-load torque

They are obtained by applying the equations (3-32) to the results in Tables 4.8, 4.9 and 4.10.

1) The speed-input reference transfer function

From equation (4-37c) the speed reference signal V_r appears in only one drive input, $u_9(t)$. Applying equations (3-32) and dividing both sides with V_r, the desired transfer function is obtained as:

$$G_1(s) = \frac{y(s)}{\delta V_r(s)} = \sum_{k=1}^{9} \frac{m_{sk}\, h_{k9}}{a(s-\lambda_k)} \qquad (4\text{-}38)$$

TABLE 4.8

MOTOR DRIVE WITH CONSTANT SLIP SPEED CONTROL

OPERATING POINT VALUES:	FREQUENCY(HZ)	VOLTAGE(VOLTS)	SPEED(RPM)	TORQUE(NM)
	60.00	127.5	1700.0	17.56

OPERATING POINT CURRENTS:			E-VALUES.REAL	E-VALUES.IMAG.	BREAK FREQUENCY(HZ)	DAMPING
STATOR 1	15.67	1	-19.87	0.00	3.16	1.00
STATOR 2	-9.89	2	-2.90	0.00	0.46	1.00
ROTOR 1	-16.02	3	0.00	0.00	0.00	1.00
ROTOR 2	1.73	4	-3.05	6.22	1.10	0.44
		5	-3.05	-6.22	1.10	0.44
		6	-170.31	-59.09	28.69	0.94
		7	-170.31	59.09	28.69	0.94
		8	-91.70	338.20	55.77	0.26
		9	-91.70	-338.20	55.77	0.26

E-VECTORS IN POLAR COORDINATES:

E-VECTOR 1		E-VECTOR 2		E-VECTOR 3		E-VECTOR 4		E-VECTOR
0.8761E 00	0.1800E 03	0.6391E 00	0.0000E 00	0.6312E 00	0.0000E 00	0.5032E 00	-0.7983E 02	
0.1000E 01	0.1800E 03	0.1000E 01	0.0000E 00	0.1000E 01	0.0000E 00	0.8271E 00	-0.7624E 02	
0.4062E 00	0.0000E 00	0.1169E 00	0.1800E 03	0.1104E 00	0.1800E 03	0.7575E-01	0.8556E 02	
0.1143E 01	0.0000E 00	0.1025E 01	0.1800E 03	0.1022E 01	0.1800E 03	0.8365E 00	0.1029E 03	
0.5926E 00	0.0000E 00	0.9273E-01	0.1800E 03	0.2110E-15	0.1800E 03	0.1821E 00	0.3875E 02	
0.5959E-01	0.1800E 03	0.6399E-01	0.0000E 00	0.6381E-01	0.0000E 00	0.5262E-01	-0.7732E 02	
0.2694E 00	0.0000E 00	0.1704E 00	0.1800E 03	0.1383E-04	0.0000E 00	0.1008E 00	0.3595E 02	
0.8136E 00	0.1800E 03	0.7503E-01	0.0000E 00	0.2409E-19	0.0000E 00	0.1.62E 00	0.1520E 03	
0.4795E 00	0.0000E 00	0.5764E-01	0.0000E 00	0.6328E-17	0.1800E 03	0.9613E-01	-0.1746E 03	

E-VECTOR 5		E-VECTOR 6		E-VECTOR 7		E-VECTOR 8		E-VECTOR 9	
0.5032E 00	0.7983E 02	0.7822E 00	-0.1808E 02	0.7822E 00	0.1808E 02	0.7125E 00	-0.1279E 03	0.7125E 00	0.1279E 03
0.8271E 00	0.7624E 02	0.6996E 00	-0.1084E 03	0.6996E 00	0.1084E 03	0.7025E 00	-0.3791E 02	0.7025E 00	0.3791E 02
0.7575E-01	-0.8556E 02	0.7962E 00	0.1615E 03	0.7962E 00	-0.1615E 03	0.6970E 00	0.5372E 02	0.6970E 00	-0.5372E 02
0.8365E 00	-0.1029E 03	0.7185E 00	0.7091E 02	0.7185E 00	-0.7091E 02	0.6859E 00	0.1438E 03	0.6859E 00	-0.1438E 03
0.1823E 00	-0.3875E 02	0.9463E-01	0.1418E 03	0.9463E-01	-0.1418E 03	0.4077E-01	0.1236E 03	0.4077E-01	-0.1236E 03
0.5262E-01	0.7732E 02	0.1050E-02	-0.5733E 02	0.1050E-02	0.5733E 02	0.2327E-03	0.1840E 02	0.2327E-03	-0.1840E 02
0.1008E 00	-0.3595E 02	0.9075E-05	0.8162E 02	0.9075E-05	-0.8162E 02	0.4734E-06	-0.7964E 01	0.4734E-06	0.7964E 01
0.1062E 00	-0.1520E 03	0.2486E-03	-0.7925E 02	0.2486E-03	0.7925E 02	0.2521E-04	0.9721E 02	0.2521E-04	-0.9721E 02
0.9613E-01	0.1746E 03	0.3352E-02	0.1213E 03	0.3352E-02	-0.1213E 03	0.7005E-03	-0.1596E 03	0.7005E-03	0.1596E 03

INPUT-MODE COUPLING MATRIX IN POLAR COORDINATES:

0.1286E 01	0.6034E-11	0.4590E 00	-0.1800E 03	0.1099E 02	-0.1800E 03	0.2172E 01	0.1800E 03		
0.1451E 02	0.2078E-11	0.8011E 00	-0.1800E 03	0.1301E 03	-0.1800E 03	0.2040E 02	0.1800E 03		
0.7280E-12	-0.1229E 03	0.7283E-12	-0.1799E 03	0.4094E-11	0.8872E 01	0.1175E-12	-0.1601E 03		
0.1157E 02	-0.6008E 02	0.1534E 01	0.5647E 02	0.1041E 03	0.1203E 03	0.1636E 02	0.1154E 03		
0.1157E 02	0.6008E 02	0.1534E 01	-0.5647E 02	0.1041E 03	-0.1203E 03	0.1636E 02	-0.1154E 03		
0.9607E 02	0.1070E 03	0.8502E 02	-0.1651E 03	0.1808E 03	-0.1467E 03	0.2013E 03	-0.6176E 02		
0.9607E 02	-0.1070E 03	0.8502E 02	0.1651E 03	0.1808E 03	0.1467E 03	0.2013E 03	0.6176E 02		
0.1861E 03	0.1587E 03	0.1821E 03	0.6836E 02	0.5405E 02	0.7231E 02	0.5500E 02	-0.9573E 01		
0.1861E 03	-0.1587E 03	0.1821E 03	-0.6836E 02	0.5405E 02	-0.7231E 02	0.5500E 02	0.9573E 01		
0.6900E 01	-0.4034E-14	0.5102E 01	-0.1397E-12	0.1121E 00	-0.1800E 03	0.5329E 00	-0.1800E 03	0.9041E 00	0.1395E-13
0.8969E 02	-0.8393E-14	0.6104E 02	-0.1782E-12	0.8675E 01	0.1800E 03	0.4606E 00	0.1800E 03	0.5999E 00	0.1800E 03
0.4121E-11	0.1799E 03	0.1567E 02	-0.3515E-13	0.9975E 01	-0.9244E-15	0.5251E 01	0.1873E-14	0.5251E 01	0.2634E-14
0.7172E 02	-0.5780E 02	0.4886E 02	-0.5960E 02	0.2891E 01	-0.1762E 03	0.3330E 01	-0.1204E 03	0.3678E 01	-0.1538E 03
0.7172E 02	0.5780E 02	0.4886E 02	0.5960E 02	0.2891E 01	0.1762E 03	0.3330E 01	0.1204E 03	0.3678E 01	0.1538E 03
0.1218E 02	0.8860E 02	0.1042E 03	-0.4276E 01	0.9231E 00	-0.9212E 02	0.2034E 01	-0.9318E 02	0.1509E 00	0.6630E 02
0.1218E 02	-0.8860E 02	0.1042E 03	0.4276E 01	0.9231E 00	0.9212E 02	0.2034E 01	0.9318E 02	0.1509E 00	-0.6630E 02
0.1263E 02	-0.1276E 03	0.1147E 03	-0.3681E 02	0.9197E 00	0.5352E 02	0.1939E 01	0.5502E 02	0.6977E-01	-0.4816E 02
0.1263E 02	0.1276E 03	0.1147E 03	0.3681E 02	0.9197E 00	-0.5352E 02	0.1939E 01	-0.5502E 02	0.6977E-01	0.4816E 02

TABLE 4.9

MOTOR DRIVE WITH CONSTANT SLIP SPEED CONTROL

OPERATING POINT VALUES:	FREQUENCY(HZ)	VOLTAGE(VOLTS)	SPEED(RPM)	TORQUE(NM)
	30.00	65.7	800.0	17.56

OPERATING POINT CURRENTS:			E-VALUES,REAL	E-VALUES,IMAG.	BREAK FREQUENCY(HZ)	DAMPING
STATOR 1	15.86	1	-23.45	0.00	3.73	1.00
STATOR 2	-9.59	2	-2.46	0.00	0.39	1.00
ROTOR 1	-16.05	3	-0.00	0.00	0.00	1.00
ROTOR 2	1.42	4	-3.41	9.15	1.55	0.35
		5	-3.41	-9.15	1.55	0.35
		6	-41.76	132.99	22.18	0.30
		7	-41.76	-132.99	22.18	0.30
		8	-218.31	-74.92	36.73	0.95
		9	-218.31	74.92	36.73	0.95

E-VECTORS IN POLAR COORDINATES;

E-VECTOR 1	E-VECTOR 2	E-VECTOR 3	E-VECTOR 4	E-VECTOR
0.9200E 00 0.1800E 03	0.6104E 00 0.1800E 03	0.6048E 00 0.0000E 00	0.4600E 00 -0.8363E 02	
0.1000E 01 0.1800E 03	0.1000E 01 -0.1800E 03	0.1000E 01 0.0000E 00	0.8330E 00 -0.7692E 02	
0.4935E 00 0.0000E 00	0.9431E-01 0.0000E 00	0.8978E-01 0.1800E 03	0.4601E-01 0.5164E 02	
0.1116E 01 0.0000E 00	0.1014E 01 0.0000E 00	0.1012E 01 0.1800E 03	0.8212E 00 0.1017E 03	
0.6586E 00 0.0000E 00	0.7770E-01 0.0000E 00	0.1193E-17 0.1800E 03	0.2544E 00 0.3133E 02	
0.5617E-01 0.1800E 03	0.6317E-01 0.1800E 03	0.6307E-01 0.0000E 00	0.5212E-01 -0.7911E 02	
0.1156E 00 0.0000E 00	0.1538E 00 0.0000E 00	0.1399E-05 0.0000E 00	0.7693E-01 0.1054E 02	
0.4097E 00 0.1800E 03	0.5750E-01 0.1800E 03	0.9269E-19 0.0000E 00	0.1141E 00 0.1210E 03	
0.3589E 00 0.0000E 00	0.4619E-01 0.1800E 03	0.5901E-17 0.1800E 03	0.1177E 00 0.1662E 03	

E-VECTOR 5	E-VECTOR 6	E-VECTOR 7	E-VECTOR 8	E-VECTOR 9
0.4600E 00 0.8363E 02	0.9584E 00 -0.9000E 02	0.9584E 00 0.9000E 02	0.7049E 00 -0.5331E 02	0.7049E 00 0.5331E 02
0.8330E 00 0.7692E 02	0.9363E 00 -0.1759E 01	0.9363E 00 0.1759E 01	0.6372E 00 -0.1477E 03	0.6372E 00 0.1477E 03
0.4601E-01 -0.5164E 02	0.9662E 00 -0.9425E 02	0.9662E 00 -0.9425E 02	0.7103E 00 0.1262E 03	0.7103E 00 -0.1262E 03
0.8212E 00 -0.1017E 03	0.9335E 00 -0.1770E 03	0.9335E 00 0.1770E 03	0.6453E 00 0.3167E 02	0.6453E 00 -0.3167E 02
0.2544E 00 -0.3133E 02	0.1278E 00 0.1664E 03	0.1278E 00 -0.1664E 03	0.6601E-01 0.1072E 03	0.6601E-01 -0.1072E 03
0.5212E-01 0.7911E 02	0.1834E-02 0.5901E 02	0.1834E-02 -0.5901E 02	0.5720E-03 -0.9171E 02	0.5720E-03 0.9171E 02
0.7693E-01 -0.1054E 02	0.2427E-04 0.3419E 02	0.2427E-04 -0.3419E 02	0.2927E-05 0.4828E 02	0.2927E-05 -0.4828E 02
0.1141E 00 -0.1210E 03	0.5141E-03 0.1416E 03	0.5141E-03 -0.1416E 03	0.1027E-03 -0.1128E 03	0.1027E-03 0.1128E 03
0.1177E 00 -0.1662E 03	0.5601E-02 -0.1160E 03	0.5601E-02 0.1160E 03	0.1799E-02 0.8723E 02	0.1799E-02 -0.8723E 02

INPUT-MODE COUPLING MATRIX IN POLAR COORDINATES:

0.3462E 01 0.1161E-12	0.1076E 01 -0.1800E 03	0.1351E 02 0.1800E 03	0.3435E 01 0.1800E 03	
0.1183E 02 -0.1800E 03	0.4444E 00 0.3962E-10	0.5108E 02 0.4437E-13	0.9289E 01 -0.1835E-11	
0.2349E-11 -0.1788E 03	0.5618E-12 0.3541E 02	0.1258E-11 0.2985E 01	0.1657E-11 -0.1026E 02	
0.1126E 02 -0.4517E 02	0.1706E 01 0.6664E 02	0.4921E 02 0.1358E 03	0.9125E 01 0.1270E 03	
0.1126E 02 0.4517E 02	0.1706E 01 -0.6664E 02	0.4921E 02 -0.1358E 03	0.9125E 01 -0.1270E 03	
0.7992E 02 -0.1771E 03	0.7428E 02 0.8923E 02	0.4368E 02 0.1172E 03	0.4565E 02 0.4430E 02	
0.7992E 02 0.1771E 03	0.7428E 02 -0.8923E 02	0.4368E 02 -0.1172E 03	0.4565E 02 -0.4430E 02	
0.2154E 03 0.9113E 02	0.1947E 03 0.1751E 03	0.2172E 03 -0.1286E 03	0.2358E 03 -0.4791E 02	
0.2154E 03 -0.9113E 02	0.1947E 03 -0.1751E 03	0.2172E 03 0.1286E 03	0.2358E 03 0.4791E 02	
0.9688E 01 0.1056E-13	0.5227E 01 -0.9655E-13	0.2557E 00 -0.1800E 03	0.9931E 00 -0.1800E 03	0.1133E 01 -0.2177E-13
0.3781E 02 -0.1800E 03	0.2057E 02 0.1800E 03	0.8332E 01 0.0000E 00	0.1185E 01 0.0000E 00	0.1475E 01 0.5412E-14
0.1740E-11 -0.1799E 03	0.1586E 02 0.1488E-13	0.1009E 02 0.4869E-15	0.5314E 01 0.5550E-14	0.5314E 01 0.4856E-14
0.3623E 02 -0.4168E 02	0.1990E 02 -0.4386E 02	0.1999E 01 -0.1556E 03	0.2970E 01 -0.1091E 03	0.2879E 01 -0.1543E 03
0.3623E 02 0.4168E 02	0.1990E 02 0.4386E 02	0.1999E 01 0.1556E 03	0.2970E 01 0.1091E 03	0.2879E 01 0.1543E 03
0.1283E 02 -0.1064E 03	0.6068E 02 -0.1820E 02	0.9930E 00 0.7542E 02	0.2115E 01 0.7920E 02	0.1942E 00 -0.2321E 02
0.1283E 02 0.1064E 03	0.6068E 02 0.1820E 02	0.9930E 00 -0.7542E 02	0.2115E 01 -0.7920E 02	0.1942E 00 0.2321E 02
0.2135E 02 -0.7462E 02	0.9605E 02 -0.2384E 02	0.1617E 01 -0.1078E 03	0.3523E 01 -0.1086E 03	0.2010E 00 0.5138E 02
0.2135E 02 0.7462E 02	0.9605E 02 0.2384E 02	0.1617E 01 0.1078E 03	0.3523E 01 0.1086E 03	0.2010E 00 -0.5138E 02

TABLE 4.10

MOTOR DRIVE WITH CONSTANT SLIP SPEED CONTROL

OPERATING POINT VALUES:	FREQUENCY(HZ)	VOLTAGE(VOLTS)	SPEED(RPM)	TORQUE(NM)
	6.67	17.8	100.0	17.56

OPERATING POINT CURRENTS:		E-VALUES.REAL	E-VALUES.IMAG.	BREAK FREQUENCY(HZ)	DAMPING
STATOR 1	16.79	1	-38.49	0.00	6.13	1.00
STATOR 2	-7.85	2	-2.24	0.00	0.36	1.00
ROTOR 1	-16.11	3	0.00	0.00	0.00	1.00
ROTOR 2	-0.29	4	-6.39	-14.79	2.56	0.40
		5	-6.39	14.79	2.56	0.40
		6	-2.03	-33.25	5.30	0.06
		7	-2.03	33.25	5.30	0.06
		8	-247.65	-26.67	39.64	0.99
		9	-247.65	26.67	39.64	0.99

E-VECTORS IN POLAR COORDINATES:

E-VECTOR 1		E-VECTOR 2		E-VECTOR 3		E-VECTOR 4		E-VECTOR
0.1[illegible]E 01	0.0000E 00	0.4717E 00	0.1800E 03	0.4679E 00	0.0000E 00	0.3834E 00	-0.1666E 03	
0.6626E 00	0.0000E 00	0.1000E 01	0.1800E 03	0.1000E 01	0.0000E 00	0.9158E 00	0.1745E 03	
0.8508E 00	0.1800E 03	0.1410E-01	0.1800E 03	0.1715E-01	0.0000E 00	0.1373E 00	0.1471E 03	
0.7811E 00	0.1800E 03	0.9615E 00	0.0000E 00	0.9597E 00	0.1800E 03	0.8204E 00	-0.2485E 00	
0.6539E 00	0.1800E 03	0.6655E-01	0.0000E 00	0.8565E-17	0.0000E 00	0.4341E 00	0.6415E 02	
0.3398E-01	0.0000E 00	0.5931E-01	0.1800E 03	0.5958E-01	0.0000E 00	0.5387E-01	0.1775E 03	
0.1235E-01	0.1800E 03	0.1384E 00	0.0000E 00	0.4012E-06	0.0000E 00	0.5162E-01	0.1326E 03	
0.7224E-01	0.0000E 00	0.4720E-01	0.1800E 03	0.4023E-20	0.0000E 00	0.1264E 00	0.1927E 02	
0.1502E 00	0.1800E 03	0.3873E-01	0.1800E 03	0.1220E-18	0.1800E 03	0.1619E 00	-0.4829E 02	

E-VECTOR 5		E-VECTOR 6		E-VECTOR 7		E-VECTOR 8		E-VECTOR 9	
0.3834E 00	0.1666E 03	0.7203E 00	-0.6084E 02	0.7203E 00	0.6084E 02	0.7470E 00	-0.8755E 02	0.7470E 00	0.8785E 02
0.9158E 00	-0.1745E 03	0.7121E 00	-0.1418E 03	0.7121E 00	0.1418E 03	0.6295E 00	0.1611E 03	0.6295E 00	-0.1611E 03
0.1373E 00	-0.1471E 03	0.4747E 00	0.8323E 02	0.4747E 00	-0.8323E 02	0.7511E 00	0.9213E 02	0.7511E 00	-0.9213E 02
0.8204E 00	0.2485E 00	0.4869E 00	0.2532E 01	0.4869E 00	-0.2532E 01	0.6349E 00	-0.1898E 02	0.6349E 00	0.1898E 02
0.4341E 00	-0.6415E 02	0.2322E 00	0.1732E 03	0.2322E 00	-0.1732E 03	0.6374E-01	0.8138E 02	0.6374E-01	-0.8138E 02
0.5387E-01	-0.1775E 03	0.1394E-01	-0.9331E 02	0.1394E-01	0.9331E 02	0.5118E-03	-0.1048E 03	0.5118E-03	0.1048E 03
0.5162E-01	-0.1326E 03	0.2816E-02	-0.1283E 03	0.2816E-02	0.1283E 03	0.2243E-05	0.6229E 02	0.2243E-05	-0.6229E 02
0.1264E 00	-0.1927E 02	0.1426E-01	0.1382E 03	0.1426E-01	-0.1382E 03	0.8490E-04	-0.1116E 03	0.8490E-04	0.1116E 03
0.1619E 00	0.4829E 02	0.3976E-01	0.6572E 02	0.3976E-01	-0.6572E 02	0.1607E-02	0.7491E 02	0.1607E-02	-0.7491E 02

INPUT-MODE COUPLING MATRIX IN POLAR COORDINATES:

0.2356E 02	0.1800E 03	0.4584E 01	0.1800E 03	0.1813E 02	0.5832E-14	0.4953E 01	-0.2416E-12		
0.1103E 02	0.1800E 03	0.1423E 00	0.1800E 03	0.7734E 01	-0.6877E-13	0.3104E 01	-0.3887E-13		
0.6404E-12	0.1691E 03	0.6653E-12	0.5883E 01	0.9576E-12	-0.1737E 03	0.1416E-12	-0.1515E 03		
0.1664E 02	-0.9169E 02	0.1937E 01	-0.1721E 02	0.1042E 02	0.8485E 02	0.4442E 01	0.7393E 02		
0.1664E 02	0.9169E 02	0.1937E 01	0.1721E 02	0.1042E 02	-0.8485E 02	0.4442E 01	-0.7393E 02		
0.1200E 02	-0.2755E 02	0.1045E 02	0.9523E 02	0.9537E 01	0.4460E 02	0.8477E 01	0.9816E 02		
0.1200E 02	0.2755E 02	0.1045E 02	-0.9523E 02	0.9537E 01	-0.4460E 02	0.8477E 01	-0.9816E 02		
0.1854E 03	0.1132E 03	0.1906E 03	0.1791E 03	0.1800E 03	-0.7132E 02	0.1980E 03	-0.4681E 01		
0.1854E 03	-0.1132E 03	0.1906E 03	-0.1791E 03	0.1800E 03	0.7132E 02	0.1980E 03	0.4681E 01		
0.1866E 02	-0.1800E 03	0.3681E 01	0.0000E 00	0.1060E 01	-0.2250E-14	0.3020E 01	-0.8425E-14	0.1453E 01	0.1800E 03
0.9548E 01	0.1800E 03	0.1959E 01	0.0000E 00	0.8510E 01	0.0000E 00	0.1560E 01	-0.2373E-13	0.1901E 01	0.4258E-14
0.4072E-12	0.2814E 01	0.1678E 02	-0.1092E-13	0.1069E 02	-0.2144E-14	0.5625E 01	-0.7127E-14	0.5625E 01	0.7636E-15
0.1339E 02	-0.9641E 02	0.3716E 01	0.9615E 02	0.1788E 01	0.2167E 02	0.3545E 01	-0.1315E 02	0.2768E 01	0.5441E 02
0.1339E 02	0.9641E 02	0.3716E 01	-0.9615E 02	0.1788E 01	-0.2167E 02	0.3545E 01	0.1315E 02	0.2768E 01	-0.5441E 02
0.6361E 01	-0.9897E 02	0.9698E 01	-0.1713E 03	0.6242E 00	0.6594E 02	0.1248E 01	0.5038E 02	0.4474E 00	0.1229E 03
0.6361E 01	0.9897E 02	0.9698E 01	0.1713E 03	0.6242E 00	-0.6594E 02	0.1248E 01	-0.5038E 02	0.4474E 00	-0.1229E 03
0.1797E 02	0.1144E 03	0.2364E 02	-0.7006E 01	0.1290E 01	-0.7291E 02	0.2807E 01	-0.7316E 02	0.1483E 00	0.1004E 03
0.1797E 02	-0.1144E 03	0.2364E 02	0.7006E 01	0.1290E 01	0.7291E 02	0.2807E 01	0.7316E 02	0.1483E 00	-0.1004E 03

The last equation can be written in the physically realizable form, by grouping together the complex conjugate pairs, in the same way as in equation (4-3).

Note that 5th row, 3rd column element (i.e., m_{53}) in the eigenvector matrix is always zero (computer results, Step 4), thus, decoupling the speed from the integrator associated with the phase angle $\delta\psi$, Fig. 3.1. This is in agreement with the previous discussion.

When the appropriate values from Tables 4.8, 4.9 and 4.10 are used in equation (4-38), the speed-speed reference transfer functions are obtained at corresponding operating points. Their Bode plots are presented in Fig. 4.26b, 4.27b and 4.28b. The same plots could have been obtained by applying equation (3-30) with the input $u_9(s)$.

When evaluated in the context of the open loop results (Fig. 4.23), these plots show the attenuation of the gain peaks (20 - 40 hz range) by the phase-lag compensating network. The full discussion of the drive frequency response is presented later, together with the analysis of the speed time response.

2) The speed-load torque transfer function

The load torque appears only in the mechanical equation. Applying (3-32) and dividing both sides by δT_L the desired transfer function is:

$$G_2(s) = \frac{v(s)}{\delta T_L(s)} = \sum_{k=1}^{9} \frac{m_{5k}\, h_{k5}}{s - \lambda_k} \qquad (4\text{-}39)$$

If the appropriate values from the computer results (Step 1) are inserted into the last equation, $G_2(s)$ is obtained at corresponding drive operating points. Its Bode plots are presented in Fig. 4.29b, 4.30b and 4.31b. These results are sufficient to assess the speed-load interaction. However, an additional insight into this interaction is obtained by calculating analytically the zeros of $G_2(s)$, using the Direct Method.

The drive reduced system is represented by (4-30), after the mechancial equation is taken out. The reduced system has five eigenvalues. Of these, four belong to the decoupled electrical system. Since they do not depend on the

drive structure, they are identical to those calculated in the constant V/hz drives (Table 4.7) and are given in Table 4.11 only for comparison. The fifth eigenvalue is located in the origin and represents the integrator which is associated with the mmf vector phase angle (Fig. 3.1). Thus, the characteristic equation of the reduced system is:

$$D_r(s) = s \prod_{j=1}^{4} (s-z_j) \qquad (4\text{-}40)$$

The speed controller has three eigenvalues, determined by equation (4-32). Obviously, none of these depend on the operating point. The eigenvalues of the speed controller and the reduced system are grouped together in Table 4.11.

OPERATING POINT	REDUCED SYSTEM			SPEED CONTROLLER		
	ZEROS	BREAK FREQ.	DAMPING	ZEROS	BREAK FREQ.	DAMPING
1700 rpm	$z_{1/2}$=-174.0±j68.2	29.75	0.931	$z_{6/7}=-\frac{1}{a}$ =-12.5	1.98	1.0
	$z_{3/4}$=-89.9±j329.6	54.39	0.263	z_8=0	0	-
	z_5 = 0	0	-			
800 rpm	$z_{1/2}$=-232.1±j78.9	39.0	0.947	$z_{6/7}=-\frac{1}{a}$ =-12.5	1.98	1.0
	$z_{3/4}$=-31.8±j130.5	21.4	0.237	z_8=0	0	-
	z_5=0	0	-			
100 rpm	$z_{1/2}$=-259.5±j28.9	41.56	0.99	$z_{6/7}=-\frac{1}{a}$ =-12.5	1.98	-
	$z_{3/4}$=-4.4±j33.9	5.45	0.128	z_8=0	0	-
	z_5=0	0	-			

Table 4.11: Zeros of the speed-torque transfer function for the constant slip speed drive calculated by using the Direct Method.

From equation (3-52) the drive speed-speed torque transfer function is

$$G_2(s) = \frac{s^2(s+1/a)\prod_{j=1}^{4}(s-z_j)}{J_T\prod_{k=1}^{9}(s-\lambda_k)} \qquad (4\text{-}41)$$

One zero at the origin will cancel the third eigenvalue, λ_3. This cancellation decouples the speed from the mmf phase angle integrator, as discussed earlier. The other zero at the origin represents the speed controller integrator which drives the speed steady state error to zero. In other words, this integrator assures zero dc value of $G_2(s)$, thus decoupling the steady state speed from the load torque. Since the four eigenvalues of the decoupled electrical system lie well above the controller bandwidth, they are very little perturbed when the speed feedback is closed. Thus, the four electrical poles (λ_5 - λ_8) are almost the same as four electrical zeros (z_1 - z_4), Tables 4.8, 4.9, 4.10 and 4.11. Consequently, some pole-zero cancellation will occur, as witnessed by the transfer function Bode diagrams (Fig. 4.29b, 4.30b and 4.31b). This means that the electromechanical coupling is weak giving poor speed regulation. Further discussion of these results is continued in the next step.

STEP 3: Speed step and frequency response

This part of the analysis gives the best insight into the drive transient performance.

As before, the speed response is calculated first for a unit step change in the input reference V_r, at rated load and then for a unit step change in the load torque with V_r constant. The results are displayed graphically together with the corresponding drive frequency response.

Following the already established procedure, the speed response is obtained in two stages:

1) Modal response to a step input

2) Speed response as a combination of modal states.

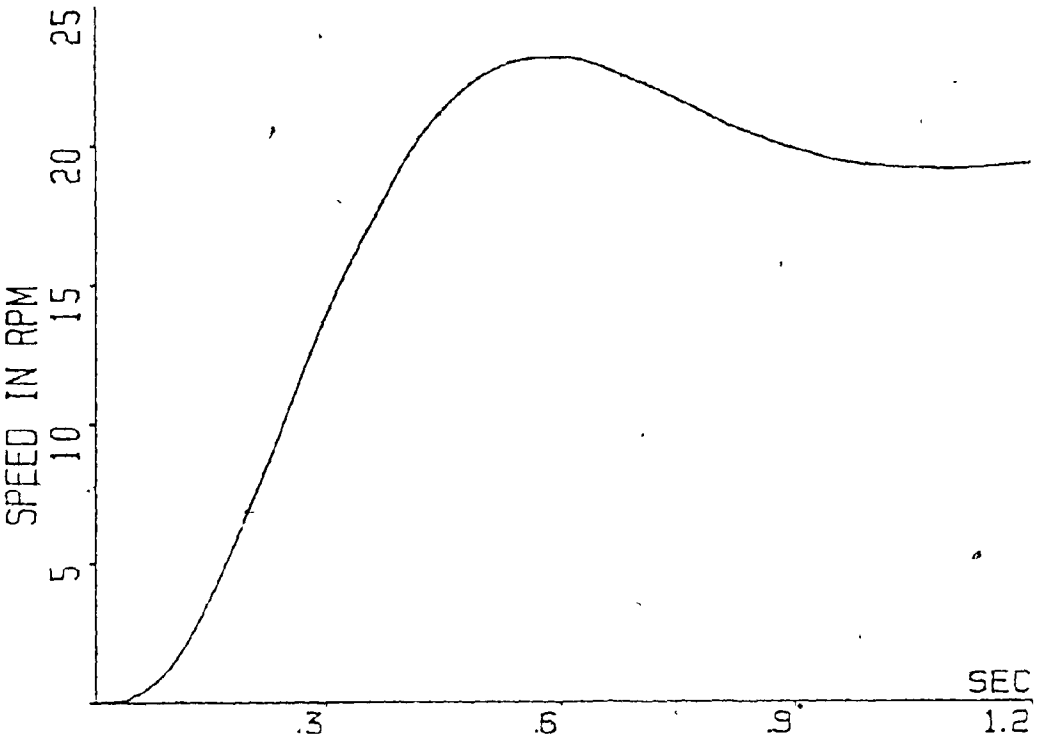

Fig 4.26a Speed response to step reference at 1700 rpm

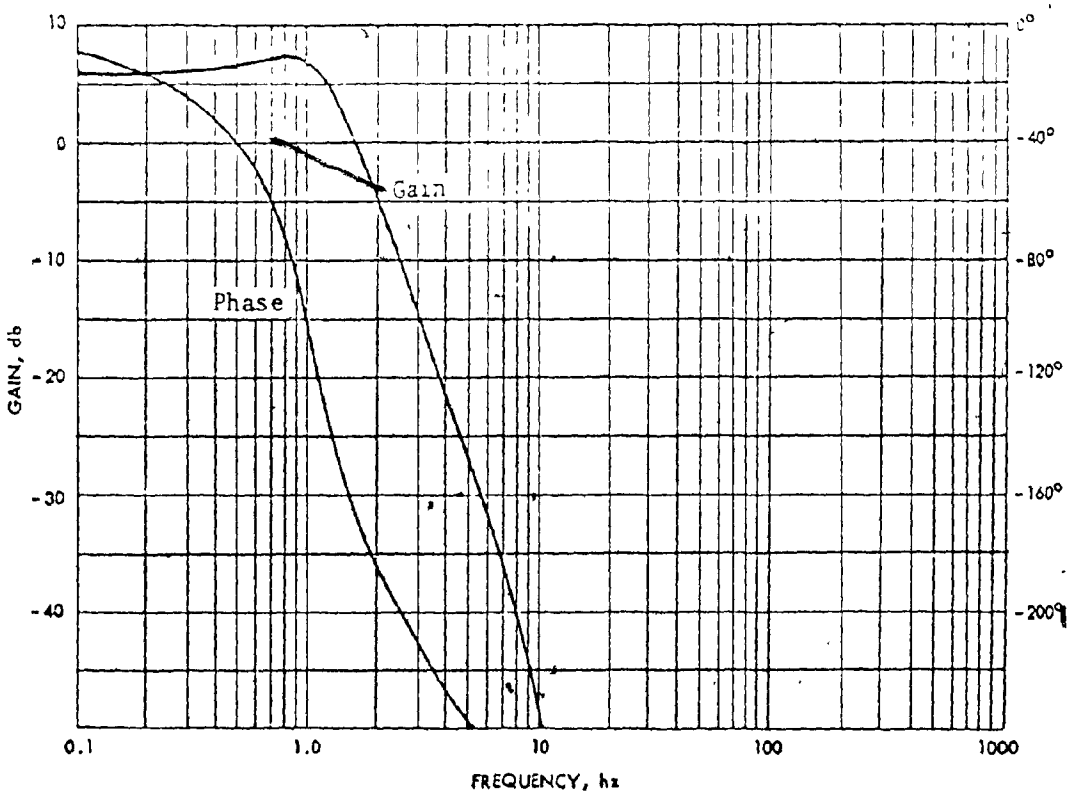

Fig. 4.26b: Frequency response of speed-input reference transfer function at 1700 rpm.

1) Response to a unit step in the input reference

From equation (4-37c), the input reference signal V_r appears only in the last input, $u_9(t)$. If the unit step in V_r is applied, the response of each modal state is given by (3-24) as:

$$q_k(t) = \int_0^t e^{\lambda_k(t-\tau)} (h_{k9}/a)d\tau \qquad k = 1 \ldots 9$$

when solved, the last equation gives:

$$q_k(t) = (e^{\lambda_k t} - 1)\, h_{k9}/a\lambda_k \tag{4-42}$$

For the special case of the eigenvalue in the origin, the last equation becomes:

$$q_3(t) = h_{39}\, t/a$$

The speed response is obtained by using (3-25) and (3-26)

$$y(t) = \sum_{\substack{k=1 \\ k\neq 3}}^{9} (e^{\lambda_k t} - 1)\, m_{5k}\, h_{k9}/a\, \lambda_k \tag{4-43}$$

The last equation gives the speed response to a unit step in the input reference. This response can be calculated for each operating point by using the appropriate values from Tables 4.8, 4.9 and 4.10. The obtained results are presented graphically in Figures 4.26a, 4.27a and 4.28a. The $G_1(s)$ frequency response, obtained from equation (4-38) is given for comparison in Figures 4.26b, 4.27b and 4.28b.

A brief discussion of these results follows:

At the 1700 rpm operating point, the drive exhibits a 15.8% overshoot (Fig. 4.26a). The rise and settling (±5%) times are 255 msec. and 800 msec. respectively. The speed response is very slow, in agreement with the narrow bandwidth of 1.3 hz, obtained on the Bode diagram (Fig. 4.26b). The slope

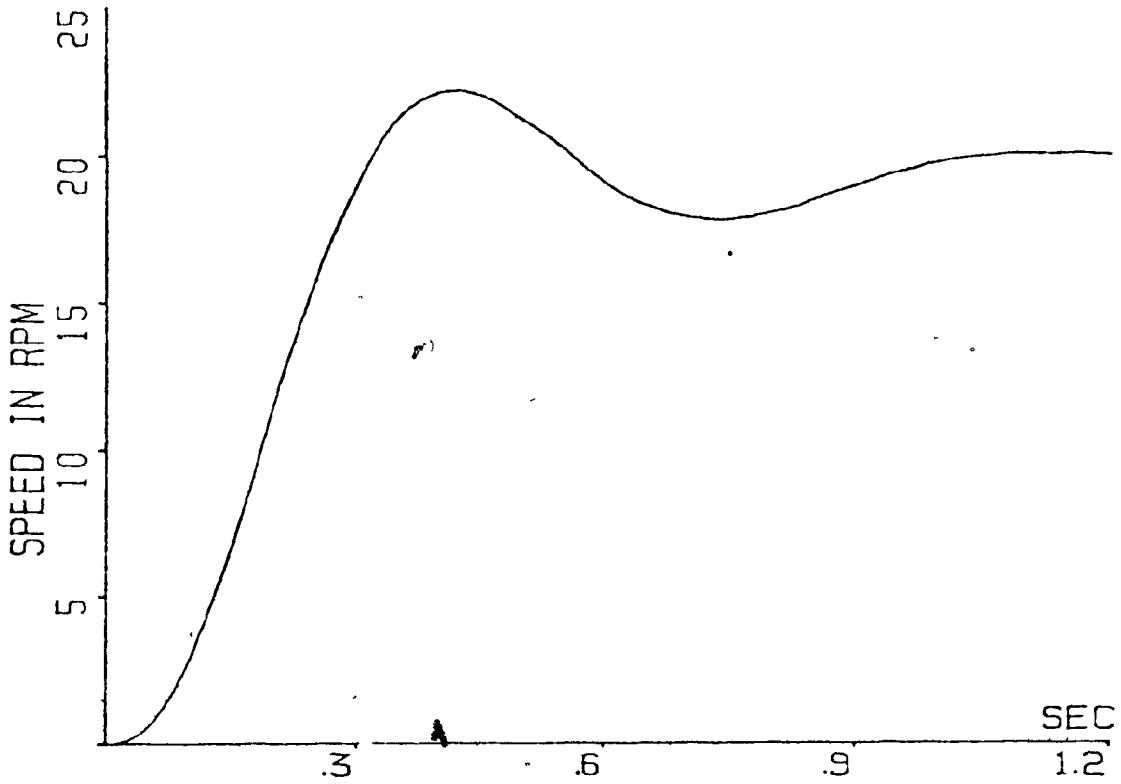

Fig 4.27a. Speed response to step reference at 800 rpm.

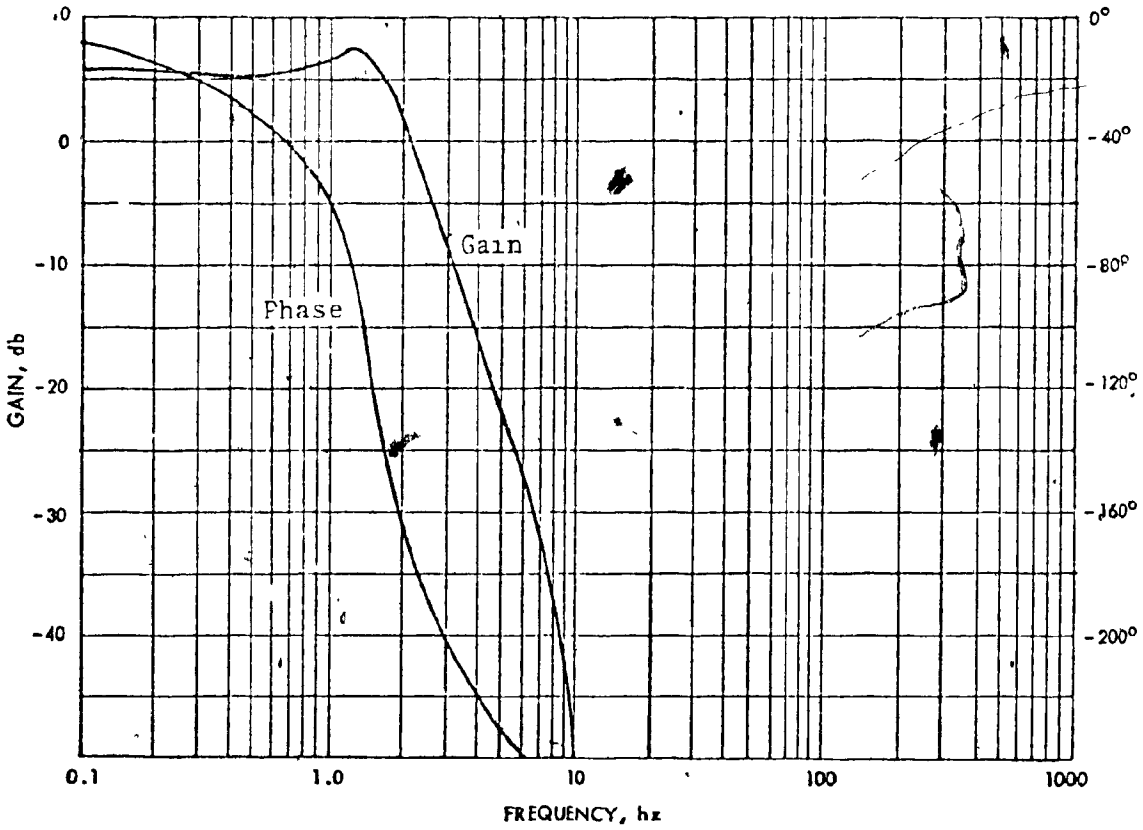

Fig. 4.27b: Frequency response of speed-input reference transfer function at 800 rpm.

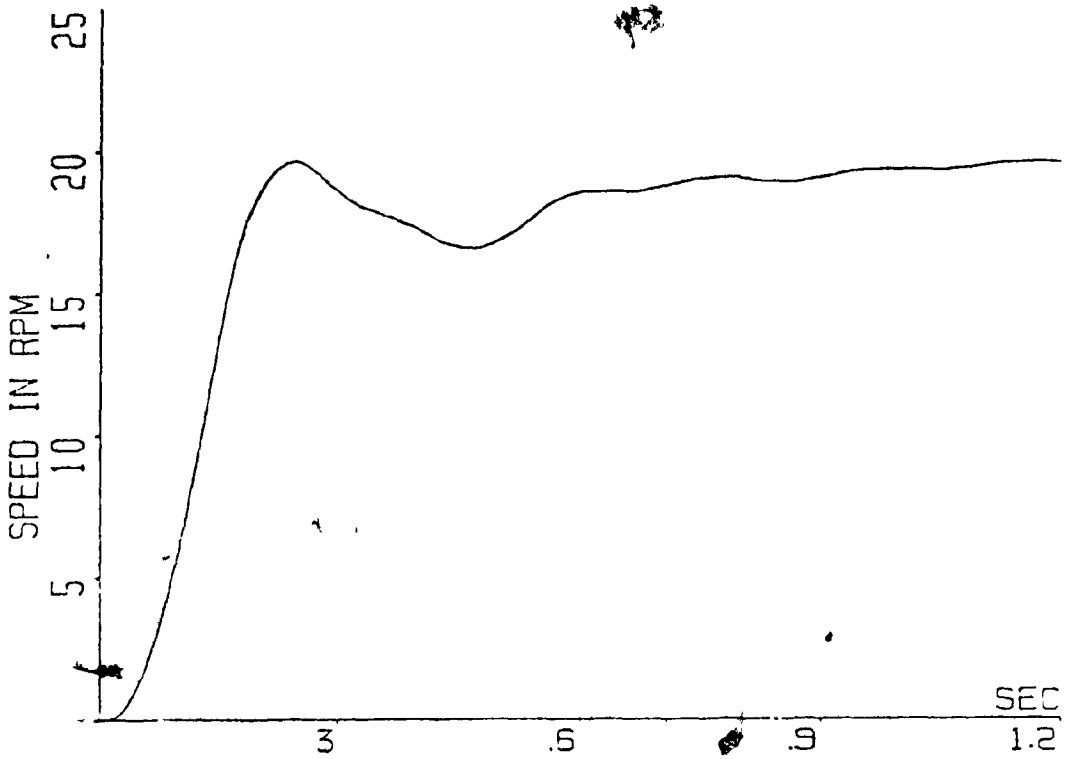

Fig. 4.28a. Speed response to step reference at 100 rpm.

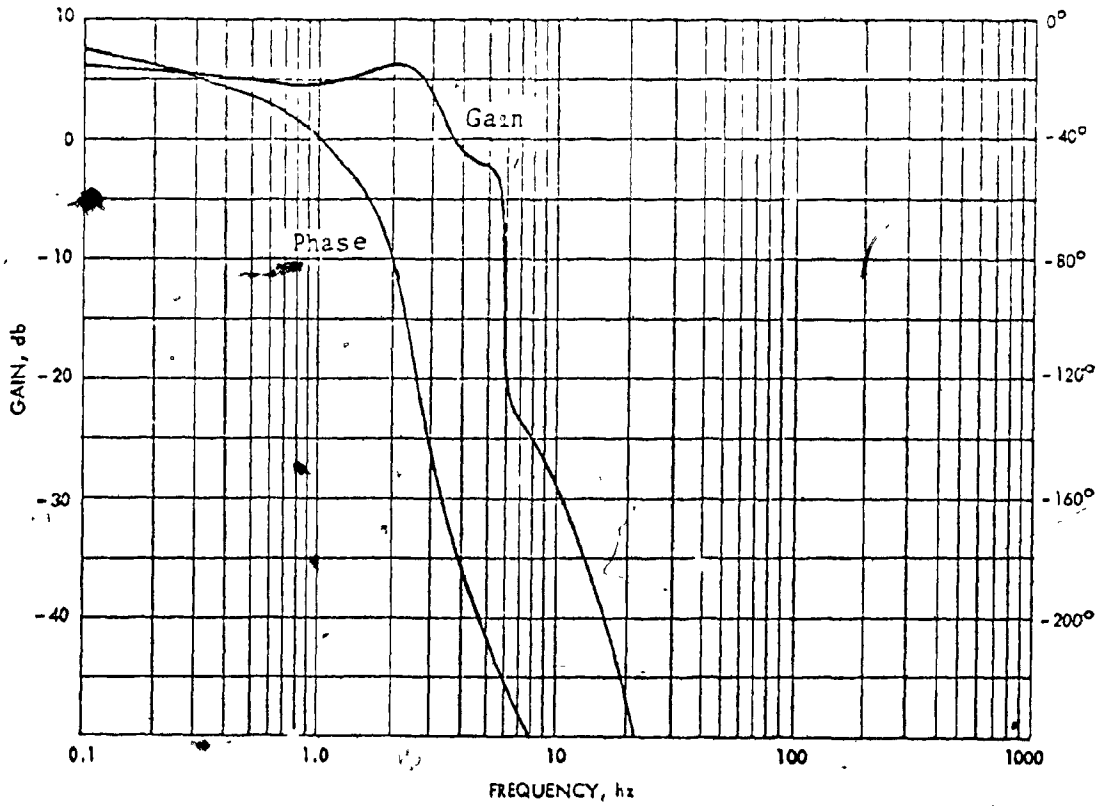

Fig. 4.28b: Frequency response of speed-input reference transfer function at 100 rpm.

of the time response curve at $t = 0^+$ is very small, corresponding to high system order at high frequencies, as indicated by the -60 db slope on the Bode plot.

The speed steady state error is ultimately zero, due to the controller integrator. However, the drive narrow bandwidth does not permit fast enough buildup of the electrical torque and the speed takes more than 1.4 sec. to reach its steady state value.

At 800 rpm, the drive behaves essentially in the same way (Fig. 4.27a). The overshoot is now 10.9% The rise and settling times are 195 msec and 515 msec. respectively, in agreement with the larger bandwidth of 1.9 hz (Fig. 4.27b). All other comments apply equally well to this operating point.

At 100 rpm, the drive gives the fastest speed response (Fig. 4.28a), corresponding to the significantly increased bandwidth, which is now at 3 hz (Fig. 4.28b) The integrator in the speed controller starts to act after 0.319 sec., pulling the speed up to its steady state value of 20 rpm. Without the integrator, the speed final value would be much lower (as it was in the open loop, constant V/hz drive at 5 hz operating point). The reason for this is the loss in the gain of the drive forward transfer function $G_1(s)$, as seen on the Bode plot where the gain starts to decrease from 0.2 hz.

Since the speed approaches its final value without the overshoot, relying entirely on the integrator, the settling time is very long: 900 msec.

The integrator action explains why the speed never exceeds its steady state value although the corresponding break point on the Bode diagram is underdamped.

Summarizing the step response results, the dominant characteristic is a very slow response, slower even than in the open loop, constant V/hz drive. The speed oscillations are not too pronounced, although the settling times are very long. Above all, the drive dynamic performance changes with the operating speed.

2) Response to the unit step in the load torque

Since the input reference, V_r, is constant, any change in the

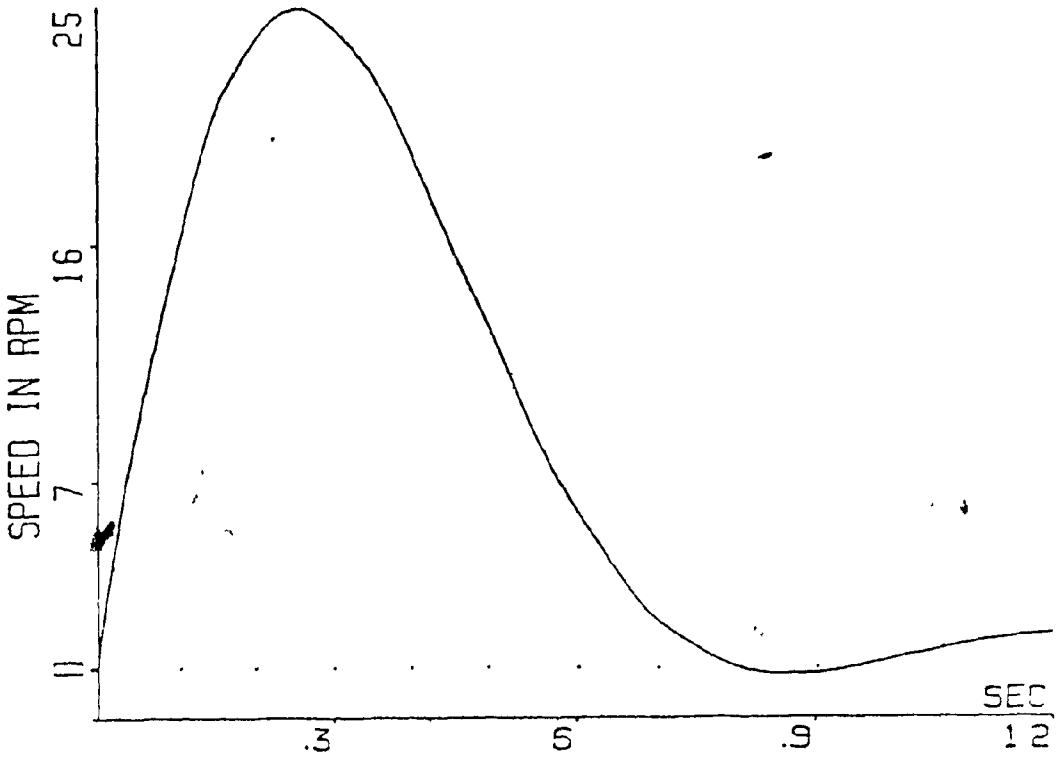

Fig. 4.29a Speed response to step torque at 1700 rpm

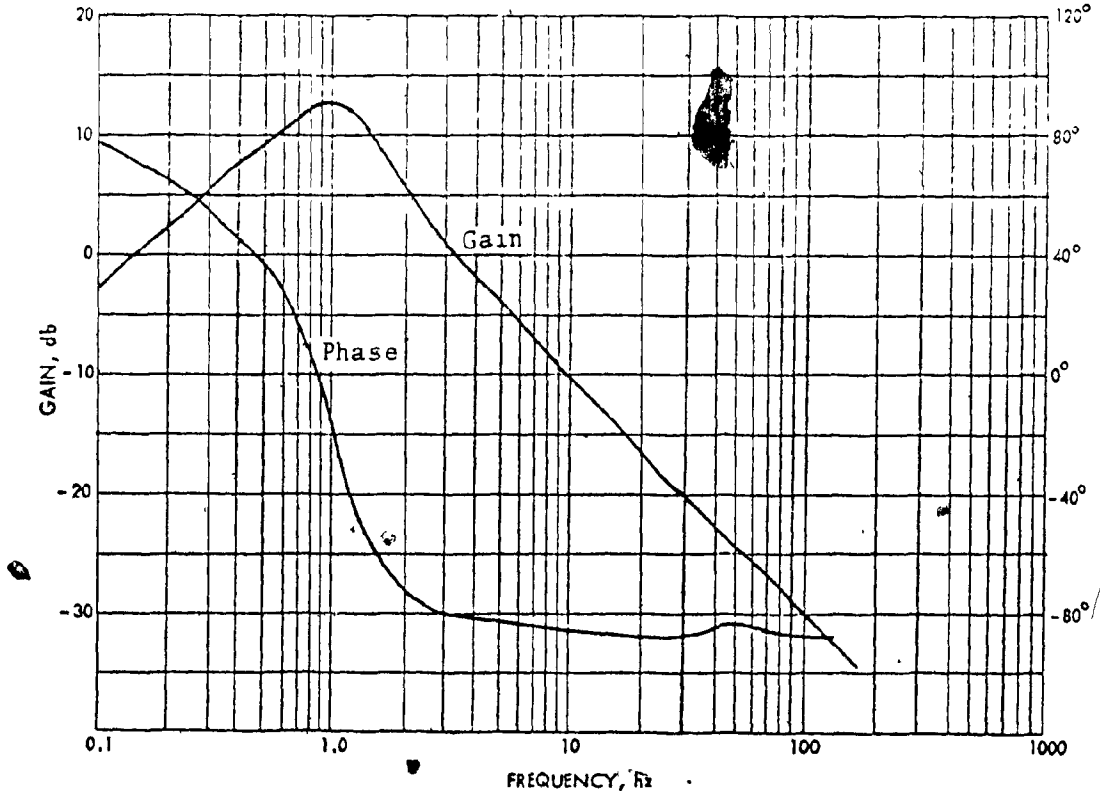

Fig. 4.29b: Frequency response of speed-torque transfer function at 1700 rpm.

output represents a speed error. The response of each modal state to unit change in torque, which appears only in the mechanical equation, is obtained from (3-24) as:

$$q_k(t) = \int_0^t e^{\lambda_k(t-\tau)} h_{k5} \, d\tau \qquad k = 1 \qquad 9$$

when solved, the last equation gives:

$$q_k(t) = (e^{\lambda_k t} - 1) \, h_{k5}/\lambda_k \tag{4-44}$$

For the special case of the eigenvalue in the origin, the last equation becomes:

$$q_3(t) = t \, h_{35}$$

From equations (3-25), (3-26) and (4-44) the speed response is

$$y(t) = \sum_{\substack{k=1 \\ k\neq 3}}^{9} (e^{\lambda_k t} - 1) m_{5k} h_{k5}/\lambda_k \tag{4-45}$$

The speed response to the unit change in the load torque is obtained at each operating point by inserting the appropriate values from Tables 4.8, 4.9 and 4.10 into equation (4-45). The results are graphically presented in Fig. 4.29a, 4.30a and 4.31a. The Bode diagrams of the drive output impedance, $G_2(s)$, are given for comparison in Figures 4.29b, 4.30b and 4.31b. The speed response at each operating point is discussed briefly.

At 1700 rpm, the speed response (i.e., error) reaches its maximum value of 25 rpm, 250 msec. after the load disturbance was applied (Fig. 4.29a). This result indicates a strong speed sensitivity to the load fluctuations. This comes as a consequence of a narrow bandwidth in the forward transfer function, $G_1(s)$, which does not permit a fast build-up of the motor electrical torque. This torque rises too slowly to block effectively the speed deviation from the value requested by the input reference, V_r. Thus,

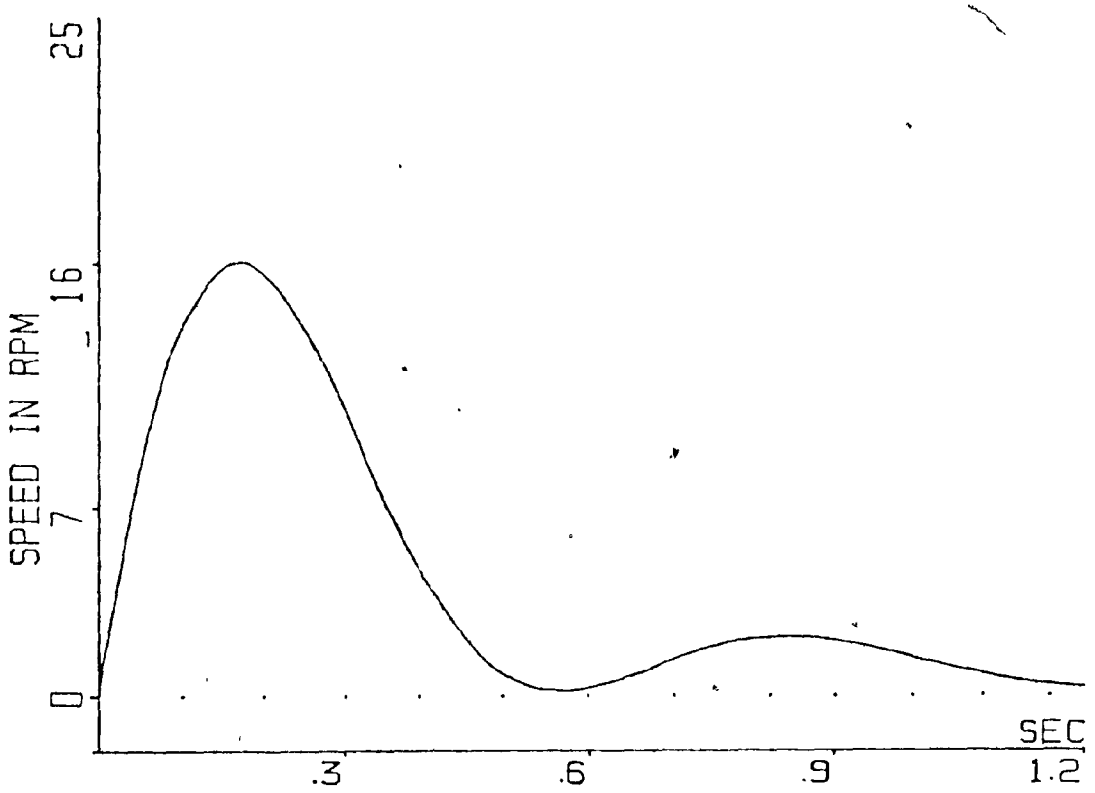

Fig. 4.30a Speed response to step torque at 800 rpm

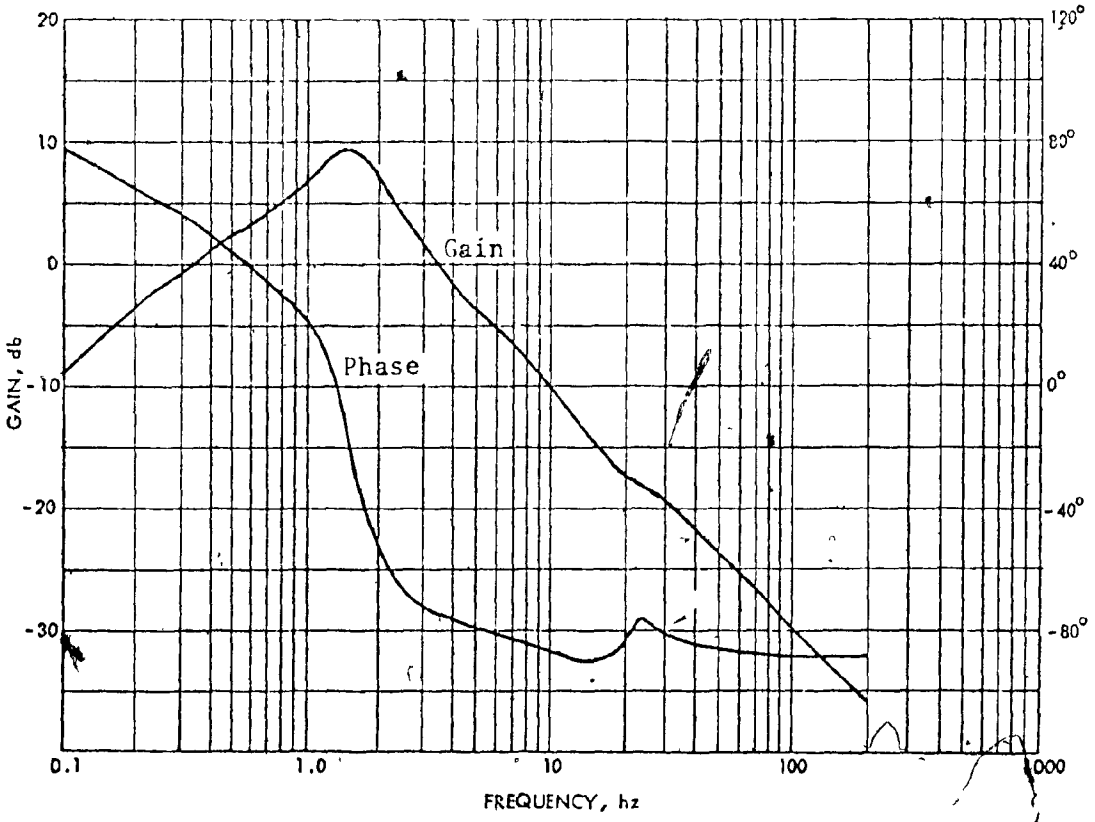

Fig. 4.30b: Frequency response of speed-torque transfer function at 800 rpm.

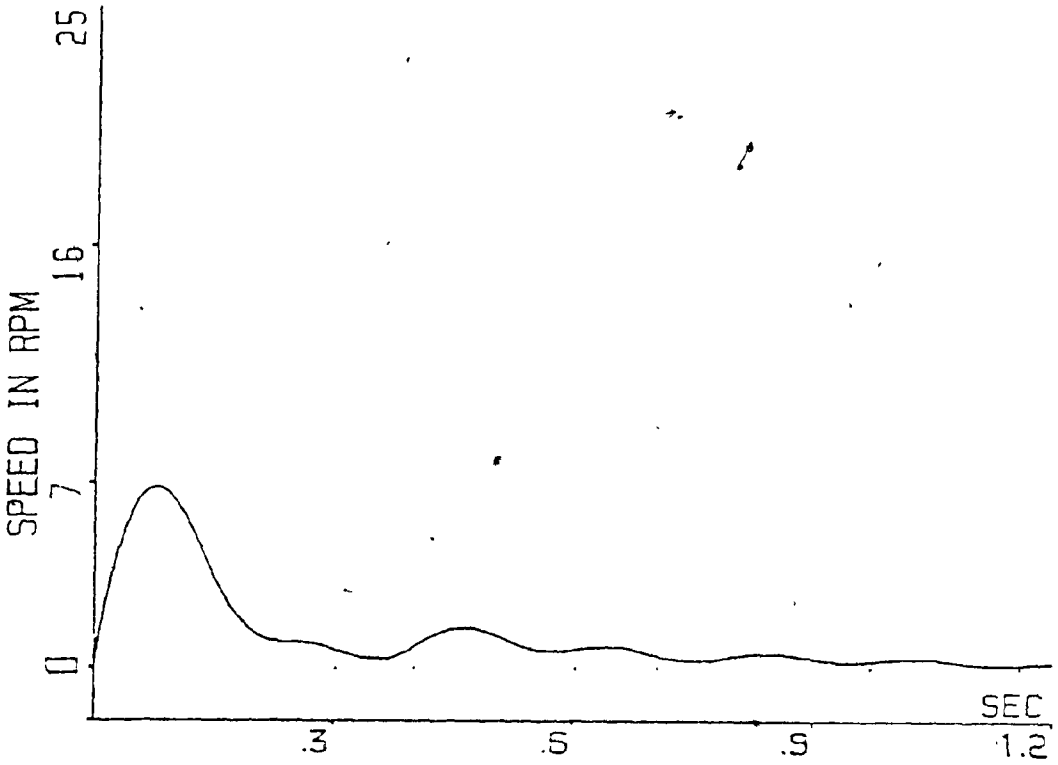

Fig 4.31a Speed response to step torque at 100 rpm

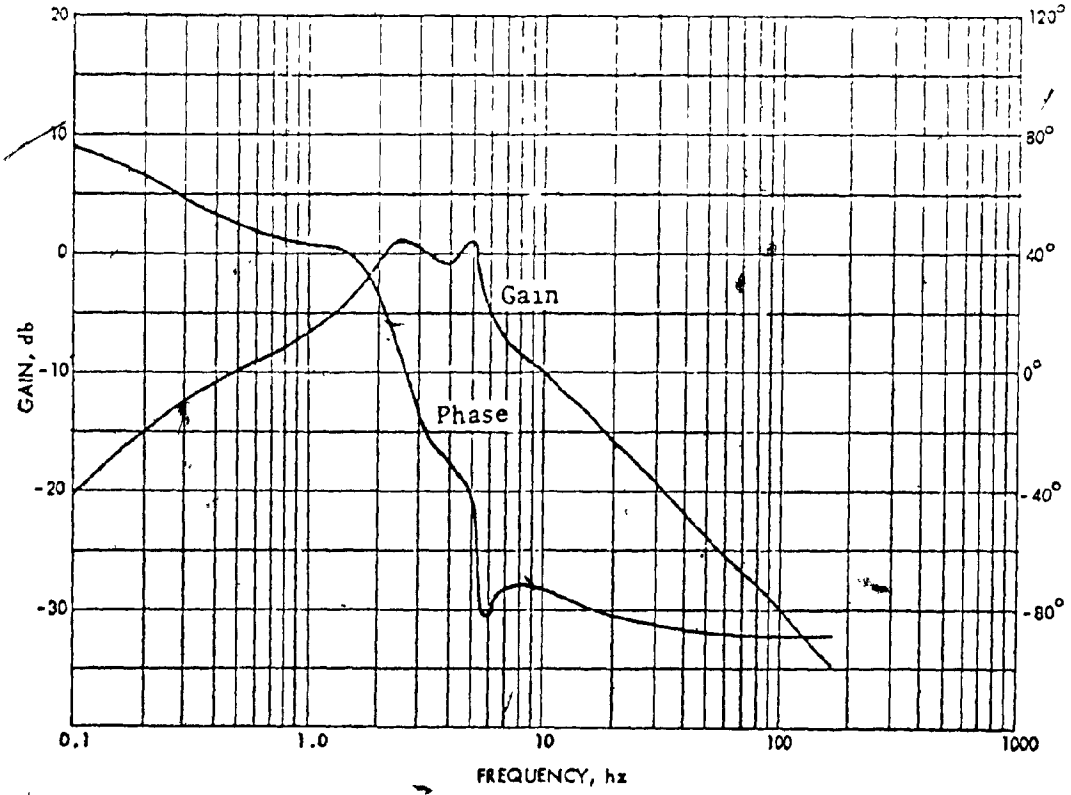

Fig. 4.31b: Frequency response of speed-torque transfer function at 100 rpm.

the speed error has time to grow and reach its large value of 25 rpm, before the electrical torque starts acting. It is clear from the expression for $G_2(s)$, equation (4-41), that this error will be reduced to zero. However, it takes 1.27 sec. to bring it below 1.25 rpm or 5% of its maximum value.

The frequency response, Fig. 4.29b, confirms the step response results

At 800 rpm, the same comments apply to this operating point (Fig. 4.30a). Due to the slightly larger bandwidth of the $G_1(s)$ transfer function (Fig. 4.27b), the electrical torque can change faster and the maximum speed error is thus reduced: .16 rpm at 170 msec. While this represents a physical explanation, the effect of the larger bandwidth is easily understood by comparing the two Bode plots, Figures 4.29b and 4.30b. The maximum gain of the drive output impedance is now reduced from 13 db at 1 hz to 9.6 db at 1.5 hz

At 100 rpm as the bandwidth of $G_1(s)$ transfer function is further increased (Fig. 4.28b) the maximum value of $G_2(s)$ is again decreased (Fig. 4.31b), making the speed less sensitive to the load disturbance (Fig. 4.31a). The maximum speed error is now less than 7 rpm, at 75 msec. The subsequent oscillations in the speed are caused by the incomplete cancellation of poles and zeros in the speed-torque transfer function. Note that two poles of $G_2(s)$ occur at 5.3 hz, with very low damping of 0.061, (Table 4.10), while the two corresponding zeros are located at 5.45 hz with the damping of 0.128 (Table 4.11).

Conclusion

The results obtained show that the constant slip speed control gives poor dynamic performance. The explanation for this is found in the shape of the drive open loop frequency response, which calls for a speed controller that necessarily gives a narrow bandwidth, low gain drive. Consequently, the speed response is slow, slower even than for the open loop, constant V/hz drive. The speed is very sensitive to load fluctuations. However, the most important fact is that the drive performance changes with the operating point.

The results obtained here determine the theoretical, upper limit of the drive dynamic performance. Several factors, not included in this dynamic study will impose additional limits on the constant slip speed strategy. One, for example, is the magnetic saturation of iron. As seen in Chapter II, any request for large electrical torques, will push the flux into saturation, resulting in further deterioration of the drive performance.

Another limitation comes from the fact that the drive power supply does not have unity transfer function, as considered in this chapter, but some, finite bandwidth. This limitation will be felt in the constant slip speed drives more than in the others, since here the frequency loop contains a positive feedback so that the voltage loop has to be faster in order to avoid instability However, the inverter frequency control is, in general, faster than its voltage control This means that the constant slip strategy subjugates a fast control loop to a slow one, with further decrease in the dynamic performance

4 4 Constant airgap flux control

As seen in Chapter II the motor torque can be controlled either by controlling the slip speed or the airgap flux. It was further seen that for the constant flux operation, the slope of the motor static torque-speed curves is constant and independent of the supply frequency. It will be demonstrated in this section that the constant flux control results in superior dynamic drive performance.

There are basically three methods by which the constant flux strategy can be implemented:[33]

1) The direct measurement of the airgap flux, by for example, Hall type probes. The signal obtained is compared with the preset, desired flux level. Any error acts to change the voltage applied to the motor and, thus, modifies the motor currents. This scheme has been proposed by a number of authors.[26,27,33] It is conceptually most straight forward, resulting in operation with truly constant flux. However, this scheme requires specially built

stators, with Hall probes installed.

2) The compensation of the stator voltage drop, as used in the Siemens Transvector drives.[80,81] In this scheme, the motor voltage consists at any time of two components: one, which is equal to the stator voltage drop and the other, which determines the flow of motor magnetizing current and, thus, the level of the airgap flux. The difficulty here lies in the need to sense both the stator current and its phase angle with respect to the applied voltage. This is necessary if proper compensation of the stator voltage drop is desired, since the two components of the applied voltage are summed vectorially. The associated controller, thus, becomes very involved, without giving any advantage over drives with direct flux measurement.

3) The regulated current principle the stator current is made of two independent components which represent respectively the magnetizing and rotor currents. If the first component is chosen to give a desired flux level at no load, while the other is made dependent on the slip speed, the drive will operate with approximately constant magnetizing current. The airgap flux will not be exactly constant since the two components are not summed vectorially. However, it will be shown that these small flux variations can be used to increase the motor efficiency. This scheme has been proposed by Phillips[58] and Magg.[66] Recently, it has received considerable attention by other authors as well.[82,83]

Due to the space limitations only one scheme for constant flux operation can be discussed here. The choice is then between the voltage control with the airgap flux measurement and current control with the slip speed measurement. The Transvector scheme (principle 2) appears to be too complex, without offering a superior drive performance.

While the constant flux strategy is best represented by the direct flux measurement, the very small airgap in induction motors makes the installation of Hall probes somewhat difficult. This is specially true when the motor is subjected to intensive vibrations, as in railway applications

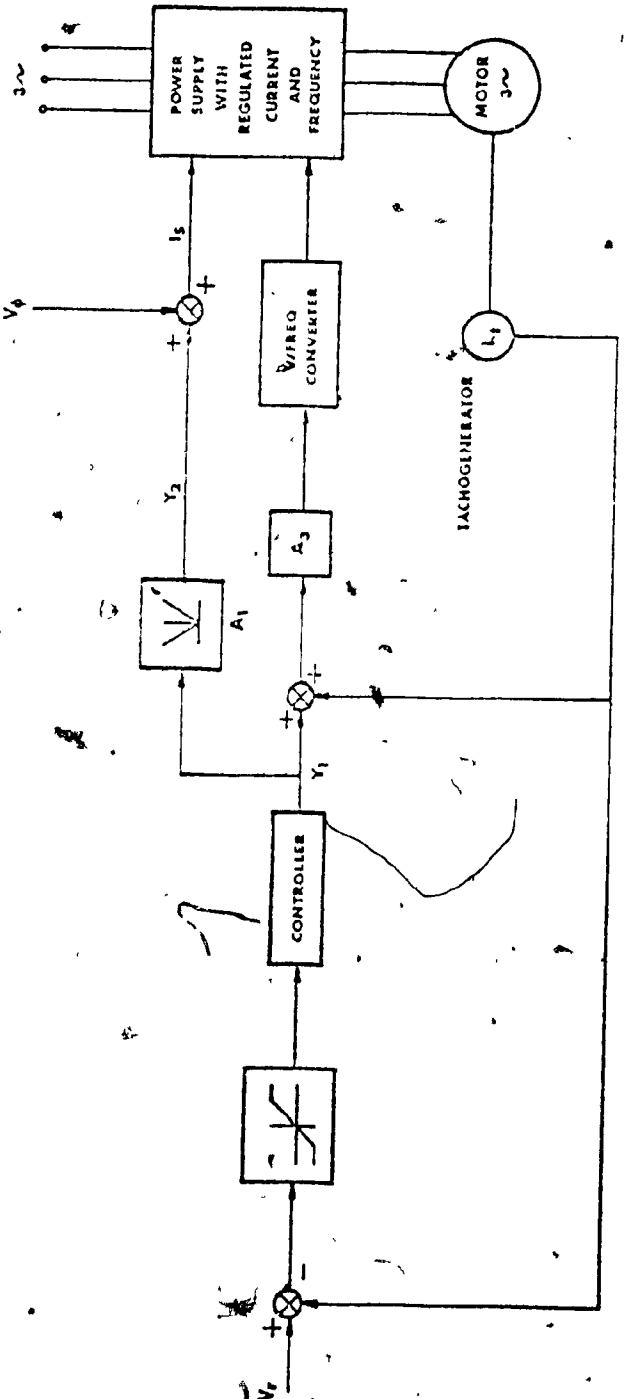

Fig. 4.32: Constant airgap flux drive

Since the current regulated method involves simpler instrumentation and since it has generated an increased interest, it is selected to represent the constant airgap flux strategy in this study

Drive description

The current regulated drive is presented in Fig. 4.32. As in previous drive structures, the power supply has a transfer function of one. The upper input, I_s, gives then directly the motor input current while the output of the A_3 amplifier is equal to the motor input frequency.

To understand the drive operation, consider first the motor running at its synchronous speed. Since the signals Y_1 and Y_2 are zero, the motor input current I_s is equal to the desired magnetizing current I_m, as determined by the reference input V_Φ.

If the motor load is now increased, some slip speed will be developed. One recalls from equation (2-2) that the rotor current depends on the motor slip speed ω_s and the airgap flux Φ.

$$I_r \cong \frac{\omega_s \Phi}{R_2} = \frac{\omega_s M I_m}{R_2}$$

The output, Y_1, of the speed controller is proportional to the slip speed

$$\omega = \omega_s + n\omega_m = (Y_1 + k_t\omega_m)A_3$$

$$Y_1 = \omega_s/A_3$$

If the gain A_1 is selected to be,

$$A_1 = \frac{A_3 M I_m}{R_2}$$

the signal Y_2 becomes equal to the rotor current, i.e.,

$$Y_2 = I_r$$

This means that, as soon as the load is applied and the slip speed is developed, the signal Y_2, representing the rotor current I_r, is added to the magnetizing current I_m, determined by the input reference V_ϕ. The resulting signal is the input into the regulated current supply and determines, therefore, the motor input current. In this way the stator current I_s is always the sum of the constant magnetizing current (V_ϕ) and the varying rotor current (Y_2).

Since the summation of these two currents is not vectorial, the stator current will be in fact larger than that necessary to produce the desired flux and load torque. Thus, the motor will tend to operate with an increasing flux as the load is increased and eventually to saturate. This can be prevented by selecting the gain A_1 so that the rated flux is reached only at the rated load. Any further increase in the load will slightly strengthen the flux and, thus, stiffen the torque-speed characteristic Operations below rated load will cause slight decrease in flux and, thus, improve the motor efficiency in this range, by reducing the magnetizing losses

Note that the A_1 block contains the absolute valued function, since the request for rotor current, Y_2, has to be always positive, even when the speed error e changes its sign during the motor braking operation.

The drive feedback equations follow now directly from Fig. 4 32.

$$I_s = V_\phi + A_1 Y_1$$

$$\omega = n\,\omega_m + A_3 Y_1$$

where I_s is the stator current per phase and $A_3 = n/k_t$.

Assuming that the desired flux level will not change during motor operation, the perturbed feedback equations are:

$$\delta I_s = A_1 \delta Y_1 \qquad (4\text{-}46a)$$

$$\delta\omega = p\delta\psi = n\delta\omega_m + A_3\delta\gamma_1 \qquad (4\text{-}46b)$$

where the variable $\delta\psi$ represents, as before, the change in the phase angle of the mmf vector (Fig. 3.1)

The next step in the derivation of the drive equations is to relate the change of the stator phase current I_s, to the change of motor currents in the synchronous reference frame. These currents are given by the same transformations which were used to obtain motor voltages, Appendix B. For the Y-connected motor, the equations are:

$$i_\gamma^s = I_s \cos((\omega - \omega_c)t + \alpha) \qquad (4\text{-}47a)$$

$$i_\delta^s = I_s \sin((\omega - \omega_c)t + \alpha) \qquad (4\text{-}47b)$$

where ω and ω_c are the supply frequency and the speed of the reference frame, respectively. If $\omega = \omega_c$ the angle α defines the position of the rotating mmf vector with respect to the γ-axis. Since the stator currents are the inputs, one can choose this angle to be zero. Thus, in the steady state, the rotating mmf vector coincides with the γ-axis and the total airgap flux is produced by the γ-current only. If now the magnitude of the stator phase current I_s and its frequency ω are perturbed, the last two equations become:

$$I_\gamma^s + \delta i_\gamma^s = (I_s + \delta I_s)\cos(\psi + \delta\psi)$$

$$I_\delta^s + \delta i_\delta^s = (I_s + \delta I_s)\sin(\psi + \delta\psi)$$

where

$$\psi = (\Omega - \Omega_c)t$$

and

$$\delta\psi = \delta\omega t$$

The speed of the reference frame, $\omega_c = \Omega_c$ is not perturbed.

If $\Omega = \Omega_c$ and the last two equations are developed while approximating

$\cos \delta\psi \approx 1$ and $\sin \delta\psi \approx \delta\psi$, and neglecting the cross products of the perturbed variables, the result is:

$$x_1 = \delta i_\gamma^s = \delta I_s, \tag{4-48a}$$

$$x_2 = \delta i_\delta^s = I_s \delta\psi \tag{4-48b}$$

These two equations give a clear insight into the current-field interaction: since in the steady state, the mmf vector lies along the γ-axis, an increase in the γ-current strengthens the airgap field, equation (4-48a). If the motor supply frequency is changed, the current along δ-axis starts to rise from its zero steady state value, forcing the mmf vector to leave its position along the γ-axis and, therefore, to change its speed. This process is very similar to that for the voltage controlled motor, Fig. 3.1.

Having established this framework, the drive equations are now considered. The basic motor is described by the matrix equation (3-10). In the regulated current drive the stator γ and δ currents (x_1 and x_2) are no longer the drive variables but become the independent inputs. Therefore, the first two rows in equation (3-10) can be deleted. If the remaining equation is rewritten so that all inputs appear on the right hand side, the drive equation becomes:

$$\begin{bmatrix} R_2+L_2p & -\Omega_s L_2 & n(L_2 I_4+M I_2) \\ \Omega_s L_2 & R_2+L_{2p} & -n(L_2 I_3+M I_1) \\ nMI_2 & -nMI_1 & -f_T-J_T p \end{bmatrix} \begin{bmatrix} x_3 \\ x_4 \\ x_5 \end{bmatrix} = \begin{bmatrix} -M_p & \Omega_s M & 0 \\ -\Omega_s M & -Mp & 0 \\ nMI_4 & -nMI_3 & 1 \end{bmatrix} \begin{bmatrix} x_1 \\ x_2 \\ \delta T_L \end{bmatrix} \tag{4-49}$$

where x_1, x_2 and T_L are the drive inputs while x_3, x_4 and x_5 are the drive states, defined by equation (3-11a). If equations (4-46), (4-48) and (4-49) were combined one would obtain the drive state equation with δY_1 and δT_L as the drive inputs. However, such equation would contain the derivatives of the input δY_1. In order to obtain a standard state space formulation, where all dynamics are confined to the system variables, one has to define

two new states

$$x_{10} = x_3 + MA_1\delta Y_1/L_2 \tag{4-50a}$$

$$x_{20} = x_4 + I_S M\delta\psi/L_2 \tag{4-50b}$$

For the sake of uniformity, denote the states of speed and phase angle as:

$$x_{30} = x_5 = \delta\omega_m \tag{4-50c}$$

$$x_{40} = \delta\psi = n\delta\omega_m + A_3\delta Y_1 \tag{4-50d}$$

When equations (4-46), (4-48), (4-49) and (4-50) are combined, the state equation for the regulated current drive is defined as:

$$[P_o]\dot{X} = [Q_o]X + U \tag{4-51}$$

where

$$P_o = \begin{bmatrix} L_2 & 0 & 0 & 0 \\ 0 & L_2 & 0 & 0 \\ 0 & 0 & J_T & 0 \\ 0 & 0 & 0 & 1 \end{bmatrix} \tag{4-52a}$$

$$Q_o = \begin{bmatrix} -R_2 & \Omega_S L_2 & -n(MI_2+L_2I_4) & 0 \\ \Omega_S L_2 & -R_2 & n(MI_1+L_2I_3) & R_2MI_S/L_2 \\ nMI_2 & -nMI_1 & -f_T & nMI_S(I_1\frac{M}{L_2}+I_3) \\ 0 & 0 & n & 0 \end{bmatrix} \tag{4-52b}$$

$$x_0 = \begin{bmatrix} x_{10} \\ x_{20} \\ x_{30} \\ x_{40} \end{bmatrix} \qquad (4\text{-}52c)$$

and

$$U = \begin{bmatrix} R_2 M A_1 \delta Y_1 / L_2 \\ 0 \\ -nMA_1 (I_2 \frac{M}{L_2} + I_4) \delta Y_1 - \delta T_L \\ A_3 \delta Y_1 \end{bmatrix} \qquad (4\text{-}52d)$$

The input Y_1 in the last equation represents the output of the drive speed controller. Thus (4-51) describes really the regulated current, open loop drive. Before the speed loop can be closed, the controller structure has to be defined.

Controller design

The Bode diagram of the open loop drive, at rated load, with Y_1 as the input and motor speed (x_{30}) as the output, is given in Fig. 4.33. Two important observations can be made from this result:

1) The drive frequency response is almost the same as that of a single pole integrator, in contrast with the open loop results obtained for the other drives. The reason for this is that the number of poles and zeros in the open loop transfer function is reduced from 6 and 4 to 4 and 3 when the stator currents become the drive inputs.

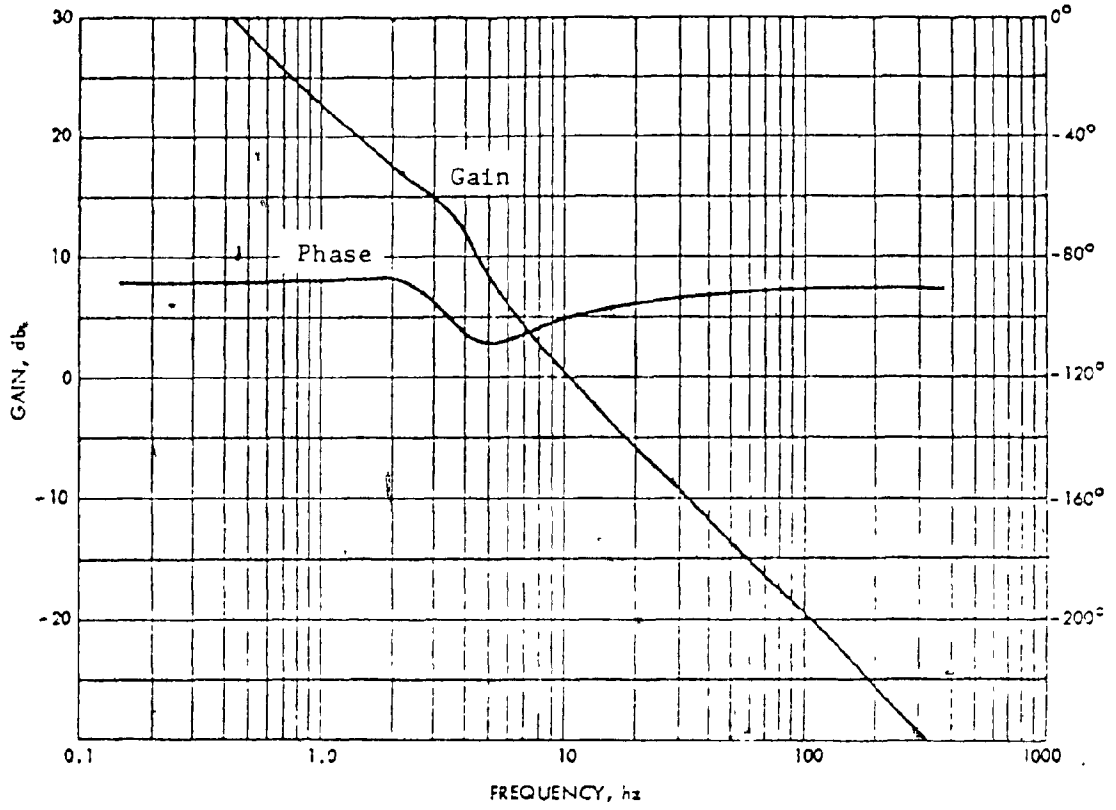

Fig. 4.33 Frequency response of the open loop system.

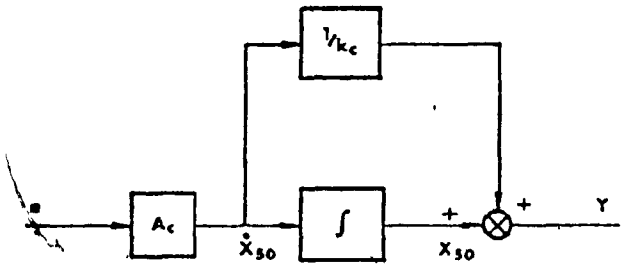

Fig. 4.34: Speed controller for the constant airgap flux drive.

The open loop frequency response indicates an unconditionally stable drive with large available phase margin. The controller design is, therefore, very easy, permitting any desired controller gain.

2) The dynamics of the current regulated drives are independent from the supply frequency. The Bode plot from Fig. 4.33 does not change with the motor operating speed. This then permits the design of an optimal, fixed structure controller, without the need to compromise between the different requirements of the two ends of a speed range.

This very important characteristic is a consequence of the operation with a constant airgap flux. A close examination of (4-52b) shows that it is not dependent on the applied frequency Ω but only on the slip speed, Ω_s. Since P_0 matrix is constant, the drive state matrix A, obtained as

$$[A_0] = [P_0]^{-1}[Q_0]$$

will depend only on the shaft load and not on the supply frequency.

The physical explanation is that the operation at a constant airgap flux reduces the motor electrical system to the rotor windings only, which "don't see" the stator frequency, only the slip speed, i.e., load. It is obvious from this discussion and from the open loop results, that any proportional-integral controller will give a well behaved drive. There is no theoretical limit on the drive bandwidth. Practically, it has to be bounded, in order to stay within the physical constraints. The controller is then so selected that the drive bandwidth is 100 hz. The controller transfer function is:

$$T_c = A_c \frac{s/k_c + 1}{s} \qquad (4\text{-}53)$$

The gain is $A_c = 10$ while the integrator zero is placed at 1 hz. The controller is represented in Fig. 4.34. If the integrator output is chosen as the new state, the controller state equation is:

$$\dot{x}_{50} = -A_c k_t x_{30} + A_c \delta V_r \qquad (4\text{-}54a)$$

while the controller output is

$$Y_1 = x_{50} - A_c k_t x_{30}/k_c + A_c \delta V_r/k_c \qquad (4\text{-}54b)$$

The final equation for the regulated current drive is obtained by combining (4-51) with (4-54):

$$[P]\dot{X} = [Q]X + U$$

The last equation can be written in the standard state space form as:

$$\dot{X} = [A]X + [B]U \qquad (4\text{-}55)$$

Defining, thus, the state and input matrices as:

$$[A] = [P]^{-1}[Q] \qquad (4\text{-}56a)$$

$$[B] = [P]^{-1}$$

where

$$P^{-1} = \begin{bmatrix} 1/L_2 & 0 & 0 & 0 & 0 \\ 0 & 1/L_2 & 0 & 0 & 0 \\ 0 & 0 & 1/J_T & 0 & 0 \\ 0 & 0 & 0 & 1 & 0 \\ 0 & 0 & 0 & 0 & 1 \end{bmatrix} \qquad (4\text{-}57a)$$

and

$$Q = \begin{bmatrix} -R_2 & \Omega_s L_2 & -T_1 - T_3 A_c k_t/k_c & 0 & T_3 \\ -\Omega_s L_2 & -R_2 & T_2 & R_2 MI_s/L_2 & 0 \\ nMI_2 & -nMI_1 & -f_T + T_5 A_c k_t/k_c & T_4 & -T_5 \\ 0 & 0 & n - A_c A_3 k_t/k_c & 0 & A_3 \\ 0 & 0 & -k_t A_c & 0 & 0 \end{bmatrix} \quad (4\text{-}57b)$$

The terms T_1 - T_5 are:

$$T_1 = n(MI_2 + L_2 I_4)$$

$$T_2 = n(MI_1 + L_2 I_3)$$

$$T_3 = R_2 MA_1/L_2$$

$$T_4 = nMI_s(I_1 \frac{M}{L_2} + I_3)$$

$$T_5 = nMA_1(I_2 \frac{M}{L_2} + I_4)$$

The input vector is:

$$U = \begin{bmatrix} T_3 A_c \delta V_r/k_c \\ 0 \\ -T_5 A_c \delta V_r/k_c - \delta T_L \\ A_3 A_c \delta V_r/k_c \\ A_c \delta V_r \end{bmatrix} \quad (4\text{-}57c)$$

The state vector is:

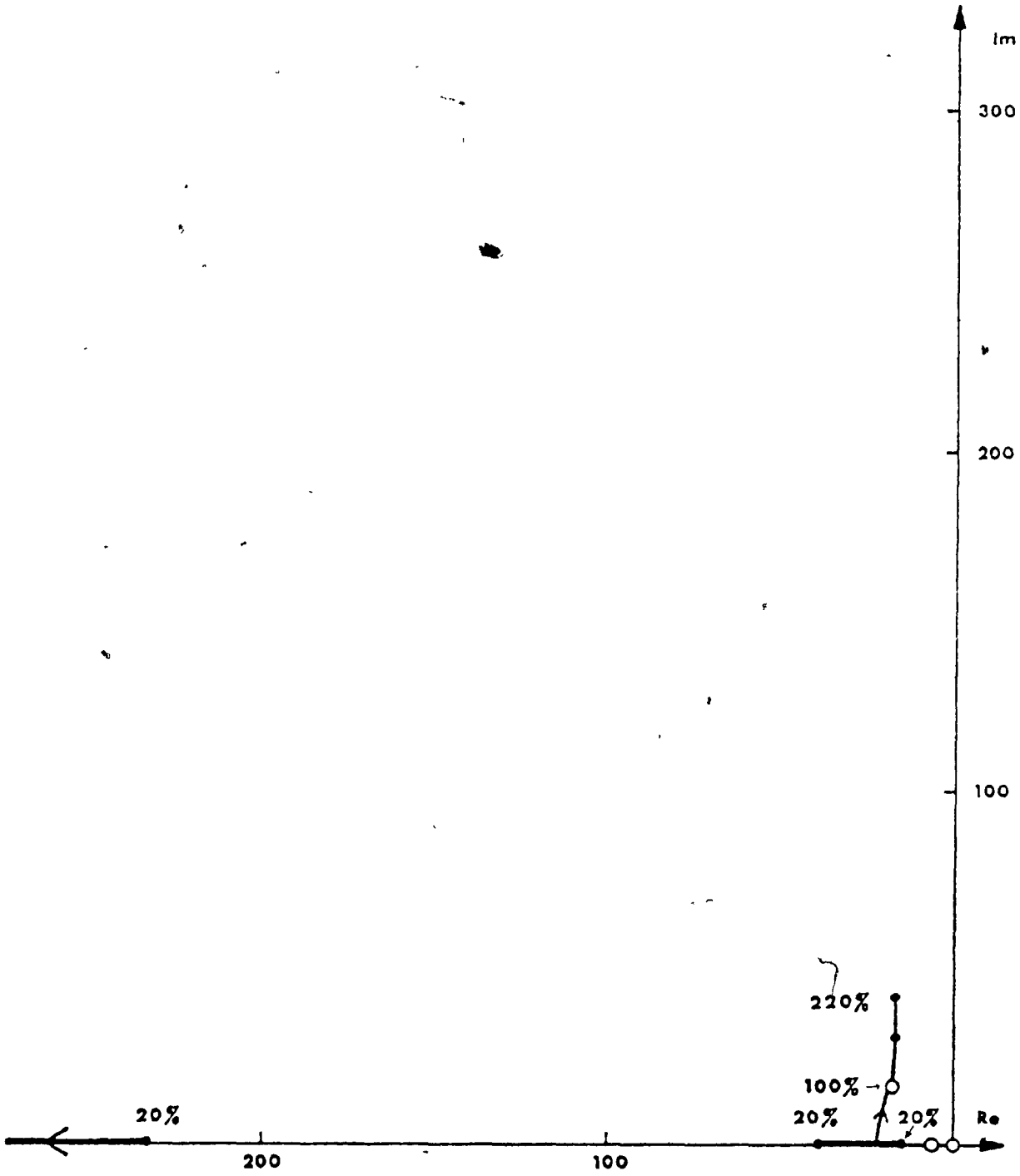

Fig. 4.35: - Eigenvalue locus for constant airgap flux drive. The effects of changing load are also presented.

$$X = \begin{bmatrix} [X_0] \\ x_{50} \end{bmatrix} \qquad (4\text{-}57d)$$

X_0 being defined by (4-52c).

Having established the drive state equations, its dynamic performance can be analyzed using the already outlined procedure.

Drive Analysis

STEP 1. Eigenvalues, eigenvector and input-mode matrices

Since the drive dynamics are independent of the supply frequency, the obtained results do not change with the operating speed, if the load is constant. The eigenvalues, eigenvectors, and input-mode coupling matrix, all calculated at the rated motor load are given in Table 4.12 The eigenvalues in the load range of 20% to 220% of the rated load are given in Fig. 4.35. As concluded before, these results are not suitable in the analysis of the drive dynamic performance. The attention is, therefore, turned to the drive transfer functions and time response

STEP 2. Drive transfer functions

The following two transfer functions have to be found:

1) $G_1(s)$: Speed-input reference

2) $G_2(s)$: Speed-load torque

1) Speed-input reference transfer function

This transfer function is obtained for the constant, rated, load, so that the only input is δV_r, appearing four times in the input vector U, equation (4-47c). From (3-25) the drive speed is given by:

TABLE 4.12

MOTOR DRIVE WITH CONSTANT AIRGAP FLUX CONTROL

OPERATING POINT VALUES:	FREQUENCY(HZ)	VOLTAGE(VOLTS)	SPEED(RPM)	TORQUE(NM)
	30.00	68.0	800.0	18.78

OPERATING POINT CURRENTS:			E-VALUES.REAL	E-VALUES.IMAG.	BREAK FREQUENCY(HZ)	DAMPING
STATOR 1	19.17	1	-635.98	0.00	101.22	1.00
STATOR 2	0.00	2	-6.33	0.00	1.01	1.00
ROTOR 1	-14.97	3	0.00	0.00	0.00	1.00
ROTOR 2	-7.33	4	-16.38	-21.25	4.27	0.61
		5	-16.38	21.25	4.27	0.61

E-VECTORS IN POLAR COORDINATES:

E-VECTOR 1		E-VECTOR 2		E-VECTOR 3		E-VECTOR 4		E-VECTOR 5	
0.5019E 00	0.0000E 00	0.1883E 00	0.1800E 03	0.1000E 01	0.0000E 00	0.7450E 00	-0.6335E 02	0.7450E 00	0.6335E 02
0.1356E-01	0.1800E 03	0.9294E-01	0.1800E 03	0.4898E 00	0.0000E 00	0.3153E 00	-0.1560E 03	0.3153E 00	0.1560E 03
0.1606E 01	0.0000E 00	0.1008E 00	0.0000E 00	0.3311E-12	0.1800E 03	0.3676E-01	-0.1095E 02	0.3676E-01	0.1095E 02
0.6207E-01	0.0000E 00	0.2644E-01	0.1800E 03	0.1364E 00	0.0000E 00	0.4764E-01	-0.5040E 02	0.4764E-01	0.5040E 02
0.9880E-01	0.0000E 00	0.1000E 01	0.0000E 00	0.8231E-06	0.0000E 00	0.8608E-01	-0.6331E 02	0.8608E-01	0.6331E 02

INPUT-MODE COUPLING MATRIX IN POLAR COORDINATES:

0.4185E-01	0.1410E-12	0.1220E 01	0.7667E-14	0.2060E 02	0.2714E-16	0.3232E 00	-0.1800E 03	0.1040E 00	-0.1800E 03
0.2800E 01	0.1800E 03	0.5262E 00	-0.6632E-13	0.1640E 01	-0.1800E 03	0.1291E 01	0.2489E-14	0.1099E 01	0.0000E 00
0.1634E 02	0.1800E 03	0.5066E 01	-0.5684E-13	0.7237E 01	0.1800E 03	0.1131E 02	0.2250E-14	0.2335E 00	0.0 E 00
0.1833E 02	0.9059E 02	0.1935E 02	0.1645E 03	0.6163E 01	0.1752E 03	0.1196E 02	-0.6592E 02	0.3512E-01	-0.1705E 02
0.1833E 02	-0.9059E 02	0.1935E 02	-0.1645E 03	0.6163E 01	-0.1752E 03	0.1196E 02	0.6592E 02	0.3512E-01	0.1705E 02

$$x_{30} = \sum_{k=1}^{5} \frac{m_{3k}}{s-\lambda_k} \sum_{j=1}^{5} h_{kj} U_j(s) \qquad (4\text{-}58)$$

where $u_2(s)$ is zero while h_{kj} and m_{3k} are the components of the corresponding coupling and eigenvectors, respectively. Define a new variable vector UE such that

$$[U] = [UE]\,\delta V_r$$

The components of this vector are obtained from (4-57c) as:

$$UE_1 = T_3 A_c / k_c \qquad (4\text{-}59a)$$

$$UE_2 = 0 \qquad (4\text{-}59b)$$

$$UE_3 = -T_5 A_c / k_c \qquad (4\text{-}59c)$$

$$UE_4 = A_3 A_c / k_c \qquad (4\text{-}59d)$$

$$UE_5 = A_c \qquad (4\text{-}59e)$$

If (4-58) is divided by δV_r, the speed-speed reference transfer function is obtained as:

$$G_1(s) = \sum_{k=1}^{5} \sum_{j=1}^{5} \frac{m_{3k}\, h_{kj}\, (UE_j)}{s - \lambda_k} \qquad (4\text{-}60)$$

Note that here, as in the drives studied previously, the eigenvector component m_{33} is zero, thus, excluding the pole at the origin, λ_3, from the speed expression.

When the appropriate values from Table 4.12 are used in (4-60) the $G_1(s)$ transfer function is obtained. Its Bode diagram is presented in Fig. 4.36b. For the constant airgap flux operation, it will not change with the drive input frequency. However, $G_1(s)$ does depend on the motor load. The full

discussion of the drive frequency response is given in Step 3.

2) Speed-torque transfer function

The speed reference is constant so that $\delta V_r = 0$. The speed is given by the equation (3-25) with the only input being the load torque. Dividing both sides by δT_L the speed-torque transfer function is obtained as:

$$G_2(s) = \sum_{k=1}^{5} \frac{m_{3k}\, h_{k3}}{s - \lambda_k} \qquad (3\text{-}61)$$

with m_{33} being of course zero, (Table 4.12). If the appropriate values computed in Step 1 are used in (4-61) the speed-torque transfer function at rated motor load is obtained. Its Bode plot is presented in Figure 4.37b. This result is discussed again, when the speed step response to load disturbance is analyzed.

Due to the low order of the constant flux drive, the Direct Method is especially effective in giving the analytical expression for the speed-load relationship.

The drive speed controller is described by (4-53) and has only one eigenvalue, located at the origin.

The state matrix of the drive reduced system is obtained from (4-57a) and (4-57b) using Definition 2.

Thus:

$$A_r = \begin{bmatrix} -R_2/L_2 & \Omega_s & 0 \\ -\Omega_s & -R_2/L_2 & R_2 MI_s/L_2^2 \\ 0 & 0 & 0 \end{bmatrix} \qquad (4\text{-}62)$$

The eigenvalues of the reduced system are obtained from (4-62) by hand:

$$s_{1/2} = -\frac{R_2}{L_2} \pm j\Omega_s = -10.28 \pm j\ 21.0 \qquad (4\text{-}63)$$

$$s_3 = 0$$

Using the equation (3-52), the speed-torque transfer function is obtained analytically as:

$$G_2(s) = \frac{s^2(s+R_2/L_2+j\Omega_s)\ (s+R_2/L_2-j\Omega_s)}{J_T \prod_{k=1}^{5} (s - \lambda_k)} \qquad (4\text{-}64)$$

where the drive eigenvalues λ_k's are given in Table 4.12.

The last expression deserves a few comments:

1) The third eigenvalue λ_3, and one zero at the origin, represent the same integrator associated with the change of the mmf phase angle, $\delta\psi$. They will cancel each other, producing the same result in s-domain as the zero eigenvector component, m_{33}, does in the time domain.

2) The second zero at the origin assures zero steady state error by decoupling the steady state speed from the load.

3) The remaining two complex conjugate zeros depend only on motor load as do all four eigenvalues.

4) When the appropriate numerical values from Table 4.12 and equation (4-63) are used in (4.64), it is seen that the pole-zero cancellation is not perfect. This is corroborated by the Bode plot, Fig. 4.37b, and comes as a consequence of the large bandwidth in the drive speed controller.

5) Although poles and zeros in $G_2(s)$ do change with the motor load, it can be shown that their ratio is approximately constant. This means that $G_2(s)$ changes very little with the motor operating point.

Further discussion of the $G_2(s)$ transfer function is continued in the next step.

STEP 3: Frequency and step response

The system performance is best understood by analyzing its time or

frequency response. They are both presented here for comparison. As previously, the time response is calculated in two stages:

- Modal response to a unit step input
- Speed response as a combination of modal states.

1) Response to the unit step in the input reference

The motor load is constant and equal to the rated load. From equation (4-57c) the speed reference, δV_r, appears in four drive inputs. With the unit step in δV_r, these inputs become:

$$[U] = [UE]$$

where the components of the UE vector are defined by (4-59).

From the equation (3-24), the response of each modal state to the unit step in V_r is:

$$q_k(t) = \int_0^t e^{\lambda_k (t-\tau)} \sum_{j=1}^{5} (UE_j) d\tau \qquad k = 1 \ldots 5$$

when solved the last equation gives:

$$q_k(t) = \frac{(e^{\lambda_k t} - 1)}{\lambda_k} \sum_{j=1}^{5} UE_j$$

For the special case of the eigenvalue at the origin, the modal state response is:

$$q_3(t) = t \sum_{j=1}^{5} UE_j$$

The speed response is obtained by using equation (3-25):

$$x_{30}(t) = \sum_{\substack{k=1 \\ k\neq 3}}^{5} \sum_{j=1}^{5} \frac{m_{3k}(e^{\lambda_k t} - 1)}{\lambda_k} UE_j \qquad (4\text{-}65)$$

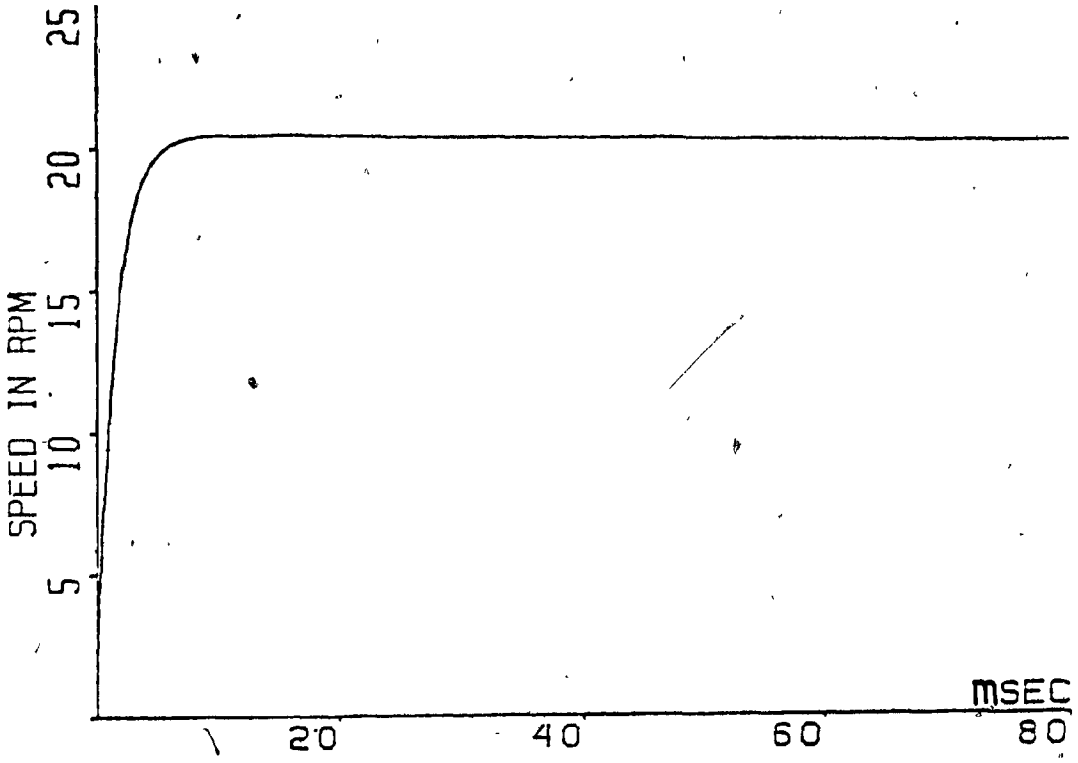

Fig. 4.36a: Speed response to step reference.

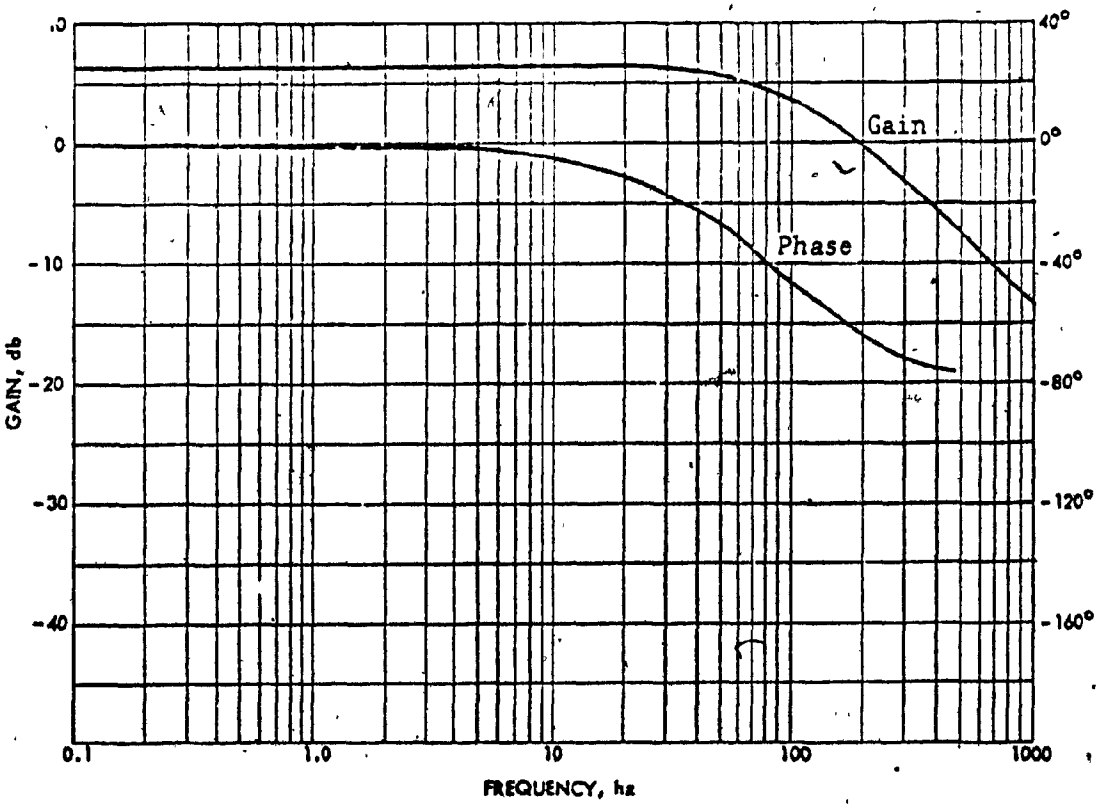

Fig. 4.36b: Frequency response of the speed-input reference transfer function.

Note that the third eigenvalue, λ_3 is unobserveable in the speed response since m_{33} is zero. This reflects the already discussed speed independence from the $\delta\psi$ integrator. The last equation gives analytically the speed response to the unit step in the reference input. The response at the rated load is obtained by inserting the appropriate values from Table 4.12 into equation (4-65). The result is displayed graphically in Fig. 4.36a while the frequency response of $G_1(s)$ is given in Fig. 4.36b for comparison.

Both results point to an extremely well behaved and fast drive. The rise and settling times are 3.1 and 4.2 msec., respectively. Since the drive responds as a pure first order system (Fig. 4.36b), the speed cannot overshoot. The only observeable eigenvalue in the speed response is the one determined by the speed controller gain, with the break frequency of 101 hz (Fig. 4.36b). All other eigenvalues have been made pseudo-observeable by the choice of the speed controller. They are cancelled by the corresponding zeros in (4-60) or, depending on a viewpoint, suppressed from the speed response by the values of the corresponding eigenvectors.

From these results the constant flux drive appears to possess ideal transient characteristic due to its speed of response and the absence of any speed oscillations.

2) Response to a unit step in the load disturbance

Since the input reference V_r is constant, any speed response represents a speed error. A step change in torque is applied with the drive operating at the rated load. As the torque appears in only one input, the response of each modal state is:

$$q_k(t) = \int_0^t e^{\lambda_k(t-\tau)} h_{k3} \, d\tau \qquad k = 1 \ldots 5$$

which, when solved, gives:

$$q_k(t) = (e^{\lambda_k t} - 1)\, h_k / \lambda_k \qquad (4\text{-}66)$$

for the special case of the eigenvalue in the origin, the last equation becomes:

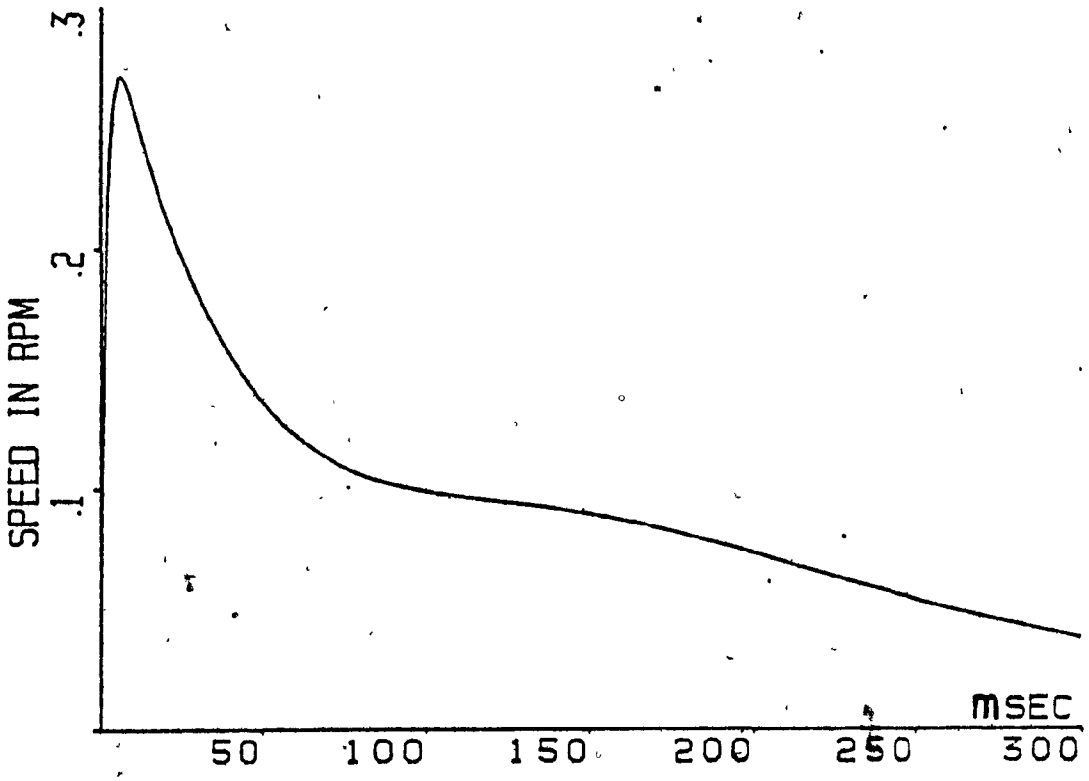

Fig. 4.37a: Speed response to step torque.

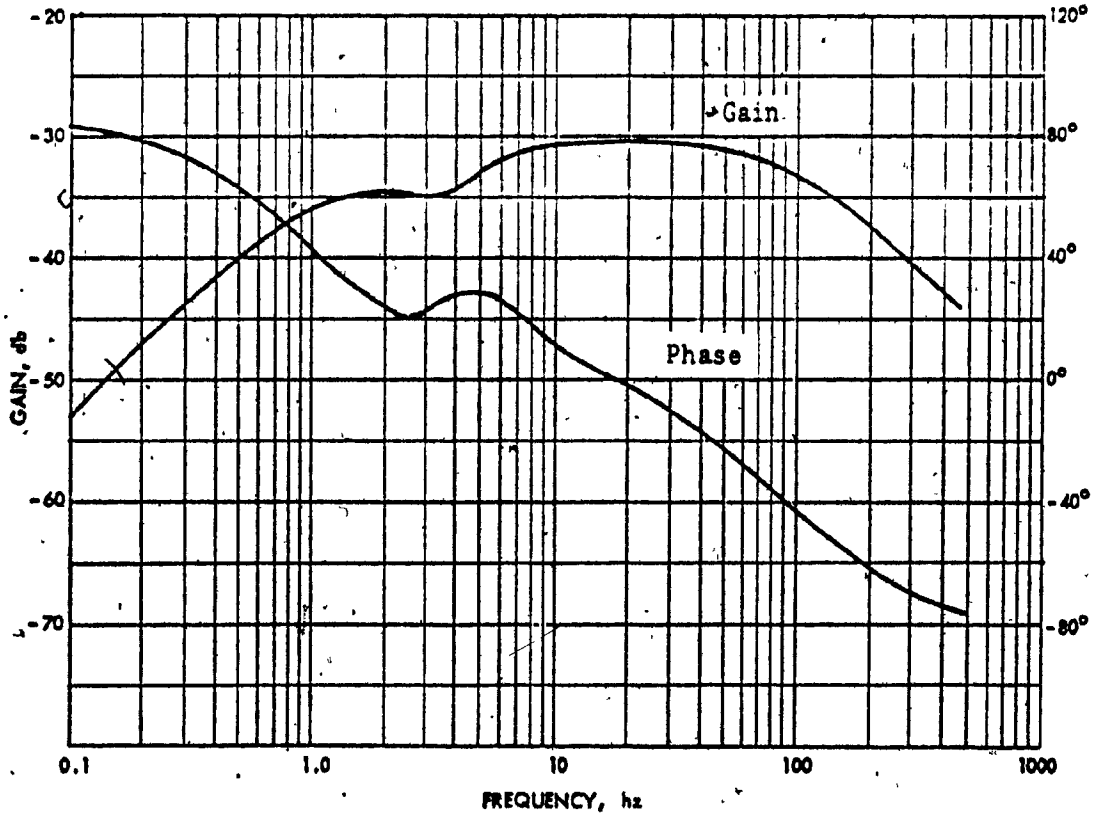

Fig. 4.37b: Frequency response of the speed-torque transfer function.

$$q_3(t) = t\,h_{33}$$

Remembering that λ_3 is unobserveable, because m_{33} is zero, the speed response, given by (3-25) is:

$$x_{30}(t) = \sum_{\substack{k=1 \\ k\neq 3}}^{5} m_{3k}\, h_{k3}(e^{\lambda_k t} - 1)/\lambda_k \qquad (4\text{-}67)$$

Using the corresponding values from Table 4.12, the speed response at the rated load is calculated and displayed in Fig. 4.37a. The Bode plot of the $G_2(s)$ transfer function is given for comparison in Fig. 4.37b.

Since the drive dynamics do not change with the operating speed, these results are valid for any input frequency.

The speed error is very small, as expected, due to the relatively large drive bandwidth. The motor electrical torque can change very rapidly and, thus, offset any load variation.

The maximum speed error is 0.272 rpm and is reached 6 msec. after the disturbance was applied. The error decreases very fast to about 0.1 rpm and then much more slowly, to reach 0.01 rpm after 0.5 sec. The fast decrease is due to the fast change in the electrical torque, as just explained. If the gain of $G_1(s)$ transfer function were finite, some error would remain. However, since the integrator in the speed controller starts to increase this gain continuously below 1 hz (or after 0.16 sec.), making it infinite at steady state, the speed error has to go ultimately to zero.

Note that complex conjugate poles are again pseudo-observable and do not cause any visible speed oscillations.

Conclusion

From these results, the constant airgap flux, regulated current strategy appears as the best of all considered here. The obtained dynamic

performance is superior to that of any other drive structure.

The advantage of the constant airgap flux control is founded on these two facts:

1) The drive dynamics do not depend on the motor operating speed. It is possible, therefore, to design a fixed structure controller which will not be a compromise between contradictory requirements at two ends of the speed range.

2) The constant flux drive behaves as the first order system. This theoretically permits an infinite range of controller gains, without any danger of instability.

The results presented here reflect the drive response with only one of many possible controller gains.

Even if the realization of wide drive bandwidths is restricted by the speed of response of the associated inverter or the noise in the speed sensor, the constant flux control permits the continuous choice of the desired bandwidth. This choice is not constrained by motor dynamics and could be, thus, optimized to match the inverter characteristics.

Although independent of the input frequency, the drive equations depend on the motor load. However, it can be shown that the speed response is very little changed as the load is increased above the rated value. The only change is a small increase in the drive bandwidth (From 110 to 120 hz when the load changes from 100% to 220% of the rated value). The Bode plot, however, remains as flat as for the rated load.

If the load is decreased, the bandwidth will decrease, to reach 50 hz at 20% of the rated load. Again, the Bode plot is perfectly flat, without any gain peaking. The decrease in the bandwidth indicates that the speed response is slower at light loads. Since the requests for large speed changes give rise to large electrical torques (i.e., current), this reduction in the drive bandwidth is not very important.

The complete comparison of the three considered control strategies is given in the next section.

4.5 Summary

Each induction motor has two independent inputs, the applied voltage and frequency. The motor performance depends very much on the control law which correlates these inputs.

In this study, the motor dynamic performance was analyzed in detail for the three most often used control strategies. The following conclusions can be made from the obtained results:

1) The constant V/hz strategy is easiest to implement and the only one which does not require any feedbacks. However, the performance of the open loop drive deteriorates significantly at lower input frequencies (below 10 hz), the most important factor being the reduction in the forward drive gain. This reduction results in the increased sensitivity to load changes and poor speed regulation.

   The drive operation improves considerably when the speed feedback loop is closed. However, due to the motor characteristics, the choice of the associated speed controller is very critical to the drive performance. This means that the controller design is constrained and is dictated first by the need to compensate the motor characteristics and only second by the process requirements. To illustrate this, consider the open loop motor characteristics obtained in Section 4.2.2. It may be desirable, for example, to filter the noise in the speed feedback signal by reducing the drive bandwidth, i.e., controller gain. However, if this is done the drive response may become lightly damped since the drive break frequency is now shifted to the region of lower phase margin. This means that the drive response cannot be selected at will, but is constrained by the motor dynamics.

   Therefore, although the constant V/hz, closed loop drives are theoretically capable of giving excellent performance, the realization of such performance may be difficult in general. Nevertheless, the constant V/hz strategy is worth considering in the design of

induction motor drives.

2) The constant slip speed control makes the motor dynamics very dependent on the operating speed. This is obviously undesirable since contradictory requirements are imposed on the drive compensating networks as the speed is changed, thus precluding a good compromise in the design of a speed controller. In this study the controller was made very sluggish in order to obtain a reasonably damped speed response. The constant slip speed strategy is, therefore, not competitive in high performance drives with the constant V/hz control.

3) The constant airgap flux control gives the most desirable drive performance. This control results in two very important drive characteristics.

   - The motor dynamics become independent of the operating speed, permitting the design of a truly optimal, fixed structure controller.
   - The drive behaves as a first order system, having, thus, an unconditional stability without any speed overshooting. Therefore, there is no need for a carefully selected compensation networks and the drive controller can be designed, without any constraints, to suit the motor application.

Thus, if a truly high performance drive is desired, one would choose the constant airgap flux control. It should be understood that the advantages of this strategy do not depend on the method used for its implementation. This means that the drive with the direct measurement of the airgap flux will have the same desirable characteristics (dynamics independent of speed, first order speed response) as the regulated current drive studied here.

In this study, the drive performance was analyzed for three different control strategies. In some applications one might use more than one voltage-frequency relationship to obtain the desired drive characteristics over the whole speed (load) range. The most common example for this approach is given by the induction motor railway application, where a fixed V/hz relationship

is maintained until the motor rated voltage is reached. Above this point, only the frequency is increased, thus, resulting in the constant horsepower locomotive operation.

All results in this chapter were obtained for the case of an infinite bus power supply, having a sinusoidal output and an instantenous response. In this way, the presented dynamic characteristics are decoupled from the inverter structure and reflect the nature of the induction machine. These results are, therefore, valid regardless of changes in the inverter technology.

However, it is desirable to make this study more relevant to the dynamic performance of present day drives. It is then obvious that these results must be reviewed to take into account various imperfections that were not considered in this chapter. Such a review is presented in the next chapter.

CHAPTER V

LIMITATIONS

5.1 Introduction

The results presented in the last chapter were obtained after making various simplifying assumptions. The validity and effects of these assumptions on motor dynamic performance are now considered. The previously obtained results may be modified by:

1) Non-ideal drive components, in particular the power supplies and the tachogenerator
2) the non-linear nature of the induction motor.

In the last chapter, the drive power supplies were assumed to have:

1) Sinusoidal output voltage
2) Zero output impedance
3) Infinite bandwidth, resulting in an instantenous response.

Realistic power supplies have none of these characteristics. While a detailed analysis of their true behaviour is beyond the scope of this study, some qualitative assessment of the effects which they have on induction motor performance is necessary. Although many good papers have been published on this topic in the last decade,[1,12] they are almost all concerned with steady state motor operation. Therefore, in order to assess the dynamic effects, limitations imposed by realistic variable frequency supplies are discussed in the next four sections. Since all supplies do not have the same characteristics, the effect of each one is evaluated separately.

In general, the four power supplies which can be used with modern variable frequency drives are:

1) Cycloconverters
2) Variable voltage input inverters, with a chopper in the dc link (VVI-1 inverters)

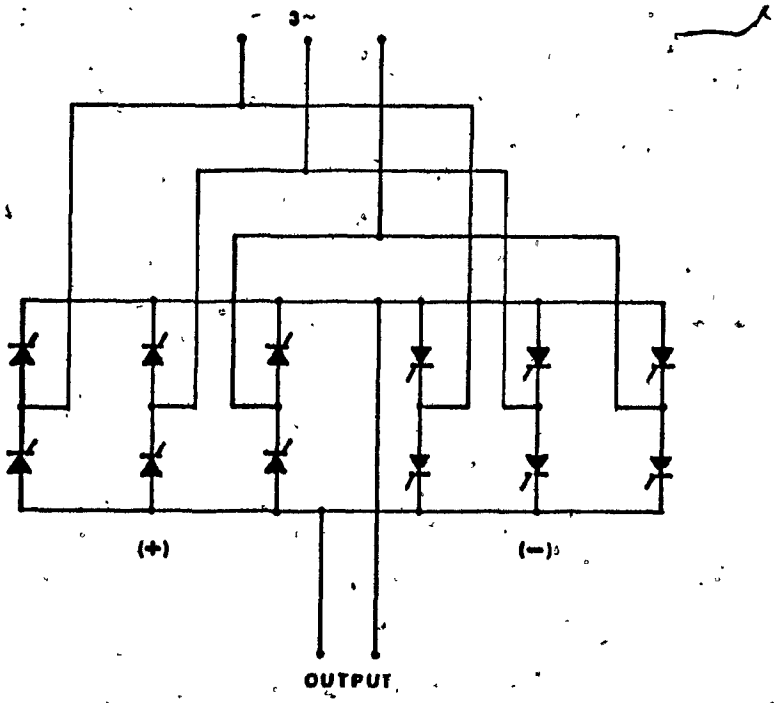

Fig. 5.1a: Single phase cycloconverter.

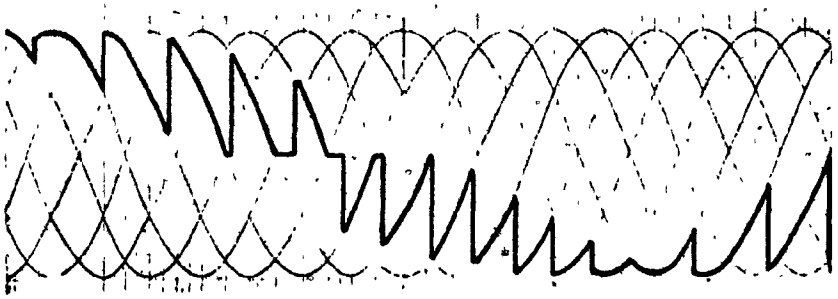

Fig. 5.1b: Cycloconverter output voltage.

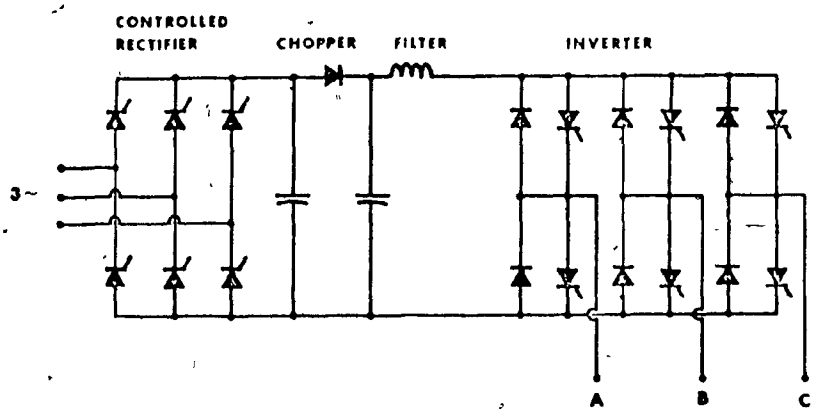

Fig. 5.2a: Chopper controlled, variable voltage input inverter

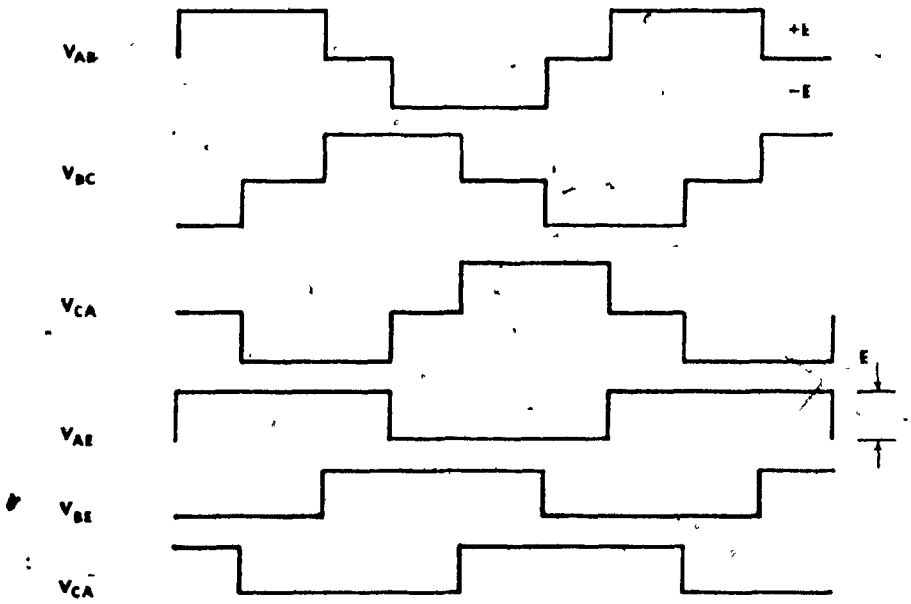

Fig. 5.2b: Inverter line and phase output voltages.

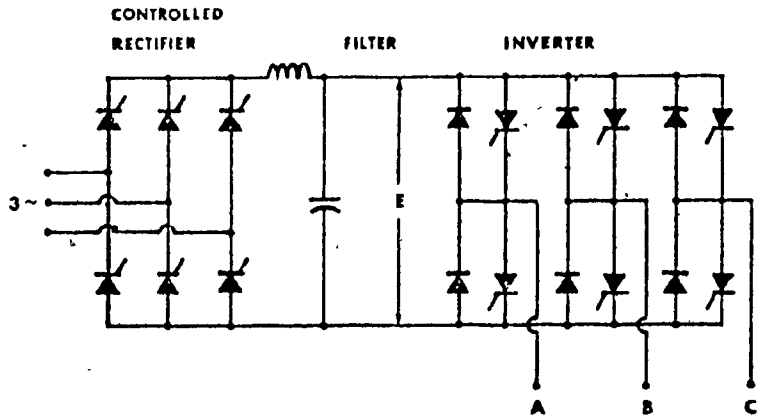

Fig. 5.3a: Variable voltage input inverter with a thyristor bridge.

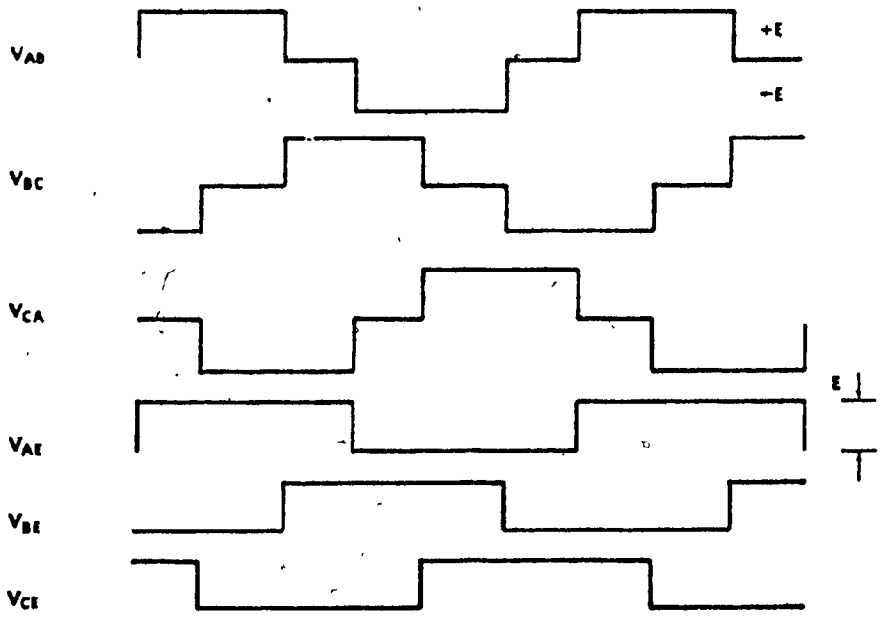

Fig. 5.3b: Inverter line and phase output voltages.

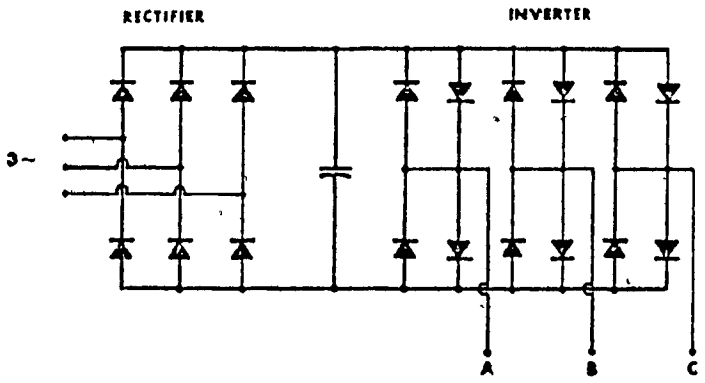

Fig. 5.4a: Pulse width modulated inverter.

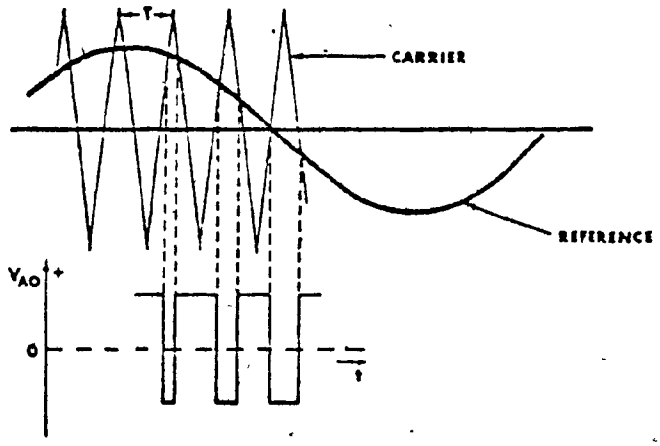

Fig. 5.4b: Sampling of a reference signal.

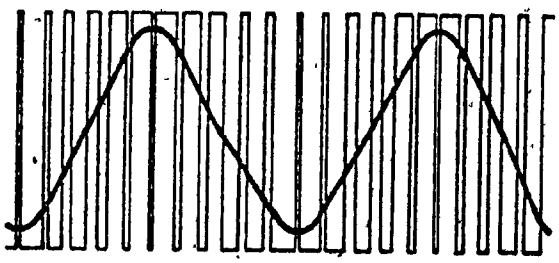

Fig. 5.4c: Inverter output voltage with a fundamental harmonic superimposed.

3) Variable voltage input inverters, with a thyristor bridge (VVI-2 inverters)

4) Pulse width modulated (PWM) inverters.

They are presented in Figures 5.1, 5.2, 5.3, and 5.4 together with the waveforms of their respective output voltages.

Cycloconverters have not found extensive application in industrial induction motor drives. The main reason is that their output frequency is restricted to approximately one half of the input frequency by the harmonic losses. Therefore, cycloconverters will not be considered here.

Since, the only functional difference between VVI-1 (Fig. 5.2) and VVI-2 (Fig. 5.3) inverters is the input power factor, these two types are similar from the dynamic point of view. The analysis is, therefore, directed mainly towards the VVI-2 type inverter, which is more commonly used. The conclusions are then extended to the VVI-1 type.

Two types of controlled current inverters are also considered. The effects of limitations for each type are briefly reviewed.

The remaining two limitations, i.e.,

- the tachogenerator noise
- the need to limit the slip speed so that the motor always operates on the negative slope of the torque-speed curve

are considered in the remaining two sections. Note that the last limitation is caused by motor nonlinearity. Therefore, it will not modify the results from the last chapter, as they were obtained for the motor linearized equations.

5.2 Effects of higher harmonics

In general, all inverters give non-sinusoidal output voltage waveforms. Therefore, the effects of higher harmonics on motor operation was one of the first topics discussed in studies of variable frequency drives.[33, 34, 40, 84-92] These effects may be divided into three categories:

1) Lower efficiency due to increased motor losses

2) Pulsating torques (cogging) at very low supply frequencies

3) Changes in the dynamic performance from that obtained for the sinusoidal voltage operation.

It is well known that the effects from the first two categories are detrimental to motor steady state performance and various techniques have been developed for harmonic suppression.[93-95] One of the most popular techniques for very high power drives is to supply each motor phase from two or more inverters connected in parallel. The selected output harmonics are then cancelled by operating the inverters out of phase with respect to each other.[95] A more direct and economic method is to use a PWM inverter with sufficiently high carrier frequency,[54] (Fig. 5.4) In this case, the inverter voltage output consists of the basic harmonic, which is a replica of the reference signal, and the carrier wave. As the carrier frequency is usually very high, the resulting carrier frequency current is greatly attenuated and appears as noise superimposed on the fundamental harmonic current.[62] Thus, harmonic effects will exist only when a variable dc link voltage inverter is used.

The impact of higher harmonics on motor efficiency and pulsating torques has been discussed extensively.[34,40,84-92] The occurrence of pulsating torques at very low supply frequencies (usually below 2-3 hz) is a property of steady state motor operation. Briefly, the fundamental and higher harmonic airgap mmf interact to produce pulsating torques of 6th, 12th, etc. harmonic frequency and zero average value. Depending on the drive total inertia, these torques may or may not cause steady state speed oscillations as the input frequency is decreased.

The possible dynamic effect of higher harmonics is obtained as the answer to the following question: "Do the drive transfer functions differ from those obtained for a sinusoidal power supply?"

The answer may be found by calculating the speed response to each harmonic component, by using the method of multiple reference frames proposed by Krause and Hake.[89] When these results are superimposed on those from the last chapter, a complete transient speed response is obtained.

For small drive inertia and low input frequencies, it will contain the oscillating component produced by pulsating torques. By taking this component out and comparing the remaining speed response with that obtained in the last chapter for the sinusoidal input voltage, dynamic effects of higher input harmonics become apparent.

A somewhat different procedure was used by Krause and Lipo,[40] who have found that higher harmonics (with pulsating torques included) produce only second order effects. Their results indicate that when steady state pulsating torques are not included, the speed dynamic response is virtually the same as for a sinusoidal input voltage.

To summarize:

- The higher harmonics in the motor supply voltage can be effectively suppressed either by feeding each motor phase from several phase shifted inverters, using transformers, or by using an appropriate PWM inverter. In both cases the drive behaves essentially as when supplied by sinusoidal voltages.
- If variable dc voltage inverters are used, the drive steady state performance will deteriorate, due to the decreased motor efficiency. Depending on the drive configuration, the pulsating torques may affect the speed of very low operating frequencies. However, for all practical purposes, drive transfer functions are not influenced by the higher harmonics and remain essentially the same as in the last chapter. The experimental results, presented in the next chapter, corroborate this conclusion.

5.3 Effects of ac source impedance

It was assumed in the last chapter that each converter-inverter group is supplied from an ac infinite bus. In reality, the drive isolation transformer, as well as the incoming ac lines have some, predominantly inductive, impedance.

For the thyristor bridge, used with the inverter of Fig. 5.3, the

net effect of this impedance would be a decrease in the dc link voltage. This decrease is caused by:

1) Lower terminal voltage on the secondary of the isolation transformer due to the line and transformer voltage drops

2) Commutation overlap in the thyristor bridge circuit. (This aspect is discussed by Pelly.[96])

To prevent the drop in voltage and generally, to improve the thyristor bridge operation, a voltage regulator is normally included. It maintains the dc link voltage at the desired level by changing the thyristor firing angle. Thus, the effect of the ac source impedance is not apparent until all thyristors are fully on, i.e., until the moment when the voltage regulator becomes inoperative (saturated).

In the case of PWM inverters, the dc link voltage is obtained from a diode bridge and, consequently, varies with the load. If an appropriate voltage regulator is included in the inverter structure, it will compensate for the changes in the dc input voltage, so that the inverter output voltage is maintained at the desired level.

To summarize:

The output impedance of the ac source has no effect on the inverter output voltage as long as the corresponding voltage regulator is in operation. For PWM inverters, the output voltage is corrected practically instantenously, the only limit being the inverter sampling delay. For the VVI-2 type inverters, the voltage regulation is performed by the input thyristor bridge which has a bandwidth of approximately 100 hz.[102] For this reason, a very large capacitor is usually connected across the dc bus. Together with the voltage regulator, it effectively shields the inverter dc voltage from load variations. The same conclusion can be made for chopper controlled inverters (Fig. 5.2).

5.4 Effects of transportation lags

In the dynamic analysis presented in the last chapter, it was

assumed that both the voltage and frequency control loops react instantenously to any input signal. In fact, this is not true due to the time lags caused by the thyristor descrete switching. As a result the voltage or frequency can be changed only at the descrete time intervals. The worst case occurs when a change is required immediately after a switching has been made. In this case the full sampling period has to pass before the change can be executed.

Since the two inverter types considered here have different voltage and frequency controls, each one is discussed separately.

In variable dc voltage inverters, the change in the output frequency is achieved by switching the thyristor in the next phase on, Figures 5.2b and 5.3b. In order to preserve the symmetry of the 3-phase wave shape, this switching can occur only at the instant which corresponds to a new requested frequency. It follows then from Fig. 5.3b that the switching delay depends on:

a) the requested change, δf, in the inverter output frequency

b) the inverter operating frequency. The delay is increased as the operating frequency is decreased. For a six step inverter of Figures 5.2 and 5.3, and very small δf, the worst case delay is approximately T/6, where T is the period of the operating frequency before switching.

For VVI-2 inverters, the control of the output voltage is done by the thyristor bridge, Fig. 5.3. As these thyristors are line commentated, the sampling period is determined by their number, N_t. For the inverter from Fig. 5.3, $N_t = 6$ and the sampling period is 1/360 = 2.78 msec.

Several studies have been made to determine a suitable converter dynamic representation.[99-102] Since the converter is a nonlinear device, most analysis were based on its linearized equations at an operating point.[99-101] It was found that a number of linear models can be derived, each one representing a converter under a particular set of conditions.[101] For the case of slowly varying signals and a stable system, the converter dc output component can be calculated using the simple continuous model proposed by Hernandex et al.[101] Finally, it was shown that the converter can be

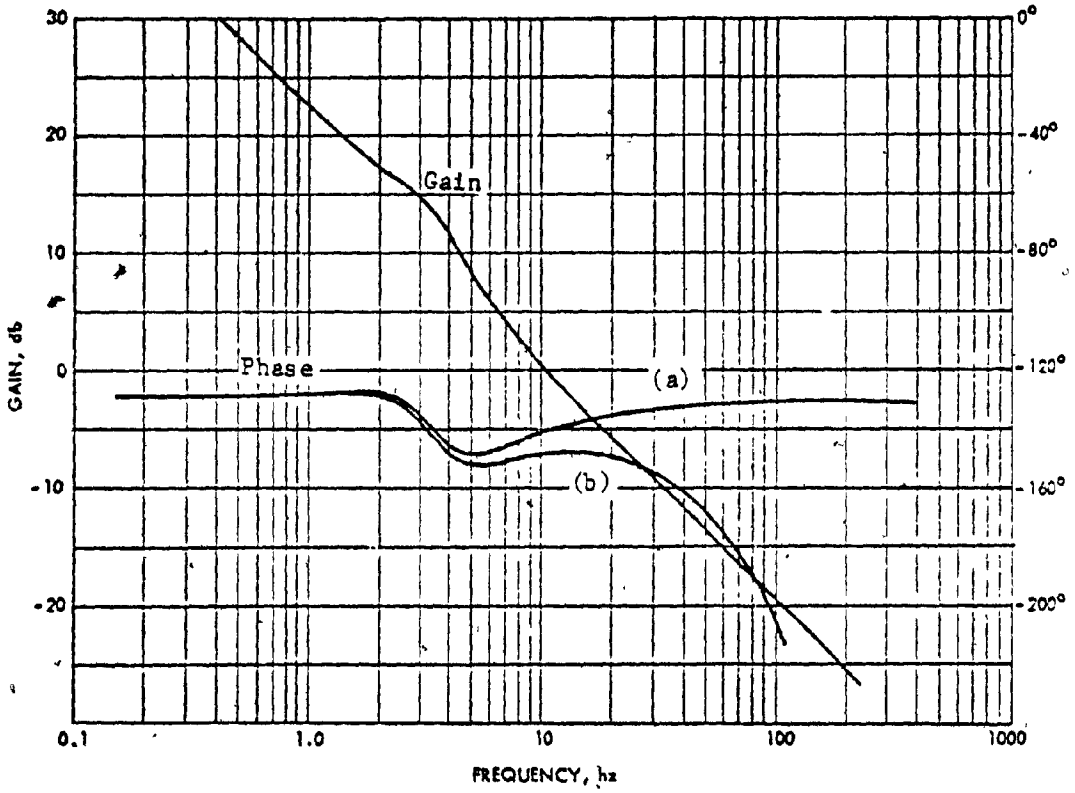

Fig. 5.5: Frequency response of the open loop constant airgap flux drive.

(a) without sampling delay

(b) with sampling delay

represented by a simple gain if its operating bandwidth is limited to approximately 50 hz.[102]

The line commutated converter is used in variable frequency drives only in conjunction with dc link filter (Fig. 5.3). It is shown in the next section that this filter may limit the bandwidth of the voltage control loop to less than 5 hz. It is then obvious that the converter can be represented in this range by a pure gain.

For PWM inverters the response of both frequency and voltage loops depends on the frequency by which the carrier samples the reference signal (Fig. 5.4). With a 600 hz carrier, the sampling time delay (worst case) is 1.67 msec.* When the response of the inverter electronics is included, the maximum total delay is less than 2.0 msec.[97]

However small, this delay is comparable to the dominant time constant of some closed loop drives (sections 4.2, part B and 4.4) and, therefore, cannot be neglected.

It may be recalled that the time delay introduces a phase lag into the system frequency response, without modifying the corresponding gain curve. Therefore, it effectively decreases the bandwidth of closed loop systems by decreasing the phase margin.

Consider, for example, the constant airgap flux drive. Its open loop response is repeated in Fig. 5.5, now with the effect of the 2.0 msec. time delay included. If a phase margin of approximately 50° is desired, the bandwidth of the closed loop drive becomes limited to 50 hz. This is a dramatic change from the situation where the inverter was represented by a pure gain, and the drive bandwidth was theoretically unlimited (section 4.4).

To summarize:

In variable dc voltage inverters the response of the frequency loop is inversely proportional to the operating frequency and the magnitude of the requested frequency change. Typically, the worst case delay for a six step inverter, operating at 5 hz is less than 33 msec.

---

* The maximum time between switching is actually shorter since the reference signal will never intersect the carrier wave at the very top, Fig. 5.4b.

For VVI-2 inverters, the voltage loop includes the line commutated thyristors which introduce appreciable delays. However, these delays do not represent a limiting factor in the drive dynamic performance, since the inverter voltage response is dominated by the very large time constant of the dc link filter.

Although the sampling delays in PWM inverters are shorter, they cannot be neglected in the study of high performance drives, since they dominate the response of both voltage and frequency loops. These delays introduce a phase shift which limits the bandwidth of closed loop drives. The delay times can be calculated on a statistical basis, but a pessimistic estimate is obtained by taking the period of the carrier wave as a sampling time constant.

When this criterion was used on the constant airgap flux drive, it was found that with a 600 hz carrier inverter the drive bandwidth is only half that obtained in the previous chapter.

5.5 Effects of the dc link filter

As seen from Figures 5.3 and 5.4, each inverter is supplied by a rectifier. The ripple in the rectified voltage is eliminated by the dc link filter. Depending on the inverter type, this filter can cause significant modifications in the previously obtained dynamic results.

In the preceding chapter, the drive power supplies were approximated by a pure gain. It is obvious that when the filter is included in a control loop, this approximation becomes invalid.

Consider first the PWM inverter, Fig. 5.4. Since the inverter controls both its output voltage and frequency, the two corresponding loops are closed in the inverter (Fig. 5.6). The dc link filter is left outside the control loop and will have no effect on the drive dynamic performance. The filter can be made as large as is economically feasible, to minimize the fluctuations in the dc bus voltage.

In the case of VVI-2 type inverters, the situation is entirely different. The inverter output voltage is controlled by controlling the dc

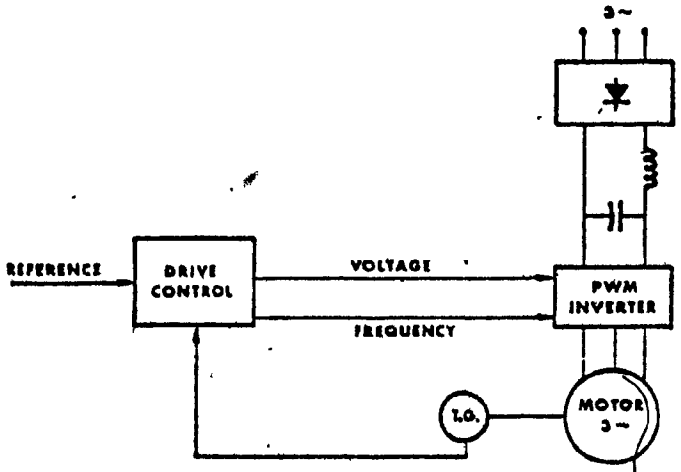

Fig. 5.6: Drive is supplied by a PWM inverter - the dc link filter is outside the control loops.

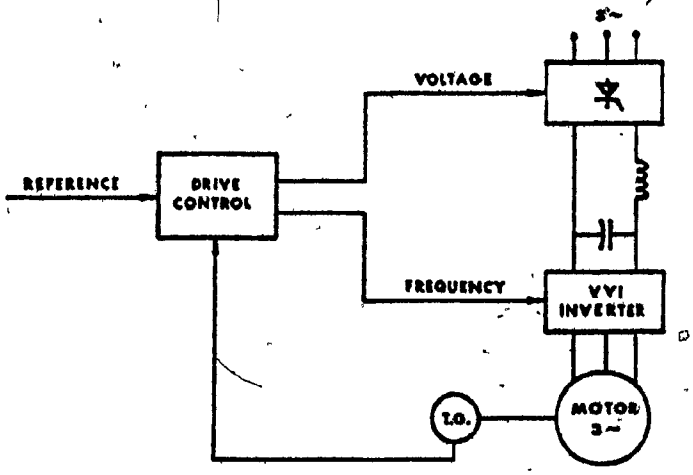

Fig. 5.7: Drive is supplied by a converter controlled VVI inverter - the dc link filter is included in the voltage control loop.

link voltage through the converter inherently included in the voltage control loop (Fig. 5.7). As seen in the last section, the response of the converter bridge is not very fast. Therefore, the role of the filter is not only to eliminate the voltage ripple, but also to supply a part of the inverter dc current at higher operating frequencies, when the converter voltage regulation becomes less effective. For this reason, the dc link filters are much larger than actually needed for ripple control. As an example, the inverter used in the experiments and described in the next chapter has a 24.000 μF capacitor connected across the dc bus. The overall converter-inverter bandwidth was measured to be less than 3 hz. Much larger filters, using up to 40.000 μF are reported in the literature.[39] It is obvious that such filter capacitance prevents any fast change in the dc link voltage and, consequently, in the motor supply voltage.

This slow response will have different effects on motor dynamic performance, depending on a particular drive configuration:

- the speed controller is made very slow so that both loops are able to track the input request. Consequently, the same control strategy exists during both steady state and transient operation.
- the speed controller is faster, but still slow enough that the response of the frequency loop may be considered as instantenous. If the frequency loop is now subjugated to the generally slower voltage loop, the desired control strategy is again preserved during the transients. If, however, the frequency loop is permitted to respond with its own speed, a particular control strategy will be lost during drive transients. For the case of constant slip speed control, this will lead directly to instability, due to the positive feedback frequency loop, Fig. 4.21. For constant V/hz and airgap flux drives, the slow voltage response will cause a deviation from the desired control strategy. The extent of the deviation will depend on the drive components, the operating point and the instant when the request for a change in speed is made. This deviation may lead to poor dynamic performance.
- the speed controller is fast so that the time constants of each

loop have to be taken into account. If each loop is allowed to respond with its own speed, the aberrations from the desired motor transient behaviour will only increase. If the faster loop is slaved to the slower one, the desired control strategy will exist at all times. Note that this may be difficult to achieve in practice due to the nonlinear and statistical behaviour of the frequency loop.

To summarize:

When PWM inverters are used, the dc link filter is placed outside the control loop and, therefore, does not influence the drive dynamic performance.

If VVI-2 inverters are used, a serious deterioration in the speed response occurs. The dc link filter slows down the inverter voltage response considerably. Depending on the interaction between voltage and frequency loops, this may either:

- limit the bandwidth of the whole inverter to the point where the drive response is approximately the same as for the open speed loop operation

or

- cause a departure from a particular control strategy during drive transients. This departure will introduce a new voltage-frequency relationship, which may lead to the drive instability.

One should note that chopper controlled inverters (Fig. 5.2) generally, have a faster voltage loop than VVI-2 inverters (Fig. 5.3). The reason is that the filter between the chopper and inverter can be smaller since the chopping frequency is usually high.

5.6 Limitations of controlled current inverters

In this discussion the effects of the component limitations were related to the performance of controlled voltage inverters. Since it was

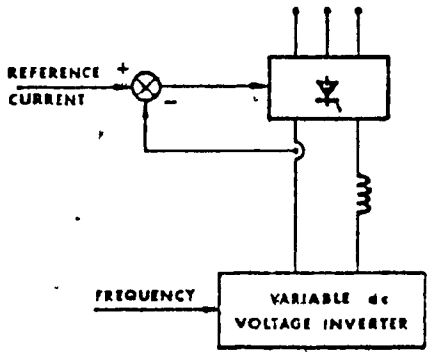

Fig. 5.8: Regulated current source with a VVI inverter.

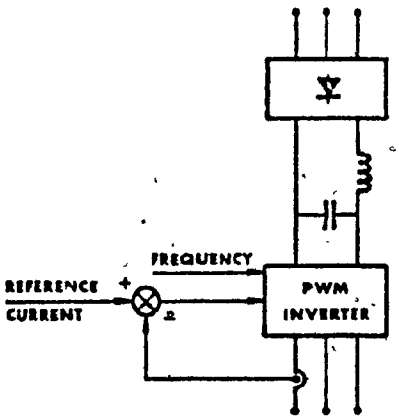

Fig. 5.9: Regulated current source with a PWM inverter.

found that the constant airgap flux strategy gives one of the best dynamic characteristics and since this strategy is most easily implemented by regulating the motor input current, controlled current supplies are now briefly considered.

Basically, two methods can be used to provide a variable frequency, regulated current. One was proposed by Phillips[58] and involves a controlled current supply and a variable dc voltage inverter, Fig. 5.8 . The other is to use a PWM inverter with current feedback, Fig. 5.9 . The inverter output voltage is continuously adjusted to provide the desired motor current.

It may be seen that the first method is inferior to the second one for the following reasons:

1) The regulated current supply consists of a thyristor bridge and a dc link inductance. It suffers, therefore, from the same slow response as the regulated voltage source, Fig. 5.3a.

2) The output is now a square wave current, as the inverter switches between the dc rails. The effect of harmonics is, thus, much greater than before, when the output was a square wave of voltage and the motor inductances acted as a filter. (Note that this disadvantage still exists when the chopper controlled inverter is used instead).

On the other hand, the PWM source (Fig. 5.9) provides a sinusoidal output current, with switching noise superimposed. The source operates essentially as a normal PWM inverter. The only difference is that now the current loop controls the output voltage. If the inner (voltage) loop is sufficiently fast (and this depends on the carrier frequency), a fast source response can be obtained, since the outer (current) loop has a wide bandwidth. Note that the inverter should have a large voltage margin to be used during fast current changes.

To summarize:

When the drive operates in the regulated current mode, better performance is obtained by using a PWM inverter, which has a superior dynamic response and gives practically sinusoidal output current, than when a voltage

inverter supplied by controlled current is used.

5.7 Effects of the tachogenerator

The tachogenerator is normally a part of closed loop speed drives. It can be one of the following types:

1) dc

2) ac

3) digital

A description of the characteristic of each type is available in the literature.[104]

The tachogenerator is usually represented by a pure gain, k_t, as in the previous chapter. However, depending on its type and installation, the tachogenerator may introduce the following effects into the speed control loop:

1) A phase shift and a magnitude attenuation

2) Noise.

The first effect results from the finite bandwidth of its transfer function, defined as the ratio between the changes in the motor speed and the tachogenerator output voltage. (Note that this definition includes all mechanical couplings between the motor and the tachogenerator.)

The second one can be caused by mechanical resonance, rotor eccentricity, brush noise, etc.

The first effect can be usually reduced to a tolerable level by mounting the tachogenerator on a very stiff shaft, as close as possible to the motor. This increases the bandwidth of the tachogenerator transfer function. At the same time, it decreases the noise level in the speed signal by pushing the resonant peak of the coupling shaft outside the drive bandwidth. However, some noise will always be present. It can be shown experimentally that its frequency is usually proportional to motor speed. As the speed is lowered, the noise falls into the drive bandwidth, the controller interprets

it as a speed disturbance and takes corrective action. Consequently, the controller and the complete drive operate continuously in a transient state, trying to respond to false speed errors. To prevent this, the speed signal has to be filtered whenever the noise amplitude or the controller gain are too high. Obviously, this decreases the drive bandwidth.

To summarize:

The tachogenerator noise is often at a level such that speed signal filtering becomes a necessity. This filtering may reduce the drive bandwidth; the actual values depending very much on the particular installation.

The use of digital tachogenerators will greatly reduce the noise problem. However, they pose problems at very low speeds.

A method by which the speed signal is reconstructed from the motor input voltage, current and their phase angle has been proposed recently.[104] Judging from the experimental results, it holds considerable promise for eliminating the noise problem.

5.8 Effects of the slip limit

All the limitations discussed previously were caused by imperfect drive components. The need to limit the slip speed is a result of induction motor nonlinearity.

Consider a squirrel cage motor, supplied from the PWM inverter and operating under constant flux control at speed n_1, Fig. 5.8. If a request for large speed change, say to n_2, is given, the voltage and frequency can change almost instantenously, transferring the motor operation to point B. This is undesirable because:

- the available accelerating torque becomes small
- the resulting motor currents are very large
- torque oscillations (not shown in Fig. 5.7) are possible if the slip is large.

If the slip speed is instead limited to ω_1, the voltage and frequency will

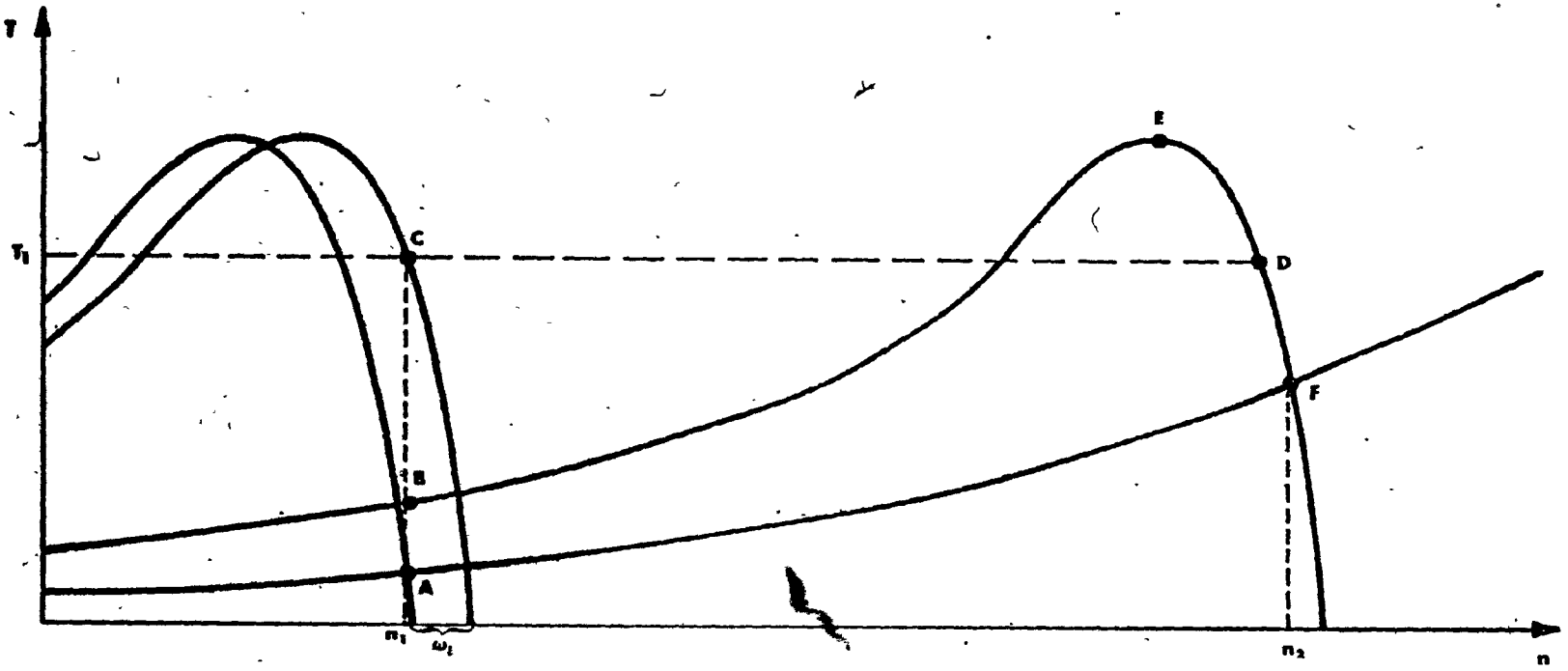

Fig. 5.10: - Large speed variation-motor accelerating with and without slip limit.

rise instantaneously only until the value of ω_1 is reached (point C). After this the limiting element (Fig. 4.30) determines their rate of change so that the motor accelerates using a much larger torque T_1, determined by ω_c. The motor maximum torque is never exceeded.

It is obvious from this example that the rates of change in motor input voltage and frequency have to be limited if the drive is to have minimum transient times during large speed changes.

Note that constant slip speed drives are an exception, since their frequency loop is subjugated to the voltage loop. Consequently, the motor maximum torque can never be exceeded and the limiting element serves only to protect the motor (and the inverter) from exceptionally high currents, (Fig. 4.20.)

Note as well that the motor static chracteristic was used for simplicity in the last example. In reality, the trajectory of the operating point follows the dynamic curve which is obtained by solving the drive non-linear differential equations.

The dynamic results, obtained in the last chapter are not affected by the slip limit, since they represent the motor behaviour in the vicinity of an operating point. However, they cannot be extrapolated without taking this limitation into account. The drive total transition time is found by solving its differential equations for each of the three trajectories indicated in Fig. 5.10. Note that the transition from point C to D requires an exact knowledge of the motor permissible torque, i.e., the slip speed limit ω_1. For constant airgap flux control this does not present a problem since the drive dynamics are independent of frequency. For constant V/hz drives the slip speed limit has to be adjusted continuously for each operating frequency, in accordance with the maximum available motor torque, Fig. 2.4b. The other alternative is to set ω_1 at the worst case level for a particular operating range. This means that the motor torque capabilities will not be fully exploited at higher input frequencies. The third alternative is obviously to break the constant V/hz ratio when a predetermined slip speed is reached and to boost the input voltage until the desired torque is obtained. Depending on the implementation, the last alternative may require additional feedback loops or, at least another limiter in the

frequency loop.

The same problem exists with constant slip speed control, since the setting of the voltage limit, Fig. 4.20, depends also on the motor input frequency. In addition to this, if the normally small value of the slip speed is not increased during large speed changes, the motor will either develop a small accelerating torque, or operate well into saturation as explained in section 2.3.

To summarize:

The slip speed limit is necessary to ensure operation on the negative slope of the torque speed curve and, thus, to provide the shortest possible transition times during large speed changes; motor starting included. This limit does not affect the previously obtained dynamic results which are valid in the vicinity of an operating point.

If the three control strategies are compared with respect to the slip limit, the constant airgap flux drive again appears to be the best one, for the following reasons:

1) It gives a fast response for the large speed changes due to the large permissible torques.

2) The limiting slip speed ω_1 can be constant over the whole operating range.

During this discussion the assumption was made that the value of the limiting slip speed ω_1 is determined only by the motor permissible torque. In this case, the inverter has to be overrated as it must supply currents which are several times the motor rated current. In order to limit these currents and, thus, to decrease the inverter cost, a lower value can be selected for ω_1. However, this will result in a slower drive response.

5.9 Summary

In this chapter a comprehensive survey was made of the factors which may limit drive dynamic performance. The first six sections were

devoted to the drive power supplies and the tachogenerator, the last one to the motor nonlinearity.

When PWM inverters are used, the effects of the higher harmonics, ac source impedance, and dc link filter are negligible. The sampling time delays have to be taken into account as they dominate the inverter response.

In variable dc link voltage inverters, the time constants of the voltage and the frequency control loops are different, the frequency loop being generally faster. Therefore, a particular control strategy is preserved during drive transients only if either the speed controller is very slow, so that both loops can track the input request, or a faster control loop is subjugated to a slower one.

When regulated current supplies were considered, it was seen that the PWM inverter with a current controlled output offers superior performance, since it yields both fast transient response and sinusoidal output currents.

While tachogenerators are being continually improved, they cannot be made absolutely noise free. With higher controller gains and faster responding drives, this noise often becomes a prime limiting factor.

In agreement with previous studies,[37] it was seen that optimal drive performance is obtained by limiting the slip speed during large speed changes. It was found that in this mode, constant airgap flux control gives the best results since it yields large and constant permissible torques over the entire operating range.

Many of limitations discussed in this chapter will become irrelevant if a drive application does not require a fast speed response. However, when high dynamic performance is desired, these limitations have to be critically evaluated so that the most suitable control strategy and correct drive components are selected.

CHAPTER VI

EXPERIMENTAL RESULTS

6.1 Introduction

Various limitations of realistic drives were reviewed in the last chapter in order to make the theoretical results more relevant to practical induction motor drives. This aim was further pursued by performing a series of experiments on an actual machine. The results of these experiments are presented and discussed in this chapter.

Within the constraints of the available equipment, the experiments have been designed with the following objectives in mind:

(1) Verification of the motor dynamic model

(2) Extension of the dynamic results to the motor nonlinear behaviour

(3) Assessment of the inverter effects on the motor transient response.

Due to the inverter limitations, to be described in the next section, it was not possible to obtain meaningful closed loop results. However, the open loop measurements are in good agreement with the predicted motor behaviour. By confirming the validity of the motor dynamic model, the experiments support also the closed loop theoretical results, within the approximations made in Chapter IV.

As in previous chapters, results in both the time and frequency domains are obtained. While the speed step response in the time domain gives overall information about system stability, it conceals the details of the motor dynamic characteristics. Therefore, the theoretical results are verified by measuring the motor transfer functions in the frequency domain while the step response is used in the study of motor nonlinear behaviour.

6.2 Apparatus

The equipment used to carry out the experiments consisted of:

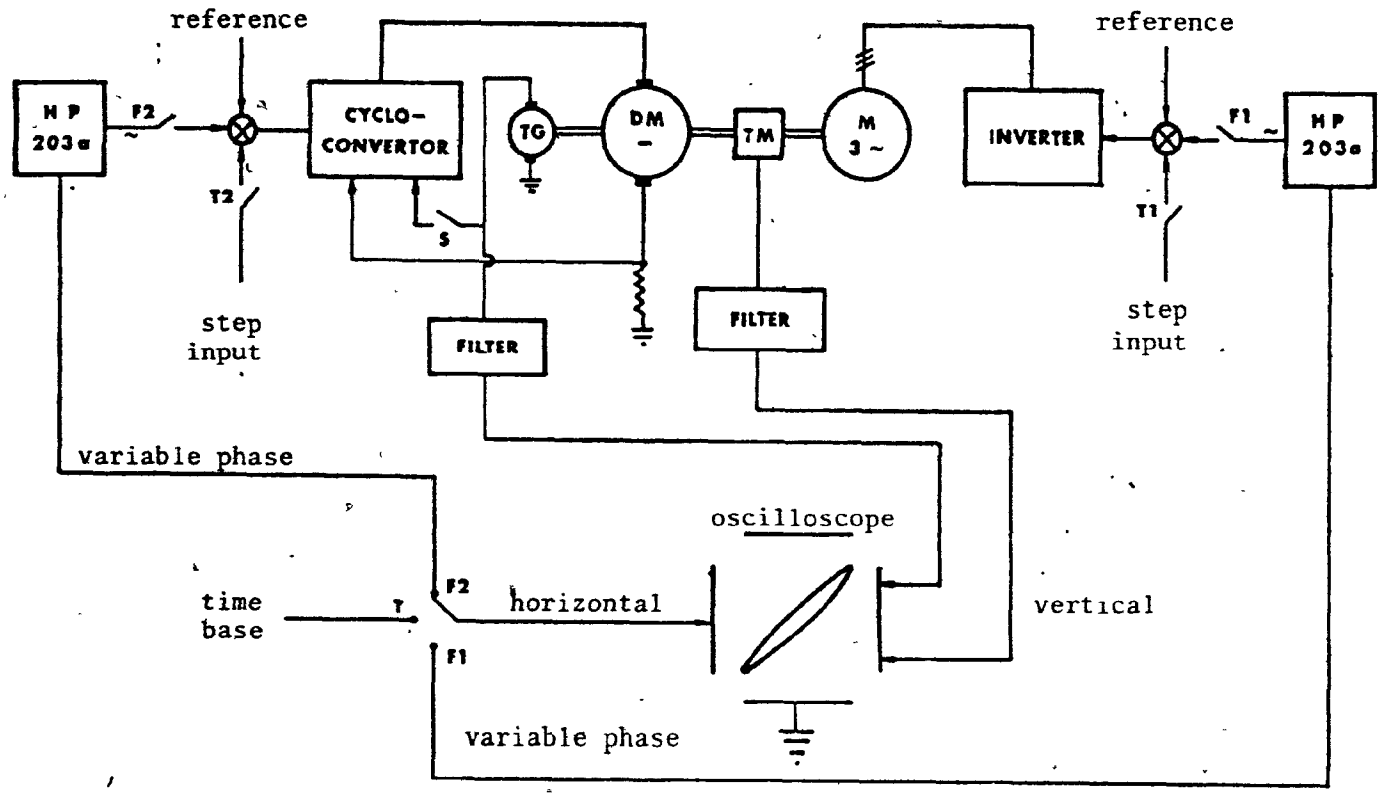

Fig. 6.1: Dynamic testing of a constant V/hz, open loop induction motor drive.

- A 3-phase wound rotor induction motor, with parameters as given in Appendix A.
- A variable voltage input (VVI) inverter, type SP-200 (General Electric) operating with constant V/hz control.
- A dc machine with inertia of 0.14 kgm^2.
- Single phase cycloconverter, used to supply the dc machine.
- A precision torquemeter.[105]
- A dc tachogenerator.
- A variable phase function generator, Hewlett Packard type 203A.
- A storage oscilloscope, Hewlett Packard, type 141A.

The cycloconverter and the dc machine form a high performance dynamometer[102]. The dynamometer is used to load dynamically the induction motor. The equipment set-up is presented in Figure 6.1.

The dynamometer can operate in either a current or speed control mode.[102] In the current mode it provides a regulated load torque for the induction motor, over the whole speed range and has a bandwidth of 50 hz. In the speed mode, it determines the speed of the whole group. In this mode, its bandwidth is at 15 hz.

All frequency response measurements were performed in a standard way, by comparing the input and the output gain and phase, using Lissajous figures. The filter is used to eliminate high frequency noise, especially present at lower operating speeds. The step response measurements were performed by applying a step reference to the appropriate power source (cycloconverter or inverter).

Altogether, four different types of measurements were made:

(1) Speed-torque transfer functions, $G_2(s)$. The inverter reference was maintained constant, while the cycloconverter sinusoidally perturbed the dc machine armature current and thus the shaft speed. The dynamometer was in the speed control mode, with speed feedback loop closed. The experiment was performed with S and both F2 switches closed and all others open. The main frequency of both filters was maintained the same as the perturbation frequency.

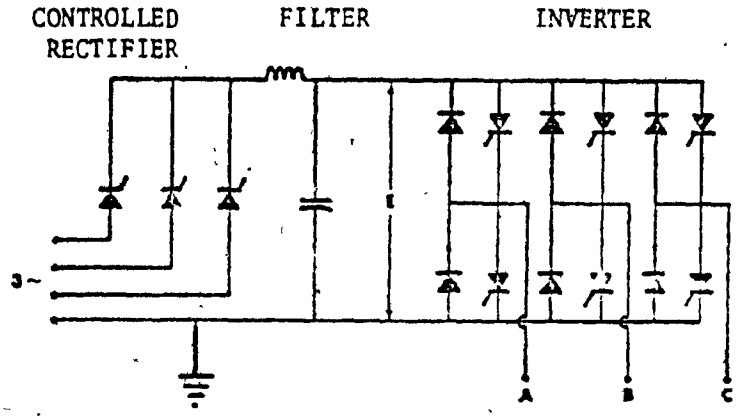

Fig. 6.2: The inverter used during induction motor dynamic measurements.

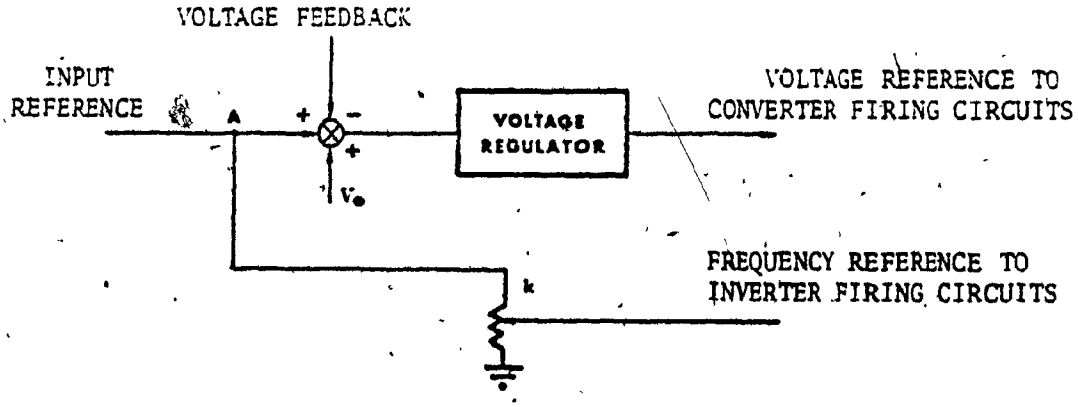

Fig. 6.3: Inverter controls giving constant V/hz strategy. The output voltage is $V = V_o + k f$.

(2) Speed response to a step torque. The corrections were the same as for (1) except that switches S, T2 and T were closed, all others being open. The break frequency of both filters was set at 200 hz.

(3) Speed-speed reference transfer function, $G_1(s)$. The cycloconverter reference was maintained constant, the dynamometer then providing a constant load torque. The inverter reference was a sinusoid. Both F1 switches were closed, all others were open. The break frequency of both filters was the same as the perturbation frequency.

(4) Speed response to step reference input. This was the same as for (3) except that both T1 and T switches were closed, all others being open. The break frequency of both filters was set at 200 hz.

In the last two types of experiments, the inverter dynamics had a considerable effect on the measured results. A brief description of the inverter is therefore presented. The inverter name plate ratings are:

INPUT:	Volts	416/240
	Amps	45
	Hertz	60
	Phase	3
OUTPUT:	hp	10
	Volts, A.C.	200
	Amps, A.C.	58
	Hertz, base	120
	Phase	3

Model No. 6V20D1003 Drive Code AF-3090

The inverter schematic is given in Figure 6.2. Both voltage and frequency can be adjusted individually to obtain the desired V/hz ratio. The input converter consists of a 3 phase, half wave thyristor converter, thereby placing stringent requirements on the ac source. As the recommended 4-wire supply transformer was not available at the time of the experiment, an existing step-up transformer was used. As the induction motor load was varied, the effect of the ac source impedance was strongly felt, especially

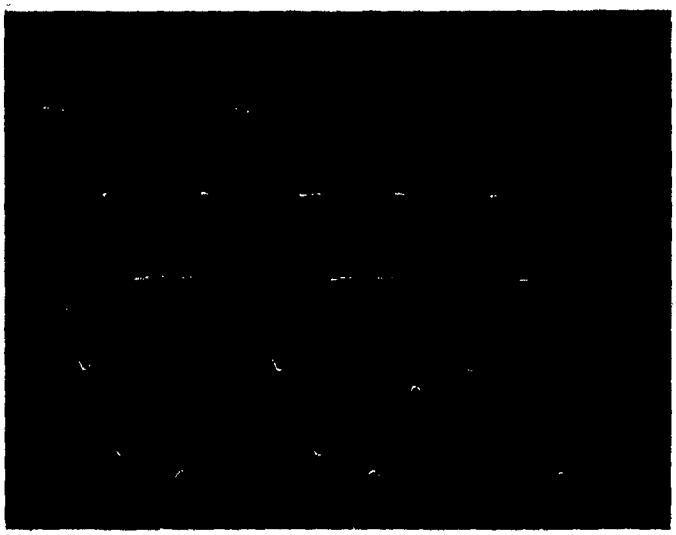

Fig. 6.4a: Inverter outputs at 60 hz.
(Trace allocation same as below).

Fig. 6.4b: Inverter outputs at 2 hz.

Trace 1: Voltage

Trace 2: Current

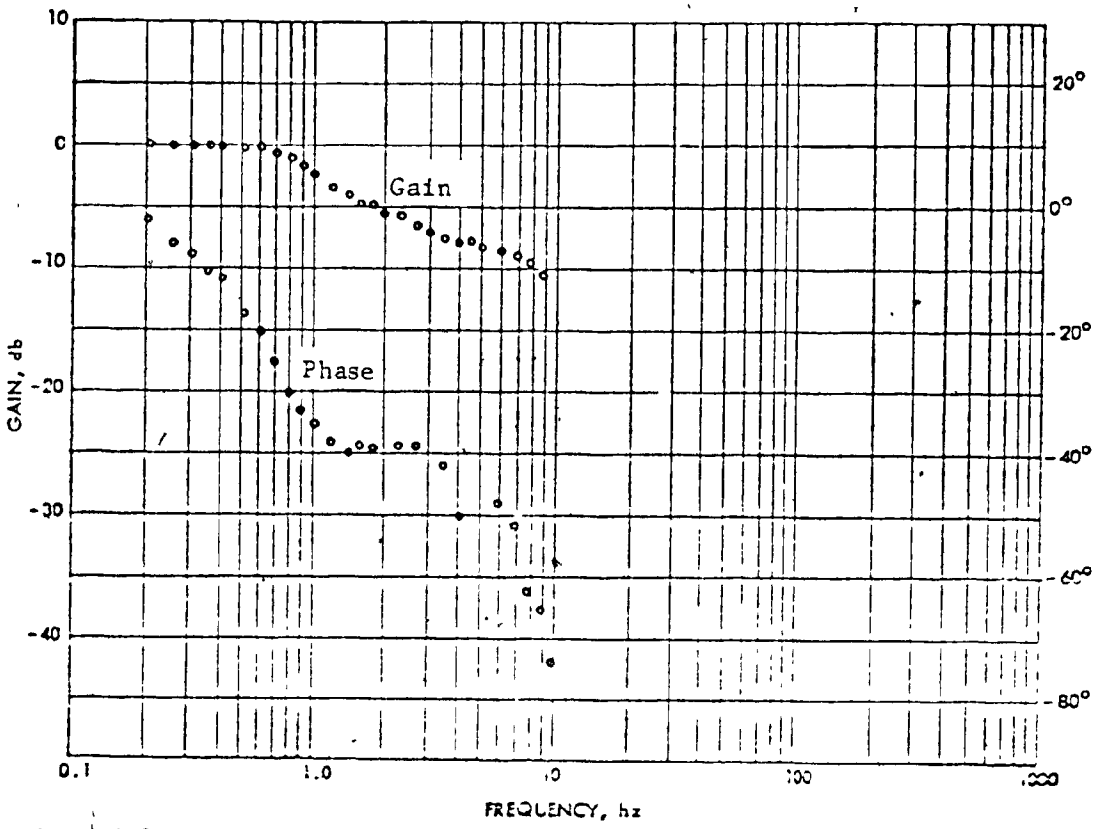

Fig. 6.5a Frequency response of the converter voltage transfer function at 60 hz inverter frequency and rated motor current.

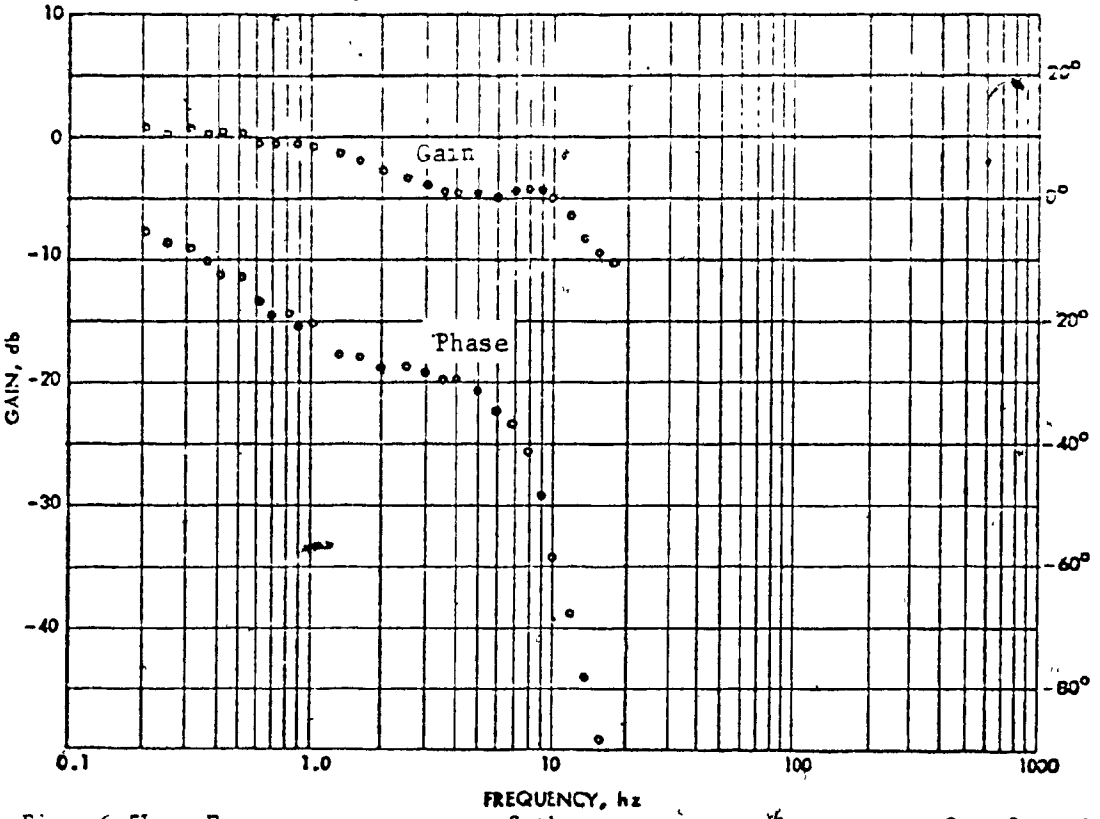

Fig. 6.5b: Frequency response of the converter voltage transfer function at 10 hz inverter frequency and rated motor current.

in the higher voltage/frequency range. For example, the inverter output voltage changed from 205V to 187V from no-load to full motor load. The voltage regulation was found to be rather poor, relying considerably on a large dc filter capacitance (24.000 μF). The voltage regulator has a narrow bandwidth and was obviously not designed for inverter dynamic applications.

The inverter is a standard McMurray type with injected commutating pulses. The inverter voltage and current waveshapes are presented in Figure 6.4a and 6.4b. Poor voltage regulation is clearly seen for 2 hz operation, Figure 6.4b. The filter capacitor is drained and cannot maintain constant voltage at low inverter frequencies, while the converter voltage regulator response is not fast enough.

The frequency response of the converter bridge at 60 and 10 hz is presented in Figures 6 5a and 6.5b. It describes the transfer function between voltage reference and the dc link voltage with the link filter included. Since the converter is highly nonlinear, this transfer function depends very much on the inverter load. The measurements were made with the motor running at the rated current. It is seen that the converter has a bandwidth of about 1.2 hz at 60 hz inverter operating frequency. At 10 hz the bandwidth is increased to 2 hz but the gain curve starts to show the filter resonant peak. Note that the fast change in the phase curve would have posed serious problems if an attempt had been made to close the drive speed loop.

These results point to the following:

(1) The converter dynamics will dominate the drive response in any speed-input reference measurements.

(2) Drive operation in a closed speed loop would require a complete redesign of the converter control circuitry. Even then, less than spectacular dynamic performance is to be expected with this type of inverter.

(3) The combination of the half-wave converter, poor voltage regulator and inappropriate isolation transformer make the inverter voltage very dependent on the motor load. The assumption of an infinite bus supply obviously does not hold. This affects the measurement of both speed-reference and speed-torque transfer functions.

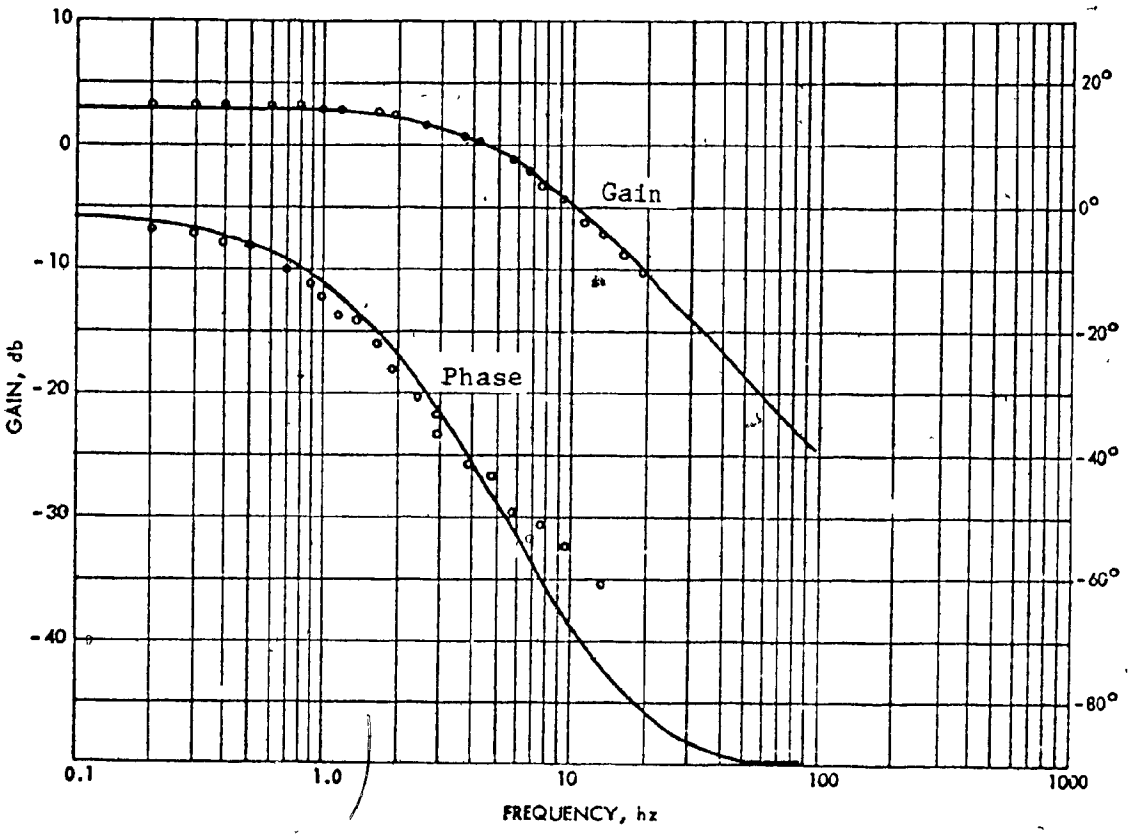

Fig. 6.6a: Frequency response of the speed-torque transfer function at 60 hz and sinusoidal input voltage.

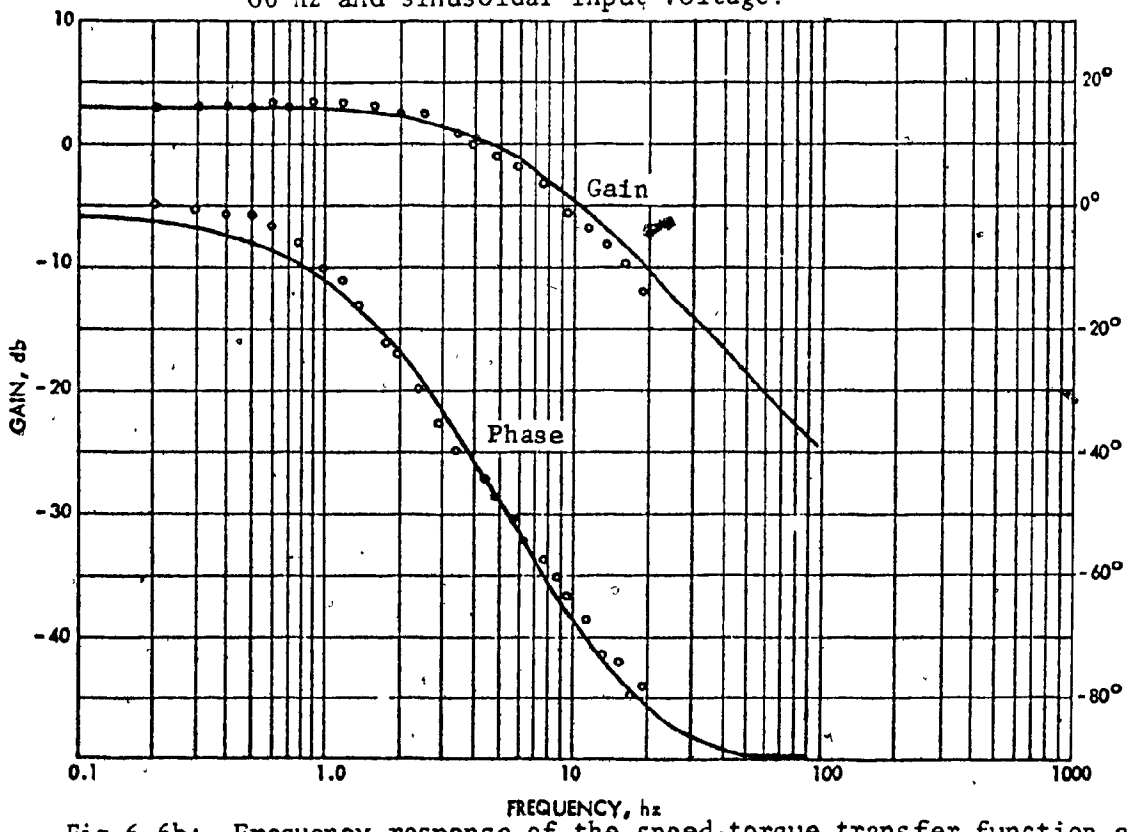

Fig.6.6b: Frequency response of the speed-torque transfer function at 60 hz, inverter supply.

While the effects of the converter dynamics were minimized by modifying the measurement procedure, the other two factors could not be eliminated. The results presented here should be examined while keeping these factors in perspective.

6.3 Small Signal Results

All results presented in this section have been obtained by sinusoidally perturbing the motor inputs around an operating point. If an allowance is made for the power supply effects, these results should confirm those from Section 4.2.1, obtained by using the motor linearized equations. Therefore, these results represent a most important group of measurements.

6.3.1 Speed-Torque Transfer Function

Although a very similar experiment had been reported by Jayawant and Bateson,[41] the narrow bandwidth of the metadyne used to perturb the motor load torque had severely restricted their results. The use of dc machine and cycloconverter enables the measurement of the motor frequency response in the 5 - 15 hz range, where the electrical eigenvalues start to appear.

The speed-torque transfer function is obtained from:

$$G_1(s) = \frac{\delta\omega_m}{\delta T_L} = \frac{\delta V_c / \delta T_L}{\delta V_c / \delta \omega_m} \qquad (6.1)$$

where V_c is the dynamometer speed reference. The procedure requires two measurements for each perturbation frequency but yields results which are independent of the dynamometer dynamics.

All experiments are performed at rated motor current and with a constant inverter reference.

At 60 hz operating frequency, with sinusoidal voltage supply, the $G_1(s)$ transfer function is as predicted, Figure 6.6a. The break point is determined by the mechanical eigenvalue. Electrical eigenvalues are obviously all cancelled, as discussed in Section 4.2.1. Since the experi-

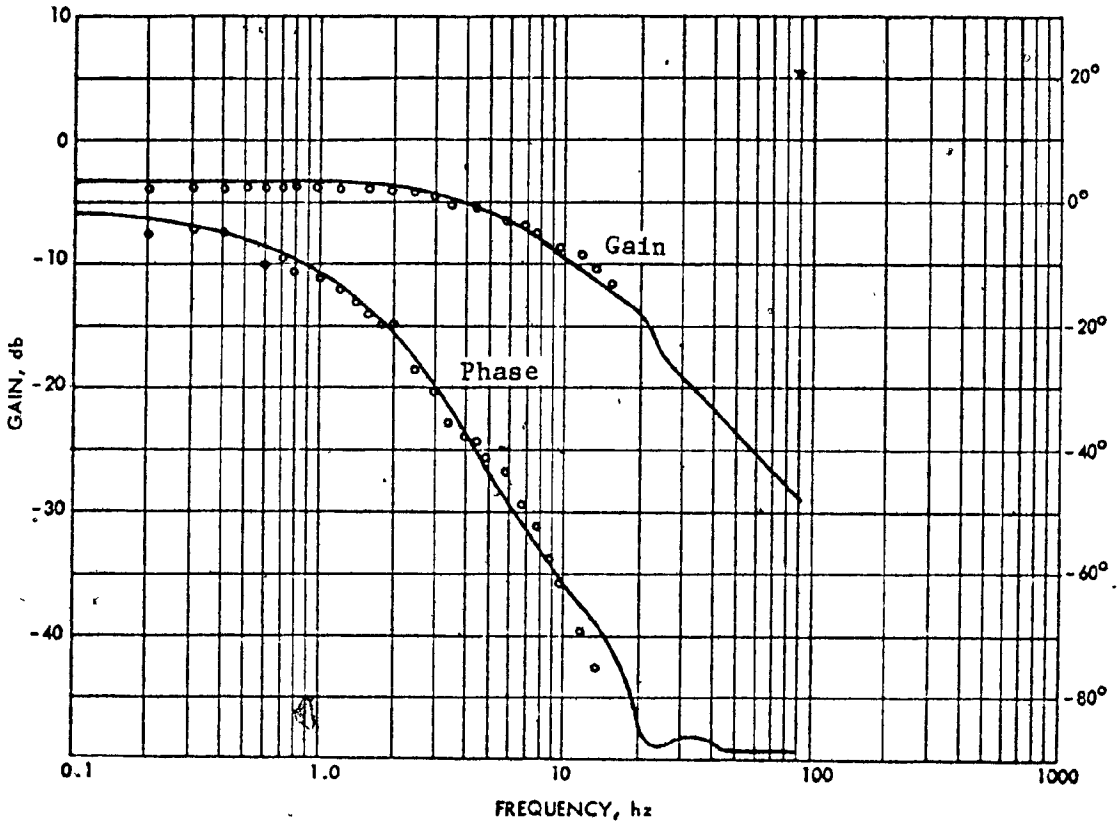

Fig. 6.7: - Frequency response of the speed-torque transfer function at 30 hz, inverter supply

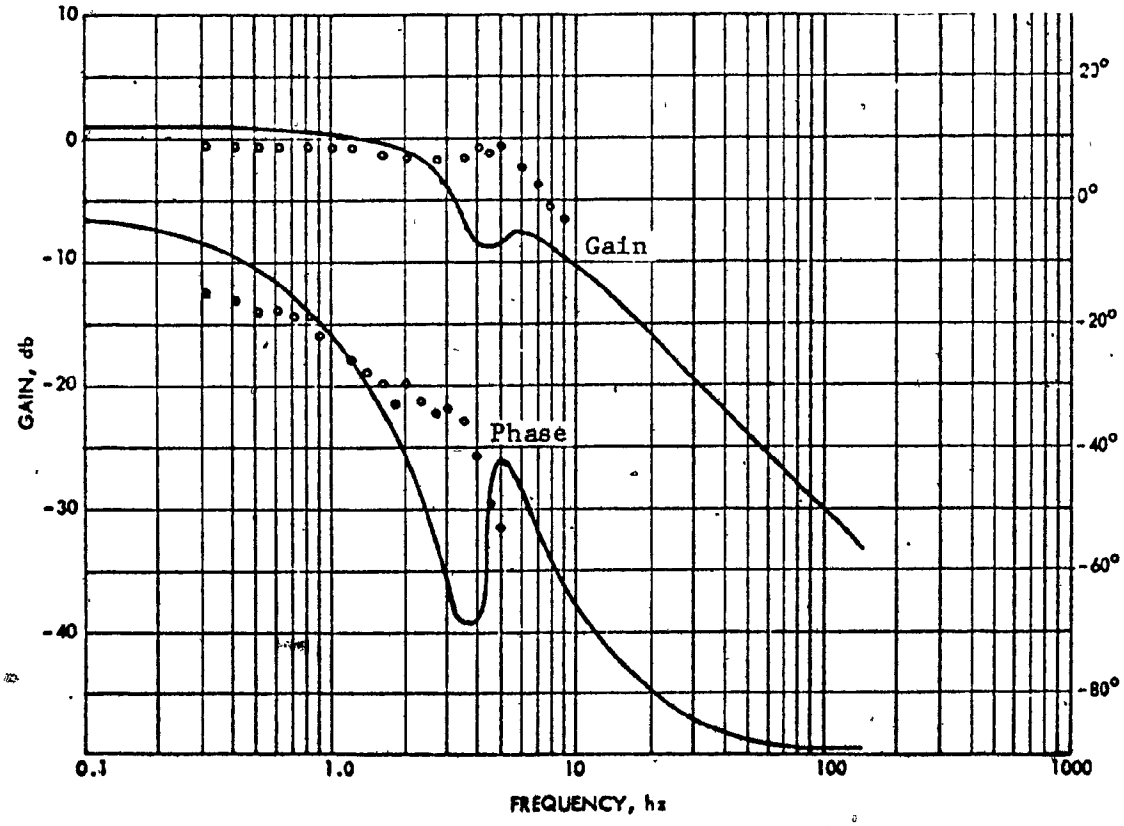

Fig. 6.8: - Frequency response of the speed-torque transfer function at 5 hz, inverter supply

ment was performed with 200 V supply voltage, (against 220 V for the theoretical results, Figure 4.6b) the break point is now at a lower frequency, in agreement with Equation (3.51).

The same results were obtained when the motor was supplied from the inverter, Figure 6.6b. This shows that the dynamic effects of the power supply are negligible at the 60 hz operating point.

At 30 hz operating frequency, the motor was supplied from the inverter. The experimental results again correspond to those obtained theoretically, Figure 6.7. The perturbation frequency is extended to 16 hz, which is not enough to detect the first pair of electrical eigenvalues at 20 hz. Measurements at higher perturbation frequency were not meaningful, since the speed signal becomes very attenuated and entirely buried in noise.

At 5 hz operating frequency, the measurements deviate from the predicted results. The main difference is in the dc level and frequency of the resonant peak. This difference could have been caused by these two factors:

- poor regulation of the motor input voltage (Figure 6.4b) which is not constant as the load is changed
- inaccurate measurements due to the noise in both speed and torque signals.

As the speed of the operating point is lowered, the noise falls into the spectrum of perturbation frequencies and cannot be filtered. It is impossible to conclude whether the speed noise was caused by the tachogenerator or represents true speed oscillations resulting from pulsating harmonic torques. The noise factor made the low speed measurements very difficult and unreliable at perturbation frequencies above 3 hz. The phase measurement was particularly affected. Therefore, the predicted shape of the phase lag curve could not be detected with any degree of confidence.

The following conclusions can be drawn from these results:

(1) The motor dynamic model, used in the theoretical study is found to be accurate. Consequently, all theoretical results are also valid when the effects of inverter dynamics are negligible. Since these effects usually have to be taken into account, the theoretical results represent an upper bound on drive performance.

(2) The pole-zero cancellation occurs for weak electro-mechanical couplings and the higher operating frequencies, as predicted by the Direct Method.

(3) The anticipated effect of electrical eigenvalues at low operating speeds could not be measured, as both speed and torque signals were swamped by noise. This is an important conclusion, indicating that at low speeds, the noise problem is more important than the low damping of the magnetizing eigenvalues. As such, this result points to a major source of problems which would have to be solved before closing the speed loop. At the same time, these results practically disqualify the VVI inverter from most applications in closed loop drives.

6.3.2 Speed-Speed Reference Transfer Function

When attempting to use the inverter in its original configuration, the following two problems were encountered in this experiment:

(1) The motor dynamics became entirely obscured by the narrow bandwidth of the converter-filter group, Figure 6.5a and b.

(2) The time constants of the frequency and voltage control loops differed so much that the constant V/hz strategy existed only when the inverter was in the steady state. It was obvious that the results obtained under these conditions would not correspond to the predicted ones.

In order to alleviate these two problems, the following was done:

(1) The faster frequency loop was slaved to the voltage loop by disconnecting the frequency input reference from point A, Figure 6.2b, and connecting it to the dc bus through an appropriate voltage divider. In this way the constant V/hz control was presented at all times.

(2) The effects of the converter and dc link filter were excluded from the results by calculating the speed-input reference transfer function as:

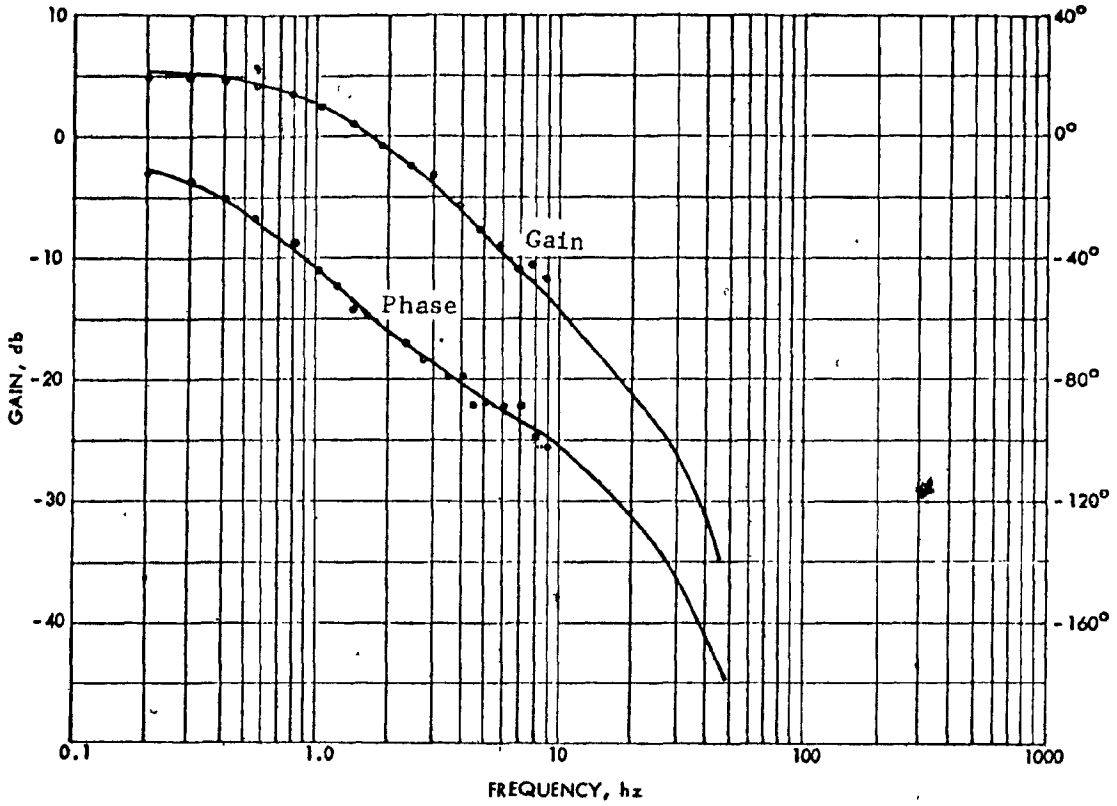

Fig. 6.9: Frequency response of speed-input reference transfer function at 60 hz.

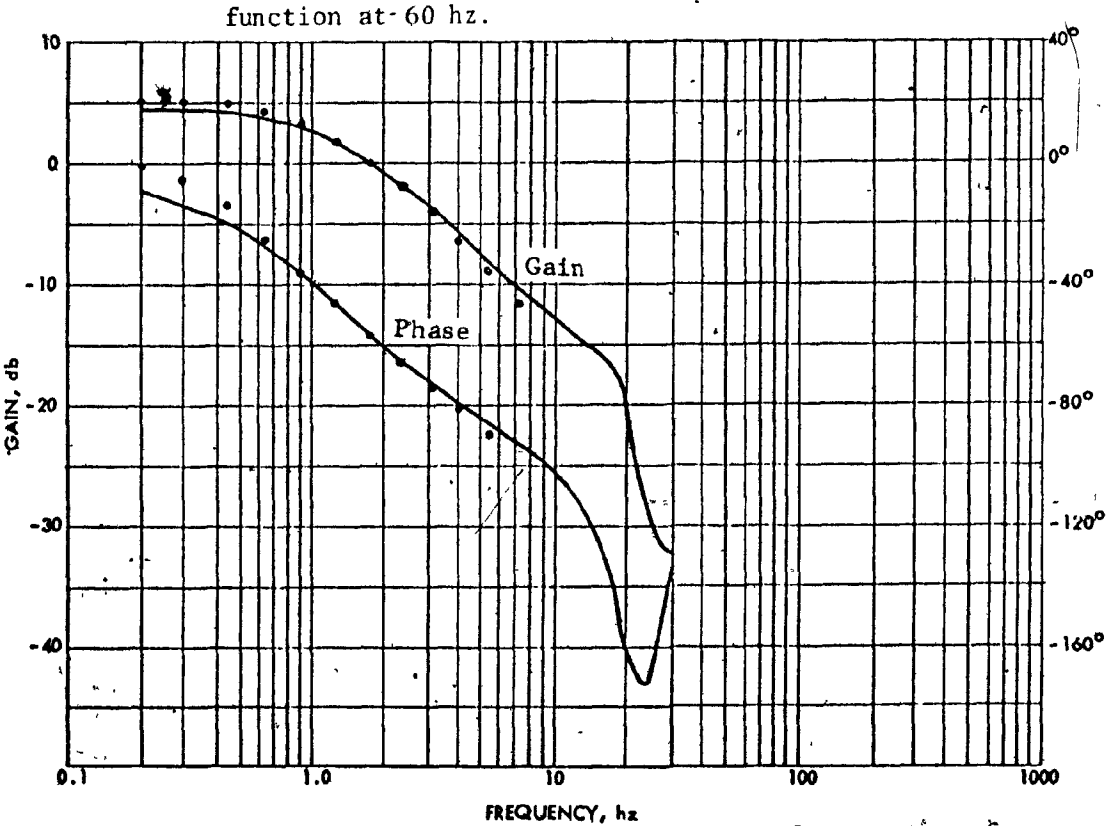

Fig. 6.10: Frequency response of speed-input reference transfer function at 30 hz.

$$G_1(s) = \frac{\delta\omega_m/\delta V_2}{\delta E/\delta V_2} = \frac{\delta \omega_m}{\delta E} \qquad (6.2)$$

where V_2 is the input reference, Figure 6.2b, while E is the inverter dc input voltage. Since the frequency reference is obtained from this voltage, δE determines the perturbation of both input voltage and frequency. If the inverter switching delays are negligible, the measured and the predicted results should be the same.

All measurements were performed at rated and thus constant motor load. As the dynamometer operates in the regulated current mode, the dc machine inertia has to be taken into account.

At 60 hz operating frequency the measured and predicted results are practically identical, Figure 6.9. The break point has moved to 1.15 hz, reflecting the increased total inertia.

When responding to the input reference, the induction motor behaves as a second order system and the gain curve rolls off at -40 db/decade. The low break frequency (1.15 hz) and the -40 db/decade slope made reliable measurements above 9 hz impossible.

At 30 hz operating frequency there is again perfect agreement between the theoretical and experimental results, Figure 6.10. The previous comments also apply here.

At 10 hz operating frequency the main disagreement between predicted and measured results exists in the different shapes of the two phase curves. As in the measurement of the speed-torque transfer function at 5 hz input frequency, this disagreement is caused primarily by the difficulty in measuring the speed signal accurately at the higher perturbation frequencies due to noise. In fact, an attempt was made to find $G_1(s)$ at 5 hz operating frequency but this was abandoned due to the inability to obtain consistent results. In addition to the noise problem, there is a possibility that the inverter also contributed to the disagreement in phase curves by introducing a switching time delay. As already pointed out, this delay may become significant at low operating frequencies.

From these results the conclusions appear to be similar to those reached during the speed-torque experiment:

- The validity of the motor dynamic model is again confirmed. This then confirms also the validity of the theoretical results.

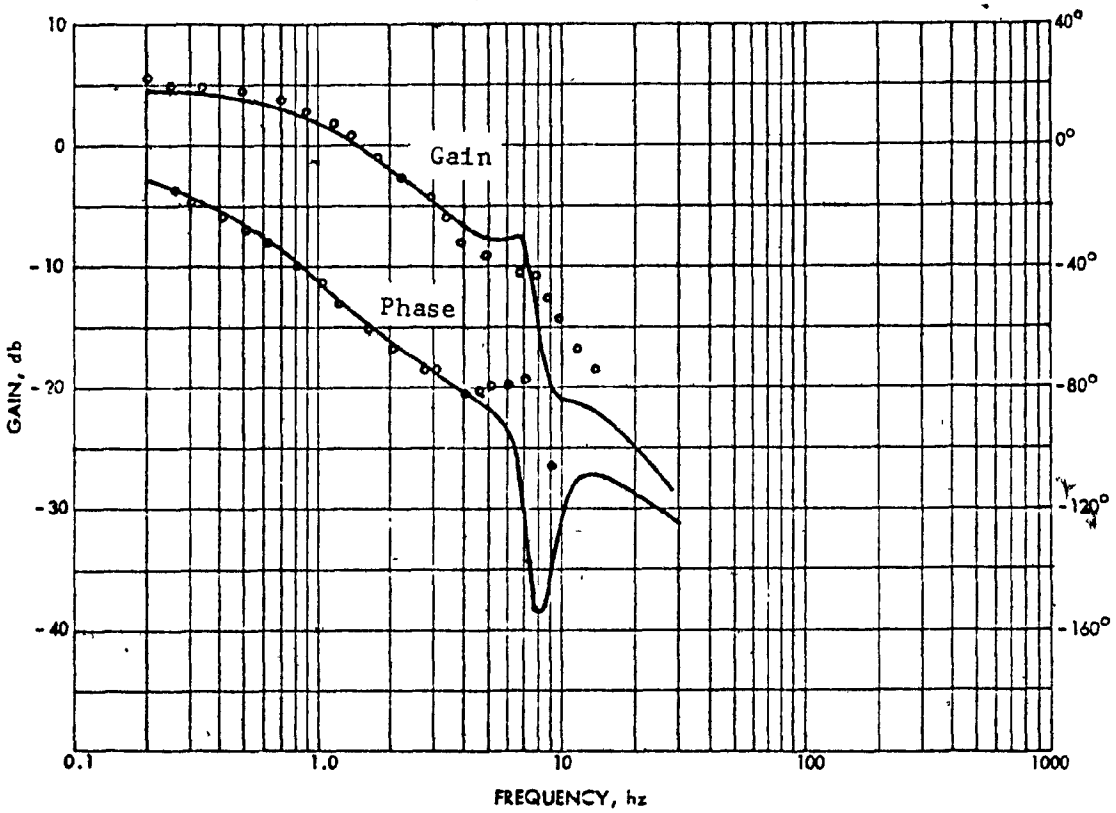

Fig. 6.11: Frequency response of speed-input reference transfer function at 10 hz.

- The electrical eigenvalues are practically unobservable at the higher operating frequencies while at the lower ones they become unmeasurable due to the torque and speed signal noise.

Note that in the addition to the noise, the problem of the converter bandwidth and stability would have to be solved before the drive could operate in a closed speed loop.

6.4 Large Signal Results

The dynamic results are extended experimentally to the motor nonlinear behaviour by applying large steps in the input reference and load torque.

6.4.1 Speed response to step torque disturbance

For this group of experiments, the speed reference is maintained constant. A step in the dynamometer armature current gives a step in the motor load torque. Although the results include the dynamometer dynamics, their effect is negligible due to the larger (50hz) bandwidth of the dynamometer which now operates in the current regulated mode. The speed change is large enough to reflect the motor nonlinear behaviour.

The results were obtained for the same input frequencies used during the measurement of the motor transfer functions in order to facilitate the comparison. Since the torquemeter circuit includes a 200hz oscillator, the torque signal had to be filtered by a fairly narrow band, low pass filter. For this reason, the dc armature current is displayed instead of the torque signal.

At 60hz input frequency 6-17 and the sinusoidal voltage supply, the motor responds to a torque stepas a first order system, fig. 6.12. Although the speed changes by 105 rpm, the result is similar to that obtained by using the motor linear model, fig. 4.6a. The only difference between the experimental and the theoretical results is in the rise time,

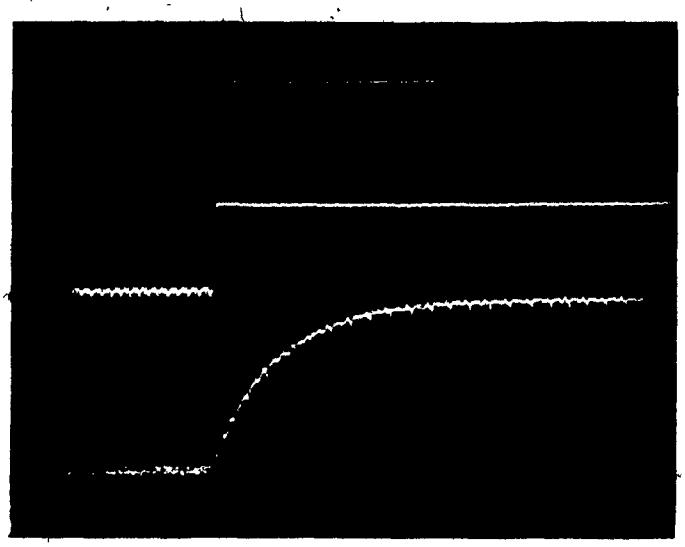

Fig. 6.12: Speed response to a load step input at 60 hz, sinusoidal voltage supply.
(Trace allocation and time base same as below)

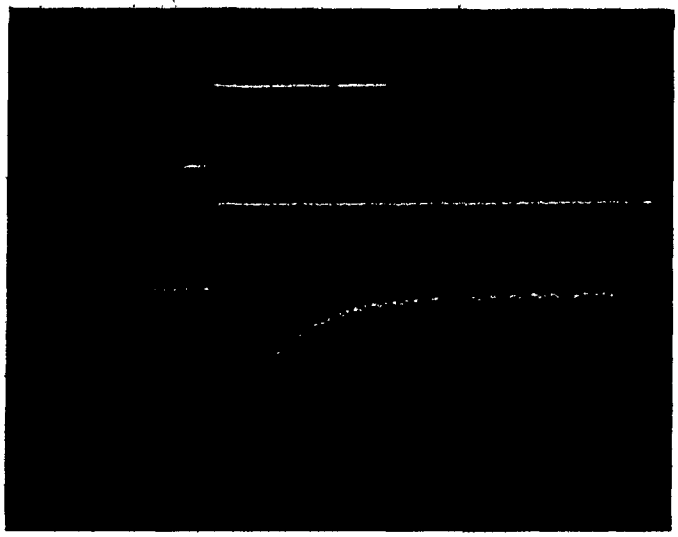

Fig. 6.13: Speed response to a load step input at 60 hz, inverter supply.

Trace 1: Dynamometer reference.
Trace 2: Dynamometer current 8.25 A/cm.
Trace 3: Speed 40 rpm/cm.
Time Base: 0.1 sec/cm.

which is now considerably larger. A full explanation of this discrepancy may be obtained by studying the motor nonlinear equations. However, some insight may be gained by pointing out that the motor was overloaded by 60% at the moment when the step torque was applied. This means that it was operating close to the top of the torque-speed curve, in the region of its decreasing slope. The speed response to the load change is determined by the mechanical eigenvalue which is directly dependent on this slope, equation (3-50). Thus, as the slope of the speed-torque curve is decreased, the break frequency of the real eigenvalue is decreased too, resulting in a slower-than-predicted response.

Although this explanation is only approximate, since the linear model is used to interpret motor nonlinear behaviour, it should account for at least part of the discrepancy between measured and predicted results.

When the motor was supplied from the inverter the results were the same as for a sinusoidal input voltage, fig. 6.13.

At 30hz, fig. 6.14, the speed step response is identical to that at 60hz and the previous comments would also apply here.

At 10hz, the result is basically the same as before, the only difference being small oscillations in the speed signal, fig. 6.15. It is difficult to determine whether these oscillations are caused by motor decreased damping, pulsating torques or represent simply tachogenerator noise.

At 5hz, the magnitude of the speed change has increased to 128 rpm, fig. 6.16 although the magnitude of the load disturbance was the same as for the other measurements. This departure from the previous results reflects the increased motor sensitivity to load disturbances at lower input frequencies, as discussed in section 4.2.1. Another important observation is that even at such low operating frequencies the speed response is well damped and there is no sign of motor instability.

One may conclude from these results that the speed response to large torque changes is essentially the same as predicted by using the motor linearized dynamic model, providing that motor operation is restricted to the stable portion of the torque speed curve.

Fig. 6.15: Speed response to a load step input at 10 hz, inverter supply.
(Trace allocation and time base same as below).

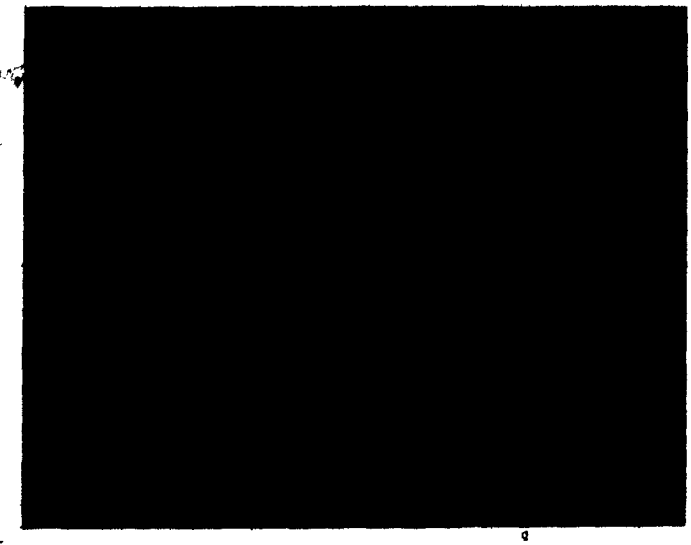

Fig. 6.16: Speed response to a load step input at 5 hz, inverter supply.

Trace 1: Dynamometer reference.
Trace 2: Dynamometer current 8.25 A/cm.
Trace 3: Speed 40 rpm/cm.
Time Base: 0.1 sec/cm.

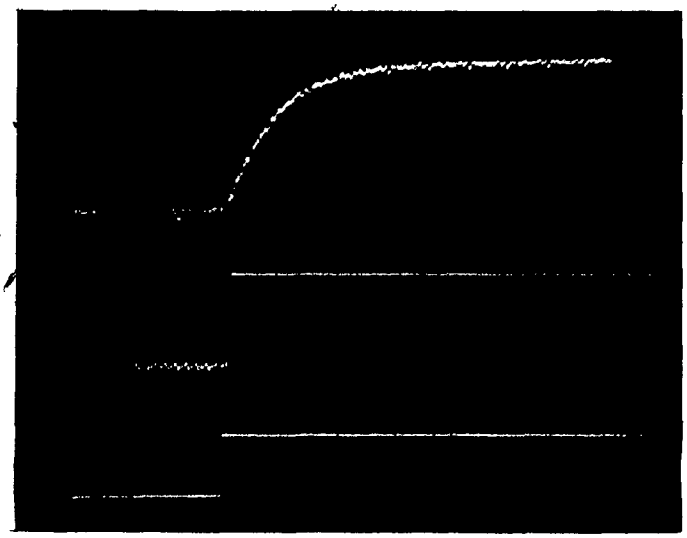

Fig. 6.14: Speed response to a load step input at 30 hz, inverter supply.

Trace 1: Speed 40 rpm/cm.

Trace 2: Dynamometer current 8.25 A/cm.

Trace 3: Dynamometer reference.

Time Base: 0.1 sec/cm.

Fig. 6.17: Speed response to a step reference at 60 hz.

Trace 1: Inverter reference 0.5 V/cm.

Trace 2: dc link voltage 6 V/cm.

Trace 3: Speed 38 rpm/cm.

Time Base: 0.5 sec/cm.

6 4.2 Speed response to step reference input

The dynamometer maintains constant motor torque by operating in the regulated current mode. A step signal is applied at the inverter reference input, fig. 6.3. The measurement procedure used to eliminate converter dynamics from the results obtained in the frequency domain was not possible here. Consequently, constant V/hz control was not maintained during the motor transients. In order to assess the effects of the converted and the dc link filter, the dc link voltage is also displayed.

At 60hz, input frequency, the response of the dc link voltage was relatively slow, fig. 6.17, resulting in a deviation from the constant V/hz control. As the motor was required to accelerate with a relatively decreased input voltage, the developed electrical torque was not very large and the speed response was slow.

While the dc link voltage exhibits a small overshoot, reflecting the structure of the converter voltage control loop, the motor speed response is overdamped.

At 30hz the results are unchanged, fig. 6.18, and the previous comments apply.

At 10hz the speed response was noticeably slower while its steady state value was decreased by 24 rpm, fig. 6.19. Both changes reflect the decrease in the gain of the forward motor loop (input reference to speed) at lower input frequencies. This decrease may be predicted by looking at the slope of the static torque speed curves, in the lower input frequency range, fig. 2.3. This was also observed in the theoretical results and extensively discussed in section 4.2.1. Finally, a loss in forward gain at low input frequencies was confirmed experimentally, fig. 6.16.

These results lead to the conclusion that the speed response to large input reference signals is very well damped. However, it is not possible to correlate the experimental and the theoretical results because they were obtained for different airgap flux distributions. The results therefore reflect motor nonlinear behaviour for one particular type of power supply.

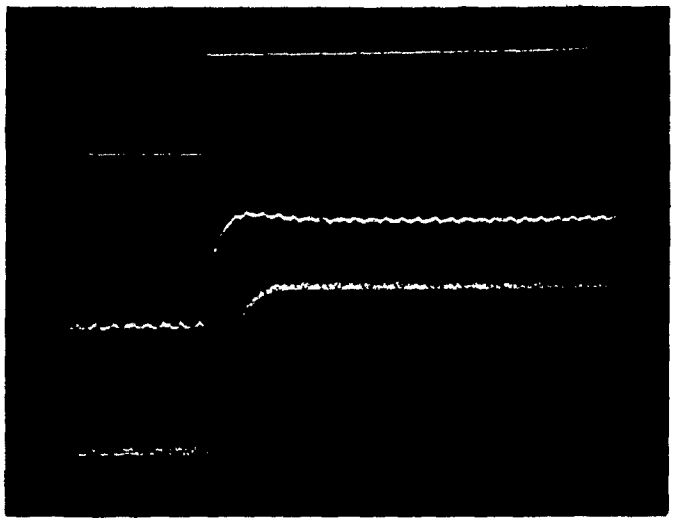

Fig. 6.18: Speed response to a step reference at 30 hz.

Trace 1: Inverter reference 0.35 V/cm.
Trace 2: dc link voltage, 7.2 V/cm.
Trace 3: speed 38 rpm/cm.
Time Base: 0.5 sec/cm.

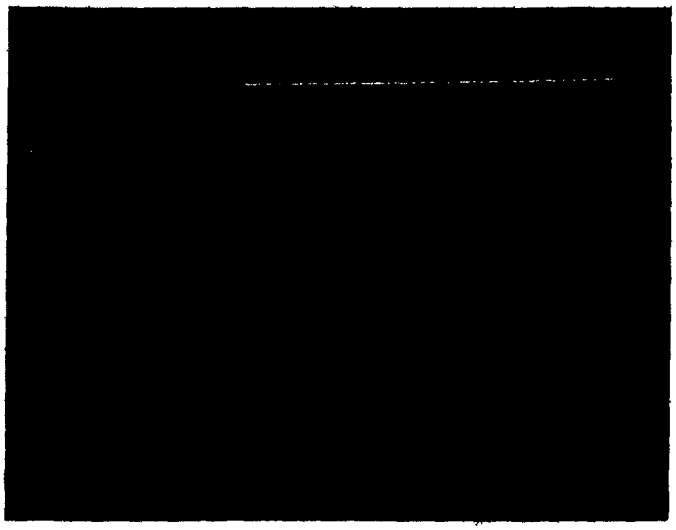

Fig. 6.19: Speed response to a step reference at 10 hz.

Trace 1: Inverter reference, 0.545 V/cm.
Trace 2: dc link voltage, 6 V/cm.
Trace 3: Speed 38 rpm/cm.
Time Base: 0.5 sec/cm.

6.5 Effects of higher harmonics

As pointed out in Chapter V, higher harmonics in the input voltage may affect the motor speed, especially at reduced supply frequencies. The following two questions have to be answered in order to evaluate these effects:

1) How much should the motor dynamic model be modified in order to account for the higher voltage harmonics?

2) What is the effect of pulsating torques on speed?

Since the first question is practically answered by looking at the speed frequency response, fig. 6.6 to fig. 6.11, only a few comments are added here:

- The linearized dynamic model predicts only the behaviour of the speed fundamental harmonic. Any corrections for the square wave input voltage have to be done by superposition of motor models for each harmonic. This might, however, severly test the linearity assumption.

- The deviation of experimental from predicted results at low supply frequency figures 6.8 and 6.11, indicate the presence of speed harmonics. However, the measurement methodology precludes any additional quantitative conclusion. One reason is that the dynamometer dynamics, decoupled from the fundamental frequency results, affect the speed higher harmonics. Another reason is that the speed harmonics appeared as a nonlinear effect in the Lissajous figures, which were very difficult to interpret. A third reason is that it was impossible to distinguish between true speed oscillations and tachogenerator noise.

In order to gain more insight into the speed harmonic oscillations, and also to answer the second question about the effects of pulsating torques, a steady state experiment was performed with the motor operating

at 1-2 hz input frequency. It was hoped that at such low speeds the relative importance of the tachogenerator noise would decrease since the effects of pulsating torques become more pronounced.

The dynamometer was used to provide a constant load torque by operating in the current controlled mode. The inverted frequency reference was disconnected from point A, fig. 6.3, and connected to an external precision dc supply, since it was not possible to obtain proper inverted operation at such low frequencies with the original connection.

The results were disappointing and encouraging at the same time. It was not possible to measure any speed oscillations caused by pulsating torques. In an attempt to get some measurements, the V/hz ratio was varied by increasing the input voltage within the range allowed by motor current considerations, but the oscillations simply did not materialize. When the load was increased so that the motor stalled, small rotor vibrations were observed and could be felt by placing one's hand on the motor shaft. However, the tachogenerator signal was not recorded as it contained different kinds of static friction and brush noise. The large added dynamometer inertia was probably the main reason why the pulsating torques could not produce significant speed oscillations.

The conclusion is then reached that the effect of voltage harmonics depends very much on drive parameters, in particular on the total system inertia; that the speed harmonic oscillations exist at low input frequencies but did not pose any cogging problems in the drive under study, and finally, that the speed oscillations would become amplified in a closed loop system if a low pass filter was not included in the speed feedback loop. Such a filter would obviously severely limit the drive bandwidth.

6.6 Summary

A series of experiments was performed on an actual machine in order to make the theoretical results more credible and relevant to practical induction motor drives.

The first of the stated objectives, confirmation of the motor dynamic model, was entirely achieved. This result has very significant implications since it also validates the predicted performance of closed loop drives.

The second objective, extension of the dynamic results to the region of motor nonlinear behaviour was mostly achieved. The speed response to large step disturbances corresponds to that of a first order system, as predicted by the motor linear model.

When large steps were applied to the input speed reference, the comparison between measured and theoretical results became meaningless due to the presence of a large dc link filter in the voltage control loop. This filter caused a deviation from the constant V/hz control during motor transients, as explained in section 5.5 of the previous chapter. Consequently, theoretical and experimental results were obtained under different transient conditions and cannot be compared. Nevertheless, the measured results show that the problem of marginal stability does not arise in this drive.

The third objective, the assessment of inverter effects on a motor transient response, was partially achieved. Only qualitative assessment was possible since an alternate power supply with sinusoidal voltage and instantaneous response was not available for comparison.

It was found that the dc link filter slows down considerably the motor response (as predicted), but does not introduce any instability. Very good agreement with theoretical results was obtained by excluding the converter from the voltage control loop. The results obtained under these conditions show at the same time that the inverter switching delays are negligible.

Of all effects, the inverter higher harmonics were by far the most important, especially at reduced input frequencies. They caused some harmonic speed oscillations and, therefore, made the frequency response measurements difficult and unreliable at low operating speeds. Consequently, the lightly damped electrical eigenvalues, anticipated in the speed response at low input frequencies, could not be observed.

Although the conclusions about the inverter harmonic effects are not new, they receive special importance when a closed loop motor operation is considered. In this case, the speed harmonic oscillations make a low pass filter in the speed feedback loop mandatory, thereby decreasing the drive bandwidth. This conclusion then tends to exclude variable voltage input inverters from applications in high performance closed loop drives.

CHAPTER VII

EPILOGUE

7.1 Summary

This thesis presents a comprehensive dynamic study of closed loop, variable frequency induction motor drives for various strategies of motor speed control.

Three control strategies were formulated and the corresponding steady state motor characteristics were presented in Chapter III.

The basic methods of time and frequency domain analysis were reviewed in Chapter III and arranged in a form suitable to this study. The classical notions of observability and controllability were examined and were found inadequate for the performance analysis of practical control systems. Therefore, the two new concepts of pseudo-observability and pseudo-controllability which are more relevant to engineering applications, were defined. In addition to this, two theorems which lead to a new analytical method for predicting the structure of speed-torque transfer functions as well as the nature and location of their zeros were formulated. The method is simple, general and applicable to any motor drive, operating in an open or closed control loop and represented by a set of linearized equations. The proof of the two theorems was presented by using the basic properties of electrical rotating machinery.

The dynamic analysis of closed loop induction motor drives, described by a set of linearized equations, was presented in Chapter IV. The results were given in both time and frequency domains, for an easy interpretation. An ideal, variable frequency, power source was assumed. Consequently, the results of this chapter reflect an upper bound of the motor dynamic performance, attainable with an instantaneous response, sinusoidal output power supply. The results of Chapter IV were reviewed in Chapter V in the light of the limitations imposed by the non-ideal drive components.

The experimental confirmation of the theoretical results was reported in Chapter VI. The measurements in both time and frequency domains were discussed. The use of a variable voltage input inverter frustrated accurate measurements at lower motor speeds and demonstrated the limitations of a square-wave power supply.

7.2 Conclusions

A number of conclusions pertinent to the analysis and the dynamic performance of variable frequency induction motor drives are now made. These conclusions are based on the results obtained in this study and the experience gained during the experimental work.

Theoretical results

1. The speed-torque transfer function $G_2(s)$ of any rotating machine, which is operating in open loop and which is represented by a set of linearized equations, has N-1 zeros, N being the number of machine eigenvalues. Furthermore, all zeros of $G_2(s)$ are identical with the eigenvalues of the machine constant speed electrical system (Theorem -1, Direct Method). In most cases the electrical poles and the electrical zeros cancel each other, leaving a first order speed-torque transfer function. The pole of this transfer function depends on the total inertia of all rotating masses and the slope of the static torque-speed curve.

2. The speed-torque transfer function of any closed loop electrical drive, described by a set of linearized equations, has N-1 zeros, N being the number of drive eigenvalues. Of these N-1 zeros, N_1 are identical to the eigenvalues of the drive reduced system, while the remaining N_2 are the eigenvalues of the drive speed controller. (Theorem 2, Direct Method). The definitions of the drive reduced system and the speed controller are given in section 3.3.3.

3. The dynamic characteristics of an induction motor generally depend on the supply frequency and the motor lead. The only exceptions are drives where the airgap flux is maintained constant at every instant of motor operation. In this case, the drive dynamics change only with load.

4. Constant Volts/hz, open loop drives exhibit a number of undesirable characteristics when operating at reduced input frequencies:

- A decreased damping of the electrical magnetizing eigenvalues. Depending on motor parameters, this may cause dynamic shaft oscillations.

- Poor speed regulation, caused by a decrease in the forward motor gain. Consequently, the motor speed is very sensitive to load changes.

- A decrease of motor maximum torques.

These factors make constant V/hz open loop drives suitable only for applications where a most elementary speed regulation is required.

5. Constant Volts/hz closed loop drives may have a very good dynamic performance, provided the speed controller and a corresponding compensating network are properly designed. In this case, motor dynamic characteristics become practically independent of the input frequency. At the same time, the motor speed becomes almost insensitive to load changes.

6. Although a constant slip speed control strategy yields constant power factor operation and reduced harmonic losses at light loads, it is not suitable for applications where high dynamic performance is expected. It was found that a motor with constant slip speed control and supplied from a voltage source has a slower speed response than when operating in an open speed loop. Furthermore, the motor characteristics depend significantly on the supply frequency, while the speed was very sensitive to the load variations, despite a closed loop operation.

7. It was found that a constant airgap flux strategy has two very important advantages over any other form of induction motor control:

a) The drive static and dynamic characteristics are independent of the supply frequency,

b) The motor electrical system is reduced to the rotor circuit. Consequently, the drive becomes unconditionally stable and responds to any input as a first order system.

Both factors enable the design of a fixed structure, optimal speed controller, which is not a compromise between the contradictory requirements at the two ends of the frequency range. Furthermore, since the drive responds as a first order system, the speed controller is not designed to improve its stability but rather to suit the drive application requirements.

8. It was demonstrated in this study that any induction motor can be made to behave in a desired fashion, provided that a correct drive structure is chosen. Thus, the most logical approach in the design of high performance induction motor drives is to optimize the motor parameters with respect to the efficiency and the steady state operation, while using control loops to obtain a desired dynamic behaviour. Note that this runs contrary to the current research practice of searching for the combination of motor parameters which gives the best open loop dynamic performance.

Practical drives

1. When different limitations of non-ideal power supplies were examined, it was found that those most important are:

(i) Time delays in the voltage control loop, introduced by a large dc link filter.

(ii) Effects of steady state pulsating torques at reduced input frequencies.

The experimental results have confirmed these conclusions.

These two factors practically prohibit the application of variable voltage input inverters in most closed loop induction motor drives.

The same conclusions were made for inverters with regulated output current, with the only difference being that the dc link filter is now replaced by a large dc choke and the effect of higher harmonics is now much stronger.

2. It was found during the measurements on the open loop, constant Volts/hz drive, that at reduced input frequencies the anticipated effect of lightly damped electrical eigenvalues could not be observed due to the effect of steady state pulsating torques. This experimental result implies that when the drive is supplied from a square-wave inverter, the effect of pulsating torques overshadows that of lightly damped eigenvalues.

3. When pulse width modulated inverters are applied, excellent dynamic performance may be achieved with the proper control strategy. In this case, the dominant limiting factor becomes the tachogenerator noise, as it necessitates the use of a low pass filter in the speed feedback loop.

4. The motor nonlinear operation was discussed and the need for slip limit during large speed changes was explained. It was found that the constant airgap flux strategy gives superior drive performance by permitting accelerations at very high, constant motor torques. Furthermore, the value of the slip limit is constant over the whole operating frequency range only with this control strategy. Therefore, a speed controller with fixed structure may be used without compromising the drive large signal response.

The overall conclusion is that the following are necessary for the realization of high performance induction motor drives:

1) Closed loop operation

2) Constant airgap flux control

3) Pulse width modulated inverter.

7.3 Suggestions for future work

The following research topics would represent a continuation of this study:

1) Further analysis of the motor nonlinear dynamic behaviour.

2) Effects of dynamic deviations from a particular control strategy due to different time constants in voltage and frequency control loops in variable voltage input inverters.

3) Investigation of dynamic characteristics of pulse width modulated inverters, in particular with respect to switching delays.

4) Design of a controlled current source with a pulse width modulated inverter and a study of its characteristics.

APPENDIX A

INDUCTION MOTOR PARAMETERS

The per phase parameters of the induction motor used in this study are given below:

Primary Leakage Inductance	L_s	=	2.22 mhenries
Secondary Leakage Inductance	L_r	=	2.20 mhenries
Magnetizing Inductance	M	=	66.84 mhenries
Primary Resistance	R_1	=	.440 ohms
Secondary Resistance	R_2	=	.708 ohms
Number of Pole-Pairs	n	=	2
Rated Frequency	f	=	60.0 Hz
Rated RMS Voltage	V_{ph}	=	127.0 volts
Rated Output Torque	T_e	=	17.37 Nm
Total Viscous Friction	f_T	=	.0014 Nm sec/rad
Rotational Inertia	J	=	.0500 Kgm^2

The total system inertia was made equal to the induction motor inertia. Therefore: $J_T = J$

APPENDIX B

PROOF: THEOREM 2

First, the state equations for the closed loop drive (Figure 3.3) are established after which the proof is given.

Controller 2

$$\dot{X}_2 = [A_2]\, X_2 + [B_2]\, U_2 \qquad \text{(C-1a)}$$

$$Y_2 = [C_2]\, X_2 + [D_2]\, U_2 \qquad \text{(C-1b)}$$

From Figure 3.3 the input U_2 is:

$$U_2 = V_2 - k_t\, \delta\omega_m$$

where V_2 is the change in the speed reference input.

Since U_2 is a scalar, $[B_2]$ and $[D_2]$ become column vectors. The output component Y_{21} is a scalar while Y_{22} is in a general case a vector. Thus, the matrices $[C_2]$ and $[D_2]$ can be written as:

$$[C_2] = \begin{bmatrix} [C_{12}] \\ [C_{22}] \end{bmatrix} \quad \text{and} \quad [D_2] = \begin{bmatrix} D_{21} \\ [D_{22}] \end{bmatrix}$$

where $[C_{12}]$ is a row vector, $[C_{22}]$ is the remaining submatrix in $[C_2]$, D_{21} is a scalar and $[D_{22}]$ is the remaining column vector. The state equations for controller 2 now become:

$$\dot{X}_2 = [A_2]\, X_2 + [B_2]\, V_2 - [B_2]\, k_t\, \delta\omega_m \qquad \text{(C-2a)}$$

$$Y_{21} = [C_{12}]\ X_2 + D_{21}\ V_2 - D_{21}\ k_t\ \delta\omega_m \qquad \text{(C-2b)}$$

$$Y_{22} = [C_{22}]\ X_2 + [D_{22}]\ V_2 - [D_{22}]\ k_t\ \delta\omega_m \qquad \text{(C-2c)}$$

Controller 1

$$\dot{X}_1 = [A_1]\ \lambda_1 + [B_1]\ U_1 \qquad \text{(C-3a)}$$

$$Y_1 = [C_1]\ \lambda_1 + [D_1]\ U_1 \qquad \text{(C-3b)}$$

From Figure 3.3 the input U_1 is

$$U_1 = V_1 - X_f + Y_{22} \qquad \text{(C-4)}$$

where V_1 is the reference input of all other states except motor speed, Y_{22} is given by (C-2c), while λ_f is the vector of feedback states. It can be written as:

$$X_f = \begin{bmatrix} \delta_1 \\ \xi \end{bmatrix} \qquad \text{(C-5)}$$

where δ_1 is the state vector of motor currents in the γ-δ frame while ξ is the vector of all other measured states (except speed), such as air-gap flux, temperature etc. Using equation (C-5) $[B_1]$ and $[D_1]$ matrices in (C-4), can be written as:

$$[B_1]\ X_f = [B_{11}\ B_{12}] \begin{bmatrix} \delta_1 \\ \xi \end{bmatrix} \qquad \text{(C-6a)}$$

$$[D_1]\ X_f = [D_{11}\ D_{12}] \begin{bmatrix} \delta_i \\ \xi \end{bmatrix} \qquad \text{(C-6b)}$$

Combining equations (C-2c), (C-4), (C-5), and (C-6) with (C-3), the state equations for controller 1 become:

$$\dot{X}_1 = [A_1]\,\lambda_1 + [B_1]\,V_1 + [B_1]\,[C_{22}]\,X_2 + \\ + [B_1]\,[D_{22}]\,V_2 - [B_1]\,[D_{22}]\,k_t\,\delta\omega_m - \\ - [B_{11}]\,\delta_1 - [B_{12}]\,\xi \qquad \text{(C-7a)}$$

$$Y_1 = [C_1]\,X_1 + [D_1]\,V_1 + [D_1]\,[C_{22}]\,X_2 + \\ + [D_1]\,[D_{22}]\,V_2 - [D_1]\,[D_{22}]\,k_t\,\delta\omega_m - \\ - [D_{11}]\,\delta_1 - [D_{12}]\,\xi \qquad \text{(C-7b)}$$

The additional states ξ depend in the general case on all drive states and all inputs. Thus, the state equation for ξ states is:

$$\dot{\xi} = [A_3]\,\xi + [H_1]\,X_1 + [H_2]\,X_2 + [H_3]\,\delta_1 + \\ + [H_4]\,\delta\omega_m + [H_5]\,V_1 + [H_6]\,V_2 \qquad \text{(C-8)}$$

where $[H_4]$ and $[H_6]$ are respectively the speed-to-ξ and speed reference-to-ξ coupling column vectors while $[H_1]$, $[H_2]$, $[H_3]$ and $[H_5]$ are the corresponding coupling matrices. The motor input voltage vector in equation (3.39) is:

$$\delta V_{\gamma\delta} = K_s\,\{Y_1 + [I_v]\,(Y_{21} + k_t\,\delta\omega_m)\} \qquad \text{(C-9)}$$

where K_s is the gain of the power source while $[I_v]$ is a unit column vector.

Using equations (C-2c) and (C-7b) the motor voltage vector becomes:

$$\delta V_{\gamma\delta} = K_s \{[C_1] X_1 + [D_1] V_1 + ([D_1] [C_{22}] + [I_v] [C_{12}]) X_2 - [D_{11}] \delta_1 - [D_{12}] \xi + ([D_1] [D_{22}] + [I_v] D_{21}) V_2 - ([D_1] [D_{22}] + [I_v] D_{21} - [I_v] k_t \delta\omega_m \} \quad (C\text{-}10)$$

Combining (C-2a), (C-7a), (C-8) and (C-10) with the motor equation (3.39), the general closed loop drive, presented in Figure 3.3 is described by:

$$[P_o] \dot{X} = [Q_o] X + U \quad (C\text{-}11)$$

where

$$[P_o] = \begin{bmatrix} [L] & 0 & 0 & 0 & 0 \\ 0 & [I] & 0 & 0 & 0 \\ 0 & 0 & [I] & 0 & 0 \\ 0 & 0 & 0 & J_T & 0 \\ 0 & 0 & 0 & 0 & [I] \end{bmatrix} \quad (C\text{-}12a)$$

$$Q_o = \begin{bmatrix} [Q_{11}] & [Q_{12}] & [Q_{13}] & [Q_{14}] & [Q_{15}] \\ [H_3] & [A_3] & [H_1] & [H_4] & [H_2] \\ -[B_{11}] & -[B_{12}] & [A_1] & -[B_1][D_{22}]k_t & [B_1][C_{22}] \\ nI^T([G]+[G]^T) & 0 & 0 & -f_T & 0 \\ 0 & 0 & 0 & -[B_2]k_t & [A_2] \end{bmatrix} \quad (C\text{-}12b)$$

$$X = \begin{bmatrix} \delta i \\ \xi \\ X_1 \\ \delta\omega_m \\ X_2 \end{bmatrix} \qquad \text{(C-12c)}$$

$$U = \begin{bmatrix} [D_1]\ K_s\ V_1 + ([D_1]\ [D_{22}] + [I_v]\ D_{21})\ K_s\ V_2 \\ [H_5]\ V_1 + [H_6]\ V_2 \\ [B_1]\ V_1 + [B_1]\ [D_{22}]\ V_2 \\ -\ \delta T_L \\ [B_2]\ V_2 \end{bmatrix} \qquad \text{(C-12d)}$$

The sub-matrices Q_{1_j} in (C-12b) are:

$$[Q_{11}] = -\ [R] - n\ \Omega_m'\ [G] - \Omega_c\ [F] - [D_{11}]\ K_s$$

$$[Q_{12}] = -\ [D_{12}]\ K_s$$

$$[Q_{13}] = -\ [C_1]\ K_s$$

$$[Q_{14}] = -\ ([D_1]\ [D_{22}] + [I_v]\ D_{21} - [I_v])\ K_s\ k_t - n\ [G]\ I_o$$

$$[Q_{15}] = ([D_1]\ [C_{22}] + [I_v]\ [C_{12}])\ K_s$$

The drive state equation is:

$$\dot{X} = [A]\ X + [B]\ U$$

where the state [A] and input [B] matrices are defined from (C-11) as:

$$[A] = [P_o]^{-1}\ [Q_o] \tag{C-13}$$

and

$$[B] = [P_o]^{-1} \tag{C-14}$$

explicitly they are:

$$A = \begin{bmatrix} [L]^{-1}[Q_{11}] & [L]^{-1}[Q_{12}] & [L]^{-1}[Q_{13}] & [L]^{-1}[Q_{14}] & [L]^{-1}[Q_{15}] \\ [H_3] & [A_3] & [H_1] & [H_4] & [H_2] \\ -[B_{11}] & -[B_{12}] & [A_1] & -[B_1][D_{22}]k_t & [B_1][C_{22}] \\ n\dfrac{I_o^T([G]+[G]^T)}{J_T} & 0 & 0 & -f_T/J_T & 0 \\ 0 & 0 & 0 & -[B_2]k_t & [A] \end{bmatrix} \tag{C-15}$$

and

$$[B] = \begin{bmatrix} [L]^{-1} & 0 & 0 & 0 & 0 \\ 0 & [I] & 0 & 0 & 0 \\ 0 & 0 & [I] & 0 & 0 \\ 0 & 0 & 0 & 1/J_T & 0 \\ 0 & 0 & 0 & 0 & [I] \end{bmatrix} \tag{C-16}$$

The drive reduced system is obtained by removing the speed controller and the mechanical system from the drive structure. The state matrix [A] of the reduced system is then obtained by deleting the corresponding equations from (C-15):

$$A_r = \begin{matrix} [L]^{-1}[Q_{11}] & [L]^{-1}[Q_{12}] & [L]^{-1}[Q_{13}] \\ [H_3] & [A_3] & [H_1] \\ -[B_{11}] & -[B_{12}] & [A_1] \end{matrix} \tag{C-17}$$

With all necessary equations defined, one can look for the speed-torque transfer function. It is given by equation (3.40) in Chapter III. The speed appears on the k-th row where $k = N - N_2$, N being the order of drive state equation (C-15), while N_2 is the number of equations in controller 2. From (3.36) and (C-16) the numerator $N_{kk}(s)$ of the speed-torque transfer function is given by

$$N_{kk}(s) = C_{kk}(s) \frac{1}{J_T} \tag{C-18}$$

where $C_{kk}(s)$ is the k-th row, k-th column element of the matrix $[C_o]$ defined by (3.34a) in Chapter III.

The element $C_{kk}(s)$ is obtained from equations (C-15) and (C-15) by using the definition for an adjoint matrix and knowing that the k-th row, k-th column element of the matrix $[s[I] - [A]]$ is $s + f_T/J_T$. Thus:

$$C_{kk}(s) = \text{DET} \begin{bmatrix} s[I]-[L]^{-1}[Q_{11}] & -[L]^{-1}[Q_{12}] & -[L]^{-1}[Q_{13}] & -[L]^{-1}[Q_{15}] \\ -[H_3] & s[I]-[A_3] & -[H_1] & -[H_2] \\ -[B_{11}] & [B_{12}] & s[I]-[A_1] & -[B_1][C_{22}] \\ 0 & 0 & 0 & s[I]-[A_2] \end{bmatrix} \tag{C-19}$$

The last equation gives:

$$C_{kk}(s) = \text{DET}\,[s[I] - [A_r]]\ \text{DET}\,[s[I] - [A_2]] \tag{C-20}$$

where $[A_r]$ is the state matrix of the drive reduced system defined by (C-17). The first and the second determinant in (C-20) represent

respectively the characteristic equations of the reduced system and the speed controller. Since only the mechanical equation is taken out from the drive state matrix (C-15), $C_{kk}(s)$ in (C-20) represents a polynomial of $N-1 = N_1 N_2$ degree, where N_1 and N_2 are respectively the number of equations in the reduced system and the speed controller.

From equation (C-18) the roots of this polynomial are the roots of the numerator $N_{kk}(s)$. Using equations (3-40), (C-18) and (C-20) the speed-torque transfer function for a general, closed loop, multi-feedback drive is:

$$H(s) = \prod_{j=1}^{N_1} (s-z_j) \prod_{i=1}^{N_2} (s-\varepsilon_i) \; / \; J_T \prod_{k=1}^{N} (s-\lambda_k) \qquad \text{(C-21)}$$

where λ_k's are the eigenvalues of the total system described by (C-11), z_j's are the eigenvalues of the drive reduced system while ε_i's are the eigenvalues of the speed controller.

Q.E.D.

REFERENCES

1. Lawson, L.J. and Amato, C.J., "An A.C. Electric Drive System for Locomotive and Multiple-Unit Traction Systems", Proc. of the Joint ASME-IEEE Railroad Conference, San Francisco, May 1966.

2. Slabiak, L., "An A.C. Electric Individual Wheel Drive System for Land Vehicles", S.A E. Automotive Engineering Congress, January 1966.

3. Agarwal, P.D., "The G.M. High-Performance Induction Motor Drive System", IEEE Trans. on Power Apparatus and Systems, Vol. PAS-88, February 1969, pp. 86-93.

4. Vutz, N., "PWM Inverter Induction Motor Transit Car Drives", IEEE Trans. on Industry Applications, Vol. IA-8, January/February 1972, pp. 89-91.

5. Brechbuhler, M. and Bohli, W.U., "Performance of Experimental Inverter Locomotive Be 4/4 No. 12001 of Swiss Federal Railways", Brown Boveri Review, No. 12, 1973, pp. 581-588.

6. Brenneisen, J., Futterlieb, E., Muller, E. and Schulz, M., "A New Converter Drive System for a Diesel Electric Locomotive with Asynchronous Traction Motors", IEEE Trans. on Industry Applications, Vol. IA-9, July/August 1973, pp. 482-490.

7. Wakefield, E.H., "An A.C. Drive Electric Vehicle", IEEE Trans. on Industry Applications, Vol. IA-10, January/February 1974, pp. 544-552.

8. Kornbichler, K., "Kernreaktoren", AEG-MITT., Vol. 57, 1967, pp. 143-150.

9. Schrufer, E., Hiesinger, L. and Lambacher, A., "Elekfrische Einrichfungen fur Kernenergieanlagen", AEG-MITT., Vol. 57, 1967, pp. 167-179.

10. Lawson, L.J., "Precisely Controlled Three-Phase Squirrel-Cage Induction Motors for Aerospace Applications", IEEE Aerospace Conference, June 1965.

11. Borland, R.P. and Puchy, C.G., "An A.C. Electric Antenna Drive System for Aerospace Applications", IEEE NAECON, May 1965.

12. Bohm, K., Fick, H. and Gebaver, W., "A.C. Cradle Dynamometers with a Static Converter Feed", Siemens Review, Vol. 39, May 1972, pp. 214-216.

13. Hamilton, R A. and Lezan, G.R., "Thyristor Adjustable Frequency Power Supplies for Hot Strip Run Out Table", IEEE Trans. March/April 1967

14. Ash, J.W and McCall, I.C , "Forced Commutated Inverters for Steelworks Roller Table Drives", IEE Conference on Electrical Variable Speed Drives, 10-12 October 1972, pp. 222-229.

15. Betke, A.C. et al, "Special Purpose A.C. Converter System for Constant Horsepower Applications", IEEE Trans. on Industry Applications, Vol. IA-8, March/April 1972, pp. 126-135.

16. Edwards, J.B. and Fawcett, W., "The D.C.-Link Inverter Induction Motor Drive Applied to the Haulage of an Underground Coal Cutting Machine", IEE Conference on Electrical Variable Speed Drives, 10-12 October 1973, pp. 8-16.

17. Hollis, C.R., "A Review of Five Types of Electrical Adjustable Speed Drives and Their Application to a Centrifugal Pump", IEEE Industrial Applications Meeting, October 1973, p. 35

18. Pollack, J.J., "Some Guidelines for the Application of Adjustable-Speed A.C.-Drives", IEEE Trans. on Industry Applications, Vol. IA-9, November/December 1973, pp. 704-710.

19. Ludbrook, A.L., "Basic Economics of Thyristor Adjustable Speed Drive Systems", IEEE Industry and General Applications Group, Conference Record, October 1969, pp. 591-596.

20. Brown, J.E. and Jones, B.L., "Variable Speed Drives, Survey of Principles and Some Costs", IEE Conference on Electrical Variable Speed Drives, 10-12 October 1972, pp. 97-101.

21. Weygandt, C.N., and Charp, S., "Electromechanical Transient Performance of Induction Motors", Trans. AIEE 1946, Vol. 64, Pt. III, p. 1000.

22. Kovacs, K.P. and Racz, J., "Transiente Vorgange in Wechselstrommaschinen", Verlag der Ungarischen Akademie der Wissenschaften, Budapest, 1959.

23. West, J.C., Jayawant, B.V. and Williams, G., "Analysis of Dynamic Performance of Induction Motors in Control Systems", Proc. IEE, Vol. 111, November 1964, pp. 1468-1478.

24. Pfaff, G., "Zur Dynamik des Asynchronmotors bei Drehzahlsteuerung mittels Veranderlicher Speisefrequenz", Electrotech. Z., 1964, {A}, Vol. 85, pp. 719-724.

25. Rogers, G.J., "Linearised Analysis of Induction-Motor Transients", Proc. IEE, Vol. 112, October 1965, pp. 1917-1926.

26. Heck, R. and Meyer, M., "A Static-Frequency-Changer-Fed Squirrel-Cage Motor Drive for Variable Speed and Reversing", Siemens Review, No. 11, November 1963, pp. 401-405.

27. Heumann, K., "Variable Frequency Speed Control of Induction Motors", Proc. of 3rd Congress of IFAC, Vol. 1, June 1966, pp. 4D1-4D9.

28. Heumann, K. and Jordan, K., "Das Verhalten des Kafiglanfermotors bei Veranderlicher Speisefrequenz und Stromregelung", AEG-MITT., No. 54, 1964, pp. 107-116.

29. Abraham, L., Forster, J. and Schliephake, G., "A.C. Motor Supply with Thyristor Converters", IEEE Trans. on Industry and General Applications, Vol. IGA-2, September/October 1966, pp. 334-340.

30. Slabiak, W. and Lawson, J.L., "Precise Control of a Three-Phase Squirrel-Cage Induction Motor Using a Practical Cycloconverter", IEEE Trans. on Industry and General Applications, Vol. IGA-2, July/August 1966, pp. 274-280.

31. Mokrytzki, B., "The Controlled Slip Static Inverter Drive", Trans. on Industry and General Applications, Vol. IGA-4, May/June 1968, pp. 312-317.

32. Hodle, H. and Stemmler, H., "New Equipment and Control Systems for A.C. Traction Vehicles", The Brown Boveri Review, Vol. 52, September/October 1965, pp. 706-719.

33. Schönung, A. and Stemmler, H., "Static Frequency Changers with 'Subharmonic' Control in Conjunction with Reversible Variable-Speed A.C. Drives", The Brown Boveri Review, Vol. 51, August/September 1964, pp. 555-577.

34. Largiader, H., "Design Aspects of Induction Motors for Traction Applications with Supply through Static Frequency Changers", The Brown Boveri Review, Vol. 57, April 1970, pp. 152-167.

35. Krause, P.C. and Woloszyk, L.T., "Comparison of Computer and Test Results of a Static A.C. Drive System", IEEE Trans. on Industry and General Applications, Vol. IGA-4, November/December 1968, pp. 583-588.

36. Fallside, F. and Wortley, A.T., "Steady-State Oscillation and Stabilisation of Variable-Frequency Invertor-Fed Induction-Motor Drives", Proc. IEE, Vol. 116, June 1969, pp. 991-998.

37. Berg, G.J. and De Sarkar, A.K., "Speed Change of Induction Motors with Variable Frequency Supply", IEEE Trans. on Power Apparatus and Systems, Vol. PAS-90, March/April 1971, pp. 500-508.

38. Nelson, R.H., Lipo, T.A. and Krause, P.C., "Stability Analysis of a Symmetrical Induction Machine", IEEE Trans. on Power Apparatus and Systems, Vol. PAS-88, November 1969, pp. 1710-1717.

39. Lipo, T.A. and Krause, P.C., "Stability Analysis of a Rectifier-Inverter Induction Motor Drive", IEEE Trans. on Power Apparatus and Systems, Vol. PAS-88, January 1969, pp. 55-66.

40. Krause, P.C. and Lipo, T.A., "Analysis and Simplified Representations of a Rectifier-Inverter Induction Motor Drive", IEEE Trans. on Power Apparatus and Systems, Vol. PAS-88, May 1969, pp. 588-596.

41. Jayawant, B.V. and Bateson, K.N., "Dynamic Performance of Induction Motors in Control Systems", Proc. IEE, Vol. 115, December 1968, pp. 1865-1870.

42. Ooi, B.T. and Barton, T.H., "The Modal Approach to Induction Motor Dynamics. Part II", Paper C 72046-6. IEEE PES Winter Meeting, January 30 - February 4, 1972.

43. Ramesh, N. and Robertson, S.D.T., "Induction Machine Instability Predictions - Based on Equivalent Circuits", IEEE Trans. on Power Apparatus and Systems, Vol. PAS-92, March/April 1973, pp. 801-806.

44. Nelson, R.H. and Krause, P.C., "Induction Machine Analysis for Arbitrary Displacement Between Multiple Winding Sets", IEEE Trans. on Power Apparatus and Systems, Vol. PAS-93, May/June 1974, pp. 841-848.

45. Lawrenson, P.J. and Stephenson, J.M., "Note on Induction Machine Performance with a Variable-Frequency Supply", Proc. IEE, Vol. 113, October 1966, pp. 1617-1623.

46. Jordan, H.E., "Digital Computer Analysis of Induction Machines in Dynamic Systems", IEEE Trans. on Power Apparatus and Systems, Vol. PAS-86, June 1967, pp. 722-728.

47. Dote, Y. and Hoft, R.G., "Liapunov Stability Analysis of Induction Motor", IEEE Industry Applications Society, Annual Meeting 1974.

48. Landau, I.D., "Wide Range Speed Control of Three-Phase Squirrel-Cage Induction Motors Using Static Frequency Converters", IEEE Trans. on Industry and General Application, Vol. IGA-5, January/February 1969, pp. 53-59.

49. Woodward, A.E., "Use of Standard Polyphase Induction Motors in Place of Synchronous Reluctance Motor", IEEE Industrial Applications Meeting, October 1973, pp. 697-709.

50. Rissik, H., The Fundamental Theory of Arc Convertors, London, Chapman and Hall Ltd., 1939, Chapters X, XI, XII.

51. Tröger, R., "Technishe Grundlagen und Anwendumpen der Stromrichter", Electrishe Bohnen, Vol. 9, No. 2, 1932, pp. 55-58.

52. McMurray, W. and Slattuck, D.D., "A Silicon-Controlled Rectifier Inverter with Improved Commutation", AIEE Trans. on Communications and Electronics, Vol. 80, November 1961, pp. 531-542.

53. Bradley, D.A., Clarke, C.D., Davis, R.M. and Jones, D.A., "Adjustable Frequency Invertors and Their Application to Variable-Speed Drives", Proc. IEE, Vol. 111, November 1964, pp. 1833-1846.

54. Mokrytzki, B., "Pulse Width Modulated Inverters for A.C. Motor Drives", IEEE Trans. on Industry and General Applications, Vol. IGA-3, November/December 1967, pp. 493-503.

55. Heumann, K., "Development of Inverters with Forced Commutation for A.C. Motor Speed Control Up to the Megawatt Range", IEEE Trans. on Industry and General Applications, Vol. IGA-5, January/February 1969, pp. 61-67.

56. Espelage, P.M., Chiera, J.A. and Turnbull, F.G., "A Wide Range Static Inverter Suitable for A.C. Induction Motor Drives", IEEE Trans. on Industry and General Applications, Vol. IGA-5, July/August 1969, pp. 438-445.

57. Veres, R.P., "New Inverter Supplies for High Horsepower Drives", IEEE Trans. on Industry and General Applications, Vol. IGA-6, March/April 1970, pp. 121-127.

58. Phillips, K.P., "Current Source Converter for A.C. Motor Drives", IEEE Trans. on Industry Applications, Vol. IA-8, November/December 1972, pp. 385-392.

59. Pollack, J.J., "Advanced Pulsewidth Modulated Inverter Techniques", IEEE Trans. on Industry Applications, Vol. IA-8, March/April 1972, pp. 145-154.

60. Penkowski, L.J. and Pruzinsky, K.E., "Fundamentals of a Pulsewidth Modulated Power Circuit", IEEE Trans. on Industry Applications, Vol. IA-8, September/October 1972, pp. 584-592.

61. Patel, H.S. and Hoft, R.G., "Generalized Techniques of Harmonic Elimination and Voltage Control in Thyristor Inverters", Part I - "Harmonic Elimination", IEEE Trans. on Industry Applications, Vol. IA-9, May/June 1973, pp. 310-317, Part II - "Voltage Control Techniques", IEEE Trans. on Industry Applications, Vol. IA-10, September/October 1974, pp. 666-673.

62. Zubek, J., Abbondanti, J.Z. and Nordby, C.J., "Pulse Width Modulated Inverter Motor Drives with Improved Modulation", IEEE Industry Applications Society, Annual Meeting 1974.

63. Nelson, R.H. and Radomski, T.A., "Design Methods for Current Source Inverter/Induction Motor Drive Systems", IEEE Trans. on Ind. Electronics and Control Application, May 1975, pp. 141-145.

64. Stefanovic, V.R. and Barton, T.H., "Static Torque Characteristics of an Induction Motor with a Variable Frequency Supply", Paper C73199-7, PASS Winter Meeting 1973.

65. Salihi, J.T., "Simulation of Controlled Slip Variable Speed Induction Motor Drive Systems", IEEE Trans. on Industry and General Applications, Vol. IGA-5, March/April 1969, pp. 149-157.

66. Magg, R., "Characteristics and Application of Current Source/Slip Regulated A.C. Induction Motor Drives", IEEE IGA Annual Meeting, October 1971.

67. Li, K.Y.G., "Analysis and Operation of an Invertor-Fed Variable Speed Induction Motor", Proc. IEE, Vol. 116, 1969, pp. 1571-1580.

68. Fitzgerald, A.E. and Kingsley, C.J.R., Electric Machinery, The Dynamics and Statics of Electromechanical Energy Conversion, McGraw-Hill, N.Y., 1961.

69 O'Kelly, D and Simmons, S , Introduction to Generalized Electrical Machine Theory, McGraw-Hill, England, 1968.

70. Horowitz, I.M. and Shaked, U , "Superiority of Transfer Function Over State Variable Methods in Linear Time-Invariant Feedback System Design", IEEE Trans. on Automatic Control, Vol. AC-20, February 1975, pp. 84-97.

71. DeRusso, P.M., Roy, R.J. and Close, C.M., State Variables for Engineers, John Wiley and Sons Inc., N.Y., 1965, p. 340

72. Ibid., p. 341.

73. Ibid., p. 349-351.

74. Ibid , pp. 336-338.

75. Chen, C.T., Introduction to Linear System Theory, Holt, Rinehart and Winston Inc., N.Y., 1970, pp. 191-196.

76. Ibid., pp. 277-281.

77. Ibid., pp. 227-229.

78. Luenberger, D.G., "An Introduction to Observers", IEEE Trans. on Automatic Control, Vol. AC-16, December 1971, pp. 596-602.

79. Lipo, T.A. and Plunkett, A.B., "A Novel Approach to Induction Motor Transfer Function", IEEE-IAS Annual Meeting Conference Record, October 8 - 11, 1973, pp. 441-449.

80. Blaschke, F., "The Principle of Field Orientation as Applied to the New Transvector Closed-Loop Control System for Rotating Field Machines", Siemens Review, Vol. 34, 1972, pp. 217-220.

81. Flotes, W. and Ripperger, H., "Field-Oriented Closed Loop Control of an Induction Machine with the New Transvector Control System", Siemens Review, Vol. 34, 1972, pp. 248-252.

82. Kume, T. and Youside, Y., "Speed Transient of Induction Motor Driven by Current-Source Type Inverter", IEEE Industrial Applications Meeting, October 1973, pp. 865-874.

83. Plunkett, A. and Lipo, T., "A New Method for Induction Motor Torque Regulation", IAS Meeting, 1974, pp. 832-844.

84. Jain, G.C., "The Effect of Voltage Waveshape on the Performance of a 3-Phase Induction Motor", IEEE Trans. on Power Apparatus and Systems, Vol. PAS-83, pp 561-566.

85. Ward, E.E., Kazi, A. and Farkas, R., "Time-Domain Analysis of the Inverter-Fed Induction Motor", Proc. IEE, Vol. 114, 1967, pp. 361-369.

86. Klingshirn, E.A. and Jordan, H.E., "Polyphase Induction Motor Performance and Losses on Nonsinusoidal Voltage Sources", IEEE Trans. on Power Apparatus and Systems, Vol. 87, March 1968, pp. 624-631.

87. Chalmers, B.J. and Sarkar, B.R., "Induction Motor Losses Due to Nonsinusoidal Supply Waveforms", Proc. IEE, Vol. 115, December 1968, pp. 1777-1783.

88. Beck, C. and Chandler, E., "Motor Drive Inverter Ratings", IEEE Trans. on Industry and General Application, Vol. IGA-4, November/December 1968, pp. 589-595.

89. Krause, P.C. and Hake, J.R., "Method of Multiple Reference Frames Applied to the Analysis of a Rectifier - Inverter Induction Motor Drive", IEEE Trans. on Power Apparatus and Systems, Vol. 88, No. 11, November 1969, pp. 1635-1641.

90. Bedford, R.E. and Nene, V.D., "Complex Frequency-Domain Analysis of Inverter Fed Induction Machines", IEEE Trans. on Industry Applications, Vol. IA-8, May/June 1972, pp. 269-277.

91. Lipo, T.A., Krause, P.C. and Jordan, H.E., "Harmonic Torque and Speed Pulsations in a Rectifier-Inverter Induction Motor Drive", IEEE Trans. on Power Apparatus and Systems, Vol. PAS-88, May 1969, pp. 579-587.

92. Robertson, S. and Hebbar, K.M., "Torque Pulsations in Induction Motors with Inverter Drives", IEEE Trans. on Industry and General Applications, Vol. IGA-7, March/April 1971, pp. 318-323.

93. Kernick, A., Roof, J.L. and Heinrich, T.M., "Static Inverter with Neutralization of Harmonics", Trans. AIEE on Applications and Industry, Vol. 81, May 1962, pp. 59-68.

94. Turnbull, F.G., "Selected Harmonic Reduction in Static D.C. - A.C. Inverters", IEEE Trans. on Communication and Electronics, Vol. 83, July 1964, pp. 374-378.

95. Jackson, S.P., "Multiple Pulse Modulation in Static Inverters Reduces Selected Output Harmonics and Provides Smooth Adjustment of Fundamentals", IEEE Trans. on Industry and General Applications, Vol. IGA-6, July/August 1970, pp. 357-360.

96. Pelly, B.R , Thyristor Phase-Controlled Converters and Cycloconverters, Wiley Interscience, New York, 1971, pp. 389-409.

97. Philibert, P., "Control Strategy for PWM Inverters", M.Eng. Thesis, McGill University (now in progress)

98. Flower, J.O. and Hazell, P.A., "Non-Linear Analysis of a 1st Order Thyristor Bridge", Proc. IEE, Vol. 118, 1971, pp. 1511-1516.

99. Bjaresten, N.A., "Static Converter as a High Speed Power Amplifier", Direct Current, Vol. 8, June 1965, pp. 154-165.

100. Parish, E.A. and McVery, E.S., "A Theoretical Model for a Single-Phase Silicon-Controlled Rectifier Systems", IEEE Trans. on Automatic Control, Vol. AC-12, May 1967, pp. 577-579.

101. Hernandez-Millan, R., Sucena-Paiva, J.P. and Freris, L.L., "Modelling of Controlled Rectifiers in Feedback Systems", IEEE Trans. on Power Apparatus and Systems, Vol. PAS-93, January/February 1974, pp. 167-175.

102. Joos, G., "A High Performance Direct Current Dynamometer", M.Eng. Thesis, McGill University, 1974, pp. 30-34.

103. Oliver, F.J., Practical Instrumentation Transducers, Hyden Book Co. Inc., New York, 1971, pp. 97-109.

104. Abondanti, A. and Brennen, M.B., "Control of Induction Motor Drives by Synthesis of a Slip Signal", IAS Annual Meeting, 1974.

105. Barton, T.H. and Ionides, R.J., "A Precision Torquemeter Based on Magnetic Stress Aniosotropy", Trans. IEEE on Power Apparatus and Systems, Vol. PAS-85, February 1966, pp. 152-159.